

Thesis  
5/10/07

**SEDIMENT AND ASSOCIATED RADIONUCLIDE DYNAMICS WITHIN THE  
RIBBLE ESTUARY, NORTH WEST ENGLAND**

**By**

**Richard John Wakefield**

**Submitted to**

**The Faculty of Natural Sciences, University of Stirling, October 2005**

**For the degree of**

**Doctor of Philosophy**

**This research was undertaken at the School of Biological and  
Environmental Science, University of Stirling, Stirling.**

05/10/07

ProQuest Number: 13917105

All rights reserved

INFORMATION TO ALL USERS

The quality of this reproduction is dependent upon the quality of the copy submitted.

In the unlikely event that the author did not send a complete manuscript and there are missing pages, these will be noted. Also, if material had to be removed, a note will indicate the deletion.



ProQuest 13917105

Published by ProQuest LLC (2019). Copyright of the Dissertation is held by the Author.

All rights reserved.

This work is protected against unauthorized copying under Title 17, United States Code  
Microform Edition © ProQuest LLC.

ProQuest LLC.  
789 East Eisenhower Parkway  
P.O. Box 1346  
Ann Arbor, MI 48106 – 1346

## ABSTRACT

Intertidal environments represent a spatially complex and dynamic system, rendering point sampling geographically and temporally isolated within the context of the entire estuarine system. Airborne remote sensing has the potential to place these spatially isolated sampling points into a quantitative spatial context. Furthermore it provides a valuable data source for quantifying processes within estuarine zones and can supply calibration and validation information for hydrodynamic models. This study focuses on the Ribble Estuary, Lancashire, England which is accumulating elevated radionuclide concentrations derived from authorized industrial discharges from BNFL Sellafield and Westinghouse Springfields.

An image mixture modeling approach was used on Airborne Thematic Mapper (ATM) data to derive accurate estimates of intertidal clay, in comparison to concurrent field sampling ( $r^2=0.828$ ) and radionuclide concentrations ( $r^2=0.822$ ). Data processed for 2003 was compared with similar data from May 1997 (Rainey 1999; Rainey *et al.*, 2000; 2003) to investigate spatial changes in intertidal clay and  $^{137}\text{Cs}$  contamination. These results compared with field sampling data demonstrates considerable reduction (c.52%) in the activity concentrations, which is primarily attributed to processes of sediment dilution. Calibrated Compact Airborne Spectrographic Imager (CASI) imagery combined with concomitant ground reference data, was used to characterize the suspended sediment concentrations and the total suspended load over each flight line. Two sets of time series image data were compared to assess the spatial and temporal changes in suspended sediment and associated radionuclide transportation within the estuarine environment. In conjunction with total volumetric estimates generated from a two-dimensional vertically resolving hydrodynamic model, this data then allowed estimation of the total flux of suspended sediment and radionuclide over the flood and ebb tidal cycle to a reasonable precision (40%). To establish whether these flux estimates are realistic, the results are compared with time series field based observations collected from monthly observations over a two year cycle. The results provide a unique quantitative insight into the understanding of

contaminant and sediment transport within this estuarine environment and the environmental processes controlling them. The contribution of field data with the intertidal and flood-ebb tide imagery has provided an enhanced understanding of the interactions of tides and fluvial flow on the spatial distribution of sediments within the Ribble Estuary. It could also be possible to apply the calibrated clay intertidal maps to other heavy metal pollutants that have a high affinity with fine-grained clay particles i.e. Pb, Zn, Cu, Al in estuarine sediments.

## ACKNOWLEDGEMENTS

I would like to thank my principal supervisor, Dr Andrew Tyler, for his continued supervision and support throughout the entire course of this work, without whom none of this would have been possible. I would also like to thank my supervisors at Westlakes Research Institute, firstly to Dr Adrian Punt for the initial period of my work and secondly to Dr Paul McDonald for his continued support and advice during the later stages of this investigation. This study was funded by the Natural Environmental Research Council, in association with Westlakes Research Institute, to whom I am very grateful for giving me the opportunity to carry out this research.

I would also like to thank all the technical staff based here at the School of Biological & Environmental Science and Westlakes Research Institute for their continued help and understanding. In particular I would like to thank Stuart Bradley for humour and field work skills, Scott Jackson for his computer wizardry, Bill Jamison for his help with all those diagrams, Philippe Gleizon for all his modelling skills and all the staff at Westlakes whom I dragged out for many sunny days of field work in the Ribble Estuary.

I would also like to extend my thanks to all my fellow Ph.D. students (some ex-) for all their help and support in that long process of Ph.D. I would especially like to thank Crona, Peter, Kevin, Gilbert and Lisa for their friendship and support. Finally, I would like to thank my family for their considerable support throughout the period of my Ph.D. here at Stirling and Westlakes.

# CONTENTS

TITLE PAGE.....	i
ABSTRACT.....	ii
ACKNOWLEDGEMENTS.....	iv
CONTENTS.....	v
INDEX OF FIGURES.....	x
INDEX OF TABLES.....	xv
INDEX OF ACRONYMS.....	xvii
<b>1 Introduction.....</b>	<b>1</b>
1.1. Rationale of Work .....	1
1.2. Aims and Objectives .....	8
<b>2 A Review of Methods of Monitoring.....</b>	<b>12</b>
2.1. Introduction.....	12
2.2. Defining estuarine sediment dynamics .....	12
2.3. Methodologies for characterising intertidal environments of estuaries.....	15
2.3.1. Intertidal environments .....	15
2.3.2. Remote sensing of the estuarine environments .....	27
2.4. Methodologies for quantifying SSC and transport in estuaries .....	30
2.4.1. Sediment flux patterns within estuarine environments .....	30
2.4.2. Point monitoring and sampling .....	32
2.4.3. Remote sensing of the suspended sediment .....	33
2.5. Radioactivity in the marine environment.....	35
2.5.1. Sources of radioactivity .....	35
2.5.2. Environmental behaviour of radioactivity in marine environments....	41

2.5.3.	Gamma ray detection .....	43
2.5.4.	Monitoring techniques .....	45
<b>2.6.</b>	<b>Modelling Estuarine Environments.....</b>	<b>47</b>
2.6.1.	Theoretical approaches.....	47
2.6.2.	Example of applications .....	51
<b>2.7.</b>	<b>Ribble Estuary.....</b>	<b>53</b>
2.7.1.	Monitoring priorities .....	53
2.7.2.	The sedimentary environment, sediment sampling and saltmarsh cores .....	54
2.7.3.	Hydrodynamic behaviour of the Ribble Estuary .....	55
2.7.4.	Hydrodynamic modelling the Ribble .....	56
<b>2.8.</b>	<b>Research priorities and the derivation of hypotheses .....</b>	<b>59</b>
2.8.1.	Intertidal characteristics.....	60
2.8.2.	Sediment flux.....	62
2.8.3.	Research milestones.....	64
<b>2.9.</b>	<b>Summary .....</b>	<b>66</b>
<b>3</b>	<b>Sediment accretion (and associated radionuclides) of the intertidal sediments in the Ribble Estuary. ....</b>	<b>68</b>
<b>3.1.</b>	<b>Introduction.....</b>	<b>68</b>
<b>3.2.</b>	<b>Locations of field study sites .....</b>	<b>69</b>
3.2.1.	Location of sampling points.....	69
3.2.2.	Lytham (Site 1).....	72
3.2.3.	Warton Bank (Site 2).....	73
3.2.4.	Savick Brook (Site 4).....	74
3.2.5.	Penwortham Bridge (Site 3) .....	75
<b>3.3.</b>	<b>Methodology for field measurements .....</b>	<b>77</b>

3.3.1.	Sampling strategy.....	77
3.3.2.	Sample collection techniques .....	77
3.3.3.	Measurement of erosion/deposition on the intertidal surface. ....	80
3.3.4.	Gamma ray analysis (procedures) .....	83
3.3.5.	Estimation of sample activity .....	84
3.3.6.	Spectral analysis of samples.....	84
<b>3.4.</b>	<b>Results and interpretation of intertidal sediment and bed elevation changes .....</b>	<b>85</b>
3.4.1.	Lytham St Anne's .....	85
3.4.2.	Warton Bank.....	89
3.4.3.	Savick Brook .....	94
3.4.4.	Penwortham Bridge.....	97
3.4.5.	Analysis of alternating clay percentage on intertidal surface.....	98
3.4.6.	Wind speed and directional impacts on intertidal clay distribution..	101
3.4.7.	Intertidal bed elevation changes.....	102
<b>3.5.</b>	<b>Specific activity and grain size associations .....</b>	<b>103</b>
3.5.1.	Relationship of radionuclide activity concentrations and clay percentage .....	103
3.5.2.	Intertidal sediment sample radionuclide inventory.....	106
3.5.3.	Depth profiles of intertidal surface .....	108
<b>3.6.</b>	<b>Discussion .....</b>	<b>110</b>
3.6.1.	Lytham .....	110
3.6.2.	Warton Bank.....	112
3.6.3.	Savick Brook .....	113
3.6.4.	Penwortham Bridge.....	114
3.6.5.	Activity concentrations of intertidal sediments.....	115
3.6.6.	Bed height elevation changes .....	116
<b>3.7.</b>	<b>Conclusions .....</b>	<b>117</b>

<b>4</b>	<b>Mapping intertidal sediments and their associated radionuclides</b>	<b>120</b>
4.1.	Introduction.....	120
4.2.	Data acquisition.....	121
4.3.	Ground truth data collection.....	122
4.4.	Image analysis procedures.....	126
4.4.1.	Image geocorrection.....	126
4.4.2.	Atmospheric correction.....	127
4.4.3.	Minimum noise fraction transformation (MNF).....	130
4.4.4.	End member identification.....	130
4.4.5.	Linear mixture modelling.....	131
4.5.	Results.....	132
4.5.1.	Transects on intertidal sediments.....	132
4.5.2.	17 <sup>th</sup> October 2003 intertidal ATM imagery.....	142
4.5.3.	Endmember selection.....	142
4.5.4.	Distribution of intertidal sediments.....	146
4.5.5.	Clay abundance transects.....	148
4.5.6.	River discharge conditions.....	151
4.5.7.	Changes in radionuclide distribution in the intertidal sediments.....	152
4.6.	Discussion.....	158
4.6.1.	Intertidal clay distribution.....	158
4.6.2.	Moisture content of the intertidal sediments.....	160
4.6.3.	Distribution of <sup>137</sup> Cs within the Ribble Estuary.....	161
4.7.	Summary.....	161
<b>5</b>	<b>Mapping suspended sediment fluxes in the Ribble Estuary.....</b>	<b>164</b>
5.1.	Introduction.....	164
5.1.1	Sediment sources within the estuary.....	166

<b>5.2. Remote sensing of suspended sediment in estuarine waters.....</b>	<b>170</b>
<b>5.3. Ground Reference Data.....</b>	<b>172</b>
5.3.1. Water sampling collection .....	173
<b>5.4. Image analysis procedures.....</b>	<b>176</b>
5.4.1. Geocorrection.....	176
5.4.2. Radiometric normalization (Atmospheric correction) .....	177
5.4.3. Sun angle normalisation .....	179
5.4.4. Image-to-Image normalisation.....	184
<b>5.5. Modelled water volume and velocity profiles.....</b>	<b>186</b>
<b>5.6. Results.....</b>	<b>191</b>
5.6.1. Introduction .....	191
5.6.2. Ground reference data .....	191
5.6.3. Time series imagery .....	194
5.6.4. Image analysis – 15 <sup>th</sup> July 2003 .....	195
5.6.5. Image analysis – 16 <sup>th</sup> April 2003 .....	213
5.6.6. Estimation of total sediment fluxes April 2003 and July 2003.....	222
5.6.7. Deposition of <sup>137</sup> Cs over tidal event.....	231
<b>5.7. Warton Bank suspended sediment transport pattern .....</b>	<b>232</b>
<b>5.8. Consideration of uncertainties .....</b>	<b>235</b>
<b>5.9. Discussion and Conclusions.....</b>	<b>238</b>
5.9.1. Warton Bank.....	240
5.9.2. Suspended sediment transportation.....	240
<b>5.10. Summary .....</b>	<b>242</b>
<b>6 Discussion and Conclusions.....</b>	<b>244</b>
<b>6.1. Introduction.....</b>	<b>244</b>
<b>6.2. Inter-annual variations in sediment deposition. ....</b>	<b>247</b>
6.2.1. Intertidal sediment properties .....	248

6.2.2. Spatial distribution of intertidal sediments. ....	249
<b>6.3. Intra-annual variations in sediment accretion and erosion .....</b>	<b>250</b>
<b>6.4. Percentage clay and <sup>137</sup>Cs relationships .....</b>	<b>252</b>
6.4.1. Intertidal clay mapping .....	254
6.4.2. Application of clay/ <sup>137</sup> Cs relationships .....	255
<b>6.5. Net sediment flux of suspended sediment.....</b>	<b>258</b>
6.5.1. Suspended sediment load estimations.....	259
<b>6.6. Further related work on the Ribble Estuary .....</b>	<b>266</b>
<b>6.7. Conclusions on method developments.....</b>	<b>269</b>
<b>6.8. Conclusions on the fate of sediment and radionuclide dynamics in the Ribble Estuary .....</b>	<b>270</b>
<b>6.9. Final conclusions .....</b>	<b>272</b>
<b>References.....</b>	<b>275</b>

## INDEX OF FIGURES

<b>Figure 1-1</b> Location of the Ribble Estuary.....	4
<b>Figure 1-2</b> The Ribble Estuary showing the major sources of radionuclides input into the estuary .....	6
<b>Figure 1-3</b> Ribble Water Framework Directive boundary (Environment Agency©).....	8
<b>Figure 2-1</b> Contact core (Ford & Honeywill, 2002).....	22
<b>Figure 2-2</b> Location of BNFL Sellafield/Drigg and BNFL Westinghouse Springfields.....	40
<b>Figure 2-3</b> Model architecture of VERSE (Gleizon <i>et al.</i> , 2001).....	58
<b>Figure 3-1</b> Ribble Estuary sampling locations.....	71
<b>Figure 3-2</b> The four sampling sites for the two year intertidal sampling campaign.....	72

<b>Figure 3-3</b> Lytham St Anne's schematic diagram generated from an extensive EDM survey obtained August 2003 and georeferenced to an accurate GPS base station. ....	73
<b>Figure 3-4</b> Warton Bank schematic diagram generated from an extensive EDM survey and georeferenced to a GPS base station. ....	74
<b>Figure 3-5</b> Savick Brook transect .....	75
<b>Figure 3-6</b> Penwortham sampling site looking west. ....	76
<b>Figure 3-7</b> Penwortham Bridge looking east. ....	76
<b>Figure 3-8</b> Comparison of clay percentages taken from the same sample, by each institutions particle sizer. Error bars are associated with the mean standard deviation of the sampled sediments for each instrument. ....	79
<b>Figure 3-9</b> Comparison of sand percentages taken from the same sample, by each institutions particle sizer. Error bars are associated with the mean standard deviation of the sampled sediments for each instrument. ....	80
<b>Figure 3-10</b> Relic footmarks surrounding field site 1 at Lytham, a month after previous sampling. ....	81
<b>Figure 3-11</b> Measurement of height elevation of the intertidal surface. ....	83
<b>Figure 3-12</b> a: Intertidal surface profile at Warton Bank. & b: Intertidal sediment surface at Lytham St Anne's .....	86
<b>Figure 3-13</b> Clay % changes at Lytham. a) Upper intertidal site, b) mid-intertidal site & c) lower intertidal site. ....	87
<b>Figure 3-14</b> Sediment surface elevation changes at Lytham a) Upper intertidal site, b) mid-intertidal site & c) lower intertidal site. ....	88
<b>Figure 3-15</b> Clay percentage changes at Warton Bank – upper intertidal zone .....	89
<b>Figure 3-16 &amp; Table 3-1</b> Clay percentage changes at Warton bank – lower intertidal section & Table 3.1 Mean summer/winter clay percentages .....	91
<b>Figure 3-17</b> a & b Bed height elevation changes at sites 1 & 2, Warton Bank .....	92
<b>Figure 3-18</b> Upper intertidal zone at Warton bank March 2002 showing erosional surface. ....	93
<b>Figure 3-19</b> a, b & c Bed height elevation changes at sites 3 – 5, Warton Bank .....	93
<b>Figure 3-20</b> a, b & c Clay percentage changes at Savick Brook .....	95

<b>Figure 3-21</b> a, b & c Bed height elevation changes at Savick Brook.....	96
<b>Figure 3-22</b> a & b Clay percentages at Penwortham .....	97
<b>Figure 3-23</b> a & b Bed height changes at Penwortham.....	98
<b>Figure 3-24</b> Coefficient of determination analyses of percentage clay and <sup>137</sup> Cs activity concentrations and daily averaged river discharge (cumecs).....	104
<b>Figure 3-25</b> Relationship between <sup>137</sup> Cs and percentage clay for 1995, 1997, 2002 and 2003.....	107
<b>Figure 3-26</b> Core profiles taken at Warton Bank August 2002.....	110
<b>Figure 4-1</b> Transect lines for Lytham St Anne's, 2 <sup>nd</sup> September 2002, showing the two transect lines and the transect-end white marker boards.....	124
<b>Figure 4-2</b> Transect lines for Warton Bank, 2 <sup>nd</sup> September 2002, showing the three transect lines. ....	124
<b>Figure 4-3</b> Percentage change in grain size along the intertidal transects at Lytham St Anne's during the September 2002 field sampling. ....	132
<b>Figure 4-4</b> a, b & c Percentage change in grain size along the intertidal transects at Warton Bank during the September 2002 field sampling. ....	134
<b>Figure 4-5</b> Percentage change in grain size fractions along the intertidal transects at Warton Bank during the October 2003 field sampling. ....	135
<b>Figure 4-6</b> Comparison of percentage sand to percentage moisture within the sediment samples (Lytham St Anne's September 2002).....	136
<b>Figure 4-7</b> Comparison of percentage sand to percentage moisture within the sediment samples from transect 1.1 & 1.2 (Warton Bank, September 2002).....	137
<b>Figure 4-8</b> Comparison of percentage sand to percentage moisture within the sediment samples from transect 2.1 & 2.2 (Warton Bank, September 2002).....	138
<b>Figure 4-9</b> a, b & c Comparison of percentage sand to percentage moisture within the sediment samples from transect 1, 2 & 3 (Warton Bank, October 2003).....	138
<b>Figure 4-10</b> Comparison of <sup>137</sup> Cs activity concentrations and clay percentages on transects from Lytham St Anne's, September 2002.....	139

<b>Figure 4-11</b> Comparison of $^{137}\text{Cs}$ activity concentrations and clay percentages on transect lines 1.1 and 1.2 from Warton Bank, September 2002. .....	140
<b>Figure 4-12</b> Comparison of $^{137}\text{Cs}$ activity concentrations and clay percentages on transect lines 2.1 and 2.2 from Warton Bank, September 2002 .....	140
<b>Figure 4-13</b> Comparison of $^{137}\text{Cs}$ activity concentrations and clay percentages on transect lines 1, 2 & 3 at Warton Bank October 2003 .....	141
<b>Figure 4-14</b> Eigenvalue plot of MNF transformation of October 2003 ATM imager.....	143
<b>Figure 4-15</b> 2D scatterplot of MNF band 1 vs. MNF band 2 (Oct'2003) .....	145
<b>Figure 4-16</b> 2D scatterplot of MNF band 2 vs. MNF band 3 (Oct'2003) .....	145
<b>Figure 4-17</b> 2D scatterplot of MNF band 3 vs. MNF band 4 (Oct'2003) .....	145
<b>Figure 4-18</b> Percentage clay map produced for the Ribble Estuary October 2003.....	147
<b>Figure 4-19</b> Comparison of measured clay percentages to image estimated clay percentage .....	148
<b>Figure 4-20</b> Percentage clay map, 1997 (Rainey, 1999).....	150
<b>Figure 4-21</b> Subset of percentage clay map (Figure 4.22), 1997 (Rainey, 1999) .....	151
<b>Figure 4-22</b> River Ribble discharge patterns 20 days prior to the flights in September 2002, October 2003 (flight on day 21) and May 1997	152
<b>Figure 4-23</b> $^{137}\text{Cs}$ map of the Ribble Estuary, October 2003 .....	155
<b>Figure 4-24</b> Subset of figure 4.24, showing $^{137}\text{Cs}$ distribution at the confluence of the River Douglas. ....	156
<b>Figure 4-25</b> Comparison of estimated and actual $^{137}\text{Cs}$ activities along sample transects at Warton Bank .....	156
<b>Figure 4-26</b> $^{137}\text{Cs}$ distribution within the estuary, 1997 (Rainey, 1999) middle Ribble & b 2003 $^{137}\text{Cs}$ distribution .....	157
<b>Figure 5-1</b> Movement of sediment within the Ribble Estuary .....	168
<b>Figure 5-2</b> Changing solar elevation azimuth for the 17 <sup>th</sup> July, 2003 and the comparison to the percentage change in radiance values of the ground control points at Warton aerodrome during each time series image.....	182

<b>Figure 5-3</b> Plot of the solar azimuth angle against the percentage change in the mean radiance value from selected ground targets for July 2003 imagery.....	183
<b>Figure 5-4</b> Solar azimuth angle against the percentage change in the mean radiance values from selected ground targets for time series imagery April 2003.....	184
<b>Figure 5-5</b> Demonstrating of the best fit equation for the image-to-image normalisation of the July 2003 imagery to that of the July 1997 imagery obtain by Atkin (2000) obtained from ground control points at Warton Aerodrome, allowing the July 2003 imagery to be normalised to the 1997 time series imagery. ....	186
<b>Figure 5-6</b> Cell velocities from Lytham St Anne's to Preston Docks showing flow in the morning 15 <sup>th</sup> July 2003. ....	188
<b>Figure 5-7</b> Cell velocities from Lytham St Anne's to Preston Docks showing flow in the morning 15 <sup>th</sup> July 2003. ....	189
<b>Figure 5-8</b> Cell velocities from Lytham St Anne's to Preston Docks 16 <sup>th</sup> April 2003.....	190
<b>Figure 5-9</b> The environmentally derived relationship between suspended sediment and the associated <sup>137</sup> Cs concentration and its temporal stability (Atkin 2000), in comparison to the July 2003 sampling data. ....	193
<b>Figure 5-10</b> SSC for the Ribble Estuary, obtained concurrently with the July 2003 time series CASI imagery. ....	194
<b>Figure 5-11</b> Measured SSC values compared to image radiance values obtained from Atkins' (2000) July 1997 imagery, band 10 CASI..	197
<b>Figure 5-12</b> Average SSC within Preston Docks a: April 2003 & b: July 2003. Blank spaces represent areas where data is not available due to reduced flight lines or cloud cover over dock area.....	198
<b>Figure 5-13</b> Image 196011b taken at 10:34 .....	200
<b>Figure 5-14</b> Image 196021b taken at 10:56 .....	201
<b>Figure 5-15</b> Image 196031b taken at 11:11 .....	202
<b>Figure 5-16</b> Image 196041b taken at 11:24 .....	203
<b>Figure 5-17</b> Image 196051b taken at 11:48 .....	204
<b>Figure 5-18</b> Image 196061b taken at 11:54 .....	205
<b>Figure 5-19</b> Image 196071b taken at 13:49 .....	207
<b>Figure 5-20</b> Image 196081b taken at 14:02 .....	208

<b>Figure 5-21</b> Image 196091b taken at 14:15 .....	209
<b>Figure 5-22</b> Image 196101b taken at 14:28 .....	210
<b>Figure 5-23</b> Image 196111b taken at 14:41 .....	211
<b>Figure 5-24</b> Image 196121b taken at 14:55 .....	212
<b>Figure 5-25</b> Image 107011b taken at 09:19 .....	214
<b>Figure 5-26</b> Image 107021b taken at 09:33 .....	215
<b>Figure 5-27</b> Image 107031b taken at 09:48 .....	216
<b>Figure 5-28</b> Image 107041b taken at 10:04 .....	217
<b>Figure 5-29</b> Image 107051b taken at 10:20 .....	218
<b>Figure 5-30</b> Image 107061b taken at 12:21 .....	219
<b>Figure 5-31</b> Image 107071b taken at 12:37 .....	220
<b>Figure 5-32</b> Variation in total suspended sediment loads for the 15 <sup>th</sup> July 2003 .....	223
<b>Figure 5-33</b> Variation in total suspended sediment loads for the 16 <sup>th</sup> April 2003.....	225
<b>Figure 5-34</b> Erosion and depositional cycle of the estuary during the July 2003 overflight. ....	229
<b>Figure 5-35</b> Comparison of suspended sediment load against <sup>137</sup> Cs loading for each flight line. ....	231
<b>Figure 5-36</b> Warton Bank – April and July 2003 suspended sediment loads during course of imagery (blue sample points are estimations of suspended sediment load prior and after time series acquisition). .....	234

## INDEX OF TABLES

<b>Table 3-1</b> Mean summer/winter clay percentages.....	91
<b>Table 3-2</b> Data used for best subset regression of clay percentage distribution in the Ribble Estuary .....	99
<b>Table 3-3</b> Correlation coefficients of changing Clay % at all estuary sites. 7 day Q (log) is the natural log of the mean daily discharge of river flow (cumecs) for the preceding 7 days prior to sampling, 3 day Q (log) is three days mean discharge prior to sampling, 5 day tide (log) is the natural log of mean tidal maximum prior to sampling, 2 day tide log (as previous) and	

before tide is the tidal maximum prior to sampling. Bold numbers represent $r^2$ values with a $p$ -value <0.05. ....	100
<b>Table 3-4</b> Best subset analysis of the effects of average wind speed and direction in comparison to the effects of changing tidal heights and riverine discharge rates in respect to intertidal clay distribution. P = Penwortham, WB = Warton Bank and L = Lytham St Anne's field sampling locations. ....	102
<b>Table 3-5</b> Best subset analysis ( $r^2$ ) of percentage clay and $^{137}\text{Cs}$ regression against oscillating river and tidal conditions within the Ribble Estuary. 7 day Q (log) is the natural log of the mean daily discharge of river flow (cumecs) for the preceding 7 days prior to sampling, 3 day Q (log) is three days mean discharge prior to sampling, 5 day tide (log) is the natural log of mean tidal maximum prior to sampling, 2 day tide log (as previous). ....	105
<b>Table 3-6</b> Inter-comparison of 1995, 1997, 2002 and 2003 intertidal sediments, assessing the relationship of percentage clay and $^{137}\text{Cs}$ ....	108
<b>Table 3-7</b> Maximum, averaged daily depositional rates (mm per day) between sampling visits for all sites within the Ribble Estuary. ....	117
<b>Table 4-1</b> Flight line requirements for intertidal sediment study, proposed, actually achieved and useable data. ....	121
<b>Table 4-2</b> Details of manual geometric correction errors for October 2003 imagery. ....	127
<b>Table 5-1</b> Flight line acquisition for flood and ebb flights, planned and obtained. ....	172
<b>Table 5-2</b> Flights lines for July 2003 time series imagery. ....	177
<b>Table 5-3</b> Flight lines for April 2003 time series imagery. ....	178
<b>Table 5-4</b> Sun angle correction factors for July 2003 imagery. ....	181
<b>Table 5-5</b> Sun angle correction factors for April 2003 imagery. ....	182
<b>Table 5-6</b> Sample locations and grain size distribution for concomitant ground control points for July 2003 CASI imagery. Also sampled SSC within the surface waters of the estuary. ....	192
<b>Table 5-7</b> Deposition and erosion of sediment over course of flood and ebb tidal cycle and the associated uncertainties with them. ....	230
<b>Table 5-8</b> The total suspended sediment and $^{137}\text{Cs}$ load for each time series flight line for July 2003. ....	232
<b>Table 5-9</b> Depositional estimation of Warton Bank sedimentation from the April and July 2003 time series imagery (Figure 5.35). ....	233

<b>Table 5-10</b> Uncertainties associated with the calculation of the net deposition of sediments during the July 2003 time series imagery (* - estimated sources of error). .....	235
-------------------------------------------------------------------------------------------------------------------------------------------------------------------------------------	-----

<b>Table 5-11</b> Absolute errors for calculated depositional values for the July 2003 time series imagery. ....	238
------------------------------------------------------------------------------------------------------------------	-----

## **INDEX OF ACRONYMS**

<b>ARS</b>	Airborne Remote Sensing
<b>ATM</b>	Airborne Thematic Mapper
<b>BNFL</b>	British Nuclear Fuels Ltd
<b>BST</b>	British Summer Time
<b>CASI</b>	Compact Airborne Spectrographic Imager
<b>DGPS</b>	Differential Global Positioning System
<b>GCP</b>	Ground Control Point
<b>GMT</b>	Greenwich Mean Time
<b>GPS</b>	Global Positioning System
<b>LIDAR</b>	Light Detection And Ranging
<b>NERC</b>	Natural Environment Research Council
<b>PEEPS</b>	Photo-Electronic Erosion Pins
<b>RMS</b>	Root Mean Square
<b>SSC</b>	Suspended Sediment Concentrations
<b>SWIR</b>	Short Wave InfraRed
<b>THORP</b>	Thermal Oxidising Re-processing Plant
<b>VERSE</b>	Vertically Resolving model of Sediment and radionuclide transport in Estuaries

# 1 Introduction

## 1.1. Rationale of Work

Estuaries are dynamic and constantly evolving regions of the natural environment, characterised by the constant, but fluctuating interaction of terrestrial and marine based processes. This constant interaction, coupled with processes which promote the deposition of fine grained sediment, often results in the consequences of human interaction being focused in estuarine environments. When this is combined with issues of usage, especially for recreational activities (e.g. fishing, shooting, sailing and house boat dwelling) and commercial activities (e.g. fishing, bait digging, disposal of domestic and commercial waste waters and water cooling processes), estuaries often become identified as an important critical interface in impact assessments. In recognition of the relative importance of estuaries, environmental policy and legislation has evolved, especially through the European Water Framework Directive (WFD), to focus regulatory activity on achieving good ecological status through revised discharge management.

Estuaries of along the eastern side of the Irish Sea are characterised by estuary wide net sediment accretion, better understanding of the estuarine process arena is required to enable future impacts from processes leading to coastal squeeze. Global warming induced sea level rise is currently the main focus of scientific concern regarding to pressures on the coastal environment.

The potential impact on the security and potential re-release of pollutants stored within the estuary needs to be evaluated to enable reliable predictions for a range of environmental scenarios. In detail, whilst estuaries may represent zones of accretion within the near-shore coastal environment, the process of sediment deposition varies over different time scales, ranging from episodic large storm events to the cyclic pattern of tidal pumping. Understanding these processes is important for assessing the geomorphic evolution of different sediment domains, and a quantification of the subsequent factors controlling this evolution (e.g. tidal forces, storm-induced wave action and the periodic storm discharge events within the riverine catchment basin) over different time scales, including single ebb and flood tide events to inter-annual change.

Efforts to quantify these processes have focussed on point sampling, modelling approach or a combination of both the two. Estuarine investigations are often based on point sampling techniques, be it through sampling or fixed logging stations, which are used to identify the environmental changes to the estuary basin. These point sampling approaches are often spatially isolated within the context of the estuary and must therefore be interpreted with caution, and this is given, tacit recognition in the literature. Modelling techniques in estuarine environments provide an important, if not essential tool, for local industries and regulatory authorities to understand the sedimentological processes within the estuarine environment (Gleizon, 1999). They take the form of either simple one-dimensional models (Burton *et al.*,

1995; Lyons, 1997), to increasingly complex two and three-dimensional models (Burton, 1995; Van der Ham & Winterwerp, 2001; Wu *et al.*, 1998; Le Hir *et al.*, 2001). These models are based on sampling or fixed logging stations based within the estuarine environment and therefore suffer from spatial isolation within the estuary.

The ability to derive spatial information of either the intertidal (Hakvoort *et al.*, 1998; Thompson *et al.*, 1998a) or flood and ebb tide states (Robinson *et al.*, 1998; Jorgensen & Edelvang, 2000) of the estuary through remote sensing would therefore appear to have much to offer estuarine research. Even the ability to provide a spatial context for conventional point samples and measurements would add significant value to data interpretation. More recently, quantitative estimates of intertidal sediment grain size distributions (Rainey *et al.*, 2003) and suspended sediment data (Atkin, 2000; Doraran *et al.*, 2001; Tyler *et al.*, *prep.*) now provide valuable quantitative information in their own right, at a spatial resolution difficult to achieve through conventional techniques. The added advantage of access to airborne remote sensing (ARS) facilities (e.g. the NERC ARSF) adds significantly to the temporal and spectral resolution with which data can be acquired.

Many studies within estuarine areas have focussed on the interaction of fine grained sediments and the associated heavy metal contaminants (Bradley & Clapman, 1998; Brenon & Le Hir, 1998; Chen *et al.*, 2001; San Miguel *et al.*, 2004). However, within the context of the Irish Sea area, the main

contaminants under investigation are the anthropogenic radionuclides released via authorised discharges from the British Nuclear Fuel Ltd Sellafield (BNFL) nuclear site based in North West England (Figure 1.1) and subsequently the distribution pathways of these radionuclides within the Irish Sea and beyond (MacKenzie *et al.*, 1999). The spatial distribution of these radionuclides has been shown to be related to fine-grained sediments (<63  $\mu\text{m}$ ) within the Irish Sea (McDonald *et al.*, 2001)

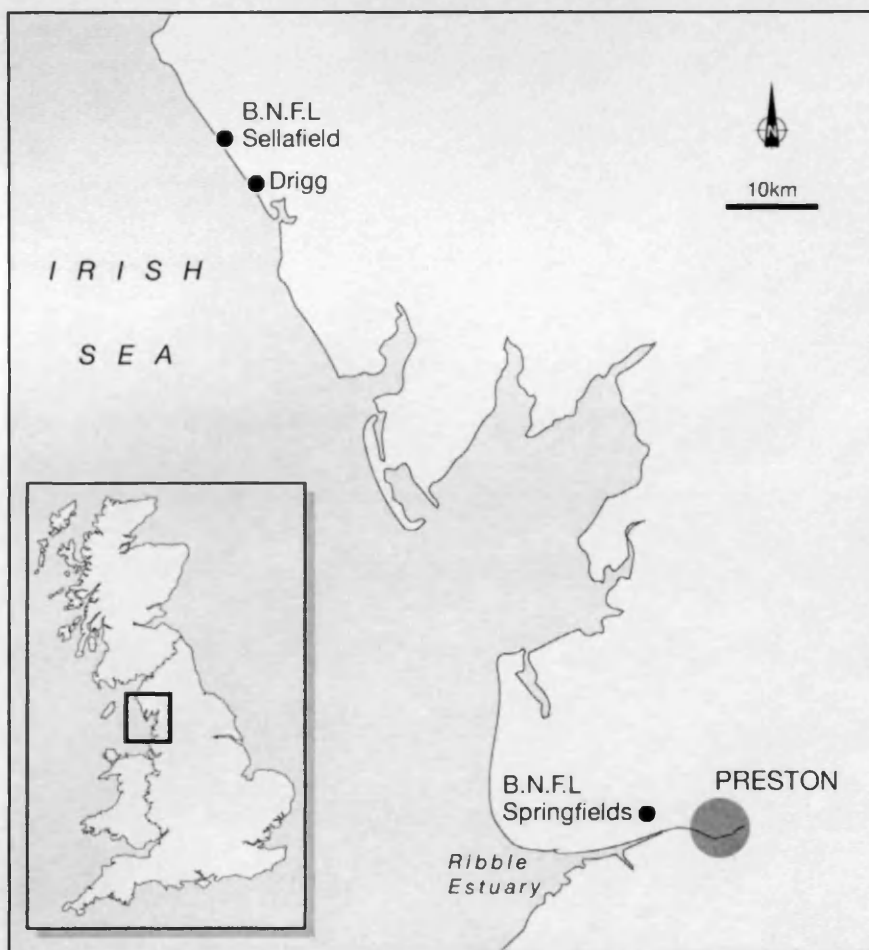


**Figure 1-1** Location of the Ribble Estuary.

Investigations have shown (Stanners & Aston, 1982), that these radionuclides are transported into the Ribble Estuary over time (Figure 1.2) and subsequently distributed over the entire estuary system, through the

interaction of freshwater and seawater, which promotes the flocculation and deposition of clays. The assessment of these contaminants has been the focus of numerous studies within the Ribble Estuary (Assinder *et al.*, 1997; Mudge *et al.*, 1997; Rainey, 1999; Brown *et al.*, 1999; Atkin, 2000). However, focusing on the anthropogenic radionuclides generated from authorised discharges from BNFL Sellafield, investigations have found that the fine grained (<63  $\mu\text{m}$ ) sediments have a high affinity for americium ( $^{241}\text{Am}$ ), plutonium ( $^{239,240}\text{Pu}$ ) and caesium ( $^{134}\text{Cs}$  &  $^{137}\text{Cs}$ ) (Stanners & Aston, 1981; Stanners & Aston, 1982; MacKenzie *et al.*, 1994; MacKenzie *et al.*, 1999; Rainey, 1999; McDonald *et al.*, 2001; Smith *et al.*, 2003; Charlesworth *et al.*, *in press*). The increased gamma dose associated with these ( $^{137}\text{Cs}$  in particular), received by critical groups within the estuarine environment (house boat dwellers, fishermen and wildfowlers), is of importance to the relevant regulatory authorities (Environment Agency, Scottish Environmental Protection Agency and Irish Environment and Heritage Service).

The assessment of the temporal oscillations and spatial pathways of such radionuclides, such as  $^{137}\text{Cs}$ , is an essential section of this investigation into the Ribble Estuary.

A combination of the ability to quantitatively map sediment grain size distributions and suspended sediment concentrations using the potential good relationship with radionuclide concentration offers a unique opportunity to

investigate the controls on the fate of anthropogenic radionuclides within estuarine environments. Whilst previous research has demonstrated the potential of remote sensing for mapping grain size distributions (Rainey *et al.*, 2003) and flood tide sediment flux (Atkin, 2000), the temporal changes, and calibration stability needs to be established. Once confirmed or refined, they have the potential of providing a unique spatial insight into the processes controlling sediment entrainment, transportation and distribution of sediments across an estuary over a range of time scales.

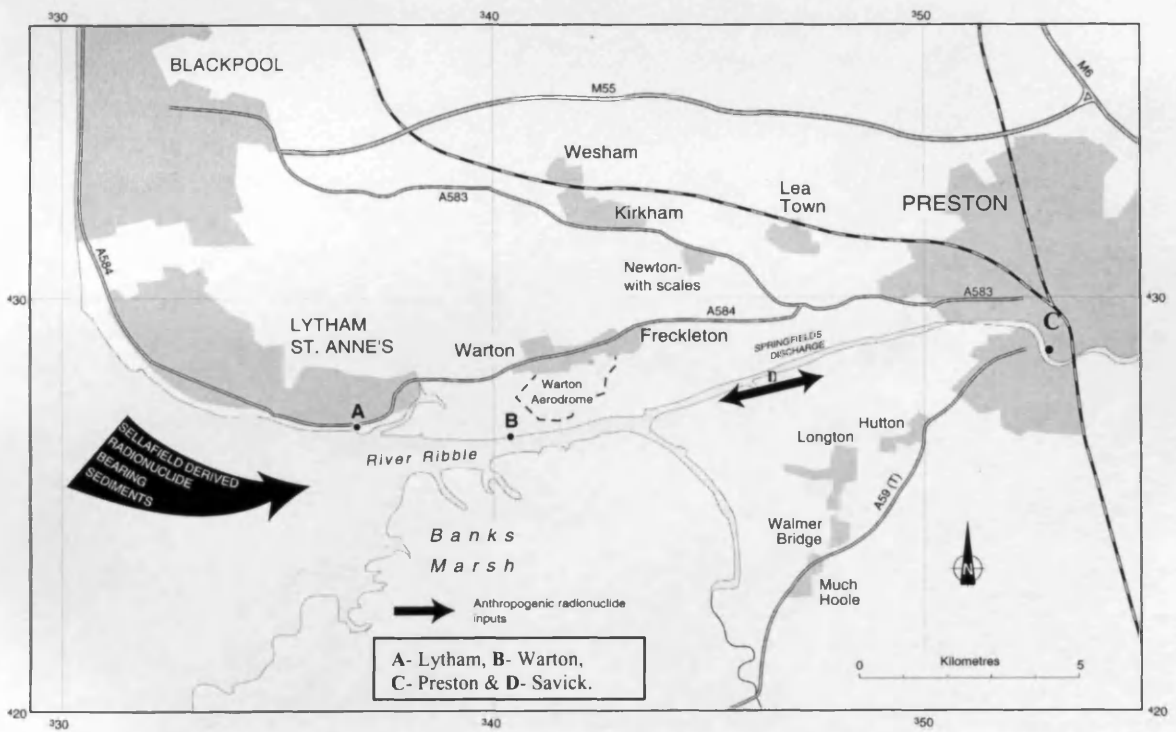


**Figure 1-2** The Ribble Estuary showing the major sources of radionuclides input into the estuary

Obtaining quantitative estimates of sediment flux transportation allows for the estimation of net sediment depositional rates within the estuary, from which estimates of changes in total radionuclide inventories within the estuary basin can be calculated. This data cannot be acquired by point sampling

investigations alone, although approximations can be made (Brown, 1997; Mudge *et al.*, 1997; Brown *et al.*, 1999).

The Ribble Estuary was the original focus for this work, as the data derived from this research would be used to validate the two-dimensional, hydrodynamic model, developed by Westlakes Scientific Institute, for the Ribble Estuary - VERSE (VERTically Resolving model of Sediment and radionuclide transport in Estuaries). Subsequently, the Ribble Estuary has become the UK's pilot estuary for the implementation of the Water Framework Directive (WFD). The WFD aims to provide long-term protection of all surface water and ground water, and within the scope of the river basin district section of the directive, it is aimed at producing a river basin management plan (RBMP) for the Ribble Basin. Whilst the estuarine zone only covers a small section of the entire river basin, it is perhaps the most complex part of the system, presenting a challenging environment to obtain direct, spatially accurate data from which quantitative estimates of sediment flux patterns can be produced.

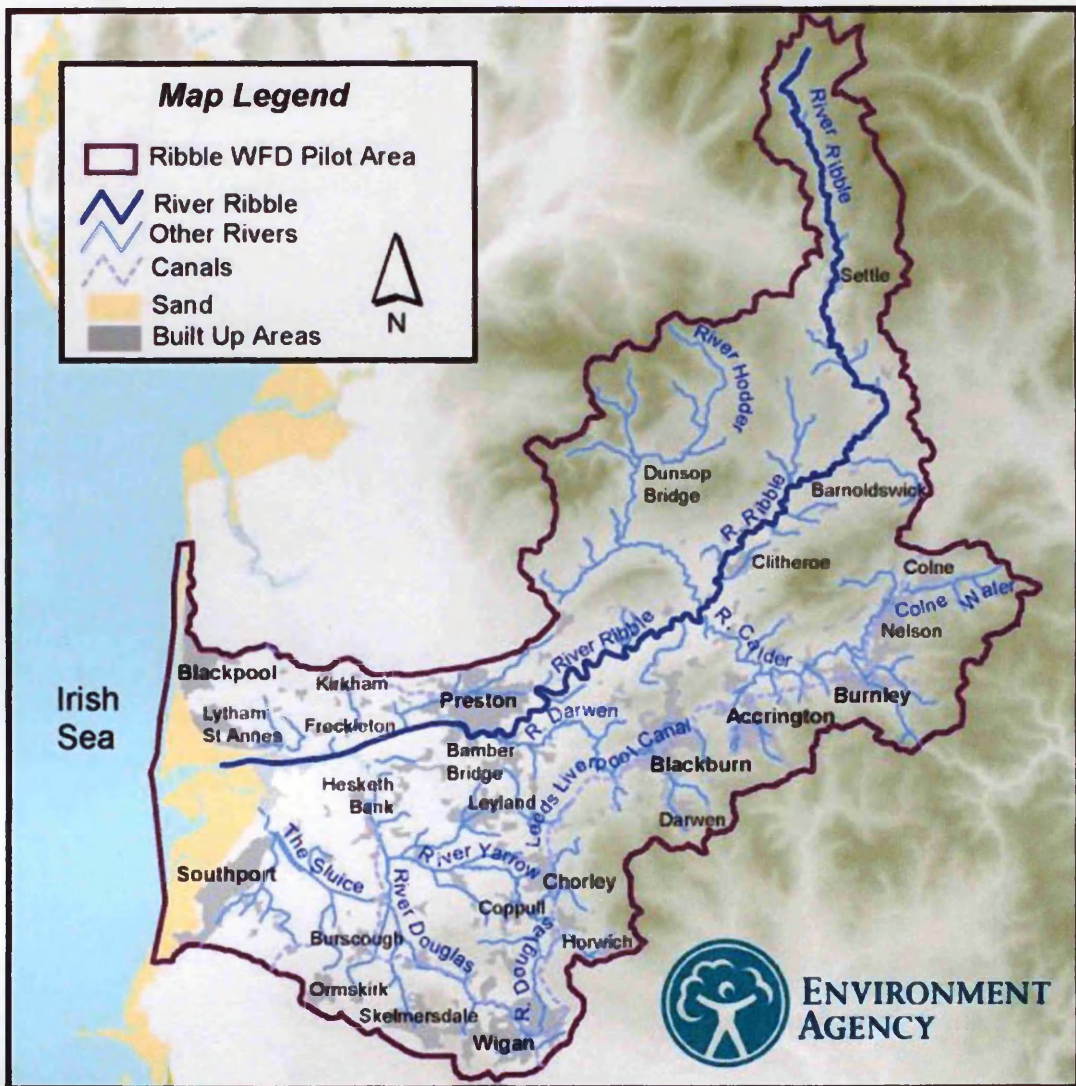


Figure 1-3 Ribble Water Framework Directive boundary (Environment Agency©)

## 1.2. Aims and Objectives

The Ribble estuary is generally recognised as an environment experiencing net accretion, exacerbated by the re-engineering of the main channel during the Victorian period. As the estuary is in a state of rebound from these engineering works (Van der Wal *et al*, 2002), the sediment dynamics (accretion and movement) are perhaps relatively exaggerated. In addition, the Ribble Estuary has been the focus for the development of a two-dimensional

model (VERSE), for which independent data has been selected, to allow the assessment of the distribution patterns of anthropogenic radionuclides generated from two distinct sources (BNFL Sellafield and BNFL Westinghouse Springfields). This dynamism provides a useful research environment in which to develop and validate techniques for quantifying estuarine processes. The primary aims of this research are:

- i) Characterise the temporal stability of the intertidal sediment environment and associated radionuclides reservoir.
- ii) Quantify the net sediment and radionuclide flux within the Ribble Estuary over an inter-annual and intra-annual (including monthly and daily) timescales.
- iii) Identify the primary environmental drivers affecting sediment stability.

The research will exploit the novel application of ARS imagery coupled with intertidal sediment studies to provide an independent means of interpreting and validating the measures derived from the remote sensing imagery over a range of temporal scales.

Initially, the inter-, intra-annual and monthly variations in the intertidal sediment properties and depositional cycle of the Ribble Estuary will be investigated through the application of a two year monthly sampling study. The sampling points will be geographically spaced throughout the estuary and will be used to examine the percentage clay/<sup>137</sup>Cs relationship within the

Ribble Estuary, originally demonstrated by Rainey (1999), assessing the seasonality and temporal stability of that relationship over time. This multi-temporal study is also aimed at identifying the primary environmental drivers within the estuarine system, which control sediment movement patterns within the estuary.

The technique of mapping intertidal grain size will be validated (Rainey, 1999; Rainey *et al.*, 2000; Rainey *et al.*, 2003) and the temporal (inter- and intra-annual) and spatial changes of the intertidal surface sediments and associated radionuclides will be investigated via the use of ARS imagery. By obtaining a time series of intertidal images throughout the year it should be possible to identify the seasonal variations of the intertidal surface sediments and highlight the spatial differences in distribution patterns of clay and associated radionuclides, as well as the distribution patterns of microphytobenthos. Through the acquisition of ARS images, it is possible to place geographically-isolated point samples within the spatial context of the estuary and allow the identification of possible sinks and sources of environmental contaminants, which could have implications for various environmental monitoring programs, such as the annual Radioactivity in Food and the Environment (RIFE) reports that are undertaken within the estuary.

Quantifiable estimates of the net sediment flux that are transported over the course of a flood and ebb tide event within the Ribble Estuary, will be gained through the application of time series ARS imagery and modelled volumetric

data. This section of the investigation will further develop the methodologies introduced by Atkin (2000), by the incorporation of the times series remote sensing imagery of both the flood and ebb sections of the tidal cycle. Quantifying the depositional budget of a tidal cycle allows for estimates to be made of sediment that are transported by the action of the tides, but also importantly it should allow the estimation of the total radionuclide inventory within these mobile, estuarine sediments.

By combining the various temporal and spatial scales of this investigation it should be possible to identify the main environmental drivers that re-distribute the sediments throughout the estuary. These findings can then be compared to other similar macro-tidal estuaries (i.e. Severn Estuary), to assess the relative strengths of each environmental driver. The application of ARS allows the spatially isolated point samples to be placed within a geographic context, which could then be used to improve existing hydrodynamic models of estuarine systems and the subsequent use within estuarine management and regulatory programs.

## **2 A Review of Methods of Monitoring**

### **2.1. Introduction**

Estuaries are critical interfaces between the marine and terrestrial environment and represent a restricted exchange environment of sediment. Their role in habitat formation and sink or source of contaminants makes them important environments for consideration in a range of environmental and ecological disciplines. Estuaries have consequently become the focus of much research and whilst they are broadly understood, have been notoriously difficult to characterise quantitatively in detail (Uncles, 2002). This chapter reviews the scientific literature to provide the appropriate definitions and mechanistic understanding of the processes and monitoring techniques within estuarine environments, relevant work which has been undertaken in the Ribble Estuary and to finally providing a framework upon which this research are based. Hypotheses are then derived from this review and the aim and objectives of the research are defined.

### **2.2. Defining estuarine sediment dynamics**

Detailed definitions of estuaries and estuarine processes can be found in many texts (Dyer, 1995; Brenon & Le Hir, 1999; Lumborg & Windelin 2003; Dyer *et al.*, 2004). However, here, a summary is presented to provide a useful definition for reference in this work (Dyer 1997). Estuaries have been defined by many different parameters, but the definition of an estuary by Cameron &

Pritchard (1963), "A semi enclosed coastal body of water which has a free connection to the open sea and within which sea water is measurably diluted with fresh water derived from land drainage" allows for most estuaries to be classified satisfactorily.

By virtue of their nature and position between the marine and terrestrial environments, estuaries have been the location for many human activities (Ridgway & Shimmield, 2002). The intertidal and sub-tidal zones form sinks for sediments and associated contaminants discharged by manufacturing industries (Beresford Hartwell *et al.*, 1995), sewage (both human and agricultural) (O'Neill *et al.*, 2004) and mining industries (Ruiz, 2001), so to understand the fate of these contaminants, an understanding of estuarine processes is necessary to underpin the methodological development that is required to appreciate the long term fate of these contaminants.

The presence of finely divided cohesive sediments in suspension or lying on sub-tidal and intertidal zones in estuaries has important ecological and economic implications (Arundale *et al.*, 1997). Cohesive sediment transport and longitudinal distribution are caused by the intricate interaction of tides, riverine inflow, waves and channel geometry. The complex interactions constantly vary, creating temporal and spatial variability in sediment distribution along the entire estuary. The salt water/freshwater interface on the flood tide is called the convergence front (Robinson *et al.*, 1996; Li, 2002), which generates high levels of turbulence (due to density gradients), which are caused by internally and boundary derived turbulence effects that

generate an area of high suspended sediment generated by the passing of the convergence front is described as the turbidity maximum. If tidal forces dominate within the estuary, a very significant quantity of fine sediment ( $<63\mu\text{m}$ ) will be transported to the upper reaches, creating a turbidity maximum (Postma, 1967; Burchard & Baumert, 1998; Brenon & Le Hir, 1999; Mitchell *et al.*, 2003). This will create a net flux of sediment being transported to the upper estuarine zone, usually called tidal pumping. Opposing tidal pumping, are episodic high rainfall events within the riverine catchment which result in the flushing of the upper estuarine fine grain sediments towards the outer estuary.

The correct modelling of such processes is important for the implementation of management strategies within estuarine zones, as a number of heavy metal and organic contaminants have a high affinity for clay ( $<2\mu\text{m}$ ) particles. An increasing tidal range plays an important factor in determining the quantities of sediment that can be transported within estuarine environments, as estuaries such as the Severn (mean spring tidal range: 12.3m (Arundale *et al.*, 1997)) and the Ribble Estuary (10m) have the capacity to transport more sediment (per unit volume) than estuaries with lower mean tidal ranges i.e. Tamar: (4.7m) (Uncles & Stephens, 2000; Tattersall *et al.*, 2003) and Trent-Humber (6.4m) (Mitchell *et al.*, 2003). The tidal propagation front, described by the velocity of the tidal wave across the intertidal zone, will cause stronger vertical mixing (Arundale *et al.*, 1997) with increased tidal range. The rate of tidal propagation can be retarded by frictional forces generated by very shallow water and by bed friction forces (Le Hir, *et al.*, 2000), which has the effect of

slowing the wave front down and creating a pronounced wave front, or bore, in high tidal range estuaries i.e. Severn and Ribble estuaries.

### **2.3. Methodologies for characterising intertidal environments of estuaries**

#### **2.3.1. Intertidal environments**

Tidal flats form at the edge of many estuaries, taking a wide variety of forms depending on the underlying environmental conditions. They are characterised by rapid and massive changes in the sediment level due to erosion, re-suspension, advection transport and wind-driven currents (Galois *et al.*, 2000). The sediments are generally composed of mud and sands, with the mudflats bound to sandflats close to the low tide mark and above the high water neap tides by a zone of vegetation (Dyer *et al.*, 2000).

#### *Characteristics of the intertidal environment*

Intertidal zones are the interface between the sub-tidal sediments and the upper shore limits. Physical environmental factors, including sediment characteristics, inundation time, tidal currents and wind waves (Bell *et al.*, 1997) all operate to help shape and define individual intertidal zones. The zones act as critical barriers, reducing and mitigating the destructive forces of wave/storm forces that interact with the shore line. Intertidal zones can vary greatly in size, shape and composition (rocky, sandy or muddy). Sharp boundaries exist between rocky shore and sandy shore environments, but the

boundary between sand flats (non-cohesive) and muddy (cohesive) shores are less well defined (Nybakken 2001). Consequently it is difficult to draw distinct boundaries between the two, although areas of muddy shoreline should experience, in general, a less energetic environment than the sandy shores, such as estuarine intertidal zones. However, the forces of tides and winds behave in an episodic manner, which can allow both low and high energy regions to exist over the same intertidal zone, which should lead to mixed grain-size distribution across the area.

The deposition of the fine 'mud' fraction occurs as a result of the interaction between currents, tides, salinity (Allen & Duffy, 1998) and river discharge conditions. Knowledge of the temporal changes within the depositional cycles of such fine grained mud is essential in understanding the distribution pathways of the sediments within the estuarine environment, which can create long-term (inter annual) to short-term (inter-tidal) changes to the sedimentological and geomorphological responses of the intertidal sediments and the surrounding saltmarsh environments. Therefore, sampling periodicity must be prolonged and at regular fixed intervals to obtain spatial and temporal understandings of sediment flux patterns and which environmental drivers dominate within such intertidal zones.

Spatially, the intertidal mudflats can be separated into three distinct zones (Dyer *et al.*, 2000):

- i) The upper tidal flats lie between the mean high water spring and mean high water neap, which are the least inundated and are often colonised by saltmarsh vegetation.
- ii) The middle flats represent the zone between mean high tide neaps and mean low water.
- iii) The lower flats lie between the mean low water spring and mean low water neap.

Characterising such intertidal zones by their vertical position in relation to the tidal height is just one of a number of features that can be applied to intertidal zones, but the use of mean high water provides a fixed parameter that can be applied to any intertidal mudflat around the world. However, present sea level rise that is generally attributed to global warming is likely to affect severely low lying coastal areas around the world (Kirchner & Ehlers, 1998) and therefore the position of the mean high water point.

Obtaining knowledge of the spatial and temporal patterns of sediment movement within estuarine environments has been approached in the past by assessing the elevation height changes at a number of geographically isolated points within an estuarine environment (Allen & Duffy, 1998; Brown, 1999) and calculating the net sediment accumulation/erosion for that area. Allen & Duffy (1998) conducted a medium term sedimentation study of the intertidal sediments of the Severn Estuary, exploring the impacts of wind and tidal oscillations on the intertidal sediments and the surrounding saltmarshes. Within that study, it was shown that the mudflats and saltmarshes do not

respond to a simple and uniform pattern to forcing factors such as wave and tidal action. However, it was demonstrated that the bed levels and sediment properties had a multi-timescale combination of periodic and episodic development, resulting from varying high water periods and wave action.

The intertidal mudflats bordering the edges of estuaries act as important sources and sinks for the sediment load and associated contaminants carried by estuarine waters (Anderson, 1983). The assessment of the effectiveness of each environmental driver is therefore important in understanding the overall sediment distribution patterns within the environment. A special focus is given to the fine grained clay particles (<2  $\mu\text{m}$ ) which have been shown to have a high affinity with anthropogenic radionuclides (Mudge *et al.*, 1997; Assinder *et al.*, 1997; Aldridge *et al.*, 2003). Consequently, identifying the temporal changes in the transportation pathways of sediment, in relation to external (marine and river catchment) and internal (mobile and *in-situ*) sources of sediment within the estuary are necessary to understand the sediment flux patterns over varying time scales.

Associated with the fine grained sediments (<2  $\mu\text{m}$ ) are authorised discharges of anthropogenic radionuclides by BNFL Sellafield ( $^{134}\text{Cs}$ ,  $^{137}\text{Cs}$ ,  $^{241}\text{Am}$  &  $^{239,240}\text{Pu}$ ) and BNFL Westinghouse Springfields (Uranium and Thorium decay chains) that are present within the Ribble estuarine environment (Mudge *et al.*, 1997; Assinder *et al.*, 1997; Brown 1997; Brown *et al.*, 1999; Rainey 1999).

### *Sediment grain size and sediment cohesiveness*

The distinction between sediment grain sizes are commonly described by reference to the Wentworth scale, which divides sediments into classes (Paterson & Hagerthey, 2001). Sandy sediments are described as comprising of grains greater than 62.5 $\mu\text{m}$  in diameter and are generally spherical and non-cohesive in nature. Smaller sediments (<62.5 $\mu\text{m}$ ) become increasingly flatter and have an increased surface to volume ratio, which leads to the formation of a cohesive (Van der Waals) force that leads to particle to particle attraction. As sandy sediments are non-cohesive, an empirical relationship can be determined and applied to numerical models (Camenen & Larson, 2005). The cohesive nature of fine grained material makes understanding sediment erosion thresholds more complex, therefore making measurements of critical erosion threshold more difficult to predict (Tolhurst *et al.*, 1999). The measurement of sediment erosion potential or erodibility is defined in terms of critical erosion threshold, erosion rate ( $\text{g m}^{-2}\text{s}^{-1}$ ) and mass of sediment eroded ( $\text{g m}^{-2}$ ) in relation to measured current velocities and estimates of bed shear stresses (Widdows & Brinsley, 2002). Sediment erosion potential will decline, in general, in a shoreward direction via the increase in sediment stability brought about by increased cohesiveness and consolidation through increasing air exposure and declining currents/wave action (Widdows & Brinsley, 2002). Benthic life has been shown to modify the critical erosion shear stress values of intertidal zone sediments, especially fine grained sediments (Black, 1997; Paterson & Black., 1999; Paterson & Hagerthey., 2001), often with a marked seasonal variability due to changing solar illumination periods. The critical erosion threshold has been shown to

increase with the mucus-like carbohydrate and sediment chlorophyll-a produced by migrating diatoms and bacteria in the sediments. These extracellular polymeric substances (EPS Perkins *et al.*, *in press*) have been shown to increase the erosional threshold, but also have considerable spatial and temporal variability (Widdows & Brinsley, 2002). Measurements of EPS can be used to estimate sediment stability of the intertidal zone (Underwood & Paterson, 2003), but other techniques can be used to gain a similar understanding on how microphytobenthos can increase sediment stability (Hakvoort *et al.*, 1998).

The measurement and classification of cohesive sediments located on intertidal surfaces are subject to much debate (Paterson & Black 2000), but it is clear that no single mathematical formula exists to describe cohesive sediment erosion and that the modelling of cohesive sediments behaviour are much more complex (Paterson & Hagerthey, 2001). EPS and other biological constituents play an important factor in such a debate, as defining the critical erosion threshold on the intertidal sediments by just using a function of grain size alone could produce unrealistic expressions of erosivity across the intertidal area. With the inclusion of more accurate measurements of EPS in modelling and classification techniques, it has been shown to provide a tool to facilitate the measurement of erosivity over intertidal sediments (Blanchard *et al.*, 2000).

Benthic life also impacts on the flow rates over the intertidal areas (Paterson, 1997). The interactions are complex, but benthic life can act to smooth the

intertidal surface, which reduces bed roughness. This is an important factor as a rough bed will be susceptible to more erosion due to increased production of turbulent eddies that can impact and erode the bed. However, the development of benthic assemblages are sporadic in nature (Paterson et al. 1998), with biofilms (areas of extensive microphytobenthos cover) developing and disappearing over the course of a few days. Thus sediment stability will be constantly changing, although relic properties of microphytobenthos i.e. EPS, can still have impacts on the sediment stability after the benthos has declined (Paterson & Hagerthey, 2001).

### *Estuarine sediment sampling*

Various methods of sediment sampling are available for studying the intertidal zone, from simple surface scrapes to the use of liquid nitrogen in freezing samples and the three-dimensional observations obtained by sediment coring techniques. Sampling strategies should be of the type and sophistication that are required to obtain the necessary field results. Strategies that require only simplistic measurements, such as grain size and water content can be conducted using simple surface scrapes (if intertidal surface characteristics are required). This method involves the use of a trowel to skim off the top 2-5 mm of the surface sediment and place it within a sealable plastic bag that will retain the water found in the sediments, so allowing estimates of surface moisture content.

To obtain a more absolute measurement of water content and also pigment analysis of the intertidal surface sediments, the contact core technique

(Honeywell *et al.*, 2002) can be deployed to gain a greater accuracy of surface sediment moisture content (figure 2.1). A metal dish (c.56 mm by 3 mm) is filled with liquid nitrogen, which freezes the underlying sediment on to the base of the dish. After 45-60 seconds it is removed from the sediment surface and any excess sediment (greater than 2 mm) are removed and then the resulting disc of frozen sediment is wrapped inside foil and immediately immersed within liquid nitrogen to stop the break down of chlorophyll *a*. Although the freezing process produces a very accurate measurement of surface sediment moisture content, the actual volume of sediment frozen are relatively small in comparison to the surface scrape technique (10 g to ~1200 g). This method allows for the extraction of chlorophyll-*a* measurements (as a measure of benthic diatom biomass within the sediments), using either high-performance liquid chromatography (HPLC) (Wiltshire & Schroeder, 1994) or more simple spectrophotometric methods (Pinckney *et al.*, 1999).

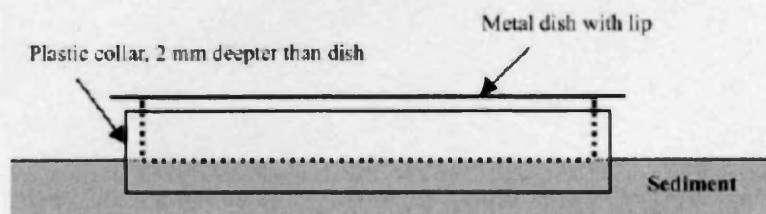


**Figure 2-1** Contact core (Ford & Honeywill, 2002)

### *Estuarine sediment redistribution*

Coring of intertidal and saltmarsh surfaces can provide a three-dimensional picture of past depositional/erosional events. Within the deposited saltmarsh sediments, the distribution of contaminants can be assessed, which with appropriate dating, can allow a chronology of contamination deposition to be

estimated (Brown *et al.*, 1999; Anderson *et al.*, 2000; Rosales-Hoz *et al.*, 2003). The coring techniques involved in obtaining depth profiles vary depending on the estuarine locations that they are being taken from. There were three distinct zones of coring operation i. Sub-tidal, ii. intertidal and iii. saltmarsh. Sub-tidal coring techniques can be found within Weaver and Schultheiss (1990), but as sub-tidal sediments are not sampled or assessed within the context of this project, they will not be discussed further. Intertidal environments can only be accessed by land during periods of low water or by boat at high tide periods. Sampling can be gathered by either using percussion corers (Parker & McCann, 1988; Tyler *et al.*, 1996; Tyler, 1999) or by a plastic piping approach (Chen *et al.*, 2001), depending on the type of intertidal surface being sampled. Both these techniques limit the depth that operators can retrieve cores from (1.5 m for percussion corer), but the use of heavier equipment from boats may allow more extensive core depth retrieval (Ridgway & Shimmield, 2002). Numerous studies have used sediment cores on salt marshes to provide valuable information on the sedimentary and contaminant history of each site (Mamas *et al.*, 1995; MacKenzie *et al.*, 1997; Brown *et al.*, 1999; Andersen *et al.*, 2000). They present a more stable working area for the use of the mechanical percussion corers and vibro-corers, but creek systems limit the accessibility of all but the most versatile work platforms.

Gamma emitting radionuclides in a core provide a range of potential tools that can allow sediment cores to be dated or act as event markers i.e.  $^{137}\text{Cs}$  from the Chernobyl accident, 1986 and BNFL Sellafield derived anthropogenic

radionuclides (MacKenzie *et al.*, 1994; Tyler, 1999). The use of  $^{210}\text{Pb}$  in sediment dating is probably the most widely used radionuclide dating technique (Andersen *et al.*, 2000; Lee & Cundy, 2001; Rosales-Hoz *et al.*, 2003; Ueda *et al.*, 2004), as it is a naturally occurring radionuclide produced by the decay of  $^{226}\text{Ra}$ .  $^{137}\text{Cs}$  is a by-product of nuclear fuel re-processing and nuclear weapons fall out, which has only been in the environment for the last 60 years. It thus provides a valuable marker in modern sedimentary records, although due to its high mobility value, it can diffuse down into the sedimentary record (MacKenzie *et al.*, 1997).

#### *Estimation of single tidal event sediment accumulation*

It is important to define what intertidal sediment accumulation actually means, as it can cover a wide range of time scales of physical, chemical, and geological processes (Thomas & Ridd, 2004). The process, if thought simply as a single depositional quantity deposited over a tidal cycle, will consist of an initial deposition of coarser sediments followed by the gradual deposition of finer material, either by gravity or flocculation of fine grained particles. The combination of the two will then produce the net sedimentation rate on to the intertidal surface. However, in nature there are constant cycles of deposition followed by periods of erosion. This can be due to changing flow rates, episodic storm and wave events and oscillating tidal cycles which together can create a very complex pattern of deposition and erosion along the length of the estuary.

Measurements of bed elevation changes are more complex than just simple vertical accumulation, due to the effects of shallow subsidence on the sediments. This can take the form of de-watering of the sediments, decomposition of the large organic fraction found in the intertidal sediments or compaction (Cahoon & Lynch, 1997). Cahoon *et al.* (1995) defined vertical accretion as the sum of sediment deposition and erosion, plant production (root systems) and decomposition. The relative importance of these components should vary with location across the estuary and are best investigated by field sampling.

The measurement of vertical elevation changes over intertidal surfaces may be measured intensively (every minute) (Lawler, 2005) to a more seasonal resolution. The methods that can be employed can be broken down into discontinuous (usually low cost methods) or continuous (usually high cost methods) (Thomas & Ridd, 2004). The use of discontinuous approaches, which reduces the temporal resolution, has the benefits of reduced destruction of the intertidal field sites. This is because intertidal zones are very susceptible to damage during monitoring visits, with effects lasting for days or months after visits i.e. compaction of bed sediments and increasing bed sediment roughness. Sediment traps are the most widely used discontinuous approach across the riverine and intertidal environments. They are often usually cylindrical in nature, but can also include novel approaches such as Astroturf matting to trap sediment (Bradley & Clapman, 1998). These Astroturf mats are used as they have similar characteristics to natural vegetation, such as the bed roughness coefficient. Traps are retrieved after

days or months after emplacement, sediment removed, dried and weighed to determine the vertical sediment flux over that time period. To produce diurnal or seasonal trends, measurements must be continuous over an appropriate time frame to identify patterns in sediment accumulation.

Sediment traps provide simple, low cost data sources both continuous and discontinuous have drawbacks associated with them. The low spatial resolution derived from emplacement locations may be hundreds, if not thousands of metres apart. However, if these simple, low cost point sampling points can be put into the larger spatial setting of the estuary system via remote sensing imagery, they would provide valuable ground calibration point data (Rainey *et al.*, 2000; Rainey *et al.*, 2003).

Measuring bed elevation changes can also involve the use of discontinuous and continuous instrumentation. Graduated pegs/pins/stakes offer a low cost tool for estimating net bed elevation changes between sampling periods and are often measured to the nearest millimetre. Unfortunately interactions with wave and current action can lead to increased turbulence around the pins, resulting in localised patterns of erosion/deposition. However, they can be emplaced in large numbers on the intertidal surface due to low cost of installation, thus obtaining multiple readings from sampling points. Photo-electronic erosion pins (Lawler *et al.*, 2001; 2005) can also be used. They consist of a vertical row of photosensitive cells that are pushed into river/intertidal sediments and connected to a data logger system. With changing sediment levels, the number of photo-electric cells exposed to the

light changes, changing the amount of current generated. The instrumentation is estimated to have an accuracy of 2 mm (Thomas & Ridd, 2004), operate throughout the day (not at night) at a high temporal resolution. However, its resolution will not pick up the very small scale change measurements and as it protrudes up from the bed, it will also have a localised effect on flow patterns. The unit also has a high cost associated with the use of the data logger, so few can be deployed over the intertidal area in comparison to the graduated pins.

### **2.3.2. Remote sensing of the estuarine environments**

The intake of contaminants into estuarine sediments by plants and bottom feeding animals can result in the contamination passing into fish, birds and mammals and eventually into humans (Ridgway & Shimmield, 2002). Therefore the ability to map the distribution of contaminants over the intertidal region is an important tool in estuarine management. Governmental agencies have a legal obligation to comply with international environmental laws and conventions i.e. the Water Framework Directive and OSPAR 1998-2003, which has 'the ultimate aim of achieving concentrations in the marine environment near back-ground values for naturally-occurring substances'. To this end remote sensing techniques have been harnessed to help with the management of estuarine ecosystems. Rainey (1999) demonstrated that it is possible to map intertidal sediment distribution (via grain size) and, if a linear relationship exist between contaminants (radionuclides) and the percentage

clay fraction in the sediments, it is possible to infer contaminant distribution across the intertidal zone (Tyler *et al.*, *in prep*).

Remote sensing allows a synoptic view of the entire intertidal surface in one survey, which cannot be completed with conventional point sampling techniques. To obtain accurate data from the remote sensing imagery, it is imperative that they are backed up with concurrent ground reference spectra/sampling points. Data can be gathered by either satellite based platforms (Folwing, 1986; Donoghue & Shennan, 1987; Yates *et al.*, 1993; Donoghue & Mironnet, 2002) or on the more flexible ARS platform i.e. Natural Environment Research Council's Airborne Resource and Survey Facility (NERC ARSF) aircraft (Thomson *et al.*, 1998a & b). Satellite platforms have the advantage of regular overpass sampling periods producing, large data series lasting up to 20 years, but crucially the poor spectral and temporal resolution of satellite data types, makes them unsuitable for detailed morphological studies of tidal flats (Rainey *et al.*, 2000). However, the use of ARS allows the user flexibility on time and location of image acquisition and most importantly the spectral and spatial resolution of the airborne platforms are at present, greater than the satellite based platforms. ARS allows for the incorporation of spatially isolated ground sampling points to be placed within a larger context of the entire estuarine system and allows user versatility in time of image acquisition. It has been demonstrated that it is possible to map the intertidal surfaces via both the compact airborne spectrographic imager (CASI) (Babey & Anger, 1989; Yates, *et al.*, 1993; Thomson *et al.*, 1998a) and the Daedalus 1268 airborne thematic mapper (ATM) (Rainey *et al.*, 2003).

Rainey *et al.*, (2003) and the use of satellite based platforms i.e. Landsat (Donoghue & Shennan, 1987; Donoghue & Mironnet, 2002) demonstrated that it is possible to map the critical interface between the fine-grained, cohesive sediment fraction and non-cohesive sands within the intertidal environment. This is an important tool, as estuaries exhibit significant spatial and temporal variability, which cannot be accurately assessed from point sampling alone. Thomson *et al.*, (1998a) demonstrated a qualitative approach to mapping intertidal sediments, identifying the constituents of the spectral variations in different classes. However, Rainey *et al.*, (2000; 2003) demonstrated a quantitative approach to mapping intertidal sediments, with the use of ATM imagery bands that are located within the short wave infrared (SWIR) range that allow identification of moisture and sediment characteristics. The estimation of interstitial moisture has also been shown by Rainey *et al.* (2003) to be very important in the un-mixing of spectral characteristics of sand over the intertidal area from remote sensing imagery. This means that areas of high interstitial moisture must be located, via concurrent ground truthing, as moisture content is important in the application of the image analysis technique.

Hakvoort *et al.* (1998) showed that it was possible to map the erosional shear stress by two main factors: benthic diatoms and the proportion of  $<63\mu\text{m}$  on the sediment surface. However, the relationships were shown to break down with an increase in non-cohesive sediment surfaces (sandier). This could be due to the lowering of benthic importance in non-cohesive sediments. With the use of remote sensing imagery and concurrent validation data, it may be

possible to produce maps of erosion shear stress, which can be used to validate input parameters for numerical modelling of sediment transport within estuarine environments. They will also allow the production of maps of benthic life on the intertidal surfaces (Rainey, 1999).

## **2.4. Methodologies for quantifying SSC and transport in estuaries**

### **2.4.1. Sediment flux patterns within estuarine environments**

The quantitative study of estuarine dynamics began with the work of Pritchard (1952, 1954 & 1956) (Uncles, 2002). Since that period, methodologies have moved towards assessing the impacts that changing tidal flow patterns have on the suspended particulate matter and in what quantities sediment are transported and deposited during the course of a tidal cycle. The use of estuarine models for sediment transport (Burton *et al.*, 1995; Gleizon *et al.*, 2003; Ganju *et al.*, 2004) has greatly increased our knowledge of estuarine processes. Hardisty & Rouse (1996) used a one dimensional model to estimate suspended sediment transport in the Humber Estuary, with an estimate of between 80 and 160 x 10<sup>6</sup>Kg for a single tidal cycle. However, obtaining direct measurements of flood and ebb tidal cycles has always created problems for researchers due to the dynamic nature of the estuarine system – especially for macro-tidal environments with the varying spring-neap tidal energies.

The position of the turbidity maximum within an estuarine system can also be dramatically altered by aperiodic events such as river floods and stormy wind

conditions (Grabemann & Krause, 1998; Uncles, 2002). Inflowing riverine flood waters into the estuarine environment can move the zone of the turbidity maximum downstream and lead to a net erosion of intertidal sediments from the upper regions of estuaries. These pulses of freshwater will not only interrupt the position of the turbidity maximum that are associated with the spring/neap cycles, but also alter the “normal” tidal variability for a number of days or even months after the flood event (Grabemann & Krause, 1998). Therefore it is imperative to have riverine discharge rates for up to 6 months prior to any field studies to enable a correct assessment of what causes changes in suspended sediment concentrations (SSC) and intertidal sediment accumulation/erosion rates within an estuary. Also, large river flood events could eject contaminants from the estuary, either in the dissolved or particulate phase, out into the near-coastal ecosystem.

The influence of the spring-neap tidal variations on the flow patterns is a very important factor in the tidal flux of sediments within estuaries. Sharples *et al.* (1994) found that during the spring tide sequence there was an increased mixing of the water column, with a reduction in the amount of stratification taking place. This pattern reversed itself during the neap period, when there was an increase in stratified conditions and a reduction in mixing. This effect has large ramifications for the utilisation of remote sensing techniques for estimating sediment fluxes within estuaries. If an assumption can be made that the water column is well mixed and uniform with depth, remote sensing imagery can be used to calculate total sediment loads on the flood tide directly from the imagery. On the ebb tide and during the neap period stratification

could be more pronounced, necessitating the use of depth profiles obtained at the time of image acquisition to produce estimates of sediment fluxes within the water column. The intratidal variation of the spring/neap tidal cycle also influences the formation and the location of the estuarine turbidity maximum (Postma, 1967; Dyer, 1986). Lyons (1997) conducted a velocity and turbidity study of the Ribble Estuary over the course of a tidal cycle and identified that the lagrangian residual circulation was dominated by the freshwater inputs into the estuary. During the neap tide the effects of tidal pumping are negligible, however, during the spring tidal cycle tidal pumping was found to be the dominant mechanism for transportation of sediment within the estuary (Guezennec *et al.*, 1999). The use of remote sensing techniques has allowed greater appreciation of how they migrate over the course of the tidal cycle, although the use of theoretical modelling approaches has increased our understanding of the main factors that drive these complex systems and the possible quantification of sediment load transportation over the course of a single flood and ebb tidal cycle.

#### **2.4.2. Point monitoring and sampling**

Obtaining measurements of intratidal variability, formation and maintenance of estuarine turbidity maximum and density driven currents from point sampling are possible with specialised rigs, but due to their cost, they are often spatially isolated. Ground based measurements, such as current speed, turbidity, salinity and water depth readings can be obtained through the use of instrument rigs and point sampling (Trowbridge *et al.*, 1999; Peters & Bokhorst, 2001; Sanford *et al.*, 2001; Uncles *et al.*, 2002; Wolanski & Spagnol,

2003). Several studies from different estuaries (Couperthwaite *et al.*, 1998) have shown that deposition rates are greatest during the spring tides, when the flow velocities in the estuary will be at their highest.

#### **2.4.3. Remote sensing of the suspended sediment**

Remote sensing techniques can generate estimates of sediment fluxes, be it airborne (Robinson *et al.*, 1998; Atkin, 2000; Jorgensen & Edelvang, 2000) or satellite based observations (Siegel *et al.*, 1999; Doxaran *et al.*, 2002; Doxaran *et al.*, 2005). It can be used to provide a spatially accurate assessment of suspended sediment in the surface layer for the whole estuary that cannot be obtained through point sampling techniques. Using ARS allows the user a much greater flexibility in selecting the ideal weather and tidal conditions for image acquisition than can be obtained from satellite imagery. Both approaches involve the use of an empirical relationship derived from imagery and point sample measurements to map the suspended sediment. These sampling points need accurately measured geographical locations via GPS, and time of actual data acquisition for image calibration. This means that remote sensing imagery often requires expensive simultaneous ground truthing measurements for image calibration. The use of ARS can provide a valuable tool for estimating surface sediment fluxes over flood and ebb tidal cycles. It can only provide information on the suspended sediment concentrations in the surface layer, when uniform mixing is assumed throughout the water column. This is especially important when assessing the sediment flux on the ebb tide, where possible stratification of the water column

will result in higher SSC in the basal flow layers than compared to the surface layers.

Deriving suspended sediment fluxes from ARS is an important tool in gaining a greater understanding of the movement of suspended sediment through the tidal cycle. It is important for a number of reasons (Jay *et al.*, 1997); the calculation of residence time for the classification of estuaries and their ecosystems; the prediction of long-term changes in estuaries and the mechanisms behind such changes; assessment of the impacts of anthropogenic influences on estuarine environments and the improved management of the coastal zone, from both environmental and socio-economic perspectives. The use of point sampling to describe the suspended sediment patterns does not provide a synoptic view of the entire estuary, but the use of point sampling for calibration purposes coupled with remote sensing imagery allows for the production of an interpolated map of suspended sediment concentrations across the entire estuarine environment. Robinson *et al.*, (1998) used the CASI to gather a series of flood tide images through a significant fraction of the tide of the Humber Estuary as part of the LOIS programme. The imagery provided information on the suspended particle matter (SPM) flux at the mouth of the estuary and allowed surface point studies to be put into a spatial context. An important point noted within the point sampling of this project is the assumption that SPM are uniform with depth on the turbulent flood tide is incorrect and that SPM increases with depth. Therefore any estimates of net sediment fluxes within the Ribble Estuary, derived from ARS imagery, will require validation data to clearly

demonstrate the stratification, if any, that occurs within the water column during the tidal cycle. Associated with such concomitant reference data for the water column, is the need for the calibration/validation data for the estimation of SSC derived from ARS.

## **2.5. Radioactivity in the marine environment**

### **2.5.1. Sources of radioactivity**

Radioactive elements occur naturally in the environment. Elements such as  $^{238}\text{U}$  or  $^{40}\text{K}$  have long half life's ( $>10^9$  years) and have been present since the formation of the Earth. However, with the advent of the nuclear industry in the 1950's there has been an introduction of anthropogenic radionuclides into the environment via atmospheric weapons testing, nuclear accidents (i.e. Chernobyl, 1986) and authorised industrial discharges (either by stack discharge or liquid effluent directly into the marine environment). Knowledge of the behaviour of these anthropogenic radionuclides once they have entered the marine and coastal environments are important and has been well studied within the Irish Sea (Stanners & Aston, 1981; Livens *et al.*, 1994; McCartney *et al.*, 1994; Kershaw *et al.*, 1999; MacKenzie *et al.*, 1999; Aldridge *et al.*, 2003). This is due to the number of potential exposure pathways that may bring the anthropogenic radionuclides back into contact with the public.

Estuarine waters are of special importance because of their high biological productivity and the greater incidence of exposure to radiation of the public i.e.

wildfowling, fishing, houseboat dwellers (RIFE 9, 2003). In addition to providing habitats for large populations of shell-fish, estuaries serve as nursery grounds for many species of fish that later move out into the offshore waters.

Desorption/sorption is the ability of some contaminants to oscillate between a fixed and dissolved phase depending on environmental conditions. The time they take to reach equilibrium can vary due to changing environmental conditions. Stanners and Aston (1981) noted that temperature changes in saline waters can have a ~40% reduction of the  $K_d$  value for  $^{137}\text{Cs}$ .  $K_d$  is the distribution coefficient where

$$K_d = \frac{\text{Activity in sedi. phase}}{\text{Activity in aqueous phase}} \cdot \rho \quad \text{Equation 2-1}$$

Where  $\rho$  is the density of the sediment (Stanners and Aston, 1981)

However, grain size is the most important factor in controlling desorption/sorption processes, with contaminants more readily attaching to fine-grained clays (< 2 $\mu\text{m}$ ) than courser sand fractions (>63 $\mu\text{m}$ ) (McCartney *et al*, 1994; MacKenzie *et al*, 1999; Rainey 1999).

### *Nuclear fuel cycle*

The production of nuclear fuel is started by the enrichment of the naturally occurring uranium ore. Uranium ore contains 99.28%  $^{238}\text{U}$ , which are not readily fissionable, but does contain 0.7%  $^{235}\text{U}$  which is fissionable (Eisenbud

& Gesel, 1997). Uranium needs to be enriched by either gaseous-diffusion plants or laser separation, allowing the concentration levels of  $^{235}\text{U}$  to increase to ~3.5%, allowing nuclear fission to take place. Enriched fuel is then converted into nuclear fuel elements and used within cores of nuclear reactors to generate heat that is harnessed to produce high pressure steam that drives turbines to produce electricity. Eventually the fuel elements become spent (for the purposes of energy production) and removed from the reactors. Only a small percentage of the  $^{235}\text{U}$  is actually used up, with a small amount being converted to  $^{239}\text{Pu}$  (via neutron capture). These used fuel rods can be re-processed through appropriate reprocessing sites i.e. THORP (BNFL Sellafield) for future use. After use, the nuclear fuel cells/rods are removed for disposal, which involves the stripping of the cladding from the cell containers and then storing the consequent radioactive material within cooling ponds. This is necessary due to the high levels of radioactivity still being generated by the 'spent' nuclear fuel.

The long term storage plans for UK radioactive waste is a source of major debate due to the potential long term environmental problems that any potential seepage would create. Although the problem of long term storage has not been completed within the UK, the United States of America has concluded that the safe disposal of radioactive waste is via the long term burial of material at Yucca Mountain, Nevada (Stuckless & Dudley, 2002; Liu *et al.*, 2004; Kemeny, 2005). However there are possible concerns regarding the long term geological stability of the region and the possible risks

associated with actually transporting the nuclear waste from around the United States to Yucca Mountain.

*BNFL Sellafield and Drigg, Cumbria (figure 2.2)*

Significant quantities of artificial radionuclides reside in the sub-tidal sediments of the Irish Sea as a result of authorised discharges from the Sellafield nuclear reprocessing plant (Aldridge *et al.*, 2003). Operations and facilities at Sellafield include spent fuel element storage, the Magnox and oxide fuel reprocessing plants, mixed oxide fuel manufacture, decommissioning of some nuclear facilities, and the Calder Hall Magnox nuclear power station (RIFE – 7, 2002). Of these, the BNFL fuel element storage ponds and the reprocessing plants represent the main sources of discharges from the site. Low level radioactive waste has been discharged under authorisation from the site since 1952 and continues to the present day; however discharge rates of transuranic radionuclides have been significantly reduced by approximately two orders of magnitude in comparison with peak discharges in the 1970s (McDonald *et al.*, 2001). The waste has consisted of a complex mixture of  $\gamma$ -,  $\alpha$ - &  $\beta$ - emitting fission and neutron activation products ( $^{134}\text{Cs}$ ,  $^{137}\text{Cs}$ ,  $^{238,239}\text{Pu}$ ,  $^{240}\text{Pu}$ ,  $^{241}\text{Am}$  (Kershaw *et al.*, 1990)). Drigg is a near-surface disposal facility operated by BNFL and is the UK's principal facility for the disposal of solid low level radioactive waste. It receives a wide range of materials from the nuclear industry, general industry, universities and hospitals. Disposals are carried out under license from the Environment Agency, under the Radioactive Substances Act 1993 (Williams *et al.*, 2002).

## *BNFL Westinghouse Springfields*

The site is situated in a rural location to the west of Preston, Lancashire and has been in operation since 1946 (Eyre, 2002). The main commercial processes that are undertaken at the site include the converting of uranium ore concentrates to Magnox clad uranium metal fuel elements for the Magnox nuclear power stations and also to uranium hexafluoride (HEX or UF<sub>6</sub>) (Eyre, 2002). This HEX is then transported to other UK nuclear plants and overseas for enrichment purposes and returned to be converted into uranium dioxide for use in Advanced Gas-cooled Reactors (AGR's). This process produces waste products relating to the uranium decay chain radionuclides (Appendix 1), notably <sup>234</sup>Th, <sup>232</sup>Th and <sup>230</sup>Th and significant quantities of daughter nuclides (McCartney, *et al.*, 1994).

Discharges are made to the atmosphere via stacks on site and to the Ribble Estuary as liquid effluent via a pipe line directly into the Ribble Estuary, close to Savick Brook. It is the Environment Agency's responsibility to authorise discharges into the two different environments. The limits at present are set up until 2007 for the discharges of authorised liquid waste into the Ribble Estuary, where it is predicted that a maximum exposure dose of 171 µSv/y will be received by the critical groups within the estuary (house boat dwellers, fishermen and wildfowlers) (RIFE-9, 2003). These critical groups have two main exposure pathways to the radionuclides contained within liquid discharges.

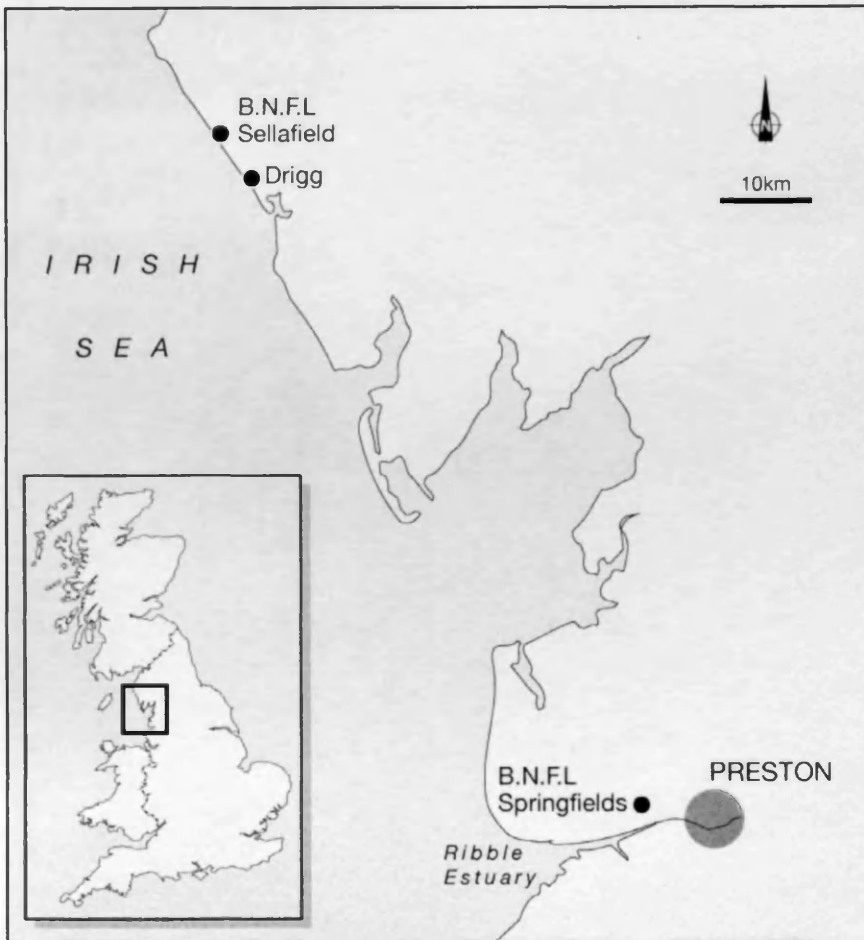


**Figure 2-2** Location of BNFL Sellafield/Drigg and BNFL Westinghouse Springfields

- i. Internal irradiation following the ingestion of radionuclides in fish and shellfish caught in and around the Ribble Estuary.
- ii. External irradiation following the incorporation of radionuclides into the estuarine sediments (RIFE -9, 2003).

It is thus important for the correct assessment, on an estuary wide scale, of the distribution of sediment bound radionuclides discharged from both BNFL Sellafield and BNFL Westinghouse Springfields along the length of the Ribble Estuary and the spatial variability in time and space (Assinder *et al.*, 1997;

Rainey, 1999). This can be conducted either by geographically isolated point sampling or more accurately by a combination of point sampling and ARS.

### **2.5.2. Environmental behaviour of radioactivity in marine environments**

The dominant control over the movement and spatial distribution of radionuclides in the marine environment is the response to changing grain size, with fine grained silts and clays having the greatest affinity for binding with a number of radionuclides ( $^{137}\text{Cs}$ ,  $^{239,240}\text{Pu}$ ,  $^{241}\text{Am}$ ,  $^{238}\text{U}$ ,  $^{234}\text{U}$ ,  $^{238}\text{Th}$  &  $^{232}\text{Th}$  (Assinder *et al.*, 1997)). Although this body of work focuses on different transuranic radioactive elements, the work investigated here will focus on  $^{137}\text{Cs}$ . This is it represents a source of anthropogenic radionuclides and are discharged from BNFL Sellafield and transported into the Ribble Estuary.

#### *Caesium ( $^{137}\text{Cs}$ - discharged by BNFL Sellafield)*

Caesium-137 is the longer lived (half life of 30.17 years (via beta and gamma radiation) (Eisenbud & Gessel, 1997) isotope of caesium that is found within the environment. It is generated through the fission process and released as low level waste from nuclear reprocessing sites (e.g. BNFL Sellafield & COGEMA Le Hague). It was initially discharged into the environment via high-yield airborne weapons testing from 1952 (Cundy & Croudace, 1996). But with the cessation of airborne nuclear weapons testing in 1963, it has mainly been due to authorised discharges from nuclear reprocessing plants after that date. An exception to this is the Chernobyl incident in 1986 which produced a radiocaesium spike in the sedimentary record across large areas of northern

Europe. Although authorised discharge levels of  $^{137}\text{Cs}$  have dramatically reduced from Sellafield since the mid 1970's due to a tighter regulatory conditions applied to the nuclear industry (Aldridge *et al.*, 2003), the historical legacy of the UK nuclear industry still remains in the UK's coastal waters.

$^{137}\text{Cs}$  solubility in the marine environment is much higher than in the freshwater environment (Eisenbud & Gessel, 1997) and it behaves 'conservatively' meaning that the bulk of its inventory is transported in solution with only 10% of the discharge being bound to sediments immediately within the marine environment. However, within the freshwater environment systems, such as estuaries, where different redox conditions allow more  $\text{Cs}^+$  ions to bind to fine grained sediments, it is possible to get higher concentrations of  $^{137}\text{Cs}$  within estuarine sediments. Since estuaries are tidal,  $^{137}\text{Cs}$  bound to intertidal and suspended sediments have the possibility of redissolution back into its soluble state. Although there is evidence to suggest that once  $^{137}\text{Cs}$  is bound to certain clay particles in soil, it is effectively fixed (Hird & Rimmer, 1995; MacKenzie *et al.*, 1999).

The distribution of  $\text{Cs}$  ions between sediments and water ( $K_d$  value) is a function of sediment-tracer contact time and radiocaesium; generally the relationship is positive (Oughton *et al.*, 1997). The  $\text{Cs}^+$  interacts strongly with clay minerals, due to its low tendency to hydrate and higher polarizability than smaller ions like  $\text{K}^+$  (Shainberg & Kemper, 1967). The nature of these interactions is dependent on the type of micaceous clays, with illite and montmorillonite reacting more rapidly with  $\text{Cs}^+$  than vermiculite (Sawnhey,

1966). Mobility of the  $^{137}\text{Cs}$  ions in the environment depends upon the interactions with the clay particles, which either act as a continuous, permanent sink for released  $^{137}\text{Cs}$ , or act as a diffuse source of  $^{137}\text{Cs}$  in the future. This is dependent on the interaction kinetics and binding mechanisms involved (Børretzen & Salbu, 2002). This interaction or ability of desorption back into solution depends on clay type that the  $^{137}\text{Cs}$  is associated with (Kaolinite, Halloysite, Illite or Smectite). The maximum  $\text{Cs}^+$  affinity with the clay minerals are located at “wedge-sites” typical of the transition zone between the 10 micaceous structure (illite) and the expanded portion of the weathered structure (smectite and/or vermiculite) (Facchinelli *et al.*, 2001). However, the  $\text{Cs}^+$  are more readily bound to the illite clay minerals due to the structure of the mineral lattice, in comparison to the smectite and vermiculite clay minerals, which have a sheet silica matrix. Therefore, where there is increased percentages of smectite and vermiculite, there is an increased chance of desorption of the Cs ions from the clay minerals back into solution, whilst illite bound  $^{137}\text{Cs}$  will be effectively bound and act as sinks for radiocaesium (Avery, 1996). This resorption is caused by the presence of other monovalent cations ( $\text{NH}_4^+$ ,  $\text{H}^+$ ,  $\text{K}^+$  and  $\text{Na}^+$ ), which can be displaced the  $\text{Cs}^+$  (Davies & Shaw, 1993).

### **2.5.3. Gamma ray detection**

Gamma spectroscopy is the measurement of maximum photon energy deposited in gamma detectors resulting from a gamma photon ionisation interacting with a semi-conducting material.

There are two main types of detectors available for the detection of gamma rays, sodium iodide detectors (NaI(Tl)) or germanium semiconductor detectors. Germanium detectors have a much higher resolution to their detection of gamma rays, but lower interaction rates. Modern germanium detectors are predominantly hyper-pure germanium detectors (HPGe), which offer high energy resolution for the detection of multiple energy gamma's. Although some impurities will remain within the crystals (even at levels of  $10^9$  atoms/cm<sup>3</sup>), if the remaining low level impurities are acceptors, then the electrical properties of the semiconductor crystal is called a *p*-type. Alternatively, if donor impurities remain, high purity *n*-type crystals are the result (Knoll, 1989). These detectors work on the semi-conductor energy band gap principle, where valence electrons are excited by ionisation until they have sufficient energy to cross the forbidden band where they are detected using an applied electric field (Knoll, 1989). The voltage that is applied across the germanium crystal represents the necessary voltage to produce a fully depleted detector, thus resulting in varying voltage requirements for each detector crystal. It is also important that the detectors are kept at 77 K (with the use of either liquid nitrogen or electronic cooling), as the germanium crystals being semiconductors, require very low temperatures to optimise detection levels.

This project will utilize two *p*-type GEM series coaxial HPGe detectors, with the first operating at a 75% relative efficiency (crystal diameter of 74.7mm and operating at a bias of 2000V) and the second operating at 15% relative efficiency, with a bias of 3000V. The efficiency of a detector is a measure of

the probability that an incident photon will be absorbed in the detector (IAEA, 2003)

#### **2.5.4. Monitoring techniques**

The UK government in 1998 signed the Sintra Statement, which stated amongst other commitments “We shall ensure that discharge, emissions and losses of radioactive substances are reduced by the year 2020 to levels where the addition concentrations in the marine environment above historic levels, resulting from such discharges, emissions, losses, are close to zero” (OSPAR, 1998). This has resulted in decreased authorised discharges by the nuclear industry.

Monitoring programs function as fundamental tools for government based organisations (Scottish Environmental Protection Agency (SEPA), Environment Agency, Food Standards Agency and CEFAS) to scrutinize industrial discharge rates by the nuclear industry. The surveillance programs are underpinned by applied research to improve analytical and assessment methods (RIFE – 7, 2002). Over 14,000 analyses or dose rate measurements were collected in 2001 alone (RIFE – 7, 2002), with the majority of them being based on point sampling techniques.

Sampling, for the monitoring organisations, can occur on a weekly to annual time scale, but the frequency and type of measurement and the materials sampled vary from site to site (RIFE – 7, 2002). These studies use a number of different techniques from routine point sampling to more spatially inclusive

studies such as airborne gamma spectrometry. Monitoring intertidal sediments and tide-washed pastures i.e. salt marsh, is considered (RIFE – 7, 2002) a cost-effective means of determining levels of activity in the environment. It allows for immediate estimates of activity concentration levels in dose assessments within these environments.

### *Gamma spectrometry*

Point sediment sampling and airborne gamma ray spectrometry has been shown to provide rapid and spatially representative estimates of environmental radioactivity across a range of landscapes (Tyler, 2004). Tyler (1999) deployed an *in-situ* n-type HPGe detector to calculate the mean mass per unit area of  $^{137}\text{Cs}$  over the Caerlaverock salt marsh, Dumfries, Scotland. This technique allows for a rapid assessment of anthropogenic activity over a large area, such as a salt marsh, over an interval of time. The benefit of this technique is that it can provide information on the vertical distribution of radioactivity that CASI and ATM imagery cannot. However the technique still employs a point sampling approach, which although spatially representative on a small area, would lack spatial resolution over large expansive intertidal zones if point samples were geographically isolated, in comparison to CASI and ATM instrumentation based studies.

### *Airborne gamma spectrometry*

This sampling method is highly appropriate for large scale environmental surveys of areas of potentially contaminated ground (Sanderson *et al.*, 2004). It finds effective application in the operation monitoring of nuclear facilities and

their vicinity, spent fuel storages and waste depositories, radioactive contamination measurements and mapping environmental, radiohygienic and radiation safety studies and geological prospecting (Kluson, 2001). Although this sampling method is evidently an effective tool in rapid monitoring/mapping of large areas, it lacks the point accuracy that ground based gamma ray spectrometry generates. It does have the possible application of mapping thorium series radionuclides in the Ribble, which are difficult to apply from point sampling techniques to remote sensing images (Rainey, 1999). However, Assinder *et al.*, (1997) did show the highest  $^{234}\text{Th}$  activity concentrations within the fine-grained sediments in the more upstream sections of the estuary.

## **2.6. Modelling Estuarine Environments**

### **2.6.1. Theoretical approaches**

Modelling and theoretical analysis has played an important role in enhancing our understanding of estuarine processes (Uncles, 2002). A simulation model allows users to gain a conceptual understanding on estuarine processes, without the need to conduct expensive and time consuming fieldwork. The model can take the form of a comparatively simple one-dimensional cross-sectional averaged model to increasingly complex two and three-dimensional models. The development of two/three-dimensional models has seen a rapid expansion over the last 15 years due to the ever increasing power of affordable computers, which has allowed researchers to make models

increasingly complex. Consequently, researchers have been able to develop more powerful models that can help in the understanding of density driven flows, tidal straining, stratification processes, variable freshwater river flow, and suppression of turbulence by stratification (Gleizon *et al.*, 2003) and surface convergence zones (Nimmo Smith & Thorpe, 1999) located within the middle of the estuary that indicate two counter rotating cells of water. All these factors must be taken into account when deriving an accurate hydrodynamic model to help gain an understanding of the complex patterns of sediment and associated contaminant transport that take place within various estuarine environments.

Some of the most complex applications of theoretical modelling involve the study of the turbidity maximum within partially mixed estuarine environments. Friedrichs *et al.* (1998) showed that fine sediment transportation within the turbidity maximum was due to three dominant factors (i) flood dominant tidal velocity asymmetry (ii) down-estuary river flow, and (iii) settling/scour lag (Uncles, 2002). Nevertheless, the choice of modelling strategy, be it a one-, two- or a three-dimensional model, will depend upon the management issues involved, the resources available and time scales the model is being designed to address (monthly, yearly or decadal). A second choice is then needed to ascertain the accuracy that the model needs to achieve in order to meet its targets and what assumptions on water and sediment interactions should be applied to the model program.

Using modelling techniques in estuarine environments provides an important, if not essential tool, for local industries and regulatory authorities to understand the sedimentological processes within the estuarine environment to assess the impact of past, present and future discharges (Gleizon, 1999). Modelling of macrotidal estuaries must simulate the hydrodynamic and sedimentological fluid dynamics in the estuary in order to model the dispersion of particle bound contaminants accurately. One-, two- or three-dimensional models can be applied to gather this information, although each have their own advantages and disadvantages associated with them. One-dimensional models (Burton *et al.*, 1995; Lyons, 1997) have the benefit of being easier to construct and operate, but as they are depth averaged, they fail to take into account any vertical stratification that takes place either on the flood or ebb tide. This means that one-dimensional models fail to predict accurately the upstream tidal pumping processes (Gleizon *et al.*, 2003).

Two-dimensional models have been extensively used in estuarine studies (Burton 1995; Liu *et al.*, 1998; van der Ham & Winterwerp, 2001; Kashefipour *et al.*, 2002; Gleizon *et al.*, 2002), to replicate sediment transport and chemical interactions that are dependent on accurate simulations not only on the flux of water, but also of sediment transport (Gleizon *et al.*, 2003). It is also possible to model fronts, which form at the interface between two water bodies that have different densities (temperature and salinity) and also velocities (Chen & Dyke, 1998). This interface creates a zone of turbulent water, which can induce higher turbidity levels within the water column (turbidity maximum). Included in such models must be an understanding of the effects of particle

size on transport properties and the chemical bonding to the various contaminants being studied. This is because certain contaminants can exhibit permanent or temporary bonding to particles e.g.  $^{137}\text{Cs}$ . However two-dimensional models, which use a longitudinal and vertical axis, cannot take into account any lateral circulation movements such as Langmuir circulation. Langmuir circulations are vortices that occur near the surface of the water and result in the formation of a convergence zone, which are often marked by buoyant flotsam on the water surface. The use of a three-dimensional model allows for the lateral transportation of sediment, which the two-dimensional models fail to take into account.

Three-dimensional models do exist for estuarine systems (Wu *et al.*, 1998; Le Hir *et al.*, 2001), but have shown that they cannot accurately replicate the complex environment that they were designed for. However, the future use of three-dimensional models may increase in frequency due to advances in computational power available to researchers in comparison to the recent past. With these computational advances, models should be able to describe and estimate both longitudinal and cross-channel hydrodynamics as well as water column changes i.e. density driven circulation. Construction of models is often constrained by the volume of input parameters that are available to the architect of the model. The initial input parameter characterised by most models (Le Hir *et al.*, 2000; Gleizon, *et al.*, 2002) is the bathymetric profile of the estuary. This defines the width of the intertidal area and the local hydraulic radius that will be associated with the tidal conditions. The bathymetric profile can be constructed by conventional surveying techniques,

side-scan surveys of the estuary or derived from ARS platforms using either radar or LiDAR instrumentation (Kashefipour *et al.*, 2002; Gilvear *et al.*, 2004).

Associated with the bathymetric parameters are the hydrodynamic input values such as water elevation, flow velocity and salinity. These are essential for defining bed sediment shear stress (Tolhurst *et al.*, 1999; 2000), dispersion coefficients for the radionuclides, and volume of water within the modelled estuary (Gleizon *et al.*, 2001). These core modules form the basis for many models of estuarine environments. It is therefore essential for accurate model predictions of the estuarine environments that these input parameters correspond to the actual conditions. These parameters therefore must be measured, over a period of time, within the estuary in question to provide validation and calibration data for the model output data.

### **2.6.2. Example of applications**

Brenon & Le Hir (1998) demonstrated that a two-dimensional depth-averaged model could be used to model the tidal propagation and fine sediment transport within the Seine Estuary, France, to simulate the behaviour of the turbidity maximum therein. The estuary is 160km long and has a similar, if somewhat larger, morphology to that of the Ribble Estuary. As with the Ribble Estuary it is a macrotidal estuary which has been modified by the emplacement of dykes to constrain the main channel for navigation purposes. The hydrodynamic model has been constructed using an up-to-date bathymetric chart, which was consequently divided into a rectilinear grid for the entire estuary. Attached to this module is the sediment transport model

which uses an advection-dispersion equation to estimate the net movement of sediment within the estuary. The model only predicts the transportation of cohesive sediments and not the non-cohesive sediments. As stated by Uncles (2002), many sediment models deliberately simplify the sedimentological processes, relying on constants to simplify the modelling process. Within this model it takes the form of a settling velocity constant, a fixed initial consolidation constant and the mud shear stress are assumed to be uniform across the entire estuary. Modelling results demonstrated that sediment patterns are strongly dependent (non-linear) on the flow characteristics (Brenon & Le Hir, 1998). This indicates that the tide has a strong effect on the position and behaviour of the turbidity maximum. However the model did fail to replicate the movement of fine-grained mud deposits during the course of the lunar cycle, indicating that there would be net deposition during the neap tide and net erosion during the spring tides.

Under the European MAST 2 program, a three dimensional model of cohesive sediment transport was constructed to replicate the formation of the turbidity maximum and the movements of fluid mud within the Seine Estuary (Le Normant, *et al.*, 1998). The model used three specific modules (suspended sediment, fluid mud and consolidation) to investigate the movement of sediments within the Loire Estuary, Western France. It demonstrated that it was able to reproduce the typical sedimentological features within the estuary through the course of a spring tidal sequence, however, no results were put forward for the sediment fluxes during the neap tidal cycle. This is important as a model must replicate the sediment flux conditions over the course of a

spring-neap tidal cycle where hydrodynamic behaviour is significantly altered, affecting the movement and distribution of sediments within estuarine environments.

## **2.7. Ribble Estuary**

### **2.7.1. Monitoring priorities**

The Ribble Estuary is located in NW England (see Figure 1.1) and is a macrotidal estuary with surrounding areas of saltmarsh that receives radionuclides from two main anthropogenic sources (Brown *et al.*, 1999). These discharged radionuclides have a high affinity for fine grained sediment (<63  $\mu\text{m}$ ) and it is this interaction that makes the identification and estimation of sediment fluxes and the depositional locations within the estuary an important priority for the Environment Agency in the UK. This is because the most significant radiation exposure pathway for the people living in the vicinity of the Ribble Estuary is through external irradiation from areas of fine-grained sediment deposits (e.g. saltmarshes and intertidal mud flats) containing elevated concentrations of radionuclides (Brown *et al.*, 1999). Therefore the monitoring program for EA is targeted mainly at *in situ* measurements of dose rates and analysis of sediments (RIFE-9). However locally caught shellfish and fish are also routinely monitored for dose rates. From these studies dose levels are then calculated for the critical groups within the estuary (Houseboat dwellers, anglers and wildfowlers, children playing in the mud and fishermen handling nets). The Ribble has now been chosen by the Environment Agency

as a pilot river basin project, which will consist of two key phases of work, firstly testing the European guidance on the planning process and public participation, but also as a prototype river basin management plan and programme of measures for the contribution to the Water Framework Directive (WFD) by May 2007.

### **2.7.2. The sedimentary environment, sediment sampling and saltmarsh cores**

Brown (1997) conducted a series of sediment trap studies at six sites evenly spaced between Lytham Jetty and Penwortham Bridge, Preston. A combination of Astroturf mats, rectangular Perspex sheets and erosion poles were used to measure the sediment accretion/erosion rates on the upper intertidal and saltmarsh surfaces. Astroturf strips (61 x 16 cm) were used to replicate the natural vegetation, which were placed flush onto the sediment surface at points close to the sampling positions for a series of saltmarsh cores and monoliths. The erosion poles were used to estimate surface sediment accretion/erosion, although erosion pole experiments have been shown to create extra turbulence around their base, distorting the natural depositional rates over the intertidal surface. They were collected on a 3-month sampling interval, which will reduce the temporal accuracy of the studies. This temporal accuracy was highlighted in the absence of any trend in  $^{137}\text{Cs}$  activity that has been reported in other estuaries i.e. the Esk Estuary (Kelly & Emptage, 1992), where  $^{137}\text{Cs}$  activity levels were seen to increase from the estuary mouth towards the estuary head from the sampling periodicity, which Brown (1997) did not detect. Assinder *et al.*, (1997)

conducted a survey of the activity concentrations of the sediments within the Ribble Estuary, demonstrating that there are significant relationships between sediment grain sizes with higher levels in finer grained sediments at upstream sites in the estuary. These findings were further investigated by Rainey (1999), who found that there are significant correlations between the percentage clay content of a surface sediment sample and the activity concentration of  $^{137}\text{Cs}$ . This allowed the use of remote sensing imagery to be utilized to map activity concentrations of  $^{137}\text{Cs}$  along the length of the intertidal sediments in the Ribble Estuary.

Numerous studies have been conducted upon the saltmarshes that surround the Ribble Estuary. Mamas *et al.* (1995) and Brown *et al.* (1999) both extracted sediment cores from the saltmarshes surrounding the estuary. Although reasons for sampling were different, with Mamas *et al.* (1995) conducting a study using  $^{137}\text{Cs}$  to assess net sedimentation rates on the saltmarshes, whilst the Brown *et al.* (1999) study aimed to determine radionuclide specific activities with depth. However, the sedimentary history of saltmarshes are different to that of the intertidal zones, which experiences cyclic patterns of erosion and depositional events. Therefore different sampling strategies must be adopted to study the intertidal sediments, than for the salt marsh environment.

### **2.7.3. Hydrodynamic behaviour of the Ribble Estuary**

The Ribble Estuary has an asymmetrical tide, which results in a short duration flood tide and a more prolonged ebb tide (Kashefipour *et al.*, 2002). This

results in flood velocities being approximately twice that of the ebb (Burton, 1995). The net effect of this asymmetry results in tidal pumping of suspended sediment and accumulation of fine grained (<63  $\mu\text{m}$ ) sediments and the associated contaminants in the upper estuary (Gleizon *et al.*, 2003). Burton *et al.* (1995) showed that during the ebb tide flow on a neap tide, there was stratification of the water column and approximately linear decline of velocity from the surface to the bed. There is less stratification on the flood tide and almost constant higher velocities, with turbulent diffusion being the main dominant mixing mechanism on the spring flood tidal sequence. However during the neap tidal flood cycle, the amount of mixing decreases due to reduced flow velocities and stratification would be present during periods of the flood tide, as well as on the ebb tide. This means that the application of remote sensing during neap tidal conditions will have to rely on turbidity readings taken concurrent to the image acquisition.

#### **2.7.4. Hydrodynamic modelling the Ribble**

To optimise estuarine models, flow mechanisms within the estuary, such as friction effects, and the mechanisms associated with sediment movement must be understood. Given the lack of this knowledge, it is necessary to approach each estuary as a new problem and to develop a model that recreates its fundamental processes (Burton *et al.*, 1995). Therefore it is important to obtain precise measurements on firstly the bathymetric profile of the estuary, as this is one of the most important factors in determining estuarine flow patterns. Following this, there is a need for long term fixed monitoring stations, which are required to build up an understanding of the

fluid and sediment dynamics that operate within the estuary. Data generated by these field measurements can then be used to construct the model and/or calibrate and validate the model output to determine model prediction accuracy.

One-dimensional models have been used in the Ribble to predict sediment transport and radionuclide dispersion (Burton *et al.*, 1995; Lyons, 1999; Gleizon, 1999). Burton *et al.* (1995) considered the intratidal solute dispersion, to gain an understanding of the estuarine turbidity maximum within the estuary, showing that predictions of sediment and radionuclide dispersion did not replicate actual conditions within the estuary. This may be due to the inability of the one dimensional model to consider the vertical variations in SSC in the water column.

Westlakes Research Institute has produced a two-dimensional numerical model, (VERSE – Vertically Resolving model of sediment and radionuclide transport in estuaries) which simulates the hydrodynamics, sediment transport and radionuclide dispersion in the x-z plan for the Ribble Estuary (Gleizon, 1999). It is designed for a relatively narrow macrotidal estuary where transverse circulation is assumed to have a minimal impact on the along-channel dispersion (Gleizon *et al.*, 2001). Using a grid system, with each cell being 250 m in the horizontal and a 0.3 m in the vertical, it divides the estuary into equal sections for its entire length from Lytham to the very upper reaches of the estuary. By using a modular system (Figure 2.3) it is then able to predict the fate of sediments and associated contaminants in the Ribble

Estuary, especially those discharged by BNFL Sellafield and BNFL Westinghouse Springfield.

The sediment module within VERSE separates the material into non- and cohesive sediments and uses a large number of uncertainties and empirical laws to predict the erosional and depositional fluxes of sediment within the Ribble Estuary. Initial bed sediment distribution and thickness are specified from site observations and then the cohesive sediment module takes into account the erosion and deposition processes, with erosion being proportional to the critical shear stress of the bed. From this, erosion and deposition rates are calculated for every inundated cell, taking into account any advection-dispersion that could take place. The model then calculates the quantities of fine-grained (<63  $\mu\text{m}$ ) sediments that are deposited over the course of the tidal cycle. It is only designed to predict movement of sediment over a relatively short time span of a year or two, but it can gather multiple data streams from a number of user defined locations throughout the estuary allowing estimates of the net flux of sediment within the estuary to be made.

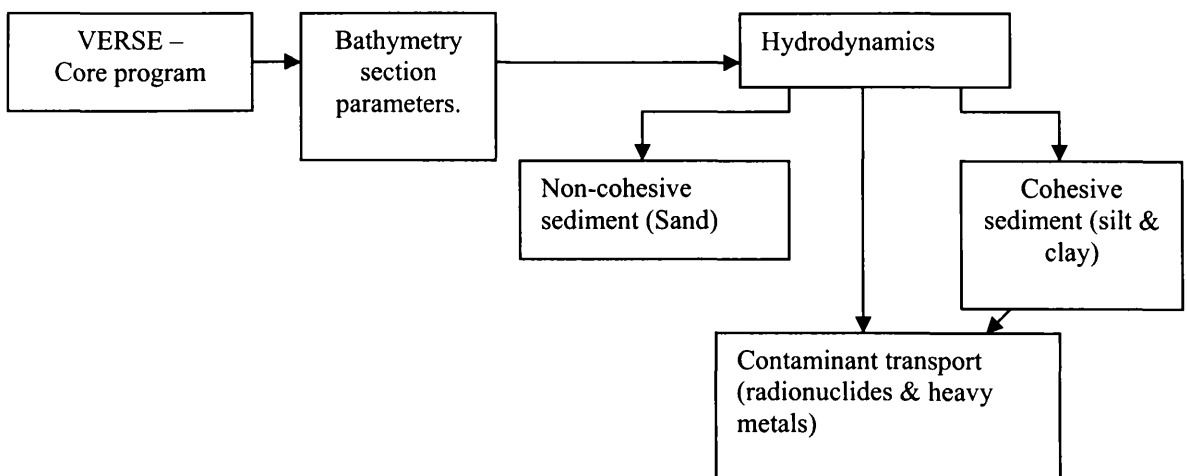


**Figure 2-3** Model architecture of VERSE (Gleizon *et al.*, 2001).

Calibration and validation of the model are based on fixed point sampling within the estuary using three instrument rig stations to log water temperature, pressure and salinity, current velocity and levels of turbidity. After testing, the model has been shown to predict tidal harmonics to a reasonable accuracy, but with some uncertainties associated with the intertidal sediment shear stress and bathymetry of the estuary (Gleizon *et al.*, 2001).

## **2.8. Research priorities and the derivation of hypotheses**

The temporal variability of sediment transportation pathways are of paramount importance in the understanding of sediment flux patterns within an estuarine basin. Interactions of sediment with cyclic tidal patterns, both on a daily time scale and the rhythmic spring and neap tidal cycle, provide the basal sedimentation patterns through tidal pumping. However, tidal pumping is affected by the differences in inter-, intra-annual, monthly and daily variations in storm generated wave action, river discharge patterns within the estuary basin and microphytobenthos stabilisation of the intertidal sediments (Black, 1999). These factors have been shown to have impacts on the erosion, transportation and deposition patterns within estuarine environments (West & West, 1991), yet the erodability of cohesive sediments remain difficult to model or predict accurately. Evaluating the effect of these factors on the temporal and spatial distribution patterns of sediments within an estuarine basin, requires the integration of sediment point sampling, selected ARS techniques to study the variations in the temporal stability of estuarine sediments.

Quantifying the long term fate of sediments and associated radionuclides is one of the key issues regarding the management, stewardship and impact assessments in estuaries. The visualisation and comprehension of estuarine processes that influence sediment flux in estuaries is important to understanding the dynamic nature of estuarine environments. This project focus on the quantification of sediment and radionuclide flux and distribution over a range of temporal scales, including ebb and flood tide sequences, intra annual variations and inter annual variations and will endeavour to increase the understanding of estuarine circulation patterns of suspended sediment and estimation of the quantity of sediment transported over the course of a flood and ebb tide by combining both ARS and a two-year monthly study of intertidal sediments. This will be achieved through the use of regular field measurements and time series ARS campaigns, complemented with data derived from a two-dimensional model (VERSE) developed by Westlakes Research Institute.

### **2.8.1. Intertidal characteristics**

The distribution patterns of intertidal sediments can be extremely dynamic and remain a fundamentally important part of the estuarine ecosystem. At the same time, they are also zones of possible erosion or deposition of sediments and therefore possible sources/stores of contaminants. The need to understand the processes that take place within these environments has been the driving force behind much research over the past few decades (Patterson & Black, 1999; Uncles, 2002).

The development of quantitative remote sensing techniques (Rainey, 1999; Rainey *et al.*, 2003) has provided a valuable approach to mapping intertidal sediment and the associated radionuclide distribution at high spectral resolution (<2 m) across the whole of the exposed intertidal zone. This technique, although relying on reference data for validation, provides a synoptic view of the entire estuarine system than can be obtained through conventional point sampling. The applicability of this technique will be verified over a number of seasonally distinct intertidal images to determine spatial changes in the distribution of intertidal sediments. In addition Light Detection And Ranging (LiDAR) data will be collected to provide data on bed elevation change, placing monthly field sampling into a spatial context. The continual balance between catchment discharges and marine influx of sediments leads us to two hypotheses which will be investigated using a combination of the field and remote sensing techniques:

Hypothesis 1: *The inter-annual deposition of marine sediments in the Ribble Estuary shows a net accretion.*

Hypothesis 2: *The intra-annual variability in sediment accretion and erosion is greater than the overall annual net accretion.*

If the strong sediment - radionuclide associations are stable over time and space, then image data can be used to provide maps of intertidal radionuclide comparisons and compared against other radiological assessments that are routinely reported, e.g. Radioactivity in Food and the Environment (RIFE). The

RIFE 9 (2004) reports variations in the observed concentrations in radioactive particles within the Ribble Estuary, from a program of fixed point sampling. This reported variability in the inter-annual variations could be due to the variations in sediment transport within the estuary, which are critical in the understanding of temporal variations of sedimentation within the Ribble Estuary. The use of ARS data could therefore be used to place these spatially isolated points within the geographical context of the estuary and produce maps of radioactive activity concentrations maps for the intertidal sediments. However, this requires that the 3<sup>rd</sup> hypothesis can be reliably demonstrated.

*Hypothesis 3: The relationship between  $^{137}\text{Cs}$  and the sediment clay percentage content is temporally stable.*

### **2.8.2. Sediment flux**

Providing a means for estimating sediment flux over flood and ebb tide cycles has numerous potential benefits for regulatory bodies, industry and conservation organisations. Specifically, the ability to make an estimate of the sediment flux within estuarine environments should allow the controls on the net flux to be evaluated and enable more informed management and engineering within the estuarine environment i.e. assessing the placement of potential discharge pipes within the estuarine system.

Fundamentally, estimates of how much sediment is deposited over flood and ebb tide events have been traditionally based on fine scale measurements of sediment accumulation at fixed sampling sites i.e. Astroturf matting (Bradley &

Chapman, 1998) or sediment plates (Brown, 1997) or application of photo-electronic erosion pins (PEEPs Lawler 2005), However, as all of these sampling methods produce point sampling, they are geographically isolated, making the individual readings spatially inaccurate when providing total estuary estimates of sediment deposition.

Atkin (2000) demonstrated that ARS imagery can be used to derive estimates of suspended sediment flux over the course of a flood tide. However, to truly understand the dynamics of estuarine sediments it is necessary to understand the fate of the suspended sediments over the course of both the flood and ebb tidal sequence. Therefore this part of the project will use calibrated imagery from the Compact Airborne Spectrographic Imager (CASI) (operated by the UK's Natural Environment Research Council) combined with concomitant ground reference data to characterise suspended sediment concentrations and the total suspended sediment load over the course of both the flood and ebb tide. This forms the final hypotheses of the project, which states that the net sediment flux of sediment and radionuclides over a single flood and ebb tide cycle can be estimated through remote sensing. To answer this hypothesis, two sets of time series imagery were obtained (April 2003 and July 2003) to assess the spatial and temporal changes in the suspended sediment and associated radionuclide ( $^{137}\text{Cs}$ ) activity concentrations over the course of a flood and ebb tide event. Data from VERSE will be used to generate estimates of total water volume for each section of the Ribble Estuary, which combined with estimates of averaged suspended sediment concentrations in the surface layers, allowing estimates of the total flux of

sediments within the estuary to be made. To demonstrate that these estimates are realistic, they will be compared to the results of the two year, monthly intertidal sediment study. However, fundamental to this work is the final hypothesis:

*Hypothesis 4: The net flux of sediment and radionuclides over a single flood and ebb tide cycle can be estimated through calibrated time series remote sensing.*

### **2.8.3. Research milestones**

As highlighted within the context of the literature review above, there are a large number of investigations focused on sediments within estuarine environments. Stemming from this, there appears to be a need to achieve an increased understanding and quantification of the temporal and spatial variability's that exists within such dynamic systems. Consequently, this project will combine four different methodical approaches (see below) to provide sediment and radionuclide distributions, evaluate their temporal stability, and quantify the flux of sediment and radionuclides over inter-, intra-annual, monthly, and single tidal event time scales.

1. Monthly intertidal sediment investigations.
2. Airborne remote sensing of the intertidal sediments (ATM).
3. Time series airborne remote sensing of a flood and ebb tidal sequence (CASI).
4. Two-dimensional hydrodynamic modelling.

## 5. Estimation of the net bed sediment movement: LiDAR.

Investigations across a combination of these timescales should enable the controls on the overall development of the intertidal area to be evaluated. Therefore, to correctly assess the sediment dynamics of an estuarine environment, it is important to obtain the temporal differences at each of these timescales to allow predictions of sediment flux and distribution patterns within the estuary to be made.

The following milestones define the direction of the research project, providing a comprehension of the temporal sediment dynamics of the Ribble Estuary.

1. Installation of intertidal erosion sampling sites to facilitate monthly monitoring of bed height elevation changes (Hypothesis 1, 2 & 3).
2. Collation of erosion monitoring data to investigate the inter-annual and intra-annual trends in bed height variations over the intertidal sediment surfaces (Hypothesis 1 & 2).
3. Placement of the erosion monitoring locations into a spatial context with the utilization of remote sensing, deriving measurements of seasonal variations in intertidal sediment grain size characteristics (using the NERC's ATM data) and bed height variations (NERC's LiDAR data) (Hypothesis 1 & 2).
4. Laboratory analysis of the monthly sediment samples, to determine the relationship between  $^{137}\text{Cs}$  specific activity concentrations and fine-grained (<2  $\mu\text{m}$ ) sediment characteristics (Hypothesis 3).

5. Acquire time series remote sensing data (NERC CASI data), to establish the temporal and spatial variations in suspended sediment concentrations over flood and ebb tide sequences (Hypothesis 4).
6. Convert time series imagery into quantitative estimates of net sediment flux over flood and ebb tides for the whole estuary (Hypothesis 4).
7. Conduct small scale study of sediment flux over a sub section of the estuary, which is comparable to a monthly field sampling site (Hypothesis 4).
8. Validation of the net sediment flux from the flood and ebb tide data with estimates derived from the erosion reference sites (Hypothesis 2).

## **2.9. Summary**

Following a review of estuaries and the typical methodologies used to investigate mechanistic process and impacts on and from estuarine environments, this chapter then identified the difficulties in providing realistic estimates of intertidal sediment concentrations and sediment flux over a range of time scales. The Ribble Estuary was identified as the chosen site, primarily as a consequence of the industrial and regulatory interest in the fate of radionuclide contamination. Coincidentally, the Ribble Estuary has become a case study site for the Water Framework Directive (WFD). Here, a combination of spatial and point sampling techniques, combined with parameterisation from an estuarine model of the Ribble will be used to provide quantitative data on sediment and radionuclide distribution and flux.

In order to provide a baseline of understanding of sediment movement within the estuary, chapter three will describe the design, location, data collection and analysis of the erosion reference sites across the Ribble Estuary and chapter four will place the monthly intertidal data within a spatial context with the use of ARS data. Chapter five will use high temporal resolution flood and ebb tide time series data to investigate the net sediment flux in the estuary, which will then be explored in context with the section of work within Chapter Six.

### **3 Sediment accretion (and associated radionuclides) of the intertidal sediments in the Ribble Estuary.**

#### **3.1. Introduction**

Estuarine intertidal zones represent an essential component of the near-shore coastal ecosystem, acting as an interaction zone for terrestrial and marine based processes, but also as diverse and productive ecosystem for many flora and fauna species. The near-shore and coastal environments have been extensively studied, however, the intertidal mudflats within estuarine environments are relatively poorly understood in comparison with sandy beaches and saltmarsh environments (Dyer *et al.*, 2000), perhaps because of their dynamic nature and general in-accessibility. This is due to the difficulties of working in such environments, but also due to the rapid spatial and temporal changes in the distributions patterns of intertidal sediments and especially the more transient fine-grained mud fraction (<63  $\mu\text{m}$ ), which are associated with radionuclides released from BNFL Sellafield and BNFL Westinghouse Springfields.

Previous studies (Tyler *et al.*, 1995; Assinder *et al.*, 1997; Brown, 1997; Clifton *et al.*, 1997; Frignani *et al.*, 2004), have found a significant relationship, typically  $r^2 > 0.8$  between  $^{137}\text{Cs}$  and clay percentage within the intertidal mudflats. This relationship was further verified by Rainey (1999) to map radionuclide ( $^{137}\text{Cs}$  and  $^{241}\text{Am}$ ) activity concentrations across the exposed intertidal mudflats of the Ribble Estuary with the use of ARS imagery.

However, it is necessary to determine whether these clay percentage/<sup>137</sup>Cs relationships are a fixed, annual relationship or merely a seasonal phenomenon as remote sensing flights are flown throughout the year. Therefore, to ascertain the temporal stability and variability of clay percentage/radionuclide relationships in mapping and the estimation of the sediment deposition/erosion cycle of the intertidal sediment, a two year monthly intertidal sampling campaign was designed to investigate these two separate intertidal sediment properties.

Obtaining this information on the sediment dynamics of the estuary will provide answers for a number of the research hypotheses outline in Chapter Two. The investigation should allow the identification of inter-annual sediment accretion rates within the estuary and consequently and which zones of the estuary are experiencing the most rapid rate of accretion. Conducting these monthly studies will also demonstrate how the intra-annual sediment accretion and erosion variability fluctuate from the net annual accretion rate within the estuary. Finally, as the sampling will be conducted continuously over a two year period, it should be possible to identify any temporal instability of the <sup>137</sup>Cs/percentage clay relationship within the estuarine system.

## **3.2. Locations of field study sites**

### **3.2.1. Location of sampling points**

Sampling locations must be selected with care within the estuarine environment to ensure a good representation of the spatial variability of the

intertidal area. Furthermore the topographic setting of each sampling site at each location was assessed, to achieve interpretation of the spatial variability and sediment regime changes across the intertidal zone. This height factor is critical for the intertidal sediments, as it affects the amount of inundation and possible exposure times for sediment drying times and consolidation. Therefore, at each sampling site it is necessary to orientate the transect lines over the vertical extent of the mudflat.

Initially, three sampling locations were selected at representative locations along the extent of the Ribble Estuary to characterize the outer, middle and upper estuary environments (Figure 3.1). The outer estuary site was located at Lytham St Anne's lifeboat station (GR SD3367 4267) (Figure 3.2a), the mid-estuary site at Warton Bank (GR SD3405 4266) (Figure 3.2b) and in the upper-estuary zone at Penwortham Bridge (GR SD3527 4290) (Figure 3.2c). However a fourth sampling location at the BNFL Westinghouse Springfields discharge pipe (GR SD3472 4285) (figure 3.2d) was added mid-estuary, during July 2003, following the initial interpretation of the 2002 remote sensing imagery which indicated that it would be difficult to validate the upper sampling site because it would not be covered by the remote sensing flight line.

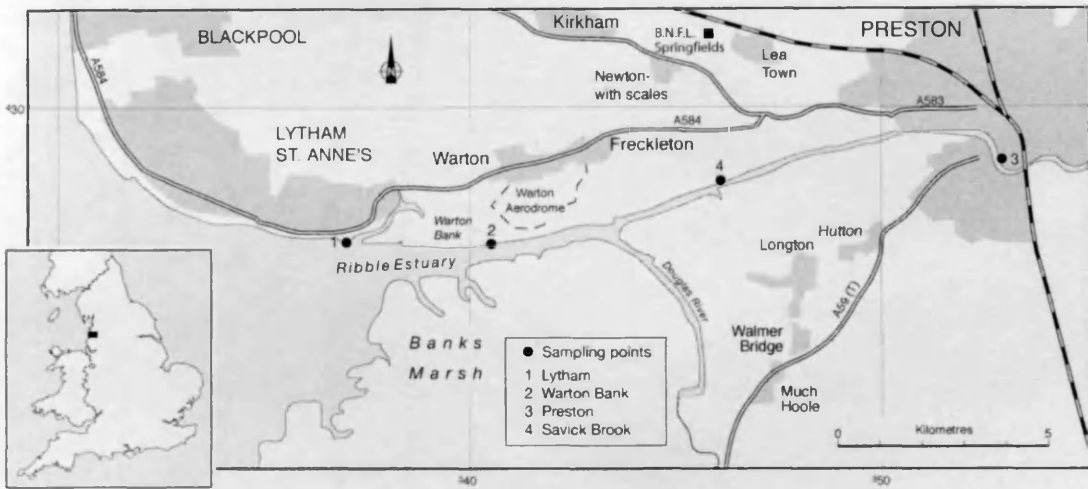


**Figure 3-1** Ribble Estuary sampling locations

After selecting sampling sites, a collection strategy was then implemented to help gain a greater understanding of the sediment movement within the estuary. It was broken down into two distinct sampling approaches i) surface scrapes of the intertidal sediment & ii) an accretion/erosion investigation.



**Figure 3.2a** Lytham St Anne's (outer estuary site) looking west.



**Figure 3.2b** Warton Bank (mid-estuary) looking South.



**Figure 3.2c** Penwortham Bridge (upper estuary) Looking west.



**Figure 3.2d** Savick Brook (mid-estuary) looking east.

**Figure 3-2** The four sampling sites for the two year intertidal sampling campaign (June 2003).

### 3.2.2. Lytham (Site 1)

The location of the field sampling sites at Lytham St Anne's was chosen for a number of reasons. Firstly, the site is located at the outer section of the Ribble Estuary, which is characterised by a large expanse of the intertidal flats that are not present within the constrained mid-, and upper estuary. Secondly the site had been previously visited by Rainey (1999) and Atkin (2000) during the course of a study of the sediment fluxes within the Ribble Estuary during a flood tide event. This allowed some visual estimation of how the

environmental conditions have altered in the intervening years. Finally, the site represents the seaward extent of the VERSE hydrodynamic model developed by Westlakes Research Institute and thus the prospective field data could be used to validate and calibrate the model predictions (Figure 3.3).

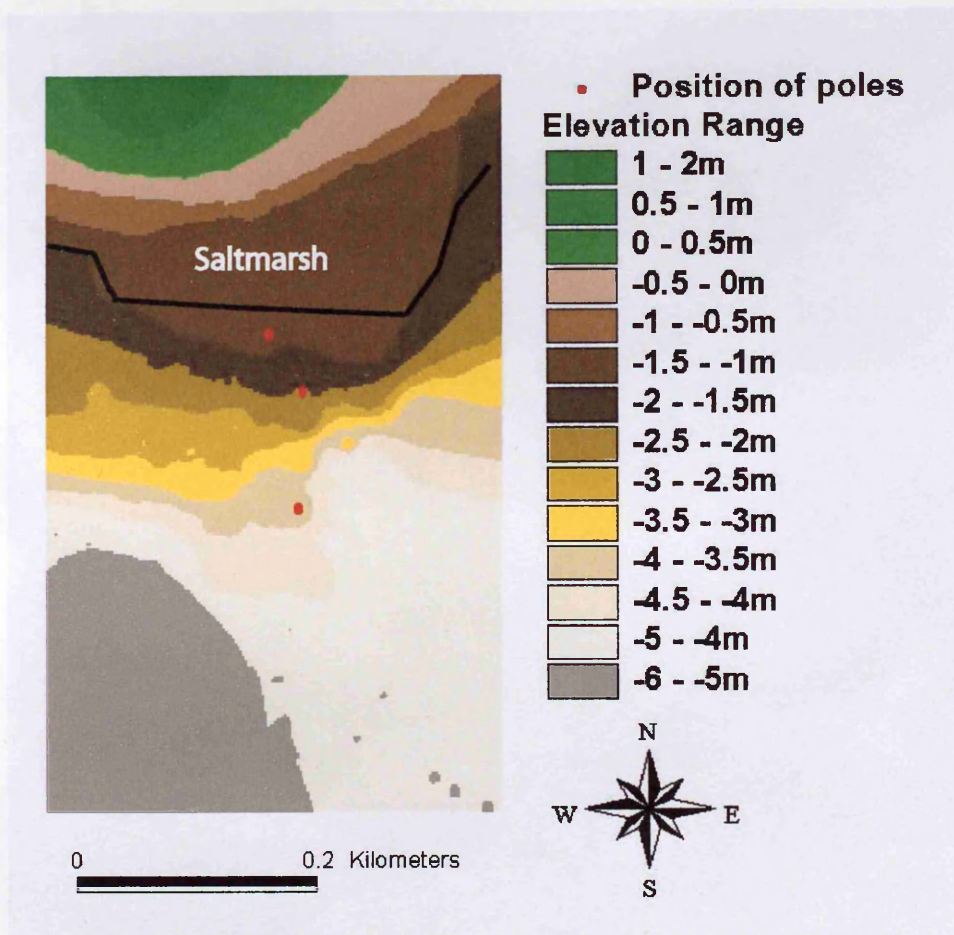


**Figure 3-3** Lytham St Anne's schematic diagram generated from an extensive EDM survey obtained August 2003 and georeferenced to an accurate GPS base station.

### 3.2.3. Warton Bank (Site 2)

Warton Bank was primarily chosen due to the past studies (Rainey 1999; Rainey *et al.*, 2000; Rainey *et al.*, 2003), which were performed over a series of intertidal sediment and moisture sampling transects across the intertidal zone from the saltmarsh edge to the edge of the main channel in the south

(Figure 3.4). Additionally the location can be considered representative of a large section of the mid-estuary within the Ribble Estuary. This is due to the wide, relatively flat lower intertidal surface adjacent to the channel and a more inclined upper intertidal surface topped with saltmarsh.

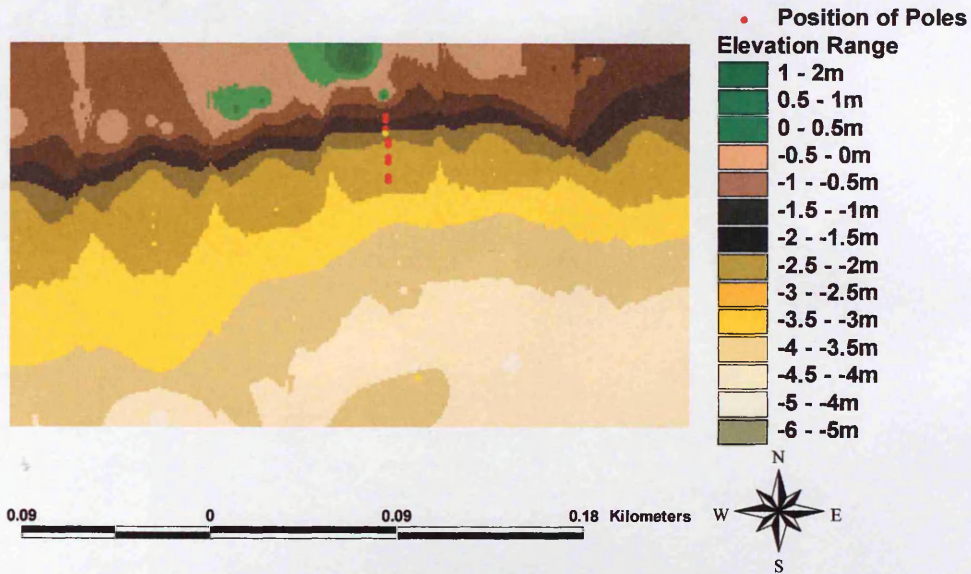


**Figure 3-4** Warton Bank schematic diagram generated from an extensive EDM survey and georeferenced to a GPS base station.

### 3.2.4. Savick Brook (Site 4)

The Savick Brook field site (Figure 3.5) represents an addition to the field sampling survey, allowing increased spatial resolution within the mid/upper estuary zone of the Ribble Estuary. Additionally the site provided an extra ground reference point for the remote sensing study of the intertidal zone. However, the close proximity of the discharge pipe from BNFL Westinghouse Springfields was also a factor in the site selection.



**Figure 3-5** Savick Brook transect (September 2003).

### **3.2.5. Penwortham Bridge (Site 3)**

Penwortham Bridge is situated within the upper reaches of the tidal inundation and was chosen to be a representative site for river-flow dominated sedimentary conditions. It is situated within a confined channel, with the predominant river channel running into the base of the intertidal surface at the transect site. The upper areas of the intertidal surface consist of a small section of eroding saltmarsh, with the remaining intertidal surface consisting of coarse boulders, which were overlain with alternating mixtures of fine to coarse grained sediments (Figure 3.6 & 3.7).

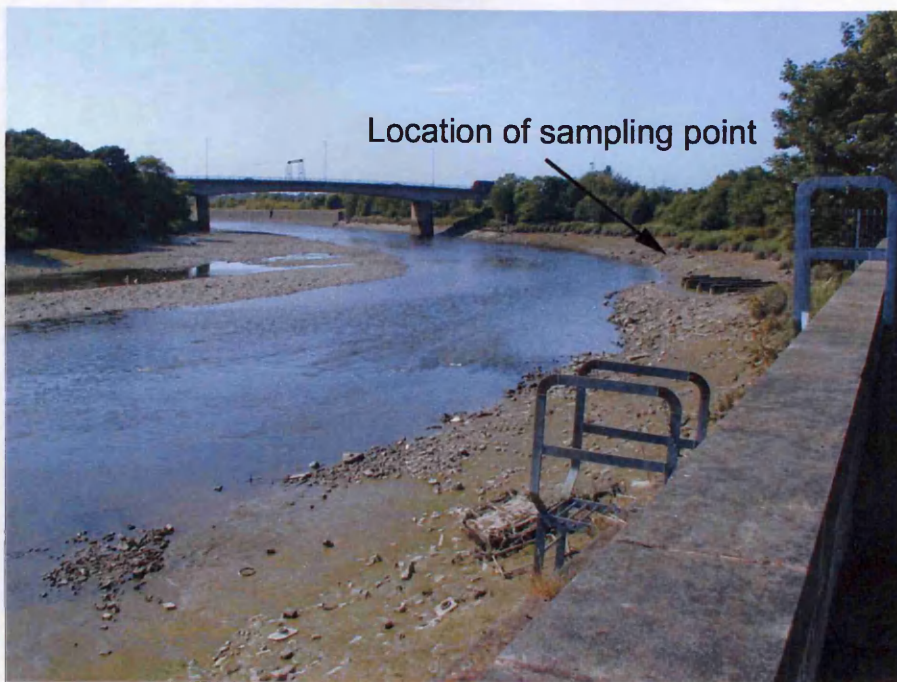


**Figure 3-6** Penwortham sampling site looking west (June 2003).



**Figure 3-7** Penwortham Bridge looking east (June 2002).

### **3.3. Methodology for field measurements**

#### **3.3.1. Sampling strategy**

Assessing the seasonal distribution of intertidal surface sediment along the length of the Ribble Estuary required the use of a monthly sampling approach at representative locations along the length of the estuary. Sediment sampling and intertidal sediment elevation changes were measured over the course of a two-year monthly sampling strategy. Sampling was carried out at low tide across four spatially representative sampling locations along the extent of the Ribble Estuary. However, due to the fixed cyclical nature of the tidal patterns within the estuary, sampling could only occur during the period of the neap tidal cycle.

#### **3.3.2. Sample collection techniques**

##### *Surface sediment scrapes, contact cores & storage bags*

Throughout the project surface sediment scrapes were used to collect the top surface sediments (<1 cm). Samples were collected using a trowel, retrieving the top layer of sediment on the intertidal surface. These samples were then placed within labelled plastic bags for laboratory analysis. However, using surface sediment scrapes does have limitations in regards to the collection of associated moisture content of the sediments. As outlined in section 2.3.1, contact cores can be employed to collect a frozen 2 mm thick section of surface sediment. This technique allows the interstitial moisture content of the

surface sediments to be accurately assessed. Due to the relatively small quantity of sediment retrieved within each sample, grain size analysis and organic composition may be limited in terms of spatial representations. Therefore surface scrapes were predominantly used within this project, allowing rapid collection of large (c. 1kg) samples from each sampling site. Contact cores were collected during the October 2003 intertidal imagery, unfortunately these samples defrosted before laboratory analysis could be performed on them.

### *Grain size analysis*

Grain size analysis was conducted jointly at Westlakes Research Institute and the University of Stirling. In both cases fresh sediment sub-samples were used to determine the sediment grain sizes. Westlakes employs a Malvern Longbed particle-sizer, which measures grain size ranges from 0.05  $\mu\text{m}$  to 3000 $\mu\text{m}$  within a large sediment sampler unit. Stirling University uses a Coulter Counter particle-sizer to measure small volumes of sediment. Subsequently the results were broken down into three size brackets % clay (<2  $\mu\text{m}$ ), % silt (2 $\mu\text{m}$ -63  $\mu\text{m}$ ) and % sand (>63  $\mu\text{m}$ ). However with the laboratories using two different particle sizing instrumentation, it was necessary to conduct an inter-laboratory comparison on the same sediment samples. This was conducted in November 2002, where sediment samples were collected from the Ribble Estuary, initially being measured at Stirling University and again the following day at Westlakes Research Institute. Comparisons of these three groups showed significant linear regression relationships between clay ( $r^2=0.98$ ) (Figure 3.8) and silt ( $r^2=0.8423$ ) and a

somewhat lower, although significant, relationship for sand ( $r^2=0.6833$ ) (Figure 3.9). This lower relationship for sand between the machines could be a result of the quantities of sediment that are placed within the sampling units of the machines (the Malvern Longbed particle-sizer has approximately four times the quantity of sediment to be sampled at one time, in comparison to the Coulter Counter).

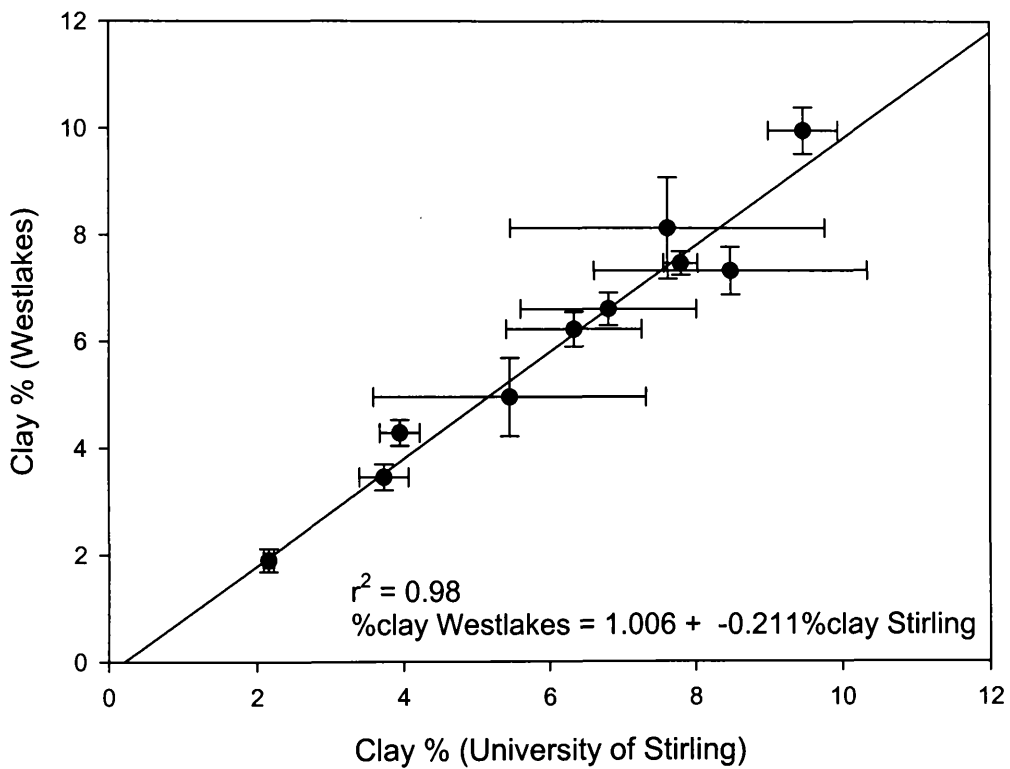


**Figure 3-8** Comparison of clay percentages taken from the same sample, by each institutions particle sizer. Error bars are associated with the mean standard deviation of the sampled sediments for each instrument.

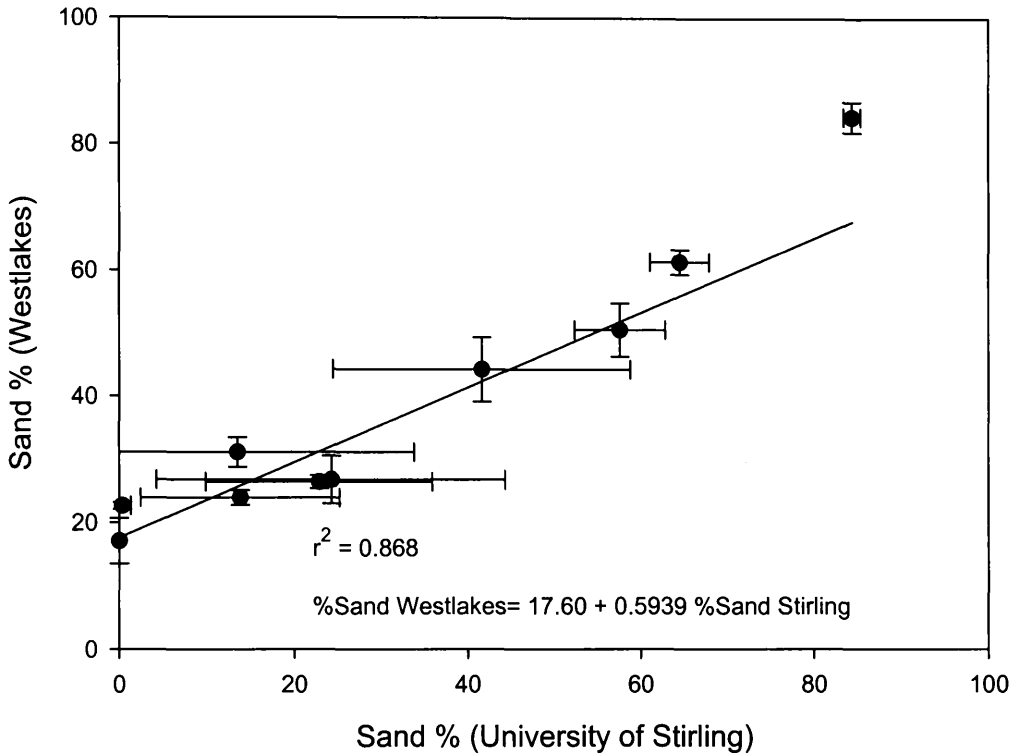


**Figure 3-9** Comparison of sand percentages taken from the same sample, by each institutions particle sizer. Error bars are associated with the mean standard deviation of the sampled sediments for each instrument.

### 3.3.3. Measurement of erosion/deposition on the intertidal surface.

Erosion and deposition lie at the heart of geomorphological explanations of sediment transport within the estuary, but obtaining the important information on the dynamics of landscape change has proved difficult (Lawler, 2005). Therefore, to truly understand the nature of erosion and deposition, it is necessary to obtain temporal field data on a number of important parameters to demonstrate the principal environmental drivers within the ecosystem. As mentioned in 3.4.2, surface scrapes were utilized to obtain information on changing sedimentological conditions of the intertidal surface, but it is also important to acquire data for the net change in the surface elevation of the intertidal sediments.

When assessing the temporal resolution of such a project, it is necessary that the sampling periodicity is adequate to obtain sufficient resolution to facilitate the identification of the main environmental drivers in the estuarine system. However, the temporal resolution must be assessed against any possible site degradation that might occur if sampling periodicity is too frequent, with the possible impacts of damage to the intertidal surface leading to enhanced erosion or bed compaction (Figure 3.10).



**Figure 3-10** Relic footmarks surrounding field site 1 at Lytham, a month after previous sampling.

#### *Erosion/deposition of the intertidal surface*

As demonstrated above (Figure 3.10), the impact of performing the sampling task on the intertidal surface could induce non-natural erosion/deposition.

Therefore, a monthly sampling strategy was implemented to mitigate the possible impacts of site survey disturbance between sampling dates.

The use of PEEPS (Lawler, 2005) can allow very short term (minutes) temporal accuracy of sediment depositional/erosional events, but due to the investigation period lasting two years, it would prevent the long-term emplacement of such expensive pieces of scientific equipment into the environment. Therefore a low cost approach was used to gain monthly temporal resolution of the oscillating sediment regime within the Ribble Estuary. The use of erosion poles has been criticised for inducing un-natural flow regimes in their vicinity (Bruesseler, 1991), therefore two poles were emplaced approximately two meters apart on the intertidal surface and height measurements were taken from the central section of a two meter long horizontal 'cross-bar' placed between the two poles (Figure 3.11), which was levelled with the use of a spirit level and metre stick. From these sample measurements, the mean was extracted for the five central points, allowing the plotting of average height accumulation/erosion for each sample locality. This was necessary as the sample measurements within 40 cm of the vertical poles demonstrated an effect from the alternating flow pathways generated around the base of the poles. Measurements were found to be inaccurate due the predominance of medium to strong wind conditions in the estuary, therefore a measuring rule was used to obtain these readings.



**Figure 3-11** Measurement of height elevation of the intertidal surface.

#### **3.3.4. Gamma ray analysis (procedures)**

Sediment samples examined at Westlakes Research Institute were freeze dried after particle grain size analysis had been completed, whilst at Stirling the sediments were placed within foil trays and dried within an oven. Following this, the samples were either ground down to powder in a pestle and mortar (Westlakes Research Institute) or within a mechanical grinder (Stirling University). A sub-sample of each was then packed into a large pre-weighed Petri dish, sealed with three strips of pre-weighed Parafilm<sup>®</sup>, which is then precisely ( $\pm 0.005$  g) weighed on laboratory balances. Using Westlakes Research Institute two gamma detectors (2.4.3), the packed samples were counted for periods between eight and sixteen hours.

### **3.3.5. Estimation of sample activity**

Using the FitzPeaks program for the detection and identification of gamma rays, it is possible to analyse the data files generated by the gamma detectors. After applying appropriate calibration files (background, energy efficiency, calibrated source and sample geometries), the program uses a peak search algorithm to find all indicated gamma peaks in the spectrum file. After the peak search has been completed, the environmental background peaks are removed, then the limit of detection is calibrated for each radionuclide and then a report on activity concentrations is produced. The program allows for the back calibration of detection files if sample times are known, which is especially important for the detection and monitoring of short lived radionuclides such as  $^{234}\text{Th}$ .

### **3.3.6. Spectral analysis of samples**

It is necessary to perform energy calibrations upon the gamma detectors on a regular basis to ensure the correct allocation of spectral peaks to radionuclides. Therefore within this project the detector was calibrated approximately every two weeks using a standard from the International Atomic Energy Agency (IAEA) (IAEA-300). This was necessitated by the continuous gamma-counting of the large number of sediment samples generated by this project.

### **3.4. Results and interpretation of intertidal sediment and bed elevation changes**

#### **3.4.1. Lytham St Anne's**

Lytham St Anne's represents the inner extent of the outer estuary zone for the Ribble Estuary and also the seaward extent of the VERSE model developed by Westlakes Research Institute for the estuary. This meant that the spatial extent of the survey had to incorporate a relatively large expanse of intertidal sediment (Figure 3.12) upon the northern bank of the estuary at that point (see Figure 3.7), obtaining representative data from sites at the upper, middle and lower intertidal zones (Figure 3.12).

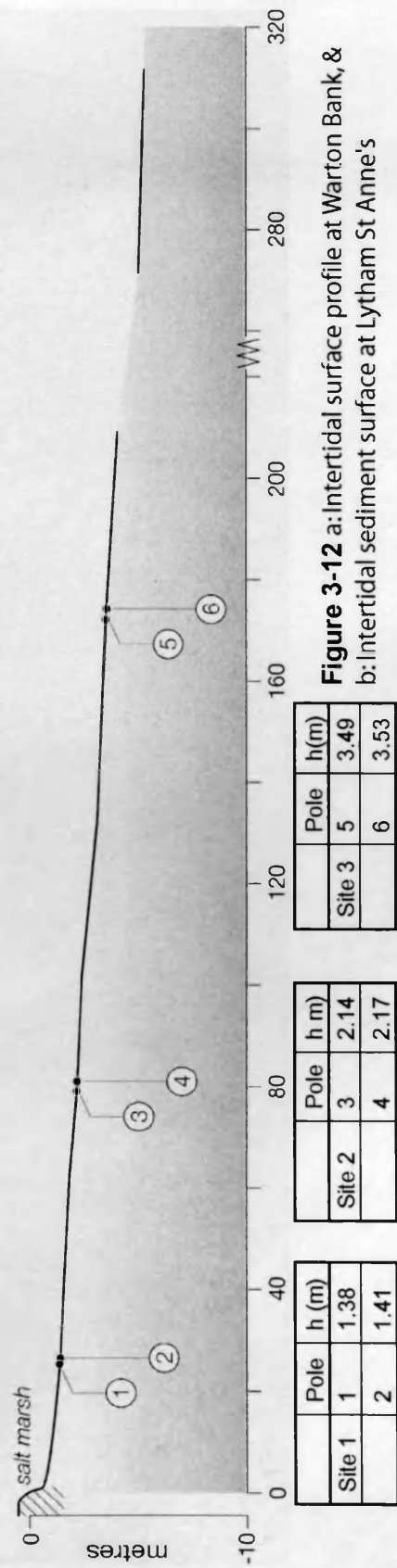
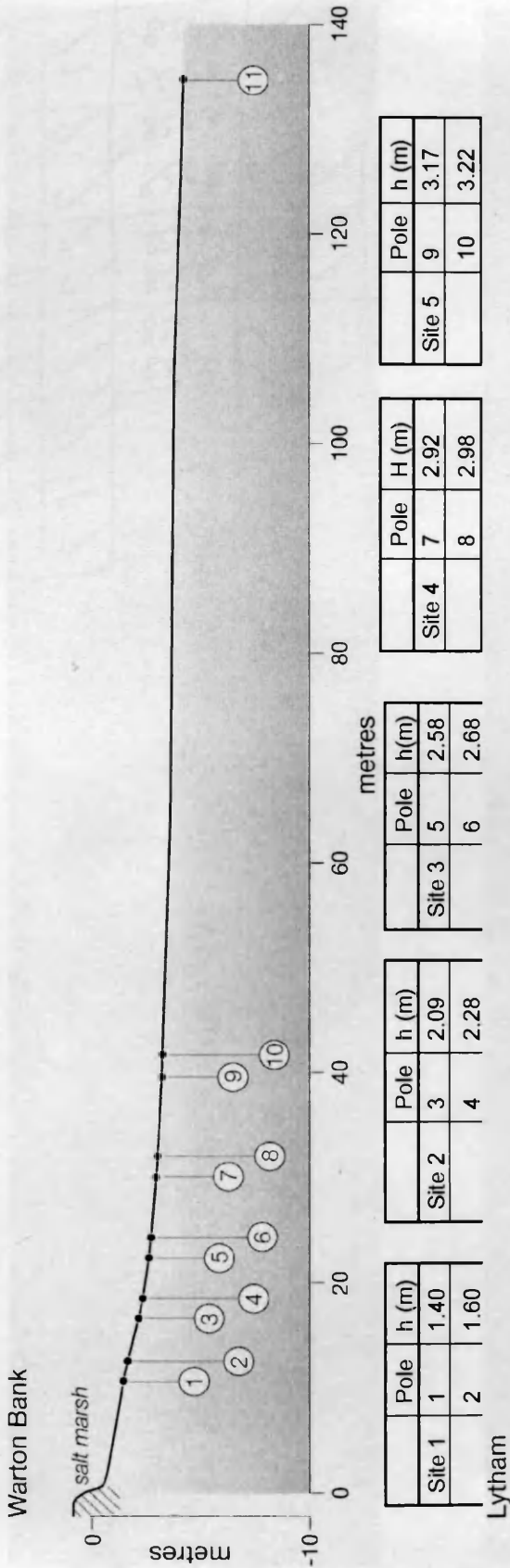


**Figure 3-12** a: Intertidal surface profile at Warton Bank, &  
b: Intertidal sediment surface at Lytham St Anne's

*Intertidal sediment properties: Clay*

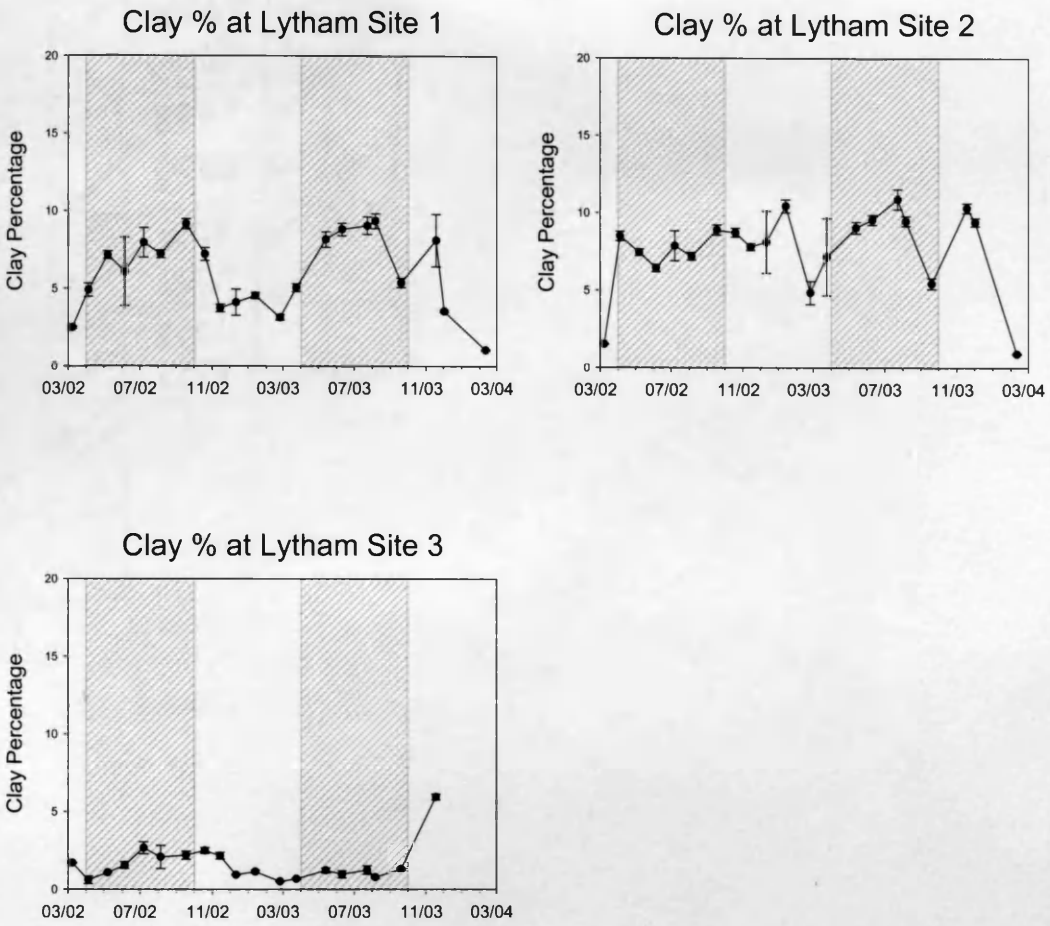


**Figure 3-13** Clay % changes at Lytham. a) Upper intertidal site, b) mid-intertidal site & c) lower intertidal site (hashed zone represents optimum summer image acquisition period for ATM and CASI imagery).

Percentage clay at the upper field site at Lytham (Figure 3.13) shows a marked summer and winter profile (summer mean = 7.1% & 8.2% & winter mean = 4.6% & 4.2%). This indicates that fine-grained sediments are deposited upon the upper intertidal zone during the summer periods and are preferentially removed during the winter periods. However, sites two and three (Figures 3.13 b & c) show little of this seasonal variation within the percentage clay distribution. Both sites show only small deviation from the

mean (Site 2 mean grain size= 7.6% & Site 3 mean grain size= 1.6%), with little variation in the summer/winter means for the study period. The sudden increase in clay percentage at Site 3 at the end of the study period results from a covering of 'mud drape' across the site (approximately 5 cm thick). This 'mud drape' consisted of a fluid, unconsolidated mud layer that overlays a sandy bed and had been identified previously in the general locality of Site 3 and are often found after a large river flow event (>100 cumecs) prior to the sampling visit.

*Sediment elevation changes*

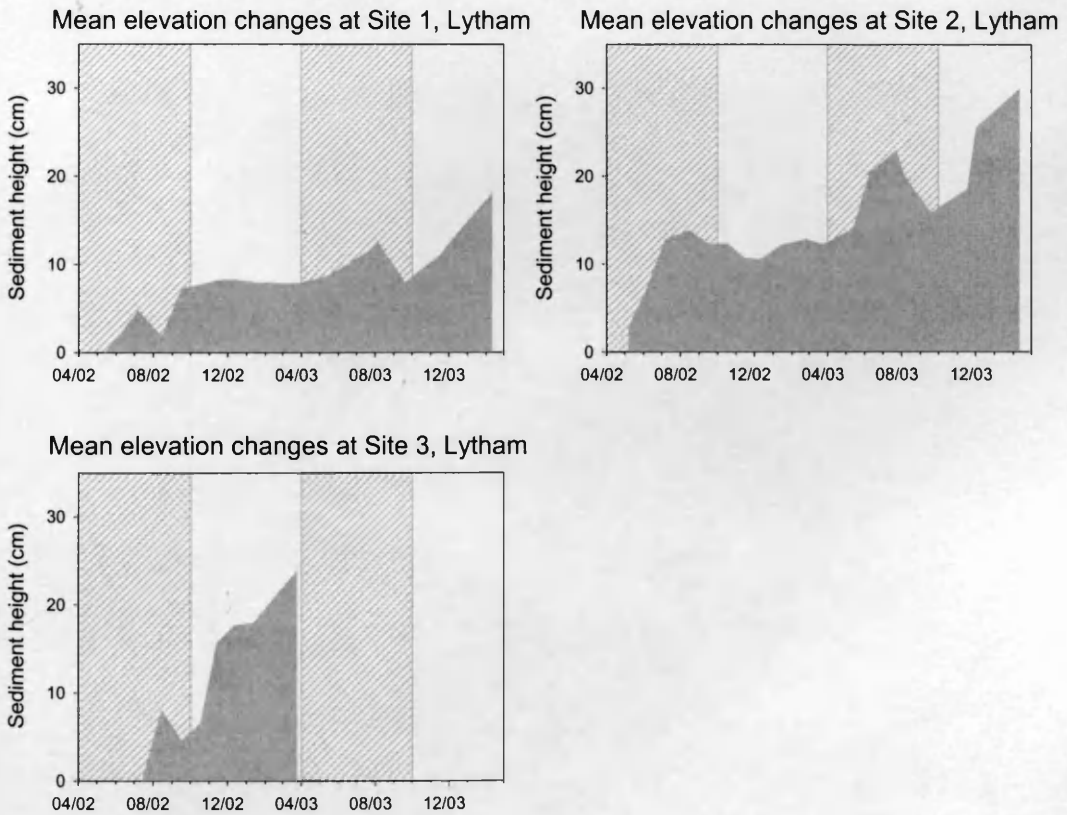


**Figure 3-14** Sediment surface elevation changes at Lytham a) Upper intertidal site, b) mid-intertidal site & c) lower intertidal site.

All sites at Lytham show a net accretion of sediments over the course of the two year sampling, although the amount of accumulation differs from site to site (Site 1= ~10 cm per annum, Site 2= ~15 cm per annum and Site 3= ~20 cm per annum). The shortened sampling period at Site 3 results from the removal/destruction of emplaced poles in the sediment surface. There is no apparent summer/winter profile for Site 1 within the survey results, opposing the results from the clay percentage.

### 3.4.2. Warton Bank

*Intertidal sediment properties: Clay*

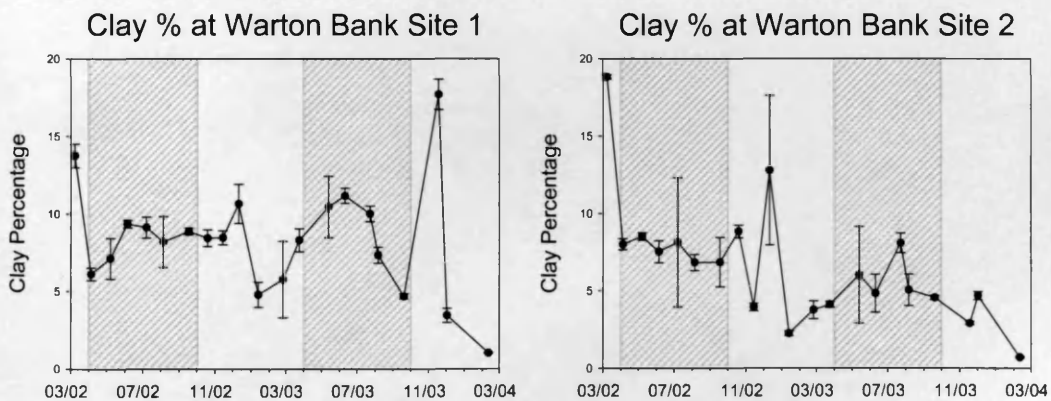
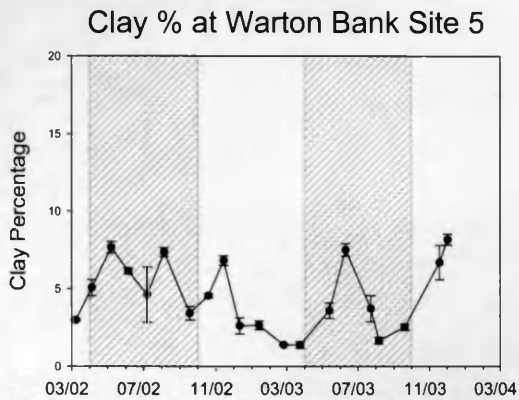
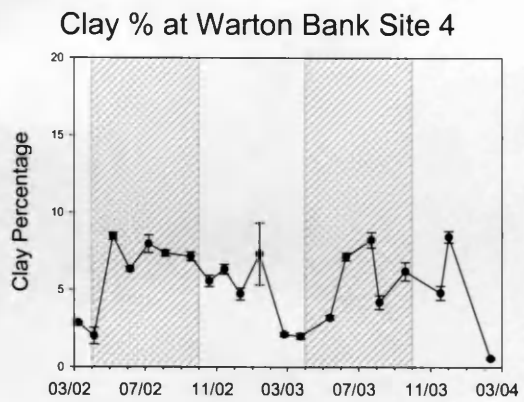
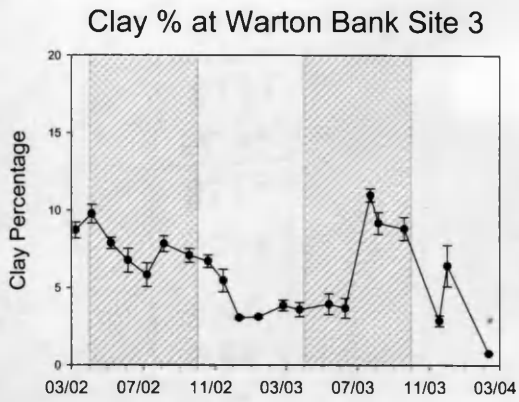


**Figure 3-15** Clay percentage changes at Warton Bank – upper intertidal zone

The survey results from Warton Bank can be split into two distinct zones due to the change in slope angle at the location. Sites 1 & 2 represent the upper intertidal zone (Figure 3.15), Sites 4 & 5 the lower intertidal zone and Site 3 the interface between the upper and lower intertidal zones (Figure 3.15).

There appears to be three separate emplacements of clay at Site 1, all occurring during the winter periods of the sampling period. Although there is little difference between the summer/winter means, the data ranges for the clay percentages span from 1.1% on the final sampling visit and 17.7% during the sample visit undertaken on the 18<sup>th</sup> November 2003. The mean values for Site 2 do show a reduced percentage of clay particles over the sampling period and the lowest percentage clay is found during the same month as Site 1. However, the maximum clay percentage sampled occurred during the initial site visit on the 8<sup>th</sup> March 2002.

Sites 3 and 4 (Figure 3.16) appear to show a seasonal variation in the mean distribution of clay percentage across the sites (Table 3.1), although this seasonal change is not replicated at Site 5. However, the (minimum and maximum) ranges appear to be similar for all three sites (Table 3.1).



	Site 3	site 4	Site 5
mean summer 2002	7.52	6.56	5.71
mean winter 2002/3	4.29	4.68	3.22
mean summer 2003	7.31	5.80	3.79
mean winter 2003/4	3.34	4.60	7.43
Minimum value	0.75	0.56	1.38
Maximum value	10.97	8.48	8.17

**Figure 3-16 & Table 3-1** Clay percentage changes at Warton Bank – lower intertidal section & Table 3.1 Mean summer/winter clay percentages

### *Sediment elevation changes*

The height elevation changes at Site 1 (Figure 3.17a) indicates a net loss of sediment on this section of the intertidal surface. This represents a loss of 7 cm of sediment per annum. Site 2 (Figure 3.17b) displays an eroded profile within the summer months and an accreting profile during the winter period. This results in net sediment erosion of 7 cm per annum over the monitoring period for the upper site at Warton.

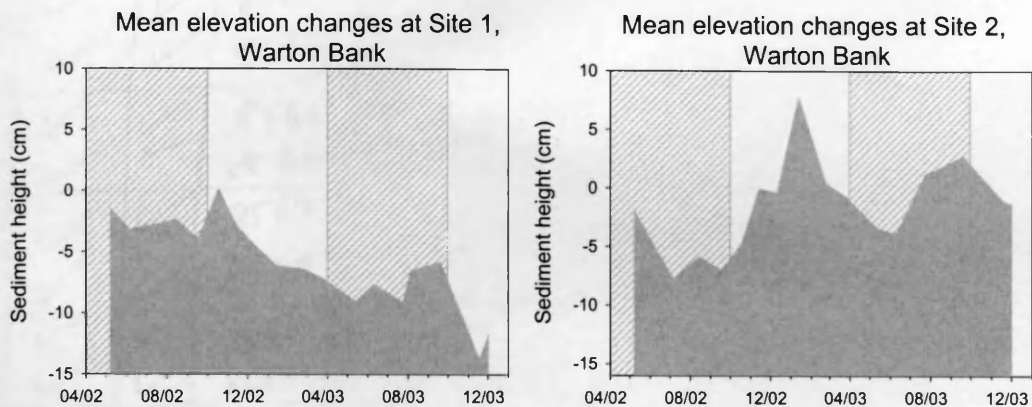


**Figure 3-17 a & b** Bed height elevation changes at sites 1 & 2, Warton Bank

Sites 3 - 5 (Figure 3.19 a, b & c) demonstrate a far more dynamic range of accretion/erosion throughout the monitoring program. They all demonstrated elevation ranges of approximately 40 cm, with large (>30 cm) monthly variations between some sampling visits. However, the net annual sediment budget for each of the Sites (3 -5) is positive, indicating that the sites are accreting over time. This accumulation cannot be directly attributed to the net erosion of sediment from the upper intertidal zone Sites (1-2), as the amount removed from the two sites does not equate to the quantity of sediment deposited over the lower intertidal area (Figure 3.18).



**Figure 3-18** Upper intertidal zone at Warton bank March 2002 showing erosional surface.

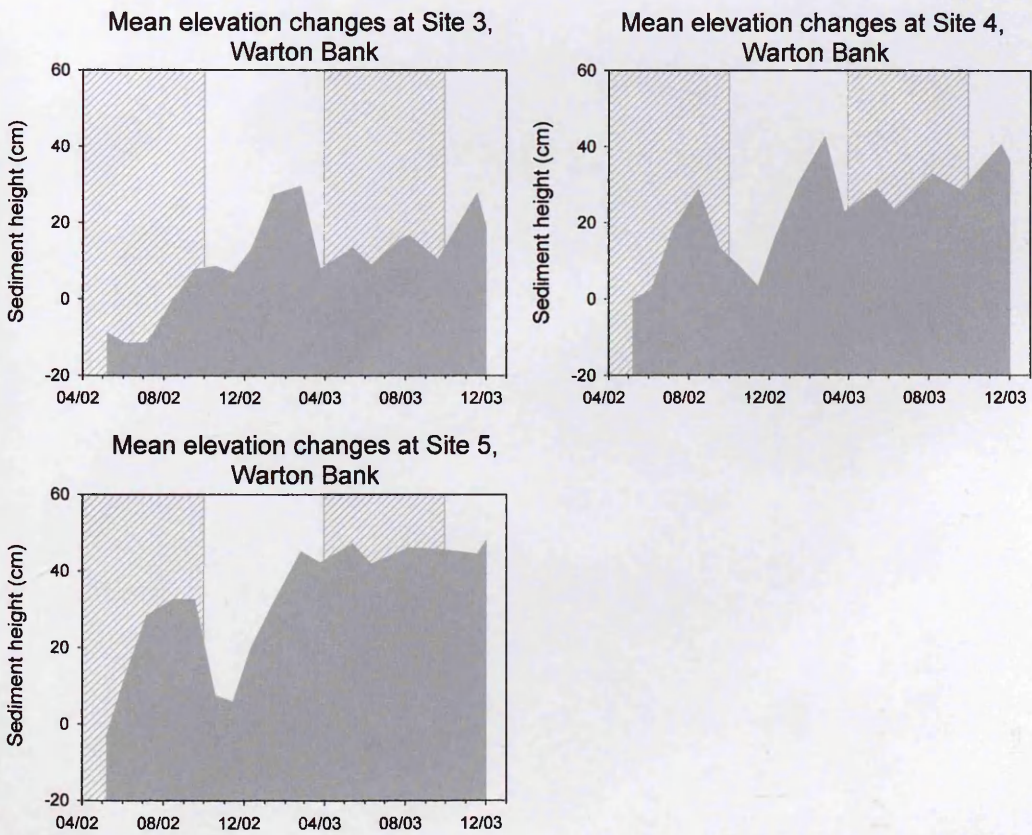


**Figure 3-19 a, b & c** Bed height elevation changes at sites 3 – 5, Warton Bank

### 3.4.3. Savick Brook

#### *Intertidal sediment properties: Clay*

Due the limited number of study visits to the site, there is a reduction in the temporal extent of the data set. The study period at this location was initiated in June 2003, continuing to the end of the study period in February 2004. The clay percentage distribution patterns indicate that the site can be split into two sections, the initially finer-grained upper intertidal zone (Figures 3.20 a & b) and the sandier lower intertidal surface (Figure 3.20 c). The upper two sites indicate that there is a steady, net loss of clay particles over the sampling period from approximately 12% in June 2003 to 1% by the end of the study period. However, the sandier lower intertidal zone at Site 3 demonstrated a low (mean 2%) clay concentration throughout the monitoring period.

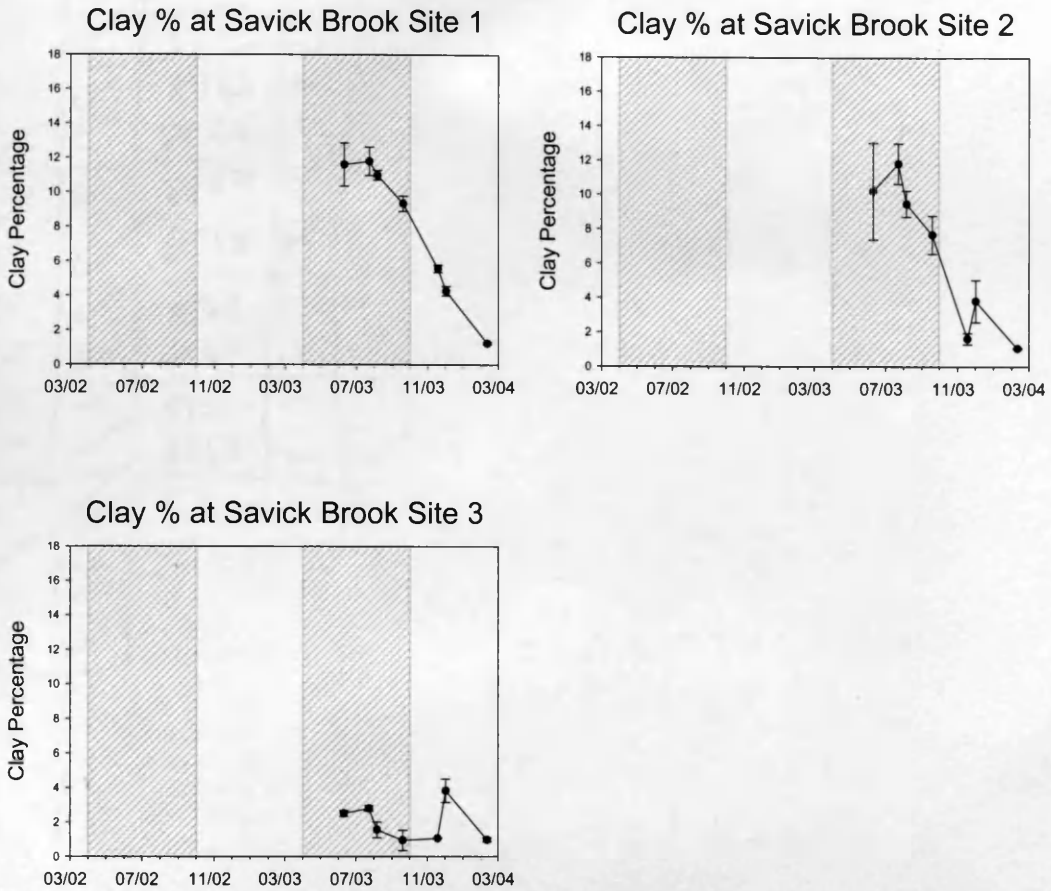


**Figure 3-20** a, b & c Clay percentage changes at Savick Brook

*Sediment elevation changes*

Although Figure 3.19 demonstrated the gradual decline in the percentage clay at the upper two sites at Savick Brook, height elevation changes at these two sites showed an overall net increase in the bed elevation of the upper intertidal surface (Figures 3.21 a & b). Site 3 (lower intertidal zone) shows a rapid increase (20cm) in the bed elevation in the initial 3 months of the survey (June to August 2003), after which there is a gradual decline back to the initial bed height elevation in November 2003. This appears to be true for both Sites 1 and 2, although the timing of the bed elevation maxima are a month later for both (November and September respectively), after which both sites appear to

undergo net bed sediment erosion. However, the increases in bed elevation changes must be attributed to the introduction of sand/silt to the sites, as there is a net reduction on the clay percentages at the upper sites.

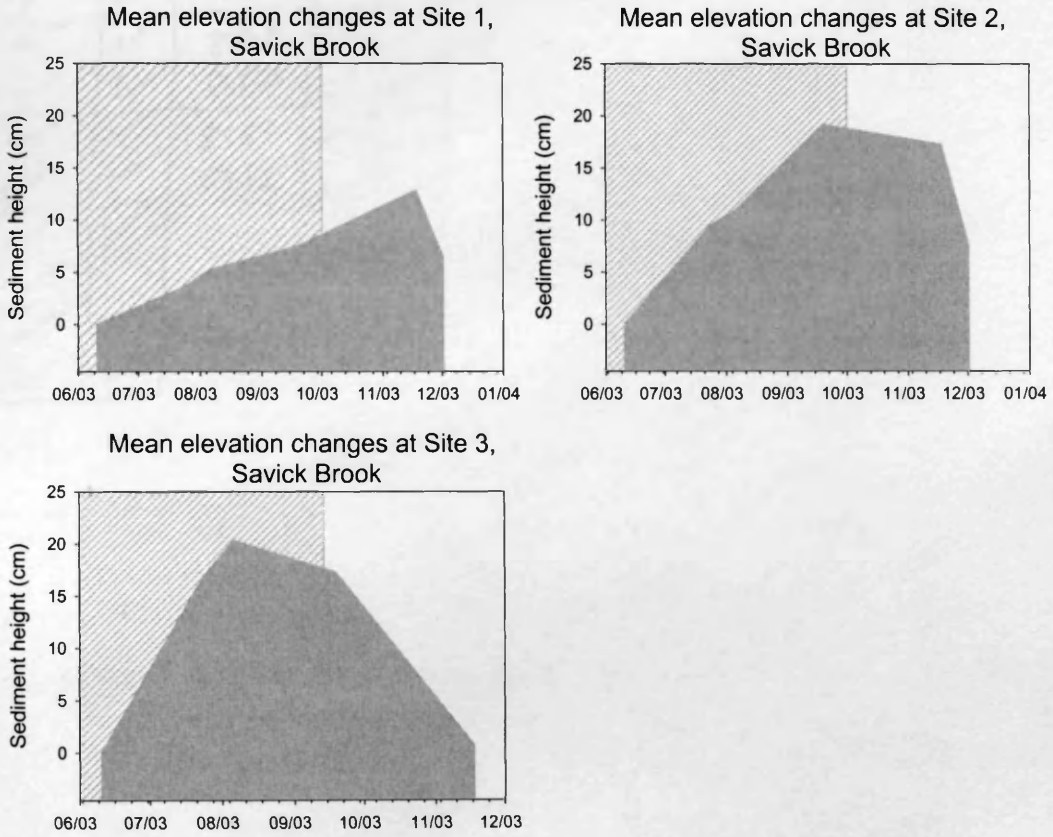
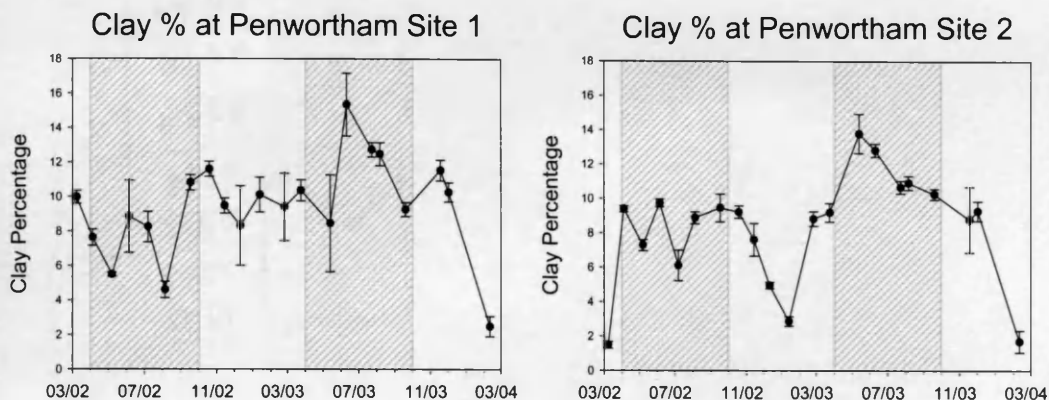


Figure 3-21 a, b & c Bed height elevation changes at Savick Brook

### 3.4.4. Penwortham Bridge

#### *Intertidal sediment properties: Clay*



**Figure 3-22 a & b** Clay percentages at Penwortham

Site 1 at Penwortham shows more homogeneity in clay percentages than the lower site. Site 2 does not appear to have any discernable seasonal patterns, with the mean clay percentages fluctuating between 2.5% and 15.3%. However, Site 2 does potentially have a summer/winter profile (summer mean = 8.5% & 11.7% and winter mean = 7.1% & 6.6%). The site does have a similar range of values (1.5% to 13.8%), but it is evident that there were four major events within the sampling period, creating large (>8%) variations in the data sets (March 2002, January 2003, May 2003 and February 2004).

#### *Sediment elevation changes*

The bed elevation height changes experienced at Penwortham are relatively small in comparison to those of the other study locations in the estuary. At the two study sites, a range of 10 cm throughout the whole two year study was measured.

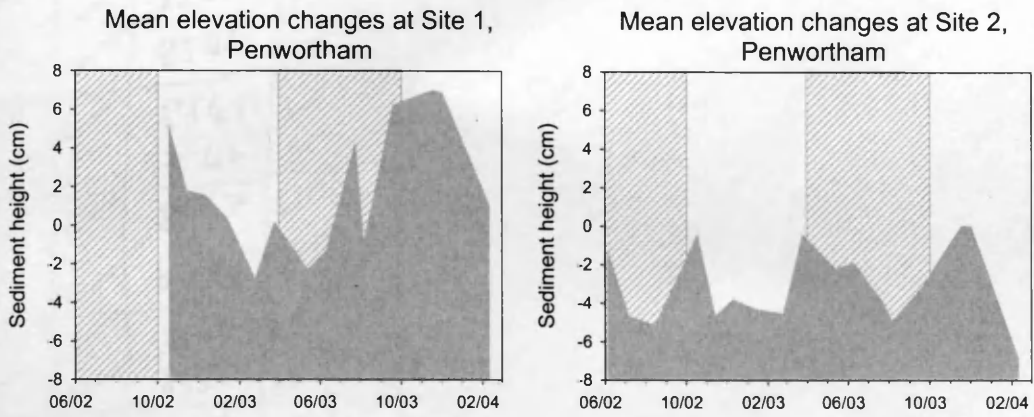


**Figure 3-23 a & b** Bed height changes at Penwortham

### 3.4.5. Analysis of alternating clay percentage on intertidal surface

Descriptive analysis of environmental data can provide important information on broad trends within ecological systems. Analysis of the monthly variable clay percentages, via Minitab<sup>®</sup>, showed that the data was not normally distributed, necessitating the conversion to natural log, where they became normally distributed. Therefore, the monthly variable clay percentage value for each site was plotted against the natural log of the various riverine discharge time periods and also varying mean tidal height maximum values prior to sampling visit (Table 3.2).

date	7 day mean pre visit (cumecs)	3day mean Q (cumecs)	2 day mean tidal height (m)	5 day mean tidal height (m)	1 day tide (m)
08/03/2002	44.25	50.73	7.33	8.28	7.18
04/04/2002	8.74	9.52	8.41	9.22	8.02
07/05/2002	37.40	12.35	6.74	7.02	6.88
05/06/2002	43.68	24.60	6.80	7.12	6.83
07/07/2002	47.57	49.28	7.29	7.12	7.44
05/08/2002	114.69	149.19	6.97	7.11	7.07
17/09/2002	16.56	6.22	7.20	7.7	7.27
19/10/2002	8.51	4.81	8.31	7.7	8.51
14/11/2002	84.06	66.33	7.17	7.7	7.16
11/12/2002	28.13	15.34	8.01	8.58	7.81
13/01/2003	14.49	13.00	7.15	7.57	7.09
24/02/2003	9.13	8.16	8.53	9.04	8.24
24/03/2003	7.84	6.75	9.09	9.47	8.8
13/05/2003	11.13	10.47	7.62	7.23	7.92
10/06/2003	7.63	9.03	7.45	7.49	7.56
23/07/2003	6.09	5.16	7.04	7.5	6.91
06/08/2003	18.67	5.98	8.02	8.34	7.86
19/09/2003	3.33	2.46	7.39	7.97	7.15
18/11/2003	35.25	47.60	7.15	7.62	7.05
02/12/2003	61.01	54.24	7.74	8.29	7.62
11/02/2004	109.12	48.23	7.54	8.8	8.24

**Table 3-2** Data used for best subset regression of clay percentage distribution in the Ribble Estuary

The comparison of the clay percentage and the mean riverine and tidal height patterns indicates that the upper estuary sampling sites at Penwortham are influenced most by the effects of alternating river discharge patterns (Table 3.3). The majority of the relationships between the variables are not significant, but this could be due to the relatively small sample set obtained at Penwortham. However, the sampling location at Warton does demonstrate correlation with the variables, although the site is split into two distinct zones by the regression analysis of the data sets. It is clear that the upper intertidal zone (Sites 1 – 3) are not significantly affected by the action of tidal flow or oscillating river discharge and that some other variable exhibits some greater control on the sediment distribution. Conversely the lower two sites appear to

be significantly effected by the complex interaction of riverine discharge and tidal height (Wb 4 clay = 47.7 - 0.209 log 7 Q - 20.2 log 5 day tide ( $r^2 = 0.608$ )), with tidal forces dominating the distribution pattern of clay particles at this locality.

Site	7 day Q (log)	3 day Q (log)	5 day tide (log)	2 day tide (log)	before tide (log)
Penwortham 1	<b>0.242</b>	0.187	0.035	0	0
Penwortham 2	0.187	0.173	0.01	0	0
Warton bank 1	0.11	0.18	0.03	0.05	0
Warton bank 2	0.06	0.04	0	0	0
Warton bank 3	0	0	0	0.04	0.08
Warton bank 4	0.09	0.019	<b>0.64</b>	<b>0.601</b>	<b>0.48</b>
Warton bank 5	<b>0.25</b>	<b>0.27</b>	<b>0.399</b>	<b>0.362</b>	<b>0.249</b>
Lytham 1	0.012	0	<b>0.266</b>	0.07	0
Lytham 2	0.033	0.04	0.07	0.08	0
Lytham 3	0.15	<b>0.214</b>	0.141	0.127	0.101

**Table 3-3** Correlation coefficients of changing clay % at all estuary sites. 7 day Q (log) is the natural log of the mean daily discharge of river flow (cumecs) for the preceding 7 days prior to sampling, 3 day Q (log) is three days mean discharge prior to sampling, 5 day tide (log) is the natural log of mean tidal maximum prior to sampling, 2 day tide log (as previous) and before tide is the tidal maximum prior to sampling. Bold numbers represent  $r^2$  values with a  $p$ -value <0.05.

Unfortunately the analysis of Lytham data does not demonstrate any significant relationships between the clay percentage distributions and mean tidal height and mean riverine discharge. This could be due to the large expansive area of the intertidal sediments at this point, which mitigates the effects of changing river discharge and tidal height conditions.

### **3.4.6. Wind speed and directional impacts on intertidal clay distribution**

Having undertaken the assessment of the distribution of the intertidal clays within the estuary in terms of changing tidal and riverine discharge conditions, it became obvious that there was another major source of disturbance within the estuarine system. After observing the destructive forces that storm wave activity can impact upon the outer estuary system (destruction of wooden jetty at Lytham St Anne's), an assessment of the effects of storminess was undertaken. However, there are no meteorological stations within the Ribble Estuary location, therefore the daily mean wind speed and directional data was obtained from the Met Office for RAF Ronaldsway, Isle of Man. The data (Appendix 1) were assessed and only the days with a wind direction between 225° and 315° were used within the study. Following this breakdown, the average wind speed and number of days of wind were taken for the seven days prior to the monthly sampling data and placed within the Minitab software for analysis with the above tidal and riverine data sets.

Assessing the best subsets (Table 3.4) suggests that the outer estuary are affected most by the number of days winds comes from a westerly direction, rather than the actual intensity of the wind speeds, conversely the upper estuary at Penwortham appears to be affected more by the actual average wind speeds than the number of days of wind from a westerly direction.

Location	Log 7Q	Log 3Q	log5 tide	log 2 tide	log day BF	No days wind	Ave wind speed	r2 (adj)
P1	X						X	17.4
P2	X		X				X	20.4
WB1						X		27.7
WB3					X		X	22.1
WB4			X			X		70.7
WB5		X	X			X		46
L1		X	X				X	42.3
L2	X		X			X		7.4
L3						X		22.2

**Table 3-4** Best subset analysis of the effects of average wind speed and direction in comparison to the effects of changing tidal heights and riverine discharge rates in respect to intertidal clay distribution. P = Penwortham, WB = Warton Bank and L = Lytham St Anne's field sampling locations.

It is clear from Table 3.4 that the best subset analysis generated at Warton Bank, is that of Site 4, obtaining a regression analysis of 70.7, which are more significant than the similar regression analysis displayed by Table 3.3.

### **3.4.7. Intertidal bed elevation changes.**

Following on from the best subset analysis of the clay distribution across the estuary, the same riverine discharge and tidal height averages were applied to the bed height elevation changes measured at Warton Bank and Lytham field sites. Unfortunately, due to limited sample data at Savick Brook and a discontinuous data record at Penwortham, these sites could not be used in the bed elevation analysis.

Analysis of the multivariate regression analysis indicated that there was little or no correlation between the riverine and tidal conditions and changes in bed height elevation. The second site at Warton Bank demonstrated a weak, but significant relationship with the combination of log 7 day discharge, log 2 day average tide height and previous tide high, with an  $r^2$  (adj) value of 31.6.

### **3.5. Specific activity and grain size associations**

#### **3.5.1. Relationship of radionuclide activity concentrations and clay percentage**

To assess the temporal stability of the clay percentage and  $^{137}\text{Cs}$  relationship demonstrated by Rainey (1999), a sequence of monthly coefficient of determinations were obtained by calculating the combined sediment sample data collected from all the estuary sites and the resultant  $r^2$  being extracted from that data sets. The coefficients of determination ( $r^2$ ) are then plotted against the daily averaged riverine discharge from the River Ribble (the contribution from the River Douglas was not included) (Figure 3.24). Descriptively the data shows that there was a low correlation between percentage clay and  $^{137}\text{Cs}$  during the initial 6 months of the project where there are relatively high riverine discharge events in close succession. However, between August 2002 and September 2002 there are noticeable absences of any >100 cumecs discharge events. The subsequent sampling visit on the 17<sup>th</sup> September 2002 produced a coefficient of determination of  $r^2=72.1$ . The ensuing three sampling visits coincided with an increased

frequency of >100 cumecs events in the estuary, that lead to a significant reduction in the regression analysis of the intertidal sediments. From December 2002 until October 2003, there appears to an improvement in the regression analysis of the percentage clay and  $^{137}\text{Cs}$  relationship. During this time frame there was only three >100 cumecs events in the river, with <50 cumecs events being the dominant river flow condition. However after November 2003, >100 cumecs events start to dominate the riverine flow conditions into the estuary, resulting in the reduction of the  $r^2$  value.

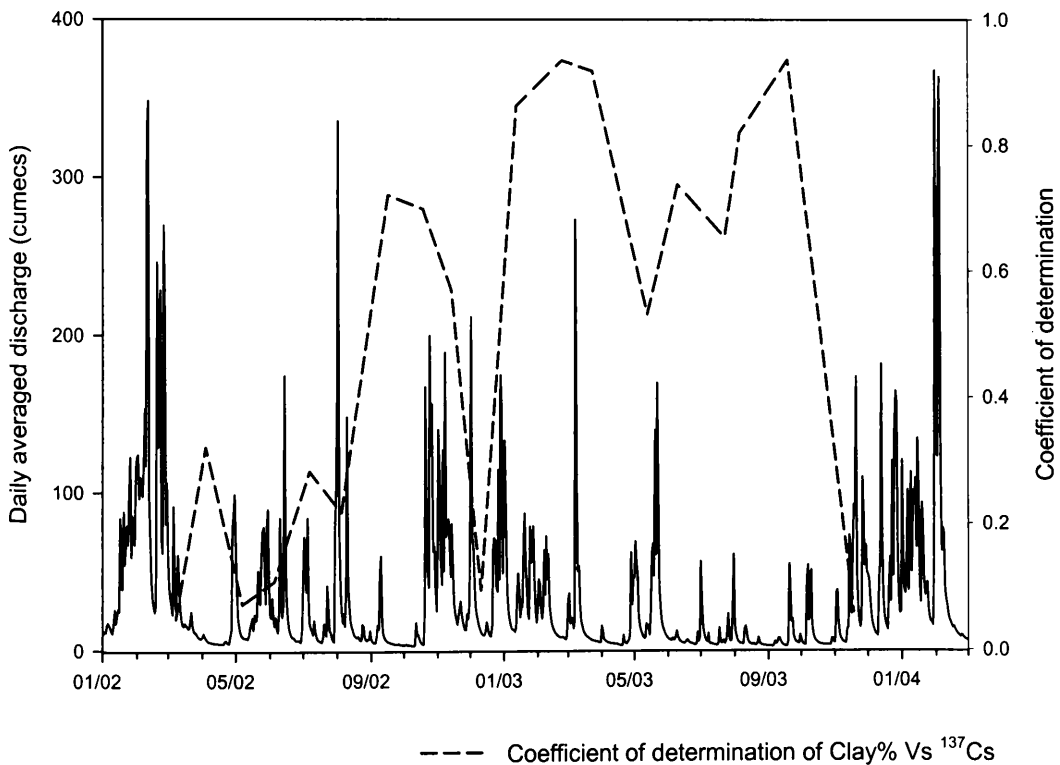


**Figure 3-24** Coefficient of determination analyses of percentage clay and  $^{137}\text{Cs}$  activity concentrations and daily averaged river discharge (cumecs).

Examination of the regression analysis of the percentage clay against  $^{137}\text{Cs}$  activity concentrations described above in Figure 3.24 shows broad trends in

the displacement of the sediments, relating to the river flow and tidal height averages. Therefore, the coefficient of determination was plotted against the same logged riverine and tidal flow conditions as described in section 3.5.5 and tabulated in Table 3.5.

Variables	r <sup>2</sup> (adj)	Mallows C-p	S
Log 7 day Q	45.1	-1.2	0.248
Log 3 day Q	41.5	-0.3	0.256
Log 7Q & log DBT	43.9	0.3	0.251
Log 7Q & log 2DT	43.2	0.4	0.252

**Table 3-5** Best subset analysis (r<sup>2</sup>) of percentage clay and <sup>137</sup>Cs regression against oscillating river and tidal conditions within the Ribble Estuary. 7 day Q (log) is the natural log of the mean daily discharge of river flow (cumecs) for the preceding 7 days prior to sampling, 3 day Q (log) is three days mean discharge prior to sampling, 5 day tide (log) is the natural log of mean tidal maximum prior to sampling, 2 day tide log (as previous).

$$\%clay/^{137}Csrelationship = 1.21 - 0.240 \log 7dayQ \quad \text{Equation 3-1}$$

Best subset regression analysis was used to differentiate between the effects of the four variables used to assess the coefficient of determination analysis of percentage clay against <sup>137</sup>Cs activity concentrations. The subsequent analysis (Table 3.5) shows that the best fitting regression model is generated by the natural log of the seven day averaged riverine discharge (log 7 day Q). This results in the equation described above (Equation 3.1), where the resultant r<sup>2</sup> value of 48.2 represents a significant. The prediction of the regression analysis of percentage clay and <sup>137</sup>Cs, with the resultant regression

model residuals being normally distributed, the fitted values are random, and there appears to be no outliers present within the resulting data (Appendix 2).

### **3.5.2. Intertidal sediment sample radionuclide inventory**

Concurrent with the collection of intertidal imagery two sets of sediment samples were collected from the intertidal sediment surface in September 2002 and October 2003. The first objective was to establish the relationship between Sellafield derived  $^{137}\text{Cs}$  and percentage clay within the surface sediments of the intertidal surface. It has been shown above that this relationship is not temporally stable for the entire estuary (section 3.6.2), however, for both the 2002 and 2003 samples there was a strong coefficient of determination for both ( $r^2 = 0.883$  and  $r^2 = 0.93$ ). Therefore, they could be both used to derive estimates for  $^{137}\text{Cs}$  activity concentrations from intertidal images of percentage clay deposition (chapter four).

Secondly, this data could be used to demonstrate the changing activity concentrations within the Ribble Estuary, in comparison with similar intertidal sampling carried out in 1995 and 1997 (Table 3.6) (Rainey, 1999).

The sediment sample data obtained during September 2002 (Equation 3.2) and October 2003 (Equation 3.3), were firstly placed within Minitab to apply a natural logarithm to the data points, so that the co-efficient of the resulting linear regressions could be compared to the 1995 (Equation 3.4) and 1997 (Equation 3.5) data plots (Rainey, 1999)

$$\ln^{137}\text{Cs} = 2.78 + 1.36(\ln \text{clay}) \quad \text{Equation 3-2 (1995)}$$

$$\ln^{137}\text{Cs} = 2.82 + 1.36(\ln \text{Clay}) \quad \text{Equation 3-3 (May 1997)}$$

$$\ln^{137}\text{Cs} = 2.19 + 1.21(\ln \text{Clay}) \quad \text{Equation 3-4 (September 2002)}$$

$$\ln^{137}\text{Cs} = 2.90 + 1.01(\ln \text{Clay}) \quad \text{Equation 3-5 (October 2003)}$$

These equations demonstrate how the percentage clay/<sup>137</sup>Cs relationship has changed over the eight year period, allowing comparisons to be made between the data sets (Table 3.6).

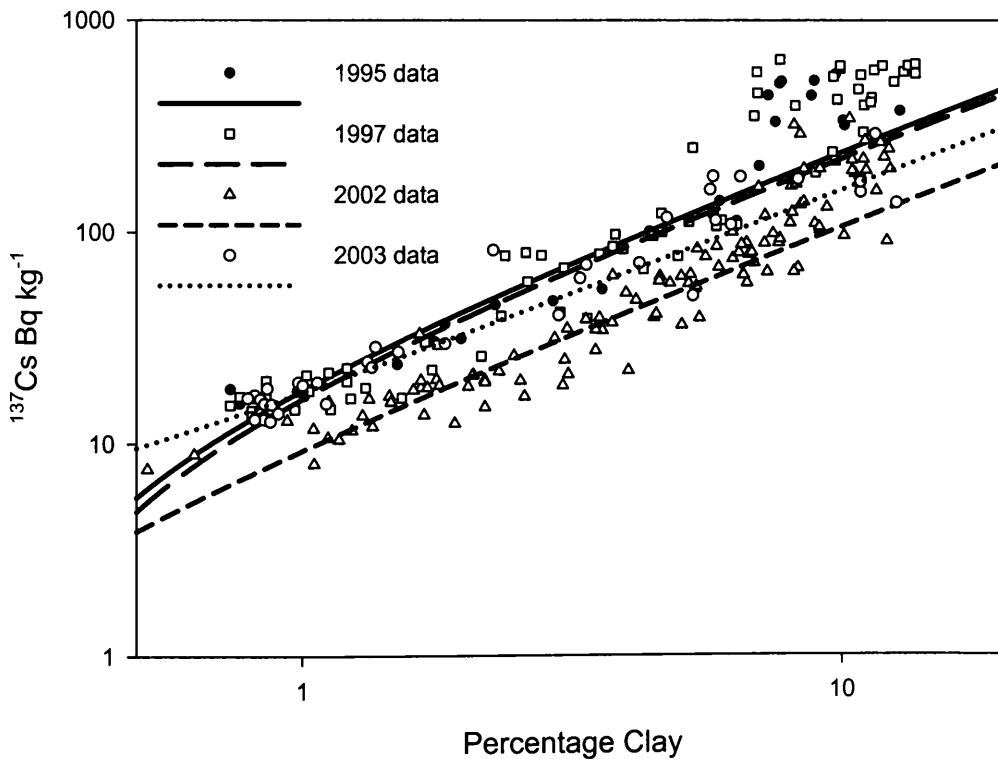


**Figure 3-25** Relationship between <sup>137</sup>Cs and percentage clay for 1995, 1997, 2002 and 2003.

It is evident that the resulting linear regression models are comparable (Figure 3.25), however, when they are used to calculate <sup>137</sup>Cs from differing clay

percentages (Table 3.6) it demonstrates that there are large differences in the two different data sets (1995 and 1997 – 2002 and 2003).

Table 3.6 demonstrates how the activity concentrations of the intertidal sediments have altered over the eight year time period. By comparing the 10 percent range for all of the samples, it demonstrates that the activity concentrations of the fine-grained clay particles have reduced by c. 64% for 2002 and c. 52% for the 2003 intertidal sediments.

Year	Month	% clay	<sup>137</sup> Cs	lower	upper
1995		1	16.1	13.9	18.6
		5	142.7	130	156.6
		10	365.5	321.4	415.5
1997	May	1	16.8	13.1	21.5
		5	152	129.9	177.9
		10	392.6	314.7	489.9
2002	September	1	8.9	7.8	10.2
		5	64.4	58.6	66.6
		10	144.3	131.4	158.5
2003	October	1	18.23	16.14	20.61
		5	92.6	82.7	103.8
		10	186.6	158.9	219.2

**Table 3-6** Inter-comparison of 1995, 1997, 2002 and 2003 intertidal sediments, assessing the relationship of percentage clay and <sup>137</sup>Cs.

### 3.5.3. Depth profiles of intertidal surface

The objective of this work was derived from observations gathered at Warton Bank during the initial field sampling visit. There had been considerable erosion of the upper intertidal bank, revealing a layered sediment structure and the resulting surface sediment samples showed very low activity concentrations. It was therefore decided to obtain cores from Warton Bank and Lytham, however, due to time limitations associated with obtaining

sediment cores at Warton Bank, no cores were obtained from Lytham. The aim in obtaining these cores was to determine the depth distribution of  $^{137}\text{Cs}$  at Warton Bank, allowing a greater understanding of the net intertidal sediment deposition rates at this location.

Intertidal sediment cores were obtained from three sites at Warton Bank in August 2002 using a 0.105 m diameter golf hole corer (ASTM 1990), which have been adapted to sample intact sediment cores with minimum disturbance and smearing to 45 cm depth (Tyler, 1994;1999). Each core was subdivided into 2 cm thick sections and placed within sealable plastic bags for laboratory analysis. The first core was extracted approximately 1 m from the saltmarsh edge (Figure 3.12), the second between sites 1 and 2 and the third core extracted between sites 2 and 3. Cores were not taken lower down the intertidal profile due to the high moisture content of the intertidal sediments at that time.

Figure 3.25 shows the depth distribution of  $^{137}\text{Cs}$  and the mean grain size for each 2 cm section of the core. The  $^{137}\text{Cs}$  profile for core 1 shows a relatively high activity concentration of  $213 \text{ Bq kg}^{-1}$ , which rapidly reduces to below detection limits at a depth of 8 cm. This pattern of relatively high surface  $^{137}\text{Cs}$  activity concentrations is also seen within cores two and three. However, the mean grain size distribution is not constant between the cores, with cores one and two having a smaller range of mean grain size (27 to 60  $\mu\text{m}$ ), whilst core three has a mean grain size range of 31 to 127  $\mu\text{m}$ .

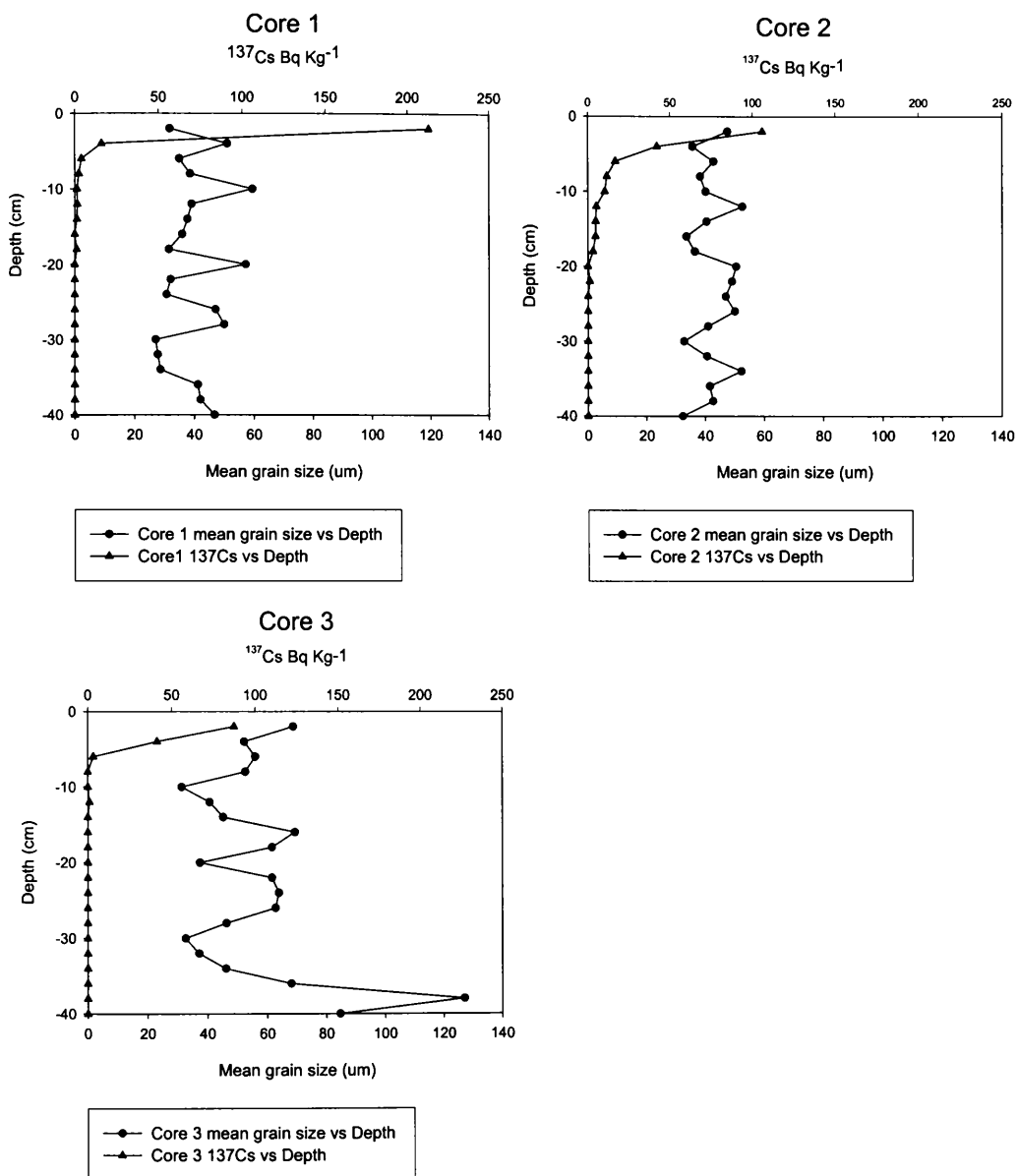


Figure 3-26 Core profiles taken at Warton Bank August 2002.

### 3.6. Discussion

#### 3.6.1. Lytham

Understanding the temporal distribution of clay particles is important due to their association with contaminant transport within estuarine environments.

The clay distribution patterns at Lytham indicate a seasonal pattern of

sediment deposition and removal, with the summer months experiencing a net increase in the clay particles and in the winter months the clay particles are removed. It is apparent from the height elevation changes that there is no removal of sediment at this time, therefore there must be either a preferential removal of the clay particles from the site or the deposition of more coarser sediments over the intertidal zone at Lytham during this period. It is also apparent from the evaluation of the data that river flow and tidal height variations have little or no effect upon the distribution of the clay particles on the intertidal surface in the upper/middle intertidal zones, so there must be other contributing factors controlling the sediment height and grain size distribution at these sites other than river flow and tidal cycles. These factors could be consolidation of surface sediments through drying of sediments after inundation. Wave effects may also play a part in the sorting of sediment grain size during high tide. This is enhanced during the high tide period where water levels remain static, allowing wave action to be focused on the upper intertidal zones for longer periods. However, due to the expansive nature of the upper and middle intertidal sites at Lytham, it may be possible that >50 cumecs river discharge events have little impact on the flow rates at these sites. One effect that could generate the seasonal pattern of clay distribution across the upper/middle intertidal sediment surface is that of increased wave/storm action during the winter months, which could have the consequence of preferentially removing the finer clay particles and depositing fresh coarser material over the intertidal surface, making the bed sediments coarser.

Conversely the clay content of the lower intertidal site at Lytham does appear to show a small positive and significant ( $r^2=0.222$ ) relationship to the 5 day averaged tidal height, indicating that this factor may be the more dominant cause in the variation of clay distribution over the lower intertidal sediment surface.

### **3.6.2. Warton Bank**

The upper intertidal zone at Warton Bank (Sites 1 & 2) had three deposits of large amounts of clay upon the intertidal surface sediments over the period of field sampling. These deposits all appear after the relatively high (>100 cumecs) river discharge events (Figure 3.24) and had the resulting effect of greatly reducing the regression value of clay percentage against  $^{137}\text{Cs}$  at those sampling periods. These three events all occurred when the underlying sediment had been exposed by severe erosion of the intertidal surface, which clearly shows that the deposited intertidal surface has been eroded back to the harder, more consolidated sedimentary layers beneath. These layers appear to pre-date the introduction of radionuclides into the environment (pre-1954 (Kircher & Ehlers, 1998)), which are correlated by the core data collected at Warton Bank during August 2002 (section 3.6.3). This demonstrates that the underlying sediments are not contaminated with any  $^{137}\text{Cs}$  at depth and indicates that these deposits were laid down prior to the presence of the nuclear industry and that the upper section of Warton bank are undergoing net erosion. This is validated by the bed elevation change results which signify that the upper intertidal surfaces at sites 1 & 2 at Warton are undergoing net erosion of sediment (Figure 3.17).

Sites 3 and 4 at Warton Bank appear to show a seasonal trend (Table 3.1) with increased clay content in the summer months, with a net reduction in the winter months, although this is not replicated at Site 5. From the regression analysis (Table 3.2) of the changing clay percentage, it is evident that Site 3 is affected by other variables than the tidal height and riverine flow conditions. Conversely the clay content at Site 4 does appear to show a positive relationship to tidal height conditions and not river discharge (Table 3.2). Site 5 appears to demonstrate that clay percentage distribution is a factor of both river discharge conditions and tidal height variations. All these results indicate that there is a very complex interaction of environmental variants (river discharge conditions and tidal height) over a relatively small section of intertidal sediments (approximately 20 m). However, the height elevation changes measured at these sites show a net accretion of sediment over the study period. This indicates that although there are varying environmental control factors operating over the lower intertidal surface at Warton Bank, the net trend for these factors is the deposition of sediments across the lower intertidal area.

### **3.6.3. Savick Brook**

The small number of sampling visits to Savick Brook means that little can be inferred about the annual change in clay percentages and bed elevation height changes, but it was important in gaining an understanding of the changing intertidal surface for the upper estuarine zone in relation to the ARS imagery. However, it is clear that coarser-grained material is prevalent across the site, making up a significant proportion of the bed sediment. This is

demonstrated by the two-fold decrease in the clay percentages at Sites 1 & 2 (Figure 3.20) and the paralleled increase in the bed elevation height changes (Figure 3.21).

#### **3.6.4. Penwortham Bridge**

Representing the riverine/saline interaction zone, Penwortham Bridge would be expected to have demonstrated greater interaction with varying riverine discharge conditions than the other three locations. However, this is not demonstrated by the analysis of the clay percentages (Table 3.3), but is confirmed within the percentage clay/<sup>137</sup>Cs regression analyses. The data show a very small positive  $r^2$  value in respect to the river discharge rates, which indicates that it is not the dominant environmental driver at the site, but there is a complex interaction between different drivers. Hypothetically this effect could be due to the tidal nature of the two sampling sites at Penwortham Bridge i.e. they will only be covered during normal or spring high tides. Therefore large river flow events that occur during periods of low water and during the neap tidal cycle may not actually inundate the site and alter the bed sediment properties.

The small changes in bed elevation at Penwortham Bridge established within this study may not be just a function of erosion/deposition events, but of the underlying bed surface. As Figure 3.11 shows, the large boulders that are present on the intertidal surface will effectively stop any further erosion of the bed sediments at this point. The small zone of salt marsh at the top of the

intertidal surface has undergone net loss over the last 5 years, which can be seen by the presence of compacted, bare mud surfaces at the top of the intertidal surface.

### **3.6.5. Activity concentrations of intertidal sediments.**

There is a good, positive coefficient of determination relationship between the clay percentage and the coupled  $^{137}\text{Cs}$  distribution patterns within the estuary as a function of the seven day average riverine discharge events on an annual basis. This relationship (based on the  $r^2$  value), demonstrates that 0.45 (Table 3.5) of the clay/ $^{137}\text{Cs}$  variation over the course of the two year field study, can be explained by the river discharge patterns seven days prior to the sampling visit. Conversely, there appears to be no direct relationships between bed elevation changes and changing tidal and river flow conditions. Therefore it could be assumed that there are other important environmental variants within the estuarine system that contribute to the temporal sediment stability of the intertidal surface. These could include exposure period (how long the sediments are allowed to dry for), microphytobenthos growth on the intertidal surface (EPS) and storm/wind induced wave action.

It has been demonstrated within section 3.6, that the activity concentrations within the Ribble Estuary are both temporally and spatially varied. The subsequent coefficient of determination analysis demonstrated that the percentage clay and  $^{137}\text{Cs}$  are also unstable during period of high riverine discharge events (>50 cumecs).

However, analysis of the sediment samples collect during ARS flights of the intertidal sediments indicate during those periods that the relationship were stable, allowing the production of  $^{137}\text{Cs}$  from clay percentage maps. The activity concentrations have been shown to have decreased since similar studies were undertaken in 1995 and 1997, in comparison to the 2002 and 2003 intertidal sediments. Table 3.6 demonstrates that the activity concentrations have dropped by between c. 64% and c. 52% for the 10% clay estimate. Clearly, there are processes within the estuary that are causing the activity concentrations of the intertidal sediments to be diluted over time. Mackenzie *et al.* (1997) estimated that the Irish Sea activity concentrations of  $^{137}\text{Cs}$  had an effective half life decay rate of 23 years, in response to resorption of  $^{137}\text{Cs}$  into the salt water. However, even this increased reduction in the activity decay rate would only account for c. 16.5% of the reduction between the 1997 and 2003 sampling periods. Therefore there are other processes that are leading to the dilution of the activity concentrations over the surface intertidal sediments within the Ribble Estuary.

### **3.6.6. Bed height elevation changes**

By assessing the maximum bed height elevation changes between monthly sampling visit it is possible to demonstrate the maximum, averaged daily depositional rates per site over the sites within the estuary. Table 3.7, shows that averaged daily depositional rates are up to 2.8 mm per day, which can be compared to the estimated quantitative depositional rates obtained from the application of time series remote sensing data in chapter five.

Site	mm per day	Month
Penwortham 1	2.4	June 2003
Penwortham 2	0.6	March 2003
Savick 1	0.4	October 2003
Savick 2	1.1	October 2003
Savick 3	1.9	October 2003
Warton 1	0.8	October 2003
Warton 2	1.2	December 2002
Warton 3	1.9	December 2002
Warton 4	1.9	December 2002
Warton 5	2.8	May 2002
Lytham 1	0.86	August 2002
Lytham 2	2.5	November 2003
Lytham 3	1.75	October 2002

**Table 3-7** Maximum, averaged daily depositional rates (mm per day) between sampling visits for all sites within the Ribble Estuary.

### 3.7. Conclusions

Amalgamating and assessing the intertidal sediment variations across the four sample locations within the Ribble Estuary requires the visualisation of how and what drives the sediments up and down the estuary. The process of tidal pumping will transport sediment in an up-stream direction and the episodic high riverine discharge events will lead to the removal of finer grained sediments in a downstream direction. However, the temporal timescales associated with each of these processes is important to understand the implications of sediment and associated contaminant transport pathways within the estuary.

The effects of wind action and associated wave action have been shown by Allen & Duffy (1998) to have significance on the bed elevation heights on the outer mudflats of the Severn Estuary, SW England. Although, there was no

direct simple or uniform way to estimate the temporal effects of wind and tides conditions on the bed sediment elevations of intertidal sediments, it is possible to identify trends and patterns on a number of spatial and temporal scales (Allen & Duffy, 1998). This has been demonstrated within the Ribble Estuary from the application of the meteorological data obtained for RAF Ronaldsway. It highlights the effects that storm induced winds and the associated wave action generated from these westerly winds (225-to-315°) has on the outer and middle estuarine zones within the Ribble Estuary. However, this wind data should be treated with caution due to the distance (c. 110 km) separating the measurement point (Isle of Man) and the Ribble Estuary and any possible localised phenomenon that may cause wave action to be altered or refracted upon experiencing the coastline at Lytham St Anne's.

Secondly, it has been shown from this intertidal study, that when an area undergoes a net loss of the clay fraction there is an inverse effect on the bed height elevation, which could indicate that there has been an emplacement of coarser material. This finding could have important implications for the mapping of the intertidal area with the use of ATM imagery, as zones of high clay content over the mid/lower sections of the intertidal area could represent zones of erosion and zones of accretion when covered in coarser sediments after high river flow events.

Thirdly, the results of the sediment core analysis on the upper intertidal sediments at Warton demonstrate that there are uncontaminated sediment

surfaces within the estuary itself, which would, if eroded, lead to a reduction in the clay/<sup>137</sup>Cs relationship within the estuary.

Fourthly, the calculation of the activity concentration change for <sup>137</sup>Cs since the 1997 field sampling in the Ribble Estuary has demonstrated that there has been a large reduction (c.52%) over the 6 year period to 2003. This indicates that there has been significant dilution of the activity concentrations of the intertidal surface sediments, which could be due to natural decay, introduction of uncontaminated catchment sediments and re-working of uncontaminated estuarine sediments, as demonstrated by the core profiles obtained at Warton Bank.

Finally, and perhaps, most importantly in terms of mapping of contaminant activity concentrations over the intertidal zones of the Ribble Estuary via the use of remote sensing, is the breakdown of the clay/<sup>137</sup>Cs relationship described by Rainey (1999). The implications for the mapping of the intertidal zone with ATM imagery could mean that individual intensive ground-truthing will be required for all imagery validation and calibration purposes. However, it has been demonstrated that the concomitant ground truthing associated with 2002 and 2003 intertidal imagery has very good coefficients of determination, allowing maps of intertidal clay to be used to generate maps of intertidal <sup>137</sup>Cs activity concentrations. Also it has been shown from the study of 1995, 1997, 2002 and 2003 image ground sampling points that the activity concentrations of the surface intertidal sediments are decreasing over time.

## 4 Mapping intertidal sediments and their associated radionuclides

### 4.1. Introduction

The intertidal zone of any macro-tidal estuarine system represents an area of sediment constant flux, coupled with a heterogeneous sediment grain size distribution. Within these macro-tidal estuaries, such as the Ribble Estuary (Beresford Hartwell *et al.*, 1995; Burton *et al.*, 1995; Assinder *et al.*, 1997; Rainey *et al.*, 2000; Van der Wal *et al.*, 2002; 2003) and the Severn Estuary (Allen & Duffy, 1998; O'Brien *et al.*, 2000), the distribution of intertidal sediments is highly variable, both spatially and temporally. The identification of the sediment types from point sampling provides assessments of the grain size distribution at specific locations, but crucially is isolated geographically. However, the application of ARS techniques has the potential for placing these point samples within the spatial context of the entire estuary system.

Rainey *et al.* (Rainey *et al.*, 2000; Rainey *et al.*, 2003) demonstrated the application of the Airborne Thematic Mapper (ATM), quantifying the spatial evidence of fine-grained sediments (<2  $\mu\text{m}$ ) over exposed intertidal sediment of the Ribble Estuary. This technique is based on the association of interstitial and surface moisture, which laboratory results (Rainey *et al.*, 2000) have shown to influence the spectral contrast between sediments of contrasting grain size. The ability of clay to retain significant volumes of moisture, unlike with sands and gravels, provides the opportunity to spectrally distinguish “muddy” sediment from coarser sediment following a period of exposure to drying conditions. Therefore, this technique will be further explored and the

temporal stability of the relationships associated with the reflectance imagery and the actual measured grain size will be assessed for two separate time periods. Having demonstrated that at times of image acquisition, good relationships exist between the percentage clay and  $^{137}\text{Cs}$ , this chapter explains the variation in  $^{137}\text{Cs}$  activity concentration dilution over time.

The ability to quantitatively map the clay concentrations within intertidal sediments provides a powerful opportunity of mapping particle reactive pollutants, including radionuclides over an estuary wide scale. It will be used within this chapter to provide answers for the first three hypotheses outlined within Section 2.7.

#### 4.2. Data acquisition

Flight line proposals	Proposed Number.	Obtained	Dates acquired	Useable data
Low tide flights 2002	4	1	02/09/2002	0
Low tide flights 2003	4	1	17/10/2003	1
Post-storm event flight	1	0	N/A	0
LiDAR flights 2003	2	2	Not delivered	0

**Table 4-1** Flight line requirements for intertidal sediment study, proposed, actually achieved and useable data.

Table 4.1 illustrates the planned flight acquisitions and the actual usable data delivered by NERC ARSF. The inclement weather of the 2002 field season resulted in only one flight being acquired. Unfortunately, this data series suffered a serious sensor malfunction that rendered the imagery unsuitable for the subsequent analysis, specifically losing the crucial moisture derivative bands in the Short-wave infrared (SWIR), as demonstrated by Rainey *et al.*

2000. Similar, inclement weather and obtaining of LiDAR flights reduced the 2003 image acquisition opportunities and resulted in the gathering of only one successful image in October 2003. Therefore, the imagery will be compared to the data obtained by Rainey (1999) in May 1997, allowing an inter-image comparison to be made and assessment of inter-annual distribution patterns of the intertidal tidal sediment within the entire estuarine intertidal environment.

Associated with these intertidal flights was the acquisition of LiDAR flights over the estuary, which were proposed to provide a vertical context for the intertidal sediment maps, showing the significant changes in bed elevation, and the bathymetric estimates for the inclusion with the flood and ebb events (Chapter Five). Data acquisition was achieved, but the subsequent imagery was not delivered by NERC ARSF and thus excluded from this study.

### **4.3. Ground truth data collection**

Concomitant with the ARS an intensive ground-truthing sampling survey was conducted over the exposed, drying intertidal sediments of the Ribble Estuary. During September 2002 data acquisition, two separate ground-truthing teams were used, one at Lytham St Anne's (Figure 4.1) and the second at Warton Bank (Figure 4.2). At the Lytham site, due to the spatial extent of the intertidal area at low tide, only two transect lines of 21 data points were used to collect ground truth data. However, at Warton Bank, with its relatively narrow intertidal area (~120 m) three transect lines of 16 data points were collected.

Each transect line was marked out at the beginning and end by a white reflectant marker board (1 m<sup>2</sup>), made from white plastic sheeting, which was used to locate the transect lines within the ATM imagery. At both sites sampling periodicity was shorter over the upper intertidal areas with the typical spacing at 5 m, gradually increasing in length between sample locations further down the transect line as the sediment surface became more homogenous, in terms of sediment grain size, from the saltmarsh edge.

During the October 2003 ATM image acquisition, logistics limited the sampling to the Warton Bank site. Three transect lines of 16 points were sampled, using similar white marker boards to mark the end of the transect lines. Surface sediment samples of <1 cm depth were obtained within a 1 m<sup>2</sup> area at each sampling point upon the intertidal sediment. All samples were collected and processed as described within section 3.3.3.



**Figure 4-1** Transect lines for Lytham St Anne's, 2<sup>nd</sup> September 2002, showing the two transect lines and the transect-end white marker boards.

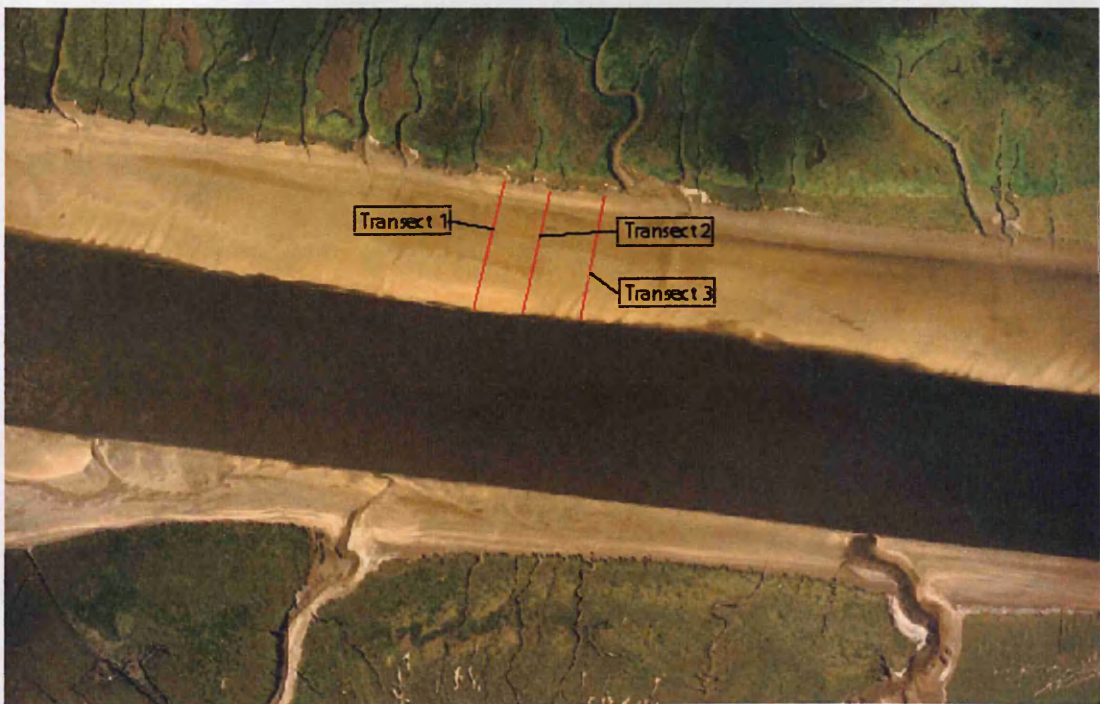


**Figure 4-2** Transect lines for Warton Bank, 2<sup>nd</sup> September 2002, showing the three transect lines.

### *Grain size*

Grain size measurements were obtained from surface sediment scrapes taken at regular intervals along the lateral extent of the intertidal surface. The same procedure for sediment collection and analysis was used as described in 3.4.2

### *Moisture content of intertidal sediment samples*

Following grain size analysis the sediment samples were placed within foil trays weighed and dried in ovens at approximately 80 °C within large vented ovens for roughly 48 hours until completely dried and moisture content calculated.

### *GPS survey*

During the acquisition of ground-truth data for the intertidal flights, two differential GPS systems were used to accurately plot the position of the ground sample locations and also to provide an accurate ground control point for the bed elevation study in Chapter Three. Initially a Magellan Promark XCM GPS system was used to provide nominal (<1 m) precision of the ground sampling points during the September 2002 flight. Accuracy was maintained by repeatedly measuring the location of a fixed, emplaced metal pole at the start of each survey. This data was processed through the MSTAR software and was also used for ground control data for the ARS imagery that was pre-processed by NERC ARSF as well as the LiDAR imagery. However, during the October 2003 flight a more accurate, real time DGPS system was used to capture this data. This system, the Leica DGPS System 300 with SR9500

DGPS receivers and AT302 antennae, provides accurate real time relative base station/rover accuracy of up to 2 cm under ideal conditions. Whilst the base stations were not fixed between surveys, the repeat surveys of the metal pole control point ensured the consistent accuracy of the points at Warton Bank. Therefore, with both of these systems it is possible to place the sampling location within a highly accurate (sub-meter) spatial context and consequently apply the transect data to the ARS imagery for calibration and validation purposes with confidence.

#### **4.4. Image analysis procedures**

##### **4.4.1. Image geocorrection**

Geocorrection of remote sensing imagery is an integral part of the image analysis procedure, allowing the accurate use of ground control points (GCP) for the calibration/validation of remote sensing imagery. Initially, the use of the automated NERC supplied AZGCORR program is utilised to quash any image warping associated with aircraft lateral rotation and pitch during image acquisition. This program incorporates GPS data obtained from the nose, tail and wingtips of the aircraft. However, it is apparent from subsequent image analysis that the AZGCORR program cannot remove the most extreme image warping and with the necessity of having the remote sensing imagery placed within a georectified context, ENVI's map warping tool was used to jointly rectify the imagery and place the image pixels within an ordnance survey grid reference. This was achieved initially by using a 1:25,000 Ordnance Survey<sup>®</sup> map to accurately place the image pixels within a spatial context and

subsequently applying an image to image geocorrection on the remaining imagery. Following the selection of these GCPs, the ENVI software was then used to apply a third order polynomial transformation, using the nearest neighbour method. The associated errors of the transformation or root mean square (RMS) error were kept below 3.0m, which is slightly greater than the 2m pixel size for the remote sensing imagery (Table 4.1). These RMS or residuals indicate the errors associated in both the east-west orientation, as well as the north-south direction and should be kept to a minimum (Atkin, 2000; Cambell, 2002). The greatest pixel error is associated with the pixels at the edges of the image swath, as they are furthest from the image centre and consequently experience the most image warping.

Image No.	a290021b
No. GCP's	128
RMS error	2.65

**Table 4-2** Details of manual geometric correction errors for October 2003 imagery

#### 4.4.2. Atmospheric correction

Atmospheric correction is an essential pre-processing step to remove the atmospheric and solar illumination signature from the ground surface reflectance (Richter *et al.*, 2002). The removal of such spectral effects ensures that the radiance values obtained through the ATM are representative of the actual spectral signal from the intertidal surface. The distortion created by atmospheric variables can be separated into three classes;

- i. Scattering: The unpredictable diffusion of radiation by particles in the atmosphere (Lillesand & Kiefer, 2000). It is caused by the

incoming radiation interacting with atmospheric molecules and other tiny particles in the atmosphere that are much smaller in diameter than the wavelength of the interacting radiation. This scattering effect is called the Rayleigh scatter and is the primary cause of haze within imagery (Lillesand & Kiefer, 2000) and can also occur in the absence of atmospheric impurities. The effects of such scattering in the atmosphere results in increased radiance values from ground targets.

- ii. Absorption: Occurs by atmospheric particles absorbing radiation (light). These absorbers, such as water vapour, tend to absorb electromagnetic energy in specific, known wavelengths and reduce the effective reflective energy from the ground target.
- iii. Refraction: Produced by the light energy reflecting from areas close to the observed pixel, due to the collision with atmospheric constituents, which deviate the light into the detector (Milovich *et al.*, 1995).

Numerous techniques exist to correct these atmospheric distortions, firstly the complex atmospheric modelling software which rely on intricate input parameters and detailed meteorological data i.e. LOWTRAN (Kneizys *et al.*, 1988), MODTRAN (Berk *et al.*, 1989; Jorgenson & Edlvang, 2000) and the 5S model (Zagolski *et al.*, 1995). Secondly, the histogram minimum method or dark pixel subtraction (Chavez, 1975), which is based on the reflectance of known or assumed surfaces in the images, which can yield the total amount of

atmospheric interference between the ground target and the detector. With this information it is then possible to apply a correction factor to the whole image to remove the effect of scattering. The third approach that can be used to remove atmospheric interference is the empirical line method, which utilizes the spectral signatures of at least two known reference objects within the scene that has strongly contrasting albedo (Perry *et al.*, 2000). The DN value of these pixels were then compared to the measured radiance of the target on the ground to estimate the degree of distortion that occurs from the signal passing through the atmosphere back to the sensor.

During this project there was no *in situ* reflectance of known ground targets or atmospheric measurements obtained from suitable ground targets. Therefore, a simple dark pixel or histogram minimum method was used to remove the effects of scattering or haze from the imagery, by utilizing the subtraction tool within the ENVI software package (Rainey *et al.*, 2003). Hence, the imagery is calibrated specifically to the estuary at the time of image acquisition and the correction factor could not be a general value for any subsequent image correction. However, if multiple images had been produced for this section of work, a series of ground reference points would have been utilized from the taxiways of the Warton Aerodrome. This process is fully discussed within section 5.4.2.

Atmospheric correction of each time series remote sensing imagery, obtained over the course of one tidal cycle, requires the use of ground calibration data to allow the application of a atmospheric correction. However, as the each

time series image will be normalised to the solar azimuth maximum for each image data series, there was no need to apply a complex atmospheric correction technique.

#### **4.4.3. Minimum noise fraction transformation (MNF)**

Rainey (1999) & Rainey *et al.* (2003) demonstrated that MNF transformations could be used to identify the spectral endmembers of the exposed, drying surface of the intertidal sediments of the Ribble Estuary. MNF transformation is an improved principal component analysis, developed by Green *et al.* (1988), which consists of two cascaded principal component transformations. This transformation process compresses the individual bands of the selected imagery and creates MNF bands of increasing noise fraction i.e. decreasing signal to noise ratios. This signal to noise relationship is expressed as an Eigenvalue and can be thus plotted to assess which MNF bands contain the most useable data. This tool is contained within the ENVI image analysis software, where the MNF transform function can be utilized to examine remote sensing imagery to identify the most important spectral bands.

#### **4.4.4. End member identification**

Selecting spectral endmembers is essential to the application of linear mixture modelling (section 4.3.5). To achieve this, the coherent MNF bands are plotted against each other in 2-dimensional scatterplots to examine the distribution of the data in feature space and the nature of the spectral endmembers (Rainey *et al.*, 2003). From the study of aerial photos and

concomitant *in situ* knowledge, it is then possible to identify the sources of these spectral endmembers identified by the two-dimensional scatterplots.

#### **4.4.5. Linear mixture modelling**

Linear mixture modelling originates from the Boardman (1989) linear mixture model. The ENVI software uses the derived endmembers from the MNF transformation to produce abundance images of the distribution of the selected endmember. However, the number of spectral endmembers used in linear unmixing must be less than or equal to one greater than the number of spectral dimensions in the data i.e. number of bands (Settle & Drake, 1993). The production of the eigenvalue plot allows the approximate dimensionality of each data set to be made. This plot permits the coherent MNF bands to be plotted within a two-dimensional scatter graph and thus identify the distinct spectral endmembers. The extreme pixels (<20) that make up the spectral endmember can then be cross referenced to inherent knowledge of the estuary and concomitant aerial photos to establish what each endmember represents within the image scene.

The selection of the endmembers from the two-dimensional scatter plots and the integration of them into the mixture modelling are discussed within Rainey *et al* (2003). The unmixed image produces a series of grey-scale images representing the spectral endmembers, with the abundance referring to each cover type (Rainey, 1999). However, due to the complexity of selecting appropriate endmembers from the image frame, the process requires

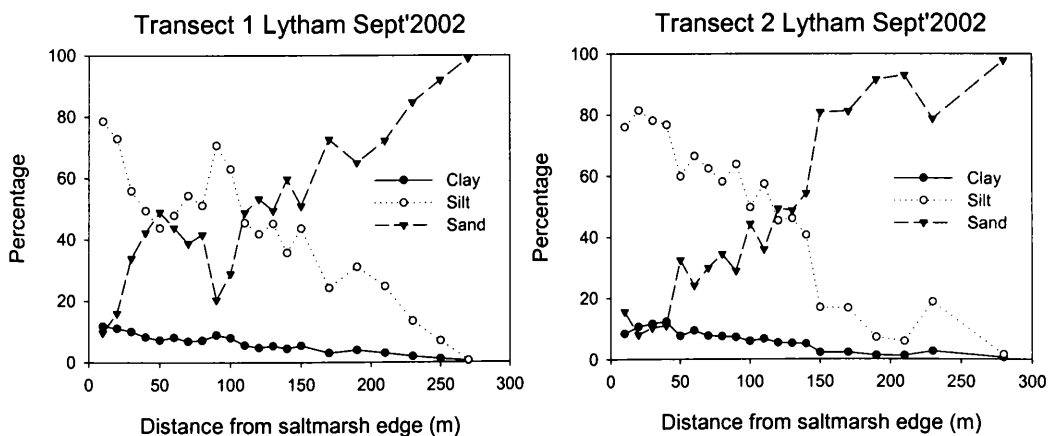
numerous iterations to achieve the correct spectral endmembers associated to the mud, sand, moisture and microphytobenthos endmembers.

## 4.5. Results

### 4.5.1. Transects on intertidal sediments

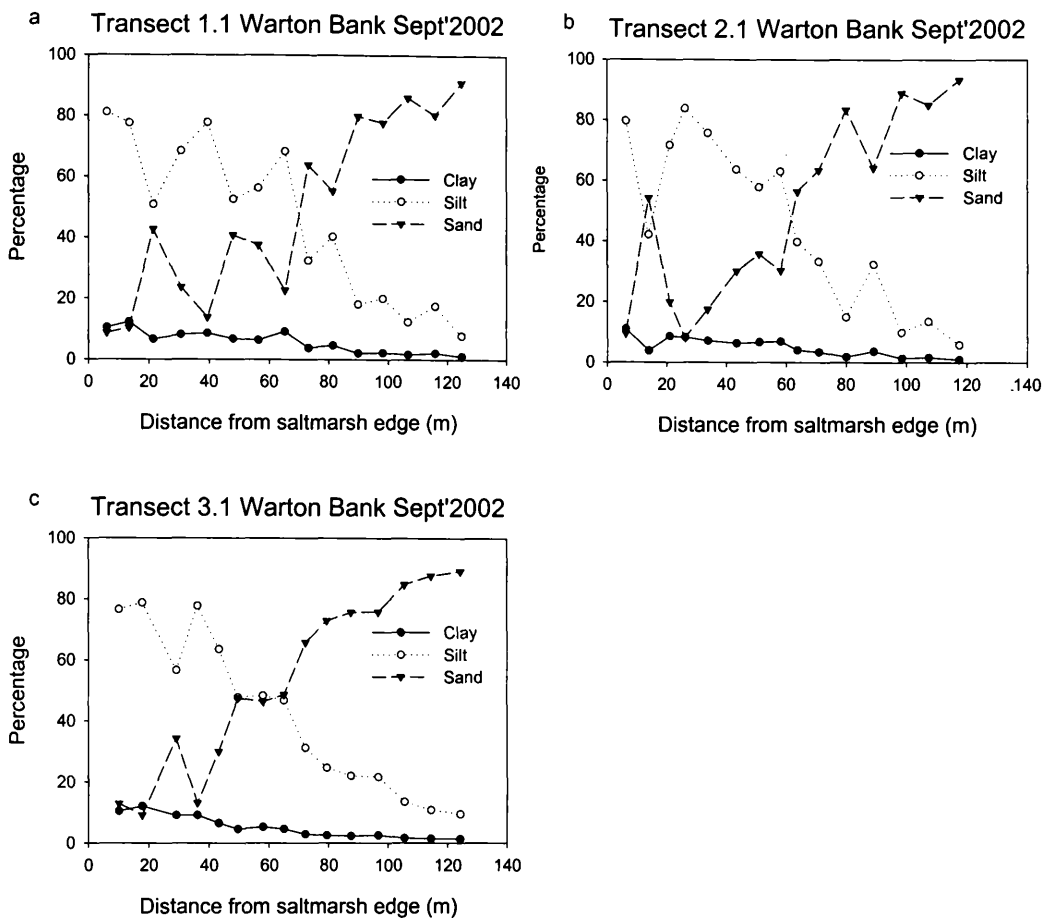
#### Grain size

Figure 4.3 shows the two separate transect lines obtained at Lytham St Anne's during the 2<sup>nd</sup> September 2002 image acquisition flight, which show a predominantly 'muddy' (<63  $\mu\text{m}$ ) profile within the first 100 metres of the saltmarsh edge, whilst the remaining section of the intertidal surface is dominated by sand. The clay percentage shows an expected maximum closest to the saltmarsh edge, with a very gradual decline towards the lower intertidal zone.



**Figure 4-3** Percentage change in grain size along the intertidal transects at Lytham St Anne's during the September 2002 field sampling.

The September 2002 transects obtained at Warton Bank (Figure 4.4) indicate that broadly, the overall pattern of grain size change is similar to that found along the Lytham transects. However, there appears to be a greater variability in the distribution of the sand and silts along the length of the transect lines. There also appears to be a marked decrease in the fine-grained material approximately 15 metres from the saltmarsh edge (Figure 4.4 b), where there is an opposing increase in the sand content of the site. This oscillation appears to be only temporary, as the next sampling point shows an increase in the percentage fines (<63  $\mu\text{m}$ ). Furthermore, the outer intertidal area appears to have a light covering of finer grained sediments that break up the expected increase in sand percentage cover over this area. This sedimentological feature may be attributed to the relatively low flow velocities experienced during the preceding seven days before the flight (8.07 cumecs) and the comparatively low mean tidal height during the previous 5 days (7.63 m). These two system drivers have been shown in Chapter Three to have an impact on the distribution of fine-grained sediment over the intertidal estuary. The most important control for sediment transport over the lower intertidal sites (3-5) Warton Bank, as identified within Chapter Three, should be that of the tidal height patterns, which coupled to relatively low river discharge conditions would result in tidal pumping of fine-grained material in an up-estuary direction. Therefore, the intertidal surface would be expected to show an increased covering of fine-grained sediment during the overflight period, which Figure 4.4 a, b & c does show.



**Figure 4-4 a, b & c** Percentage change in grain size along the intertidal transects at Warton Bank during the September 2002 field sampling.

Conversely within the October 2003 data set (Figure 4.5) there appears to be little fine-grained material over the lower intertidal area, with the percentage sand over 80% after approximately 50 metres from the saltmarsh edge. Although there also appears to be a sandier layer at about the 10 meter mark (from the saltmarsh edge), as seen in the September 2002 transects (Figure 4.4). Therefore, in the ATM imagery obtained for this time period a large expanse of sand should be expected to be seen over the lower intertidal zone, with two relatively narrow strips of mud (approximately 5 m each, in a north-south orientation), identified within the first 20 metres from the saltmarsh edge.

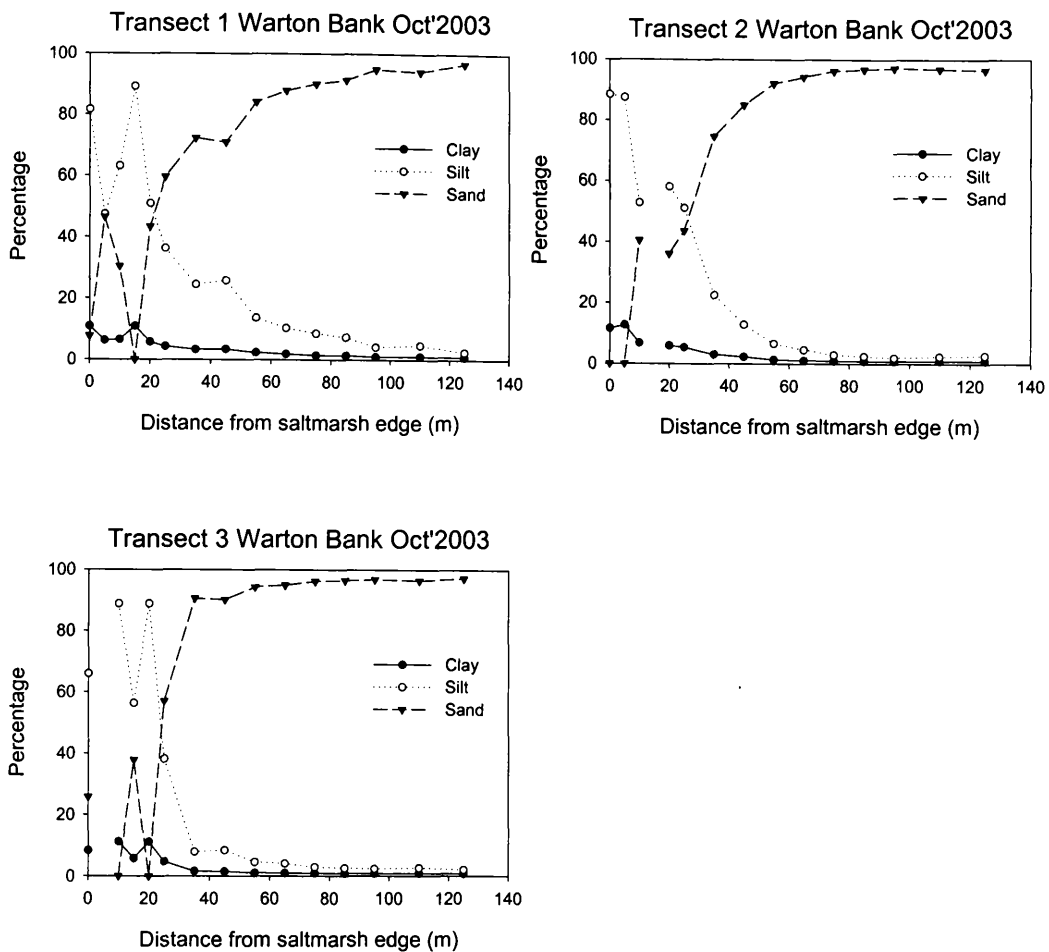


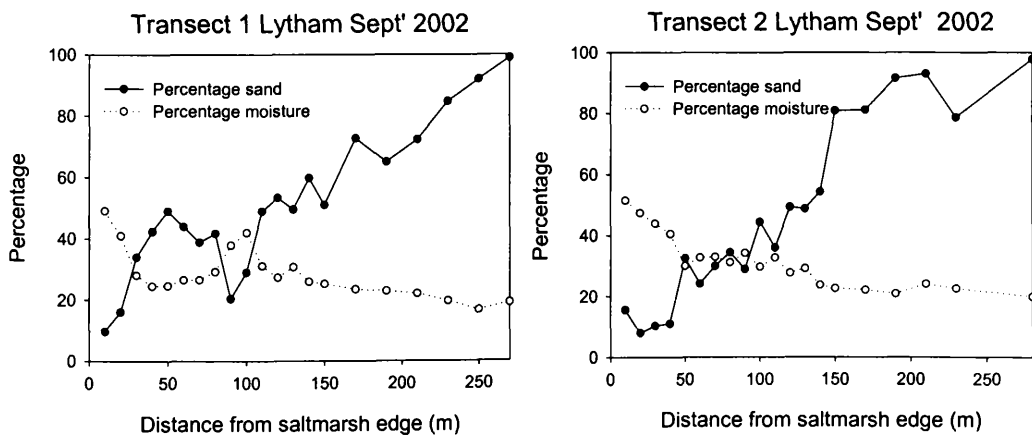
**Figure 4-5** Percentage change in grain size fractions along the intertidal transects at Warton Bank during the October 2003 field sampling.

The sand variability displayed within Figure 4.5 indicates that there is none of the spatial variability of the transect lines that is located within the September 2002 transect lines (Figure 4.4). This observation could be due to two possible reasons; either the variability is real and that it is a function of environmental effects or that it is an artefact of particle size measurement. The 2002 sediment transects samples were analysed using the Malvern Particle sizer based at Westlakes Research Institute, whilst the 2003 transects samples were assessed using the Coulter counter at the University of Stirling. It has been shown that an inter-laboratory comparison (section 3.3.3) for the

clay particles produces a very good correlation between the instrumentation. However, there were discrepancies in the sand content produced discrepancies in the inter-laboratory comparison in the comparison of the Malvern particle sizer and the Coulter counter, which is demonstrated in chapter three.

*Moisture content*

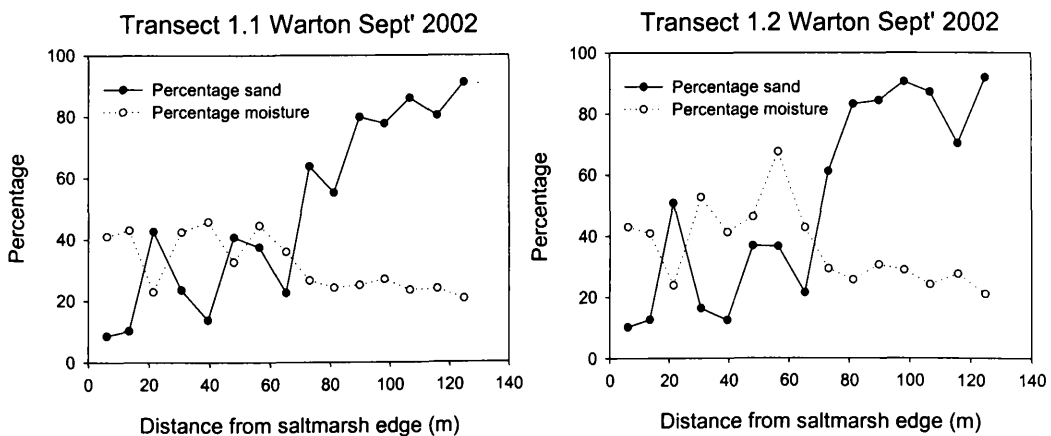
Figure 4.6 shows that the moisture content of the sediment samples which is related to the quantity of sand within each sample. This is due to the larger pore space of the sand grains, which can only retain smaller volumes of water. However, where there are higher percentage of finer grained sediments (<63  $\mu\text{m}$ ) the percentage of water that the sediments can retain increases due to increased pore water retention capacities. This is demonstrated in Figures 4.6, 4.7, 4.8 & 4.9, where a reduction in sand percentage reflects, in general, an increase in the amount of moisture that is retained within the sediment sample.



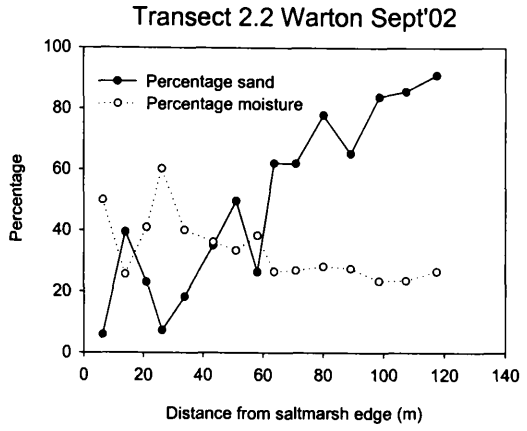
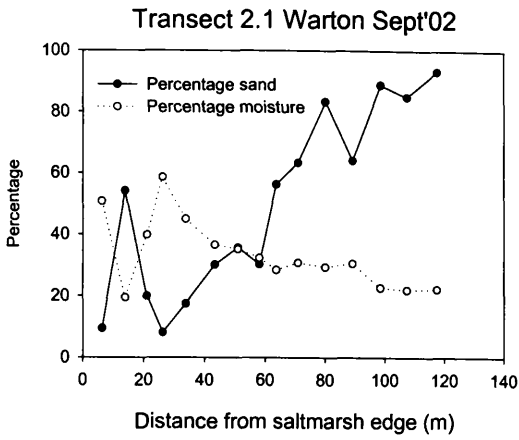
**Figure 4-6** Comparison of percentage sand to percentage moisture within the sediment samples (Lytham St Anne's September 2002)

Figure 4.6 shows that the moisture content of the sandier zone of the intertidal surface (starting approximately 100 m from the saltmarsh edge), does not appear to decrease over the length of the transect, even though the actual mean grain size for the sediments actually increases. The only zones where there was elevated moisture levels, is close to the saltmarsh edge, where the percentage of fine-grained sediments is higher than the subsequent sediments on the transect (Figure 4.3).

The two transect lines (Figures 4.7 & 4.8), show a marked difference to that of the Lytham transects, as they all show a much more spatially variable distribution pattern for the percentage sand and moisture content along the transects. It is clear however, that the moisture percentages are related to the percentage of sand at each site, as was the Lytham St Anne's transect lines. It is apparent that the actual moisture percentages in the surface sediments are roughly comparable to that of the Lytham transects, with the moisture proportion being between 20 % and 50 % for both sites.



**Figure 4-7** Comparison of percentage sand to percentage moisture within the sediment samples from transect 1.1 & 1.2 (Warton Bank, September 2002)



**Figure 4-8** Comparison of percentage sand to percentage moisture within the sediment samples from transect 2.1 & 2.2 (Warton Bank, September 2002)

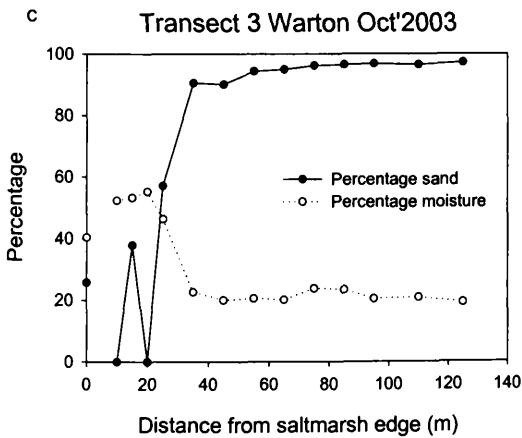
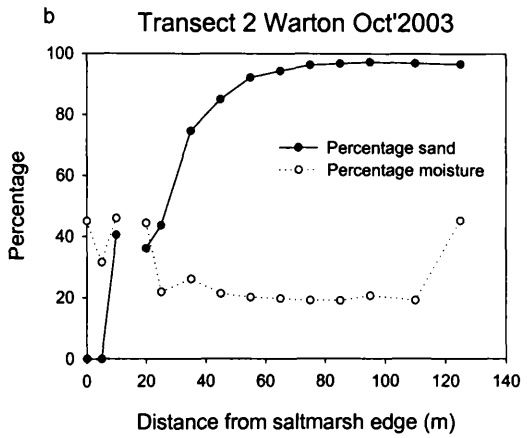
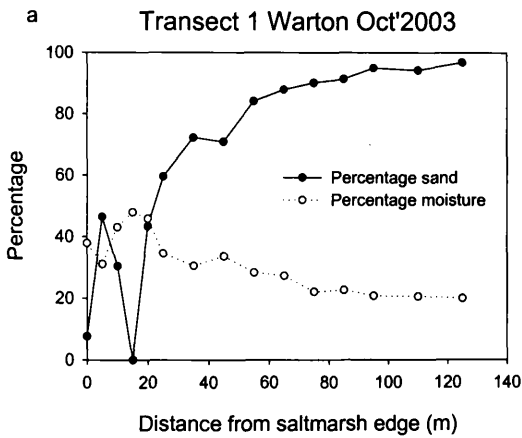


**Figure 4-9 a, b & c** Comparison of percentage sand to percentage moisture within the sediment samples from transect 1, 2 & 3 (Warton Bank, October 2003).

Comparatively, the percentage sand and moisture transects obtained for the 17<sup>th</sup> October 2003 flight (Figure 4.9 a, b & c) demonstrate a relatively smooth profile with a good fit between the sand distribution and the moisture percentage. It is clear that most of the changes in moisture content occurs during the first 40 metres of the transect lines.

### Radionuclide activity concentrations

Estimates for the activity concentrations for the surface sediments of the intertidal surface were gathered by the same procedure outlined in section 3.3.5. After gamma-counting the activity concentration data were compared to the percentage clay fraction at each site to identify any correlations between the two data sets (Figures 4.10 to 4.14).

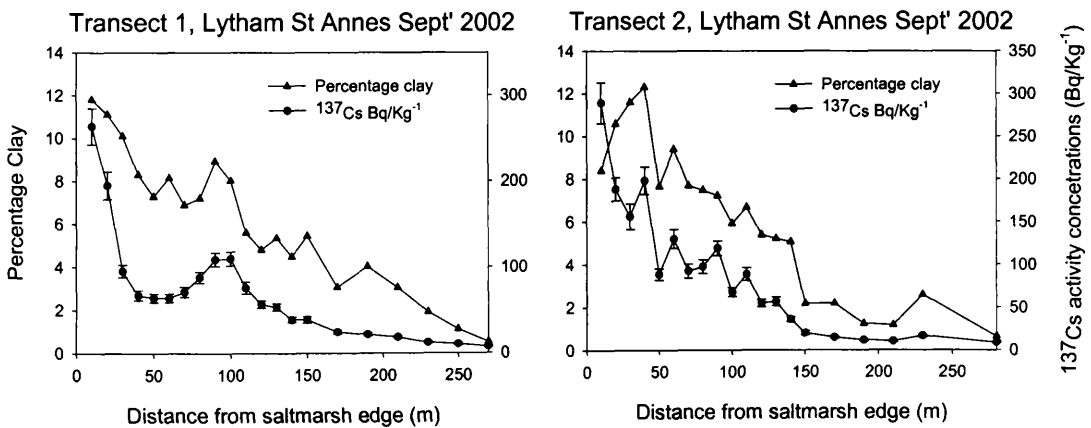


**Figure 4-10** Comparison of <sup>137</sup>Cs activity concentrations and clay percentages on transects from Lytham St Anne's, September 2002.

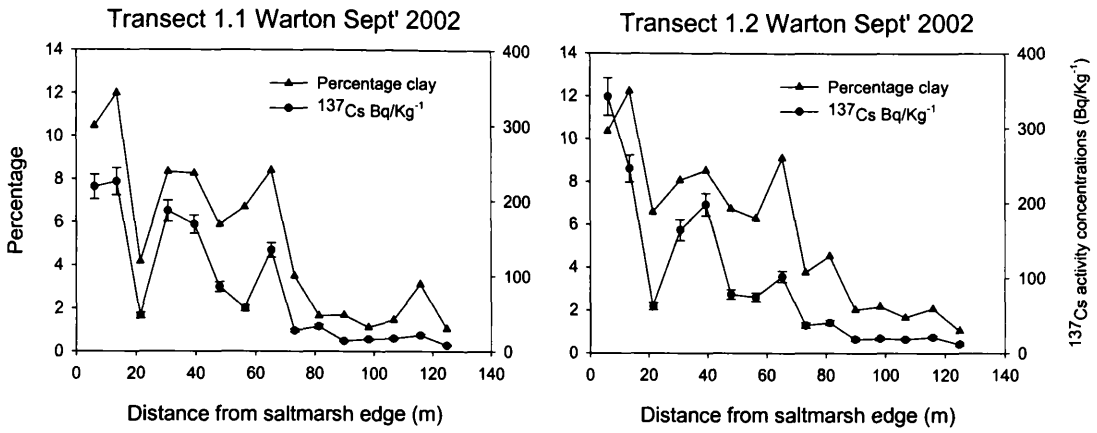


**Figure 4-11** Comparison of <sup>137</sup>Cs activity concentrations and clay percentages on transect lines 1.1 and 1.2 from Warton Bank, September 2002.

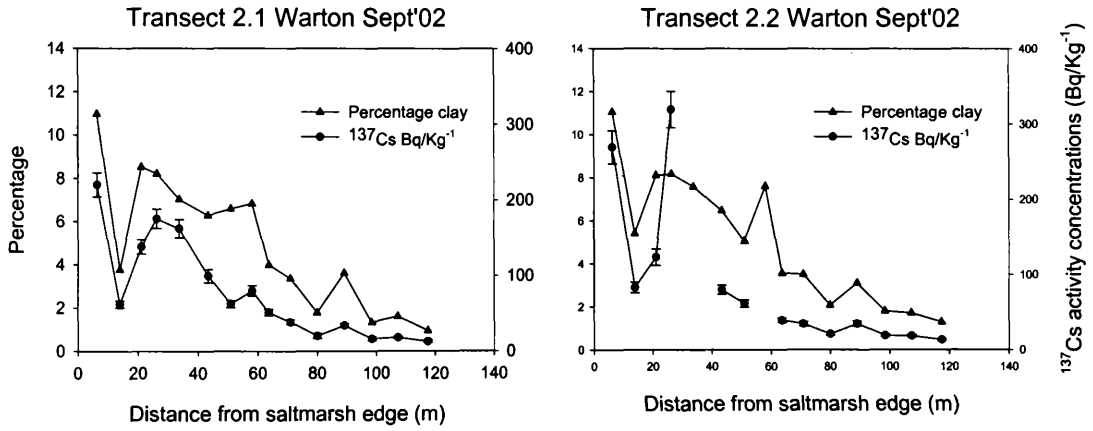


**Figure 4-12** Comparison of <sup>137</sup>Cs activity concentrations and clay percentages on transect lines 2.1 and 2.2 from Warton Bank, September 2002

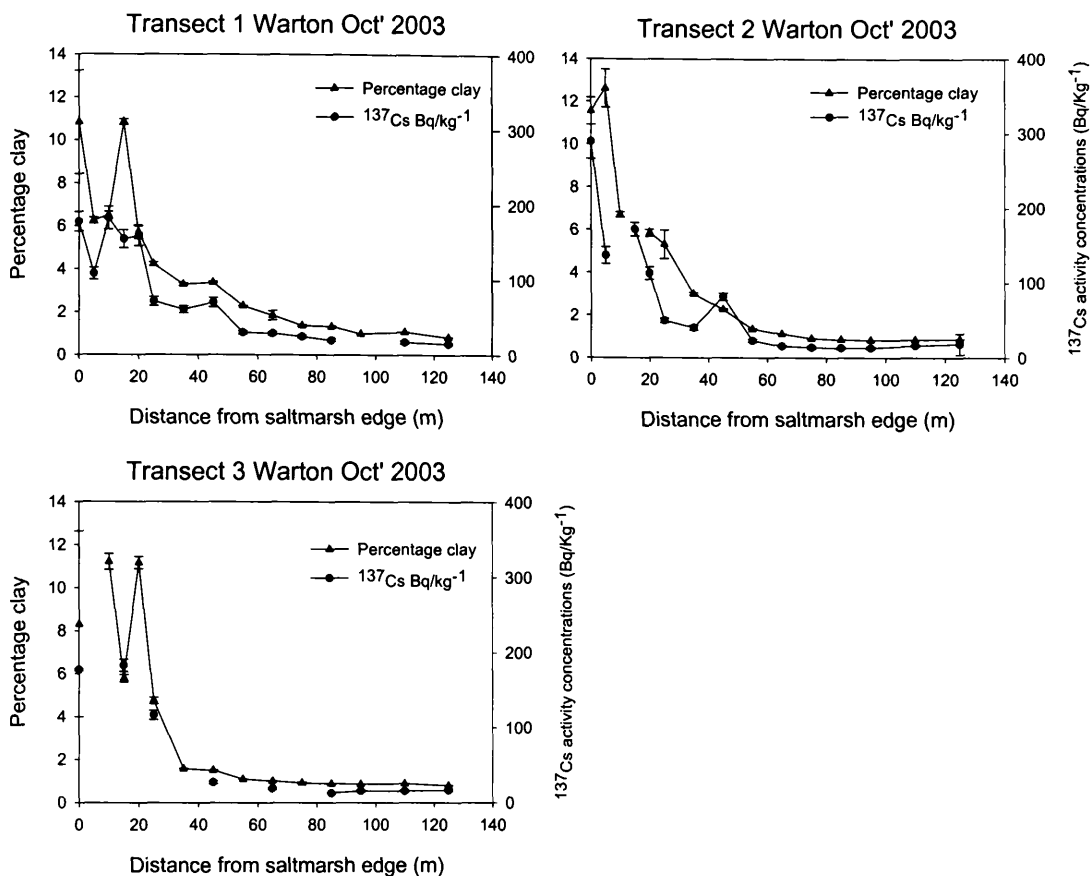


**Figure 4-13** Comparison of <sup>137</sup>Cs activity concentrations and clay percentages on transect lines 1, 2 & 3 at Warton Bank October 2003

Following on from the 2002 transect profiles of the clay/<sup>137</sup>Cs relationships, Figure 4.13 demonstrates that the relationship between the two components is still relatively stable for the October 2003 transects at Warton Bank. Therefore, the hypothesis that by quantifying the percentage clay draped over the intertidal surface the subsequent creation of a map of activity concentrations for <sup>137</sup>Cs can be produced for the intertidal sediments in the Ribble Estuary are true, as long as the samples are collected concomitantly with the ARS imagery.

Figure 3.25 demonstrates the linear relationship between clay percentage and  $^{137}\text{Cs}$  activity concentrations in the fine-grain sediments within the Ribble Estuary, for 1995, 1997, September 2002 and October 2003. The objective of deriving such relationships is the application of these associations to the ATM imagery of the estuary, which should allow the mapping of  $^{137}\text{Cs}$  activity concentrations. Consequently, the linear regression model for 2003 (Figure 3.25 & Equation 3.3) can be used to produce maps of activity concentrations for the intertidal sediments of the Ribble Estuary, from intertidal clay maps.

#### **4.5.2. 17<sup>th</sup> October 2003 intertidal ATM imagery**

##### *Image geocorrection*

A single ATM image was produced by the image registration software located within ENVI (section 4.3.1) allowing the pixels to be georectified and thus accurately assessed against the transect samples. The dark pixel subtraction method was applied to the imagery within the ENVI software,

#### **4.5.3. Endmember selection**

MNF transform of the October 2003 masked intertidal imagery used all 11 bands of the ATM imagery, which differed from Rainey *et al* (2003) as the thermal band was included within the principal component analysis. The inclusion of this extra band was found to have importance in the selection of the spectral endmembers that are displayed within figures 4.15 to 4.17.

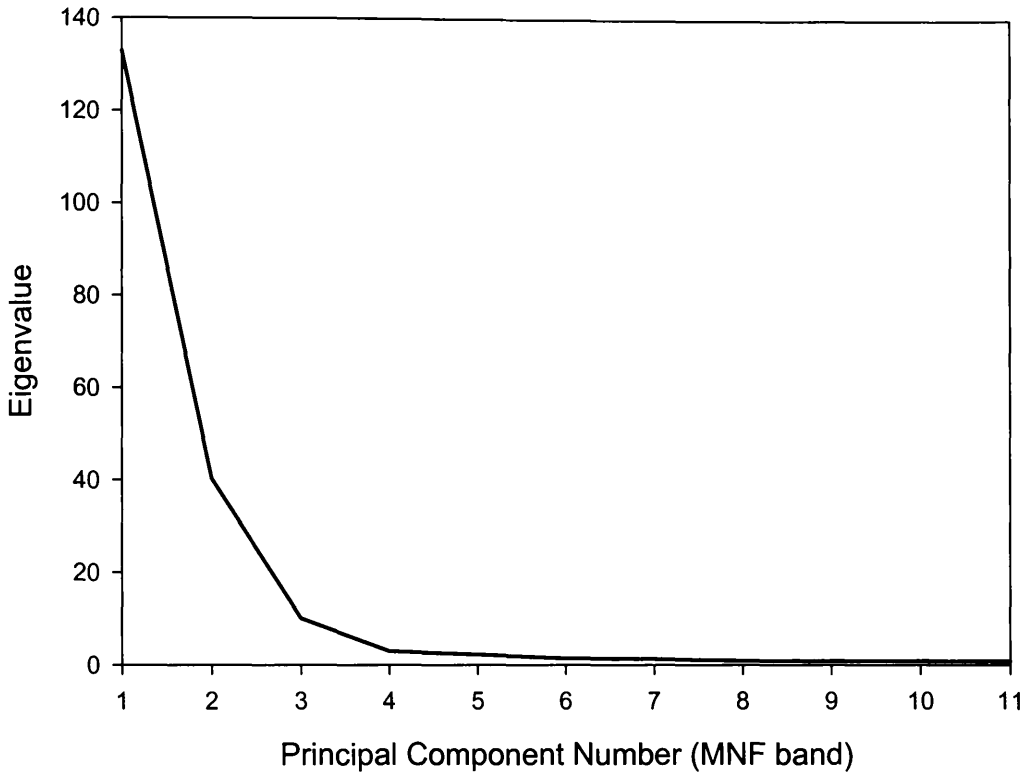


**Figure 4-14** Eigenvalue plot of MNF transformation of October 2003 ATM imager

The initial 4 bands were selected for use in the two-dimensional scatterplots, after analysis of the eigenvalue plot (Figure 4.14), which demonstrates that most of the variance is located within these bands. The remaining 7 bands were discarded from the linear mixing process. Identifying the spectral endmembers utilises these 4 bands with two-dimensional scatterplots and the imager window within ENVI to identify the spectral endmembers are located within the imagery. This allows these points to be cross-referenced with the locations detailed in the aerial photos taken during the course of the October 2003 flights. Once each endmember is identified from the four selected MNF bands (Figures 4.15 – 4.17), the selected endmembers are transferred into the linear mixture modelling sub-program within ENVI. Upon transferral the

program assesses the relative contribution in each endmember and produces separate abundance bands for each selected endmember. These endmember spectral bands can then be selected and assessed against the transects obtained during image acquisition. This process, however, requires numerous iterations to complete as the correct spectral endmember must be identified from within the spectral window.

Study of the MNF plots (Figures 4.15 – 4.17) demonstrates that the comparison of the separate bands generates some clearly distinct endmembers, whilst others are less readily defined. It can be seen that the sand and moisture endmembers generates a distinct plot, whilst the mud and microphytobenthos plots are more ambiguous when comparing MNF 2 & 3 (Figure 4.16)

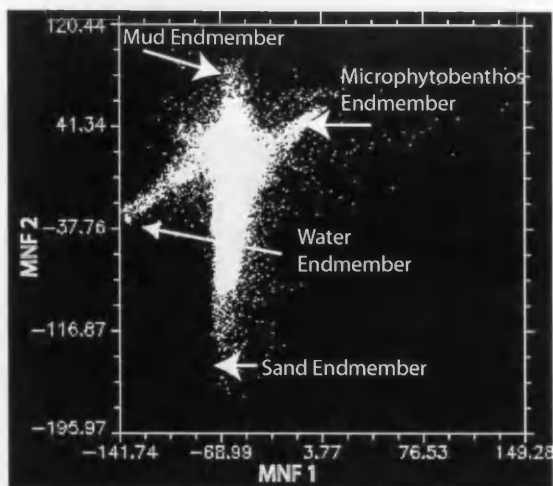


Figure 4-15 2D scatterplot of MNF band 1 vs. MNF band 2 (Oct'2003)

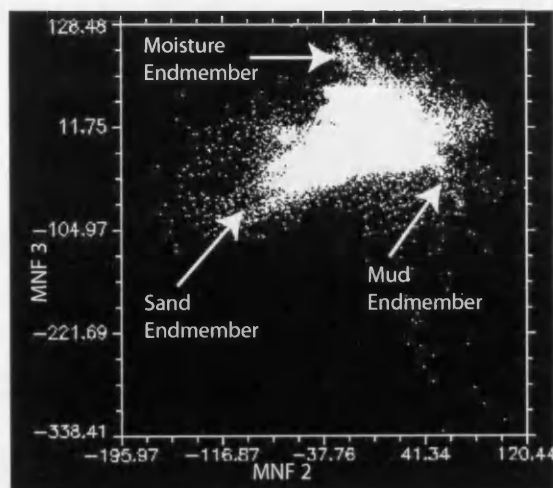


Figure 4-16 2D scatterplot of MNF band 2 vs. MNF band 3 (Oct'2003)

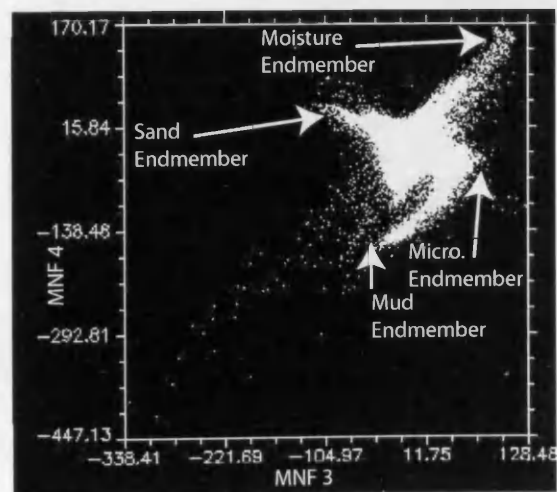


Figure 4-17 2D scatterplot of MNF band 3 vs. MNF band 4 (Oct'2003)

#### 4.5.4. Distribution of intertidal sediments

Following the identification of the spectral endmembers of the MNF transformation bands (Figures 4.15 to 4.17) and the application of the linear mixture modelling, the resultant image transects were obtained from the mud abundance and microphytobenthos end member images. Image transects were obtained and compared to the point sample measurements obtained simultaneously with the ATM imagery. This generates the empirical relationship described below (Equation 4.1) ( $r^2 = 0.828$ ,  $p < 0.001$ ) (Appendix 3).

$$\%Clay = \exp(-0.856 + 10.7MudAbundance + 0.24Microphytobenthos) \quad \text{Equation 4-1}$$

The subsequent mud abundance transect data generated from the linear mixture modelling does not directly identify the surface intertidal clay percentages; nonetheless it can be utilized to calculate the relative abundance of the clay after spectral unmixing. The above empirical relationship is based on three sampled concomitant transects obtained from Warton Bank during the course of the over flight. The resulting clay distribution (Figure 4.18) demonstrates that the spatial cover of clay over the intertidal sediments is visually less than demonstrated by Rainey *et al.* (2003) (Figure 4.20), which was obtained on the 30<sup>th</sup> May 1997.

However, microphytobenthos does appear visually within the aerial photos obtained simultaneously within the ATM imagery, which Rainey *et al.* (2003) showed to have the effect of generating underestimates of mud abundance over the intertidal surface.

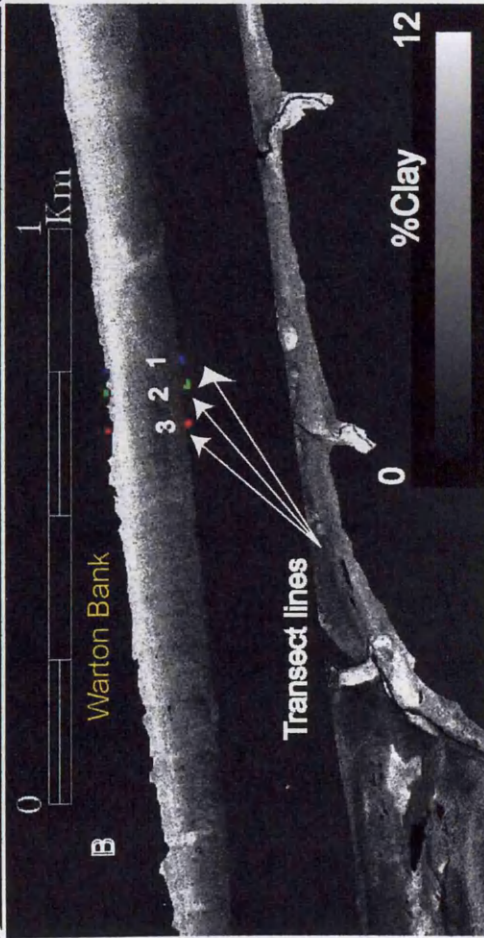
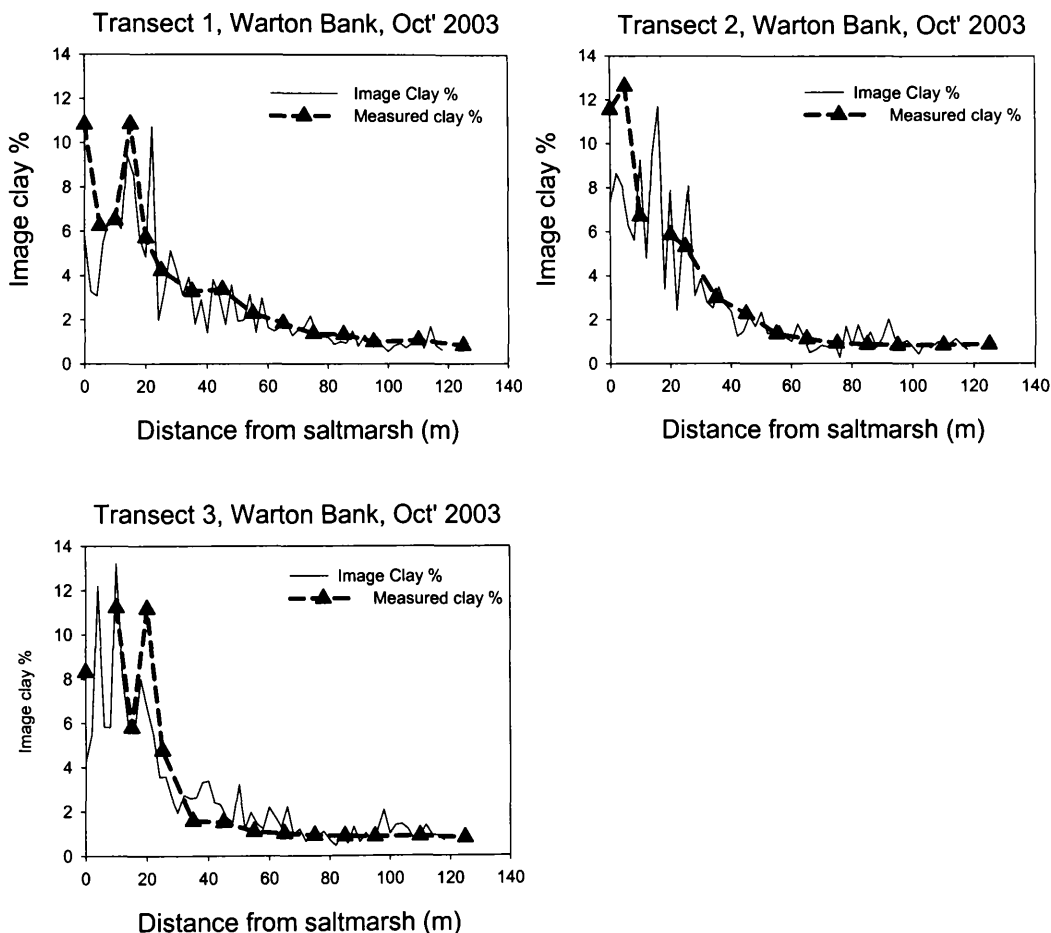


Figure 4.20 a: Clay distribution across intertidal sediments of the Ribble Estuary obtained in October 2003  
 b: Magnified section of intertidal sediment at Warton Bank, showing three transect lines

Demonstrates upper and middle estuary are more dominated by clay fraction, whilst outer estuary has lower percentages of clay particles on intertidal surface.

#### 4.5.5. Clay abundance transects

To assess how accurately the derived clay abundance image (Figure 4.18) fits the clay percentages transects for Warton Bank, transects from the imagery have been compared against the transects (Figure 4.19).



**Figure 4-19** Comparison of measured clay percentages to image estimated clay percentage

The measured clay distribution for each transect appears to replicate the image generated transect. However, the image values do appear to be more noisy across the spatial extent of the transect line.

Subsequent comparison of the intertidal clay deposition images (Figure 4.18) produced from the October 2003 ATM imagery to that of the intertidal clay distribution generated by Rainey (1999) and Rainey *et al.* (2003) in May 1997 (Figures 4.20 & 4.21a) demonstrate differences in mud/clay distribution patterns across the estuary system. Figure 4.18 shows that clay distribution is significantly lower over the northern intertidal surface, than compared to Figures 4.20 & 4.21a. It can be seen from Figure 4.21b that the clay distribution for the October 2003 intertidal surface is not as clearly defined, but the clay distribution is visibly lower than the 1997 imagery (Figure 4.21a).



Figure 4.22 a. Percentage clay map, 1997 (Rainey, 1999) & b Percentage clay map October 2003. Demonstrates that there is an increased covering of clay particles in the May 1997 image, in comparison to the October 2003 image.



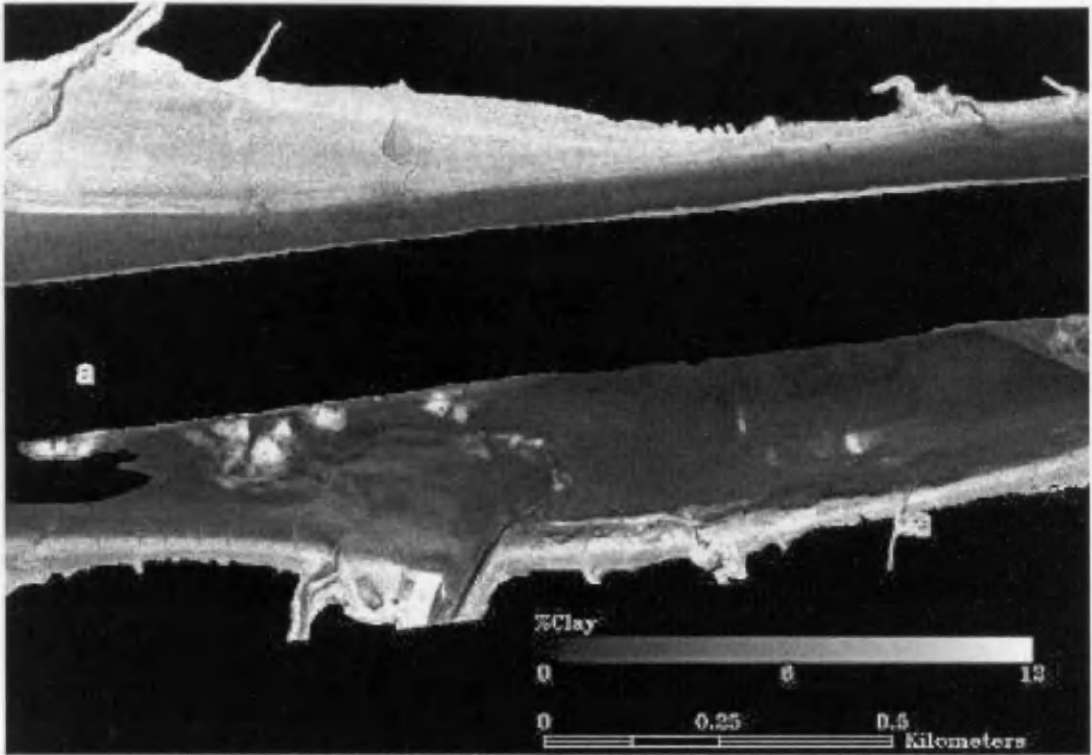
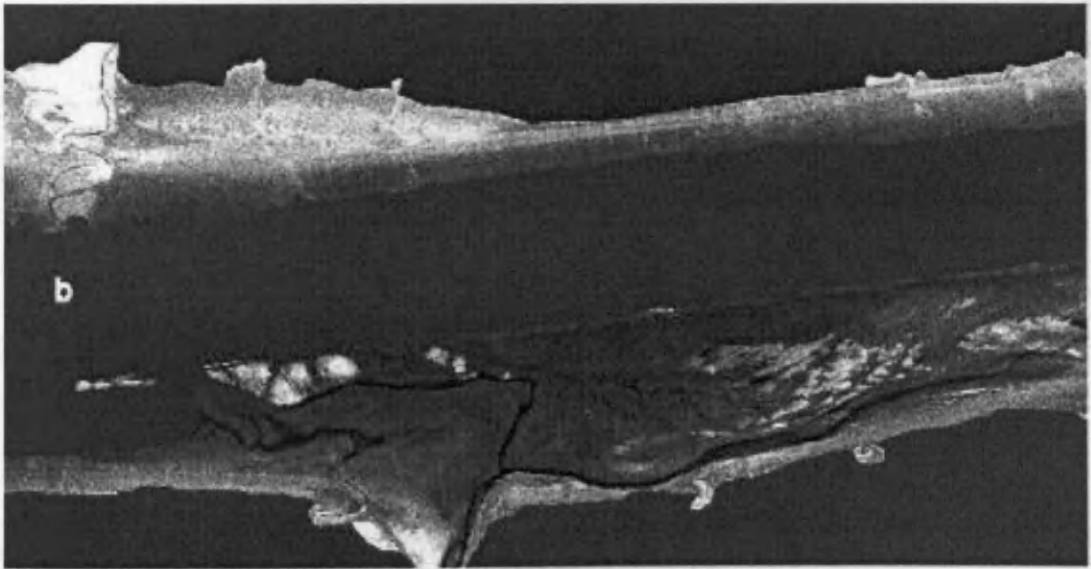


Figure 4.21 a. Subset of percentage clay map (Figure 4.20), 1997 (Rainey, 1999)  
 b. Subset of percentage clay map (Figure 4.18), October 2003.



#### 4.5.6. River discharge conditions

Comparing the discharge conditions seven days prior to the ground transects (Figure 4.22), demonstrate marked differences in the flow patterns of the river,

which could be responsible for the removal of the finer grained sediments from the lower and mid – tidal areas within the October 2003 transects. Also there was a relatively high 5 day mean tidal height of 8.41m during this period, which chapter three has demonstrated to be of importance within the sediment dynamics of the estuary.

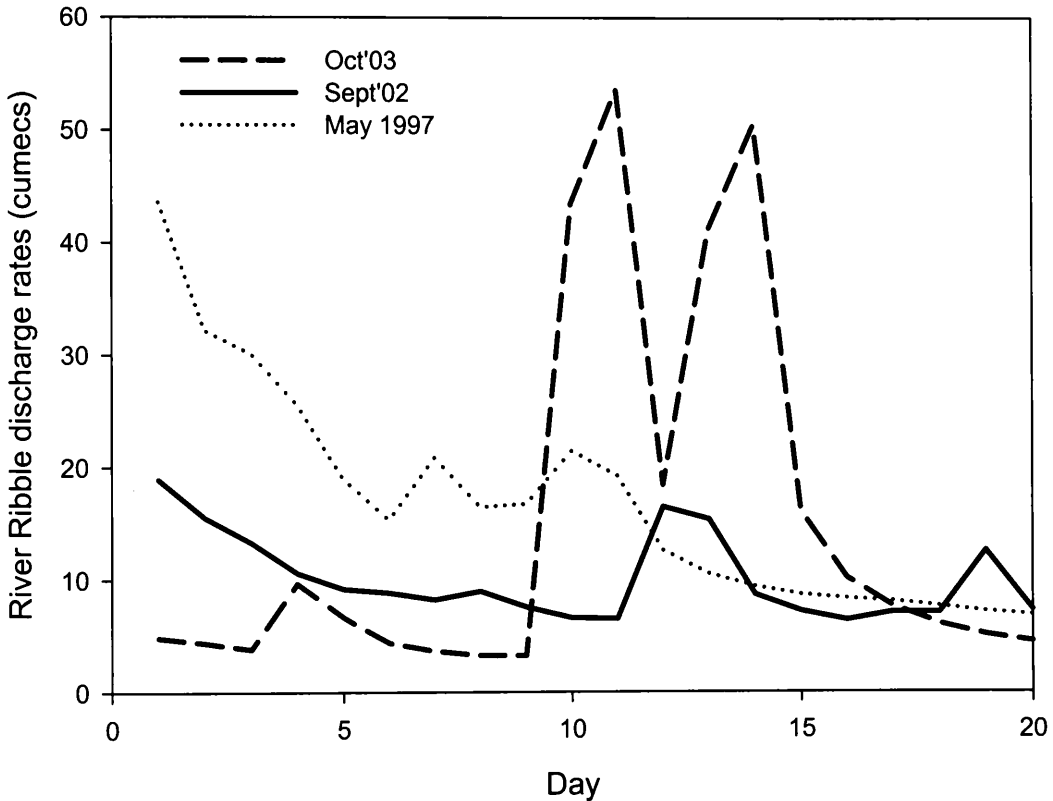


**Figure 4-22** River Ribble discharge patterns 20 days prior to the flights in September 2002, October 2003 (flight on day 21) and May 1997

#### 4.5.7. Changes in radionuclide distribution in the intertidal sediments

The distribution of  $^{137}\text{Cs}$  over the spatial extent of the intertidal sediment surface is determined by the percentages content of clay that are present

within each pixel. This relationship is derived from the comparison of the clay percentage and  $^{137}\text{Cs}$  content of the sample transects obtained concurrent with image acquisition and demonstrated within Figure 3.25. Therefore, this significant linear relationship between  $^{137}\text{Cs}$  and percentage clay can be applied to the derived clay image (Figure 4.18) to derive maps of  $^{137}\text{Cs}$  distribution across the Ribble Estuary. This procedure is carried out within ENVI's band math tool, thus allowing the use of a linear equation to be applied directly to the image data. However, as shown within figure 3.25 and Rainey (1999), the best fit relationship between clay and  $^{137}\text{Cs}$  is best expressed when the two data sources are converted to natural logarithms.

The spatial distribution of  $^{137}\text{Cs}$  shown within figures 4.23 and 4.24 demonstrate that the radionuclide is mainly distributed within the middle and upper intertidal areas of the Ribble Estuary, with reduced intertidal distribution over the outer intertidal sections of the estuary. It is also perceptible from Figure 4.23a that  $^{137}\text{Cs}$  is most concentrated towards the upper intertidal area of the transect lines, where there is an increased clay content. The actual activity concentrations for the middle and lower intertidal areas are similar to the estimated activity concentrations for all three transect lines. However, at the upper intertidal areas closest to the saltmarsh, the estimates of  $^{137}\text{Cs}$  appear to be lower than the actual activity concentrations relative to clay percentages predictions. This could be related to polygonated mud at the upper section of the intertidal surface, which would induce underestimation of the clay percentages generated in section 4.6.4.

Comparing the October 2003  $^{137}\text{Cs}$  distribution map to the May 1997 map (Figure 4.26) (Rainey, 1999), clear differences are evident between the two maps. The maximum activity concentrations in 1997 are approximately twice the values obtained by the later 2003 imagery and the spatial distribution patterns show that there is a more extensive coverage of  $^{137}\text{Cs}$  across the entire middle and upper intertidal sediment surfaces within the estuary in 1997. The October 2003 imagery is shown to be accurately replicating the actual activity concentrations collected from the ground sampling undertaken concomitantly with the imagery (Figure 4.25).

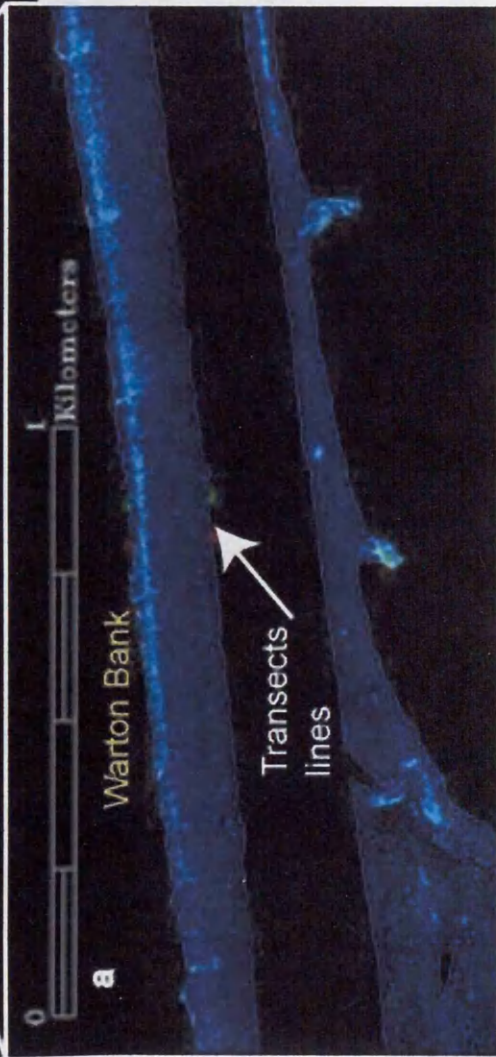
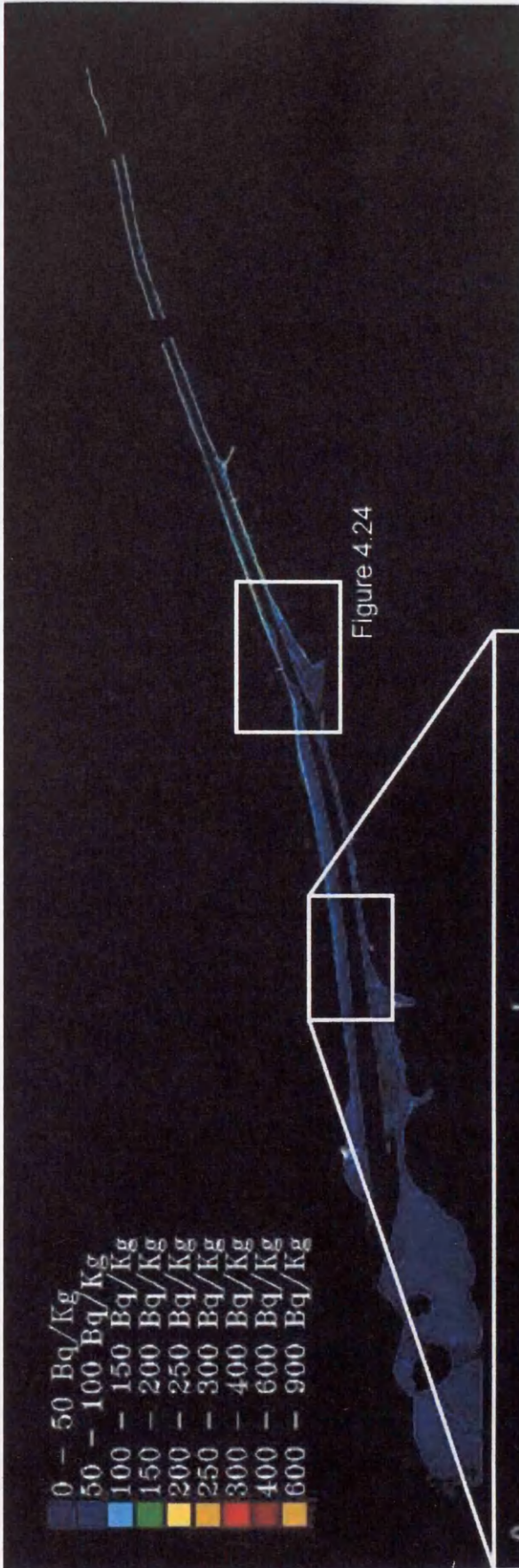
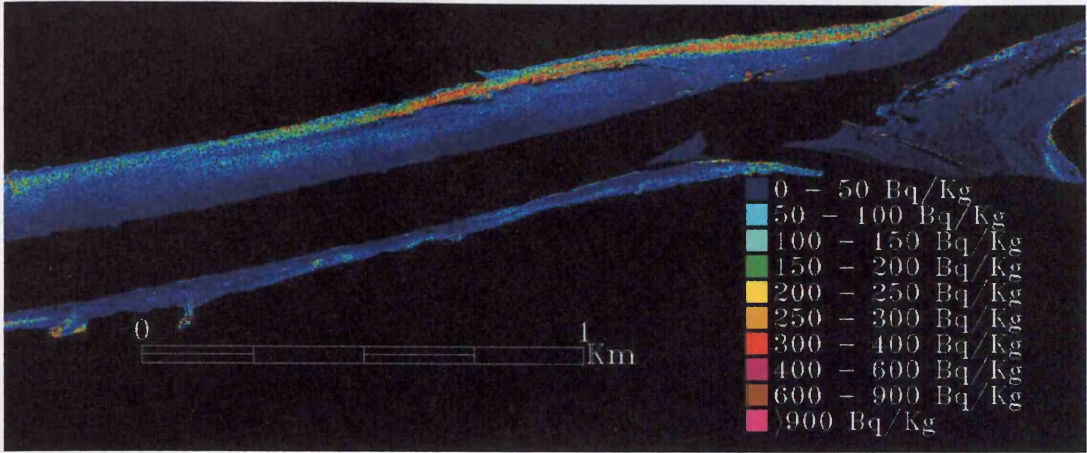
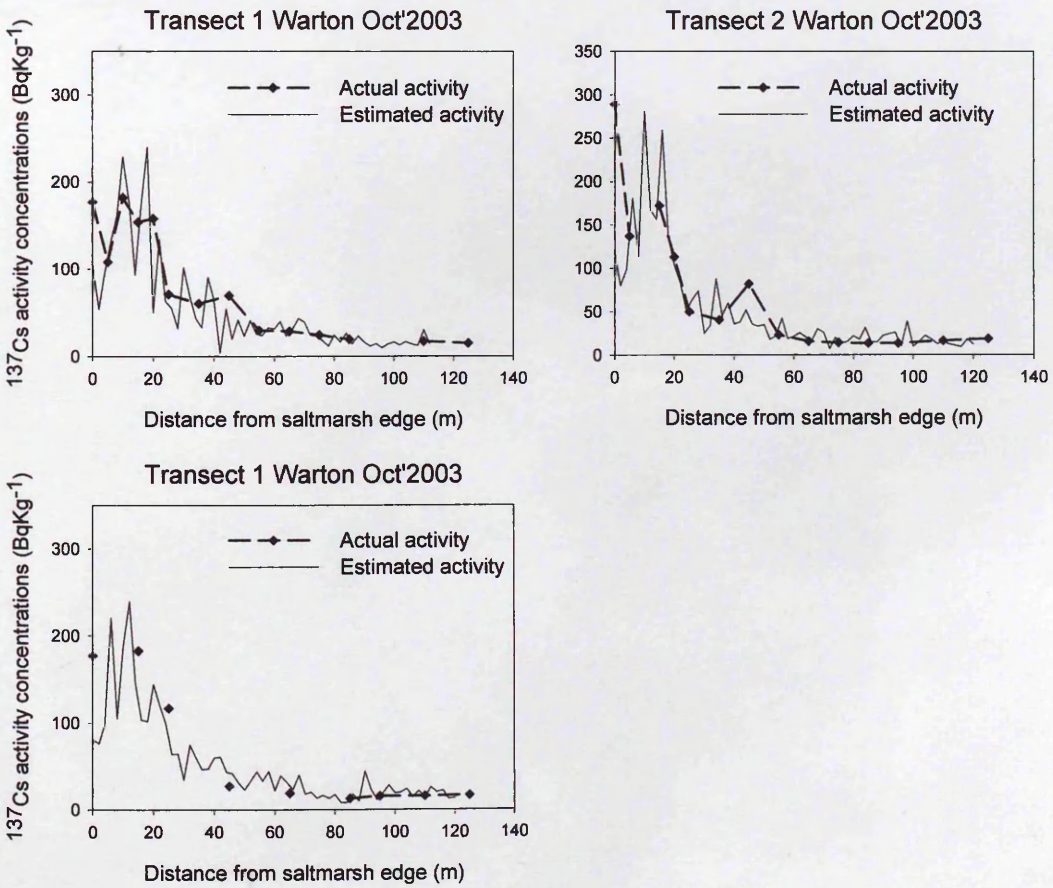


Figure 4.23 Distribution of  $^{137}\text{Cs}$  activity in the Ribble Estuary.  
 a. Magnified section of the  $^{137}\text{Cs}$  activity at Warton Bank, also showing the transect lines.



**Figure 4-24** Subset of figure 4.24, showing  $^{137}\text{Cs}$  distribution at the confluence of the River Douglas.



**Figure 4-25** Comparison of estimated and actual  $^{137}\text{Cs}$  activities along sample transects at Warton Bank

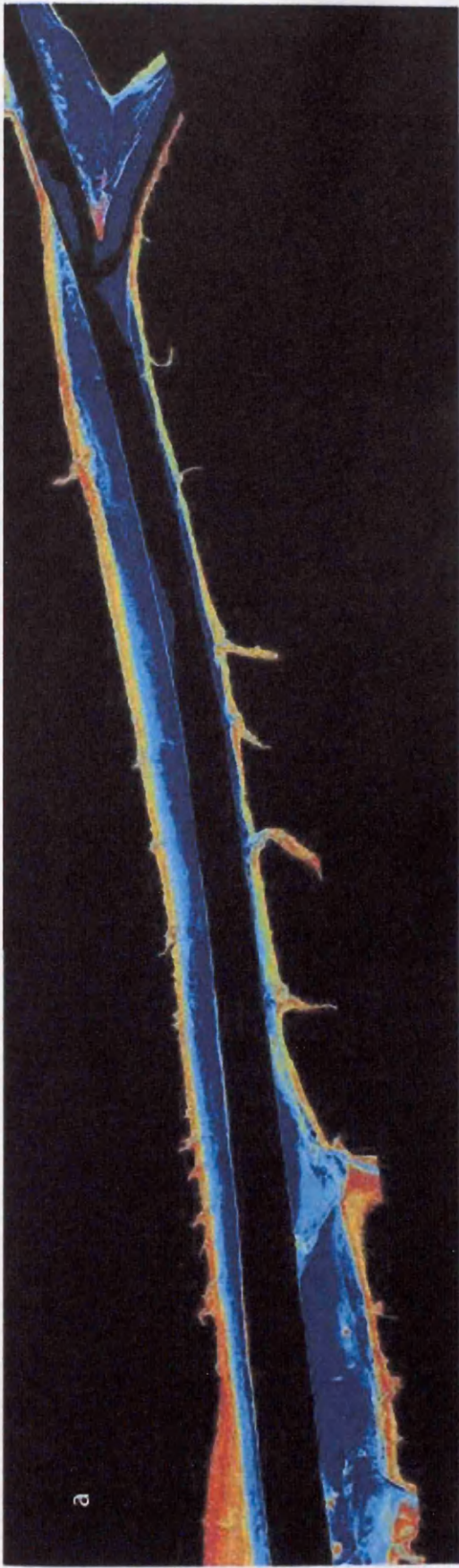
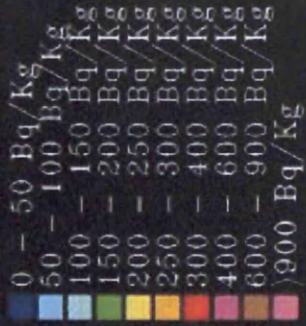
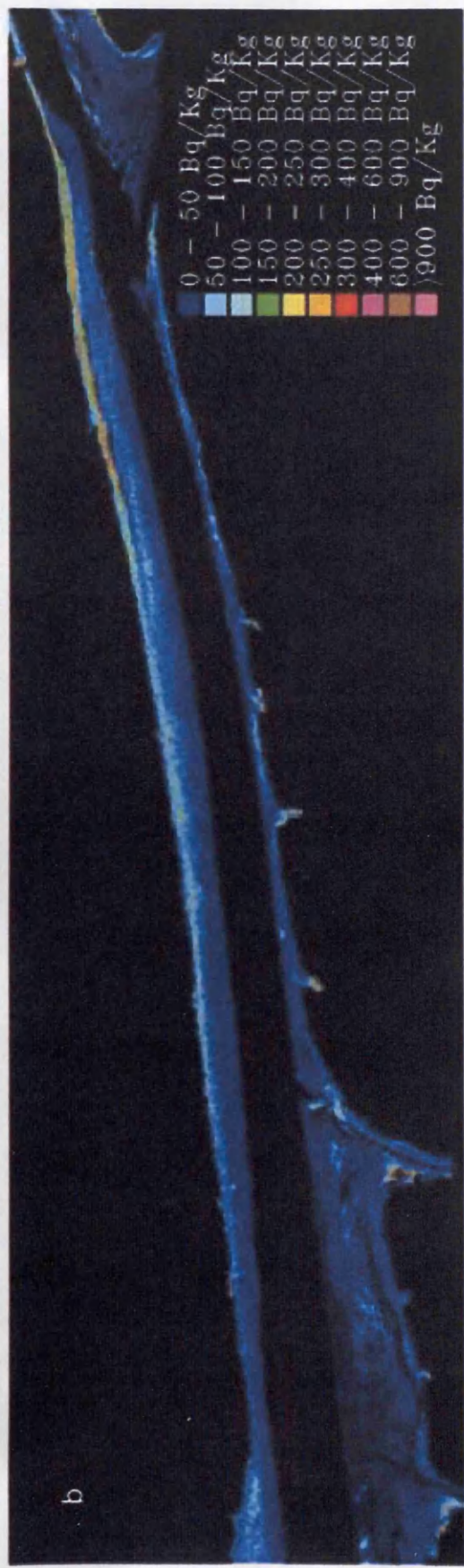


Figure 4.26 a.  $^{137}\text{Cs}$  distribution within the middle Ribble Estuary, 1997 (Rainey, 1999) & b 2003  $^{137}\text{Cs}$  distribution



## 4.6. Discussion

Following on from Rainey, 1999, Rainey *et al.* 2000 and Rainey *et al.* (2003), this study aimed to capture a series of intertidal images to characterise both the spatial and temporal variability of the surface intertidal sediments. However, due to a number of factors out with the control of this project (poor weather conditions associated with ideal tidal conditions and the sensor malfunctions) it was not possible to fulfil this aim. Nevertheless, some valuable insight can be obtained from the inter-comparison of the point measurements associated with the 2002 and 2003 flights and by comparing the inter-year comparison of Rainey's (1999) 30<sup>th</sup> May 1997 intertidal image and the one acquired on the 17<sup>th</sup> October 2003. The application of LiDAR data to these maps of activity concentrations would have given the data a third dimension, allowing the possible assessment of the effects of bed elevation has on the spatial distribution of <sup>137</sup>Cs.

### 4.6.1. Intertidal clay distribution

The associated ground-truth data gathered from the two flights (2<sup>nd</sup> September 2002 and 17<sup>th</sup> October 2003) can be compared to assess the temporal changes in sediment and <sup>137</sup>Cs distribution at Warton Bank. Comparison of the sand, silt and clay content of the transect lines at Warton Bank (Figure 4.5 & 4.6) demonstrate significant differences in the spatial distribution of the sediments. It is apparent that the percentage clay distribution during the 2002 transects (Figure 4.5) is much more extensive than the covering demonstrated within the 2003 transects. This illustrates that there has either been a removal of

fine-grained sediments or deposition of a more coarse layer of sediments has occurred from the 2003 data. The low distribution levels of fine-grained sediments over the intertidal sediment from the 2003 imagery could be related to the discharge patterns of the River Ribble (Figure 4.25) in the preceding 20 days.

There is a good correlation between the estimated clay percentages and the measurements of sampled clay percentage (Figure 4.20) for the October 2003 intertidal image. Therefore, it is possible to compare the derived clay image (Figure 4.19) with the imagery produced using the mixture modelling approach demonstrated by Rainey *et al.* (2003) for the Ribble Estuary intertidal sediments (Figures 4.20 & 4.23). Assessing the spatial and temporal differences between the two image sub sets (Figure 4.20 & 4.21) demonstrates significant changes to the surface intertidal sediments. The upper intertidal clay distribution from the 1997 imagery clearly shows that there is a more extensive covering of clay than compared with the 2003 image. However, the mid- to lower intertidal surfaces appear to have similar clay distributions at and around the Warton Bank location (Figure 4.21). This could be related to the relative narrowing of the channel at this section of the estuary, which would generate increased tidal currents and hence increased erosion and transportation of the finer grained sediments, which do not differ greatly over the course of the tidal cycle.

It should be noted that the MNF transform performed on 2003 imagery, used the thermal band, which was excluded by Rainey (Rainey *et al.*, 2000; Rainey

*et al.*, 2003) was used within this investigation, as it generated a better signal to noise ratio within the MNF forward rotation. It was assumed that the intertidal area had been exposed for a sufficient time that the sediments had reached thermal equilibrium, allowing the use of the thermal band.

The increased distribution of clay on the intertidal surface in the mid-upper reaches of the estuary in the 1997 image, is related to the net effect of tidal pumping of sediment associated with a period of reduced river discharge conditions (Figure 4.22), resulting in the transportation of fine-grained sediments in an upstream direction. This process of tidal pumping has been mitigated by the large river discharge events in the period prior to the October 2003 image (Figure 4.22), leading to flushing of the finer grained sediments out into the outer estuary and tidal pumping having an insufficient time period to transport the finer grained sediments back in an upstream direction.

#### **4.6.2. Moisture content of the intertidal sediments.**

Moisture content of the point measurements sediments sampled during the 2003 intertidal imagery show (Figure 4.10) show relatively uniform patterns across all three transects. The upper 40 metres of the transect line (closest to saltmarsh) contains approximately 20 percent more moisture than the remaining sediment profile. This coincides with the spatial distribution patterns of the grain size associated with these transect lines (Figure 4.6). The percentage moisture content of the sediment has been shown by Rainey *et al* (2003) to have important impacts on the spectral signal of the intertidal muds, with drier sediments producing improved correlations between the ARS

imagery and the point measurements of the clay content.

#### **4.6.3. Distribution of $^{137}\text{Cs}$ within the Ribble Estuary**

Distributions of  $^{137}\text{Cs}$  within the estuary alternate from the wide expansive intertidal zones of the outer estuary to the more confined middle and upper estuary intertidal regions. The outer estuary is dominated by sandier sediments (Figures 4.4, 4.7 and 4.18), which consequently have lower percentages of clay distributed across them. Therefore, as there is a significant correlation with percentage clay and  $^{137}\text{Cs}$  activity concentrations (Figure 4.14) the outer estuary and lower intertidal zones of the middle estuary zones (Figure 4.24 & 4.26) have on average less than  $50 \text{ Bq kg}^{-1}$  of  $^{137}\text{Cs}$  distributed over the intertidal surface. However, the upper intertidal sediments of the middle and upper estuary zones exhibit relatively high clay percentages, which consequently generate higher quantities of  $^{137}\text{Cs}$  activity concentrations in comparison to the lower intertidal zones.

#### **4.7. Summary**

This section of work has clearly demonstrated the application of ARS for the mapping of intertidal clay and radionuclides distributions within the Ribble Estuary, from the modification of the methodologies demonstrated by Rainey 1999, Rainey *et al.* 2000 and Rainey *et al.* 2003. The ability to map the distribution of the clay particles and their associated radionuclides provides a spatially accurate map of clay and  $^{137}\text{Cs}$ , distributions that are strongly influenced by river discharge.

Comparing the May 1997 and October 2003 images for percentage clay distribution and  $^{137}\text{Cs}$  activity concentrations, demonstrates that the patterns are both spatially and temporally complex. It is clear from the inter-year comparison (Figure 4.25) that there is significantly more  $^{137}\text{Cs}$  activity within the 1997 image, in comparison to the 2003  $^{137}\text{Cs}$  map even when the reduction in clay percentage distribution is accounted for. This finding could be due to a number of possible causes;

- Reduction in the activity concentrations of the marine sediments.
- Dilution of activity concentrations by uncontaminated riverine sediments.
- Dilution by un-contaminated, per-nuclear industrial age estuarine sediments.
- De-sorption of  $^{137}\text{Cs}$  back into the water column (MacKenzie *et al.*, 1997)

It is apparent that the river discharge conditions for the preceding 20 days are dissimilar for the 1997 and 2003 intertidal images (Figure 3.22). Clearly, prior to the 2003 flight there was a significant increase in the riverine discharge rates, which have been shown in Chapter Three to cause the erosion of the intertidal fine grained sediments and flush them out of the estuary. Conversely, prior to the 1997 imagery the average flow rates were relatively low, encouraging tidal pumping of marine sediments in an upstream direction. Although it may be likely that there is combination of factors that generate lower values of  $^{137}\text{Cs}$  over the spatial extent of the estuary.

However, the percentage clay and  $^{137}\text{Cs}$  relationship within the Ribble Estuary during the flight on the 17<sup>th</sup> October 2003 did still demonstrate a high coefficient of determination, which allows the production of maps of  $^{137}\text{Cs}$  within the estuary. This provides evidence in support of the third research hypothesis outlined in Chapter Two, indicating that the percentage clay/ $^{137}\text{Cs}$  relationship were stable for a given point in time, but this relationship has been shown to temporally unstable over time.

The use of ARS data allows conclusions to be drawn on the inter-annual research hypotheses as well as the temporal stability of the clay/ $^{137}\text{Cs}$  relationship. The inter-annual distribution of sediments within the estuary and the temporal stability of the percentage clay/ $^{137}\text{Cs}$  relationships is shown to vary with the two intertidal images. However, definitive answers to the research hypotheses of the inter-annual sediment flux and temporal stability of the percentage clay/ $^{137}\text{Cs}$  relationships cannot be conclusively derived from just this section of work. Due to the reduced number of intertidal images obtained during this investigation and the lack of LiDAR data, it is not possible to identify any intra-annual variability in the sediment accretion and erosion within the estuary.

## **5 Mapping suspended sediment fluxes in the Ribble Estuary**

### **5.1. Introduction**

The erosion, transportation and deposition of sediments and their associated contaminants within estuarine environments is dynamic in space and time. Obtaining measures of such processes and their products is important not only in terms of understanding and quantifying the mechanisms controlling sediment and contaminant transport, but also in the requirements of river/channel engineering and coastal defence and effective effluent discharge management.

Within the Ribble Estuary, the Victorian re-engineering of the estuary, evidenced by the presence of the fixed entraining walls constraining the main channel, has resulted in rapid siltation of the main channel and formation of extensive saltmarshes (Van der Wal *et al.*, 2002). Rapid siltation remains a problem, even with the development of new structures such as the millennium funded Ribble Link canal, which is experiencing rapid siltation rates within the confined mid-estuary Savick Brook area.

There is therefore value in developing a better understanding within a spatial context of the processes and fluxes associated with sediment and contaminant transport. Here, time series ARS image data sets will be used to estimate the net flux of sediment within the estuary over two sets of flood and ebb tide sequences. Atkin (2000) demonstrated that a linear relationship exists between suspended sediment concentrations (SSC) and reflectance

values within the estuary over a range of 0-300 mg l<sup>-1</sup>, beyond which the relationship can be better described with a natural logarithmic relationship. A linear SSC relationship with the time series CASI data (radiance values) was used over a turbulent well mixed flood tide event and this has been applied to provide an estimate of the amount of sediment deposited.

Chapter Three demonstrated that the relationship between percentage clay in intertidal sediments and <sup>137</sup>Cs is a temporal one. There is therefore a further need to validate whether SSC can be used as a surrogate for contamination transport, specifically <sup>137</sup>Cs, as indicated by Atkin (2000).

This section of the investigation is focused on obtaining quantitative estimates of sediment flux within the Ribble Estuary via the acquisition of time series ARS imagery of the flood and ebb tide. Methodologies presented by Atkin (2000), will be validated and the approach further developed to obtain quantifiable estimates of the net flux of sediment and radionuclides over both the flood and ebb tidal sequence. Therefore, this chapter will provide answers to the last research hypotheses;

*The net sediment flux of sediment and radionuclides over a single flood and ebb tide cycle can be derived through time series remote sensing.*

To provide answers to this hypothesis, a number of aims were identified;

- i) Further develop the approach initially defined by Atkin (2000) to obtain estimates of total suspended sediment load over the

duration of two flood and ebb tidal events to gain estimates for the net deposited sediment rates within the estuary,

- ii) Demonstrate that the relationship between fine grained sediments and  $^{137}\text{Cs}$  are temporally or spatially stable within the Ribble Estuary.
- iii) Derive quantitative estimates of suspended sediment loads and associated radionuclide activity concentrations in the water column.

These aims will be achieved by;

- The acquisition of a number of separate time series airborne remote sensing imagery over the course of a flood and ebb tide within the Ribble Estuary.
- The collection of ground reference data for SSC and associated radionuclide activity concentration ground reference data. This will provide calibration and validation data for the remote sensing imagery.
- The collection of depth profile measurements of SSC within water column, concomitant with image acquisition.
- Estimation of water volume within the estuary for each time series image.

### **5.1.1 Sediment sources within the estuary**

From Chapter Three it is possible to start to build a model of the controls on the sources of sediment within the estuary and its associated radionuclide

contamination. Sediment sources within the Ribble Estuary can be classified as fluvial, marine or re-mobilisation of historic intertidal sediments (Figure 5.1). Fluvial sediments are generated within the river catchment area, with the greatest quantities transported during periods of heavy rainfall events within the catchment, which should increase the capacity of the river to entrain and transport sediment into the estuary. This material may be ejected out into the outer estuary whilst tidal conditions are on the ebb, whereas during the flood event some of the material may be deposited within the inner estuary system. However, the velocity of fluvial flow could also have the effect of scouring the intertidal sediments during the ebb tide, as the volumes of the ebb tidal flow and elevated river flow will combine to increase flow rates above normal ebb flow rates. These fluvial sediments, which are transported into the estuarine system during storm events, may be characterised by weapons-fallout and Chernobyl sourced radionuclides. Therefore after high (>50 cumecs) river flow events, it could be expected that intertidal surfaces may be covered by a layer of relatively uncontaminated sediments or the exposure of older uncontaminated sediments at the intertidal sediment surface. The freshly deposited sediments are likely to have lower critical shear stress values, and therefore be more likely to be entrained on the subsequent flood tide event and redistributed and mixed with the Irish Sea sediments containing Sellafield derived radionuclides.

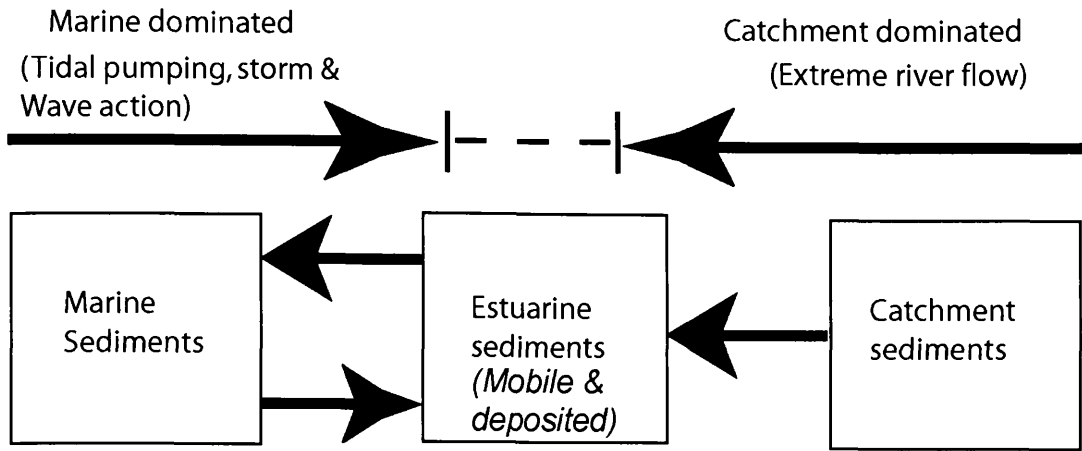


**Figure 5-1 Movement of sediment within the Ribble Estuary**

The second source of sediments are those derived from the marine environment that are transported into the estuary by onshore storm events and during the tidal cycle from the Irish Sea. These sediments are dominated by anthropogenic radionuclides derived from BNFL Sellafield (see section 2.4) and because they are derived from a well mixed source, they should tend to show good relationships with clay concentrations. The third possible source of sediments may be generated by the remobilisation of existing sediment sources within the estuary itself. These fine, mobile sediments should be readily remobilised by the action of the tide, but mobilisation of consolidated sediments requires more energy i.e. wave action and/or heavy rainfall on exposed intertidal sediments. Brown (1997) conducted an extensive mineralogical study of the intertidal and saltmarsh sediments within the Ribble Estuary, indicating that the Illite mineral is the dominant clay mineral present (48 – 68.5 %) within the estuary and that other clay minerals (Smectite, Kaolinite and chlorite) are present in much lower abundances (<35 %). The type of clay mineral present is important for the potential resorption of  $^{137}\text{Cs}$

(Section 2.3.1), as higher levels of smectite-type minerals can result in an increased resorption rates within the marine environment.

Clay mineralogy compositions remained relatively constant throughout the entire estuary, which indicates that the marine and fluvially derived clay particles have been homogenised throughout the estuary and that the marine source sediments dominate in the estuary environment. However, there were indications that there were occasional inputs of fluvial sediments from the River Douglas (Brown, 1997).

The erosion, transportation and deposition of clay particles is a function of current velocity, particle size, and water content of the materials, which Postma (1967) integrated into a set of velocity curves or Hjulstrom Curves. Sediments can be split into two separate classes i. non-cohesive (gravel, and sand) and ii. Cohesive sediments (clays). The fine grained clay particles can, due to inter-particle bonds, have an increased critical erosion threshold than would be expected by the linear decrease in critical shear stresses associated with the non-cohesive, coarser particles. Furthermore, the critical erosion threshold for the cohesive clay and finer silt particles can be further increased by microphytobenthos and EPS (Section 3.2.1). If consolidation can occur (de-watering and compaction), then the critical erosion threshold will be increased and encourage net deposition. However, the increase in the critical erosion threshold may still be lower than the actual flow velocities of the incoming tide and therefore erosion and transportation of the fine-grained sediments will still take place.

## 5.2. Remote sensing of suspended sediment in estuarine waters

In addition to the novel use of ARS for mapping intertidal radionuclide concentrations (Chapter Four), ARS within estuarine environments also has the potential of providing a valuable tool in gaining a greater understanding of the spatial movement and distribution patterns of suspended sediments and associated monitoring of contaminants such as radionuclides within these environments. This is important for a number of reasons:

- The calculation of residence times for the contaminants within estuarine ecosystems.
- Assessing the anthropogenic influences (e.g. engineering structures, effluent discharge) on estuarine environments.
- Prediction of long-term changes in estuaries and the mechanisms that drive these changes.
- The improved management of the coastal zone.

The application of point sampling and fixed sampling sites generates important data for the interpretation of flow patterns at those zones and forms the basis for many estuarine hydrodynamic models i.e. VERSE. However, only ARS can provide the time specific, spatial coverage of the entire estuarine system. By using such ARS systems i.e. CASI, it has been shown (Novo *et al.*, 1991; Han 1997; Atkin, 2000) that it is possible to retrieve SSC values from reflectance values obtained over case 2 coastal and estuarine systems.

The use of ARS to assess the spatial patterns of sediment entrainment during the initial flood event and the subsequent ebb tide presents many complex problems in terms of obtaining estimates of total sediment load transportation. As Mikkelsen (2002) noted, the use of several different algorithms to empirically derive total suspended matter (sediment or organic particles) have been conducted in the past for numerous coastal and marine waters. One of the reasons for these discrepancies is the reflectance qualities of different averaged grain sizes (Bale *et al.*, 1994). This change in mean particle size affects the net cross-sectional area or net projected area of the particle (Mikkelsen, 2002). Therefore, where the averaged particle size is small ( $<10\ \mu\text{m}$ ), the projected specific surface area is much greater than that of a larger particles ( $>100\ \mu\text{m}$ ) and will therefore reflect increased amounts of solar radiation (Atkin, 2000; Tyler *et al.*, *in prep.* (b)). This could potentially affect turbid estuarine environments during periods of slack water, where, due to settling and flocculation, the average grain size located within the surface waters may decrease (in mean grain size terms), having the effect of increasing the net surface reflectance values of the surface waters, even though the actual SSC may have decreased. Conversely, where high levels of coarse ( $>100\ \mu\text{m}$ ) suspended sediment are in suspension i.e. convergence front, a linear regression model may overestimate the SSC within the surface waters. However, these algorithms, demonstrated by Mikkelsen (2002), do use band settings, which will receive interference from dissolved constituents such as organic matter and chlorophyll i.e. below  $700\ \mu\text{m}$  (Hudson *et al.*, 1994). Selecting wave bands greater than  $700\ \mu\text{m}$  will remove any reflectance associated with dissolved organic matter and chlorophyll, therefore

potentially improving the reflectance relationship for SSC (Atkin 2000). Interestingly, it is the clay fraction of the SSC dominating the reflectance measurement that is responsible for the majority of  $^{137}\text{Cs}$  activity concentration. Thus, there is a very good relationship not only between SSC and  $^{137}\text{Cs}$ , but also reflectance and  $^{137}\text{Cs}$  (Tyler *et al.*, *in prep.* b).

Flight line proposals	Proposed Number	Obtained	Spring	Mid-cycle	Neap	Flight lines	Useable data
Flood & ebb 2002	2	0	n/a		n/a	n/a	
Flood & ebb 2003	2	2	1	1	n/a	13 & 7	12 & 7

**Table 5-1** Flight line acquisition for flood and ebb flights, planned and obtained.

Table 5.1 shows the proposed flight line acquisition schedule for the investigation. It had been proposed that one time series ARS would be acquired each year, with one capturing a neap tidal event and the other a spring tide. However, due to the tidal harmonics of the Ribble Estuary it is not possible to acquire a mid-day high water neap tidal cycle. Unfortunately, due to unfavourable weather patterns with 2002 no time series data was acquired. Nevertheless, in 2003 two separate time series images were acquired. The first in April and the second in July, but due to logistical problems (see section 5.3) it was only possible to obtain ground calibration data for the July data set.

### 5.3. Ground Reference Data

It is important to obtain accurately georeferenced concomitant ground control data to assess/quantify ARS data. However, in the Ribble Estuary, there are limited launch sites that are operational only two hours either side of the high

tide. Atkin (2000) solved this problem by launching on the preceding tidal high, mooring up to a mile marker pole and then waiting for the tide and incoming ARS flight paths the next day. Due to limitations in logistics and suitable boat hire for this project and utilizing Atkins (2000) past work, it was decided to launch just two hours prior to high water. Unfortunately, due to difficulties in launching into the estuary, data collection did not begin in the estuary until high water slack and ended only three hours later. This restricted the quantity of data that could be gathered, thus Atkins' (2000) suspended sediment calibration was used as the basis to quantify the sediment load and the data collected during the April and July 2003 time series imagery, with the July 2003 ground calibration points used as validation points.

### **5.3.1. Water sampling collection**

#### *Grain size analysis*

Samples of suspended sediment grain sizes from the turbid estuarine waters were obtained by the use of 1 litre, wide necked plastic sampling bottles. These samples were obtained concomitantly with CASI ARS flights lines collected by the NERC ARSF Dornier aircraft. Each sampling location was located with the use of a handheld GPS system and the subsequent identification of the boat within the imagery, therefore allowing for the sample to be located to within 3 to 4 m accuracy and within short time frame of flight overpass

The pre-acid washed sampling bottles were used to collect water from the side of the boat that was utilized during the estuarine sampling. Following

sample acquisition, the samples were returned to the Westlakes Research Institute Laboratories where they were placed in a cold dark store (5°C). Prior to grain size analysis the sample bottles were agitated for approximately one minute each and half of the water poured into the large sampling unit of the Malvern Longbed particle-sizer (Section 3.3.3).

#### *Activity concentration of suspended sediment*

For the purposes of this investigation, as demonstrated by Atkin (2000), it is important to establish whether there is a relationship between SSC and the associated radionuclide concentrations within the water column. As described in chapters three and four, it is clear that the relationships between fine-grained sediments and the associated radionuclides ( $^{137}\text{Cs}$ ) is temporally variable. Therefore, it is important to obtain precise measurements of the grain-size/radionuclide relationships during image acquisition to allow correct estimations of total activity concentrations to be calculated for the estuarine flux.

Atkin (2000) demonstrated that there is a linear relationship between suspended sediment and radionuclide concentrations (between 50 and 250  $\text{mg l}^{-1}$ ). This relationship was found by comparing two separate sets of sampling data (June 1996 and July 1997), which demonstrated a clear temporal stability over time. But as Chapter Three has demonstrated, the relationship between fine-grained sediments and radionuclide contaminants are not constant during the course of the year and so imagery that had not been ground-truthed obtained after high river flow events may have to be

treated with some caution with regards to the total activity quantities within the estuary.

This work demonstrated that it is imperative to obtain concomitant SSC samples during image acquisition. Therefore eight, wide necked 10 litre sampling bottles were used to acquire enough suspended sediment to allow for gamma counting to take place on the collected sediment. Also eight one litre sample bottles were used to collect measurements of the mean grain size of the suspended sediment. After collection they were transported back to Westlakes Research Institute Laboratories, where they were placed in a cold store (5°C). These samples were then filtered through a pre-weighed 293 mm diameter cellulose-nitrate membrane filter, via the use of an air compressor to draw the water through the small pore size (0.2 µm). After filtration, the samples were folded and dried within an oven (~50°C) for twenty-four hours and accurately weighed ( $\pm 0.001$ ). They were then placed within large petri dishes and gamma counted using the Westlakes Research Institute gamma detectors (2.4.3).

#### *Depth profiling of estuarine water column*

Estimates of suspended sediment concentrations were obtained through the depth of the water column over the course of a flood/ebb tidal cycle, to validate the assumption of relative uniform depth distribution of SSC. A uniform distribution may be anticipated in macrotidal estuaries where strong tidal currents will induce intense vertical mixing on the flood tide and stratification of the water column during the ebb tide. Measurement of vertical

suspended sediment variations in such a dynamic estuary as the Ribble remains problematic. Previous studies (Gleizon, 1999), have used fixed bed instrument rigs at Lytham, Clifton Marsh and Preston. Each station was equipped with temperature/conductivity/depth and suspended sediment transmissometer probes to assess changing river flow conditions over a yearly time period. These rigs provided valuable data for studying the basal flow patterns of the channel bottom flow, but did not provide any information on the overlying water column.

Therefore it was decided to employ a turbidity/temperature/depth/salinity probe during image acquisition in July 2003, to obtain SSC measurements through the water column. The probe, a Hydrolab Quanta (temperature, dissolved oxygen, pH, depth and turbidity), was purchased by Westlakes Research Institute with an aim to provide a valuable water quality tool for environmental studies. The probe was attached within a robust instrument rig and suspended from the sampling boat, being lowered at one meter intervals every two minutes. The subsequent log files were cross correlated to GPS timing to accurately assess the location of the depth profile in relation to the ARS data.

## **5.4. Image analysis procedures**

### **5.4.1. Geocorrection**

Image correction is necessary for the retrieval of reliable spectral data from ARS imagery (Table 5.1 & 5.2). Initially, as discussed in Chapter Four, the

imagery is geocorrected via the NERC supplied azgcorr software to correct any in-flight roll at time of image acquisition. Following this correction, a further geocorrection is performed to place the image pixel locations into a national grid format. This enables the application of GPS's ground control points to assess the validity of modelled SSC.

#### 5.4.2. Radiometric normalization (Atmospheric correction)

Following this image correction procedure, a sequence of correction procedures were performed to obtain estimates of the SSC from the imagery data. Initially, an automated dark pixel subtraction was applied to the data, then a sun angle normalisation was calculated for each time series imagery data set and finally image-to-image normalisation must be completed between the 1997 and the 2003 data to ensure comparable image radiance values for the targets, such as roads and runway surfaces.

15th July 2003

Flight line	196	Alt (ft)	3650	pixel size (m)	2 - 2.5
-------------	-----	----------	------	----------------	---------

Number	Dir	Time start	Time stop	spd kts	CASI	ATM	RC10
196011b	O78	10:34	10:40	122	Yes	Yes	Yes
196021b	O78	10:56	11:02	120	Yes	Yes	No
196031b	O78	11:11	11:16	121	Yes	Yes	No
196041b	O78	11:24	11:31	123	Yes	Yes	Yes
196051b	O78	11:40	11:46	122	Yes	Yes	No
196061b	O78	11:54	12:00	119	Yes	Yes	No
196071b	O78	13:49	13:54	117	Yes	Yes	Yes
196081b	O78	14:02	14:07	120	Yes	Yes	No
196091b	O78	14:15	14:20	120	Yes	Yes	No
196101b	O78	14:28	14:34	120	Yes	Yes	Yes
196111b	O78	14:41	14:46	120	Yes	Yes	No
196121b	O78	14:55	15:00	120	Yes	Yes	No

**Table 5-2** Flights lines for July 2003 time series imagery

17th April 2003

Flight line	107	Alt (ft)	4900	pixel size (m)	3
-------------	-----	----------	------	----------------	---

Number	Dir	Time start	Time stop	spd kts	CASI	ATM	RC10
107011b	O78	09:19	09:24	131	Yes	Yes	Yes
107021b	O78	09:33	09:38	132	Yes	Yes	No
107031b	O78	09:48	09:54	129	Yes	Yes	Yes
107041b	O78	10:04	10:10	126	Yes	Yes	No
107051b	O78	10:20	10:26	130	Yes	Yes	Yes
107061b	O78	12:21	12:27	135	Yes	Yes	No
107071b	O78	12:37	12:42	139	Yes	Yes	Yes

**Table 5-3** Flight lines for April 2003 time series imagery

### *Dark pixel subtraction*

Atmospheric correction is an essential pre-processing step to remove the atmospheric and solar illumination signature from the ground surface reflectance (Richter *et al.*, 2002). The distortion generated by atmospheric variables i.e. scattering, absorption and refraction, will induce a degradation in the resulting ARS imagery. Radiometric pre-processing seeks to remove the undesirable impacts of atmospheric distortion on the images and can fall into the category of image restoration (Estes *et al.*, 1983). In the case of time-series images, any omission of atmospheric correction will give unreliable results (Hadjimitsis *et al.*, 2004). Song *et al.* (2001) demonstrated the effectiveness of seven absolute atmospheric correction models, based on the darkest pixel (DP) correction principle. It was found (Song *et al.*, 2001; Hadjimitsis *et al.*, 2004) that the simple DP method demonstrated the best overall results for image classification and change in detection accuracies. Also there is a lack of necessary atmospheric input parameters to perform the

more complex atmospheric model correction i.e. LOWTRAN 7 (Kneizys *et al.*, 1988) and MODTRAN (Berk *et al.*, 1989; Jorgenson & Edelvang, 2000).

### **5.4.3. Sun angle normalisation**

The application of sun angle normalisation is important in the comparison of time series airborne remote sensed imagery. Due to the extended collection periods of image acquisition, the sun's solar elevation azimuth is constantly changing, resulting in a change of the relationship between SSC and the reflectance value. Atkin (2000) demonstrated that it is important to normalise known ground control points in order to achieve image to image normalisation. Atkin (2000) used fixed stable ground control points located at Preston docks, a tarmac road surface, a field and sewage works filter bed.

In attempting to improve data the 1997 data set, a review of the above ground control points indicated that they were no longer suitable for image-to-image normalisation. The spectral properties of the tarmac surface at Preston Docks has been changed due to re-surfacing. The fields will have different crops and rates of growth and so the spectral signals associated with them will have changed and finally the filter beds are subjected to periodic wetting, substantially changing the spectral signal. Consequently, new ground control points had to be located within the 1997, April and July 2003 imagery that were present and importantly un-altered over that time period and comparable with the 1997 data set.

Warton Aerodrome (north of the estuary at Warton Bank) was identified as a suitable site for image radiometric normalisation. Subsequent communications with the operators of the site (BAe) confirmed that the taxiway tarmac surfaces had not been re-surfaced in the intervening years between image acquisitions. For that reason, 30 separate ground control points were located upon the aerodrome taxiways. At each location, 5 by 5 grids of pixels were sampled to give an average value and an indication of the variation within those sample grids.

Subsequent analysis of the change in radiance values at these 30 localities in comparison to the near midday image (196061b – July 2003), allowed for separate linear regression equations to be calculated and the subsequent regression models applied to the non-midday imagery to normalise the entire image data set back to the midday image values. Unfortunately, due to a number of problems with obtaining the necessary ground control points, another image correction tool was required to correct for the changing sun azimuth during image acquisition. Therefore the imagery was corrected for the change in solar radiance that is resultant from the changing solar azimuth angles throughout the image acquisition timeframe.

Consequently, the solar azimuth information for the Ribble Estuary was obtained from the Astronomic Application Department, U.S. Naval Observatory, Washington DC. These data (Figure 5.3) show the changing solar azimuth angle throughout 17<sup>th</sup> July 2003 (it is important to note that each individual day will result in a different solar azimuth plot (Table 5.3)). Against

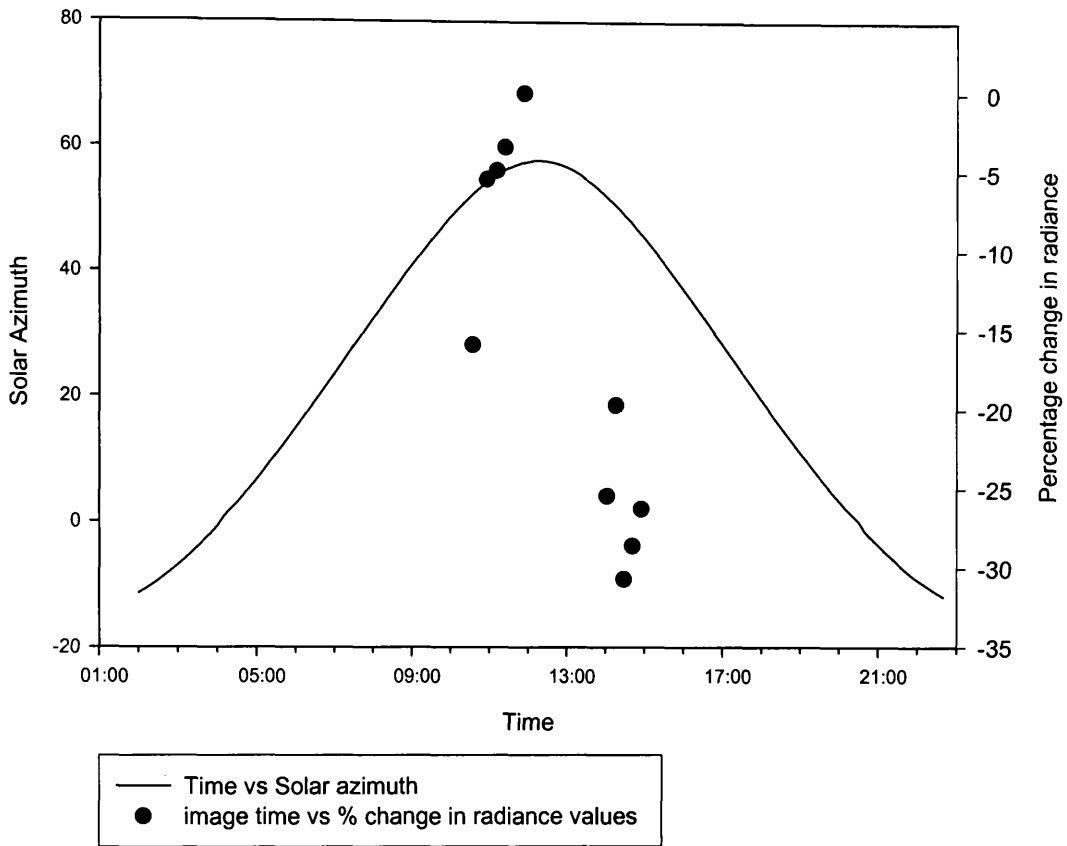
this, the averaged percentage change in radiance values from the aerodrome's ground control points were plotted, in comparison to the near-midday image. These data points were then compared to the solar azimuth angle for the time point that the image acquisition was started at (Table 5.3) and plotted in Figure 5.3.

image	time (s)	% change	Sun azimuth angle	correction of imagery		Fractional change
196011b	-4800	-15.938	51.900	-16.449	16.449	1.197
196021b	-3480	-5.460	54.600	-9.029	9.029	1.099
196031b	-2580	-4.902	55.400	-6.831	6.831	1.073
196041b	-1800	-3.420	56.000	-5.182	5.182	1.055
196051b	-360	-0.684	57.400	-1.335	1.335	1.014
196061b	0	0.000	57.600	-0.785	0.785	1.008
196071b	6900		53.300	-12.602	12.602	1.144
196081b	7680	-25.439	52.300	-15.350	15.350	1.181
196091b	8460	-19.713	50.300	-20.846	20.846	1.263
196101b	9240	-30.703	49.100	-24.143	24.143	1.318
196111b	10020	-28.602	48.000	-27.166	27.166	1.373
196121b	10860	-26.259	45.500	-34.036	34.036	1.516

**Table 5-4** Sun angle correction factors for July 2003 imagery

This allows the formulation of a linear regression model (Figure 5.4) that can be used to calculate the percentage change and thus the fractional change in the radiance values for the ground control points for that day. Furthermore, it permits the correction of the two images that had the aerodrome ground control points covered by cloud shadow, thus allowing the use of all the time series data set. This technique was also performed upon the April 2003 (Figure 5.5) and imagery obtained by Atkin (2000) on the 20<sup>th</sup> September, 1997, thus generating a standardised technique that can be applied to time series data sets that span both pre- and post midday solar azimuth maximum. This is important for the investigation of both flood and ebb tide SSC, due to

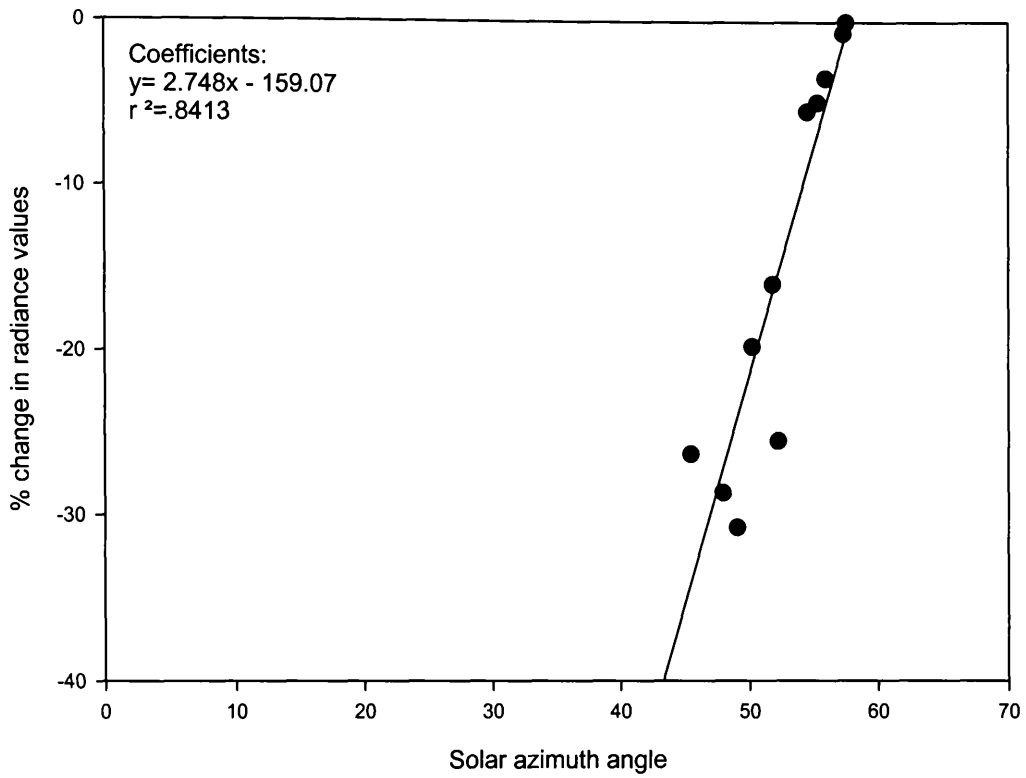
the extended flight period associated with the acquisition of tidal time series data.



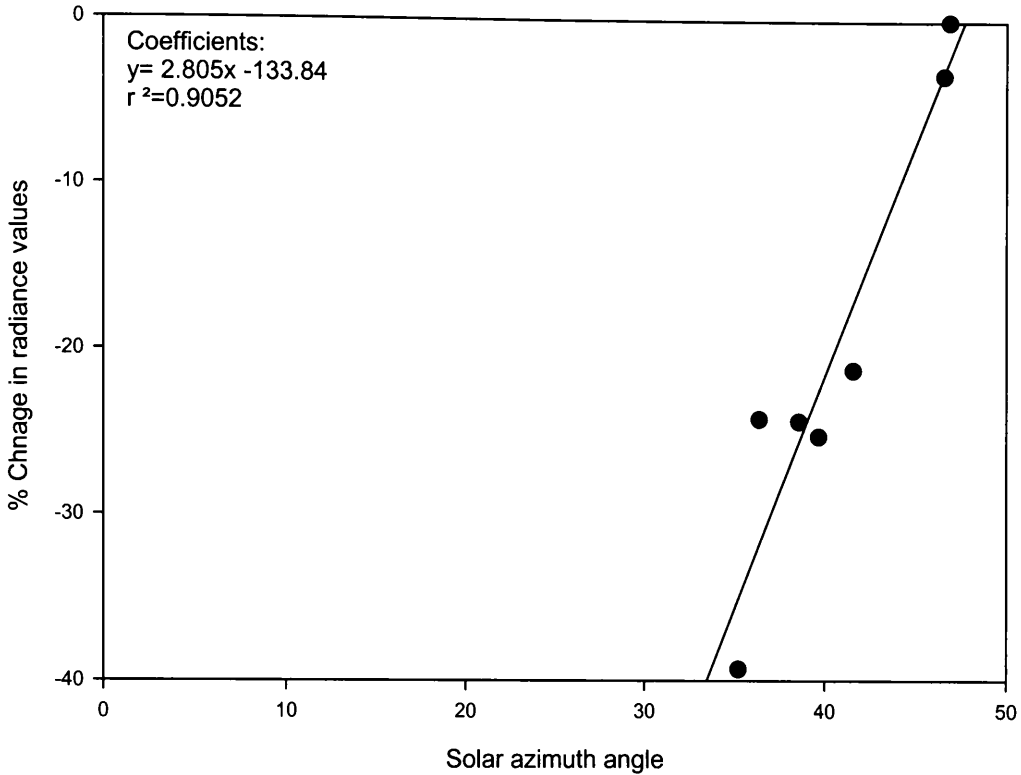
**Figure 5-2** Changing solar elevation azimuth for the 17<sup>th</sup> July, 2003 and the comparison to the percentage change in radiance values of the ground control points at Warton Aerodrome during each time series image.

Image	time (s)	% change	Sun azimuth angle	correction of imagery		fractional change
c107011b	-10860	-39.302	35.2	-35.093	35.093	1.541
c107021b	-10020	-24.140	36.4	-31.727	31.727	1.465
c107031b	-9120	-24.276	38.6	-25.555	25.555	1.343
c107041b	-8160	-25.189	39.7	-22.470	22.470	1.290
c107051b	-7200	-21.163	41.6	-17.140	17.140	1.207
c107061b	0	0.000	46.9	-2.271	2.271	1.023
c107071b	1020	-3.284	46.6	-3.113	3.113	1.032

**Table 5-5** Sun angle correction factors for April 2003 imagery



**Figure 5-3** Plot of the solar azimuth angle against the percentage change in the mean radiance value from selected ground targets for July 2003 imagery



**Figure 5-4** Solar azimuth angle against the percentage change in the mean radiance values from selected ground targets for time series imagery April 2003.

#### 5.4.4. Image-to-Image normalisation

The lack of ground reference data obtained for the 2003 image data series, required that a previous calibration of SSC had to be applied from the 1997 data. However, due to changes in wavelengths in the data sets (1997 and 2003), it required that the entire 1997 data set had to be reprocessed enabling same wavelength calibrations to be applied to the 2003 time series imagery. This correction, incorporating the above sun angle correction allowed the use of the 1997 image data sets SSC calibration to be used (Figure 5.2).

Following the sun angle normalisation correction to all the time series imagery (July 1997, April & July 2003) and the lack of a SSC calibration derived from the July 2003, it was then necessary to normalise the April and July 2003 to the July 1997 time series imagery. This image-to-image normalisation was achieved by comparing the reflectance values of approximately 35 ground control points obtained from the taxiways at Warton Aerodrome for the sun angle corrected midday images from July 1997 and the midday images from April and July 2003 (Figure 5.6). This regression equation is then applied to the other normalised images in the July 2003 time series, so that the SSC calibration model generated from Atkin (2000) imagery can then be applied to the time series data sets obtained in 2003.

Unfortunately, due to the application of a sun angle normalisation to the April and July 2003 time series imagery, it became apparent that an identical sun angle normalisation would be required on the Atkin (2000) July 1997 data series and thus the subsequent construction of a new linear calibration model for this newly corrected imagery. However, due to the deficiency in the number of ground control points collected during the ground truthing for the July 2003 imagery for calibration purposes, these points were set aside for the validation purposes (no ground truth data was available for April 2003 data). It was necessary to utilize the SSC calibration model generated by Atkin (2000) for the 1997 imagery of the Ribble Estuary to calculate the SSC within the 2003 imagery.

Prior to the application of the SSC regression equation, it was necessary to apply a mask to the imagery to remove any non-estuarine zones from the subsequent SSC calibration.

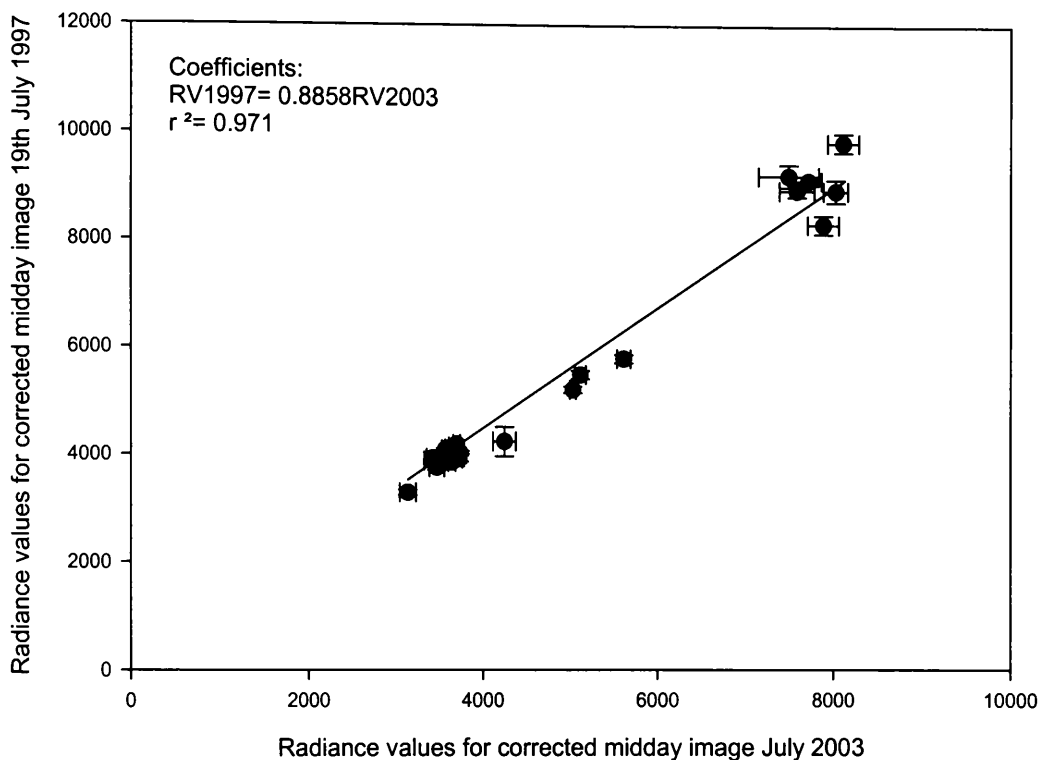


**Figure 5-5** Demonstrating of the best fit equation for the image-to-image normalisation of the July 2003 imagery to that of the July 1997 imagery obtain by Atkin (2000) obtained from ground control points at Warton Aerodrome, allowing the July 2003 imagery to be normalised to the 1997 time series imagery.

### 5.5. Modelled water volume and velocity profiles

Ideally the estimation of the water volume for each image would be derived from a combination of both LiDAR data and CASI data. However, as LiDAR data was not processed in time for image processing only modelled water volumes from VERSE were used. So modelled horizontal velocity, volumetric

data and suspended particulate matter estimates were obtained from the VERSE model for the two time series dates. The modelled area selected within this study stretches from GR337800/426100, close to Site 1 (Figure 3.1), to Bull Nose at Preston Docks. This zone encompasses 50 longitudinal 250m cells that VERSE can individually calculate the water volumes for. VERSE also generates a depth component within each cell for the above criteria, however, within this study the results were averaged for each individual cell.

The model allows the estimation of the average horizontal water velocities for each cell (Figures 5.6, 5.7 & 5.7) along the length of the study area at the time of each overflight. It can be seen from the figures below that the modelled horizontal flow patterns appear to show a net reduction in flow velocity around the River Douglas confluence. This may be due to the impact of two flow patterns converging and generating increased turbulence, effectively retarding the horizontal flow speed. It may also increase the suspended sediment load within the water column due to the increase in horizontal mixing that will take place within this zone of increased turbulence. It should be noted from figures 5.6 & 5.7, that flow velocities are registered as negative flow velocities. These values represent down-estuary flow, whilst positive flow velocities indicate an overall landward flux.

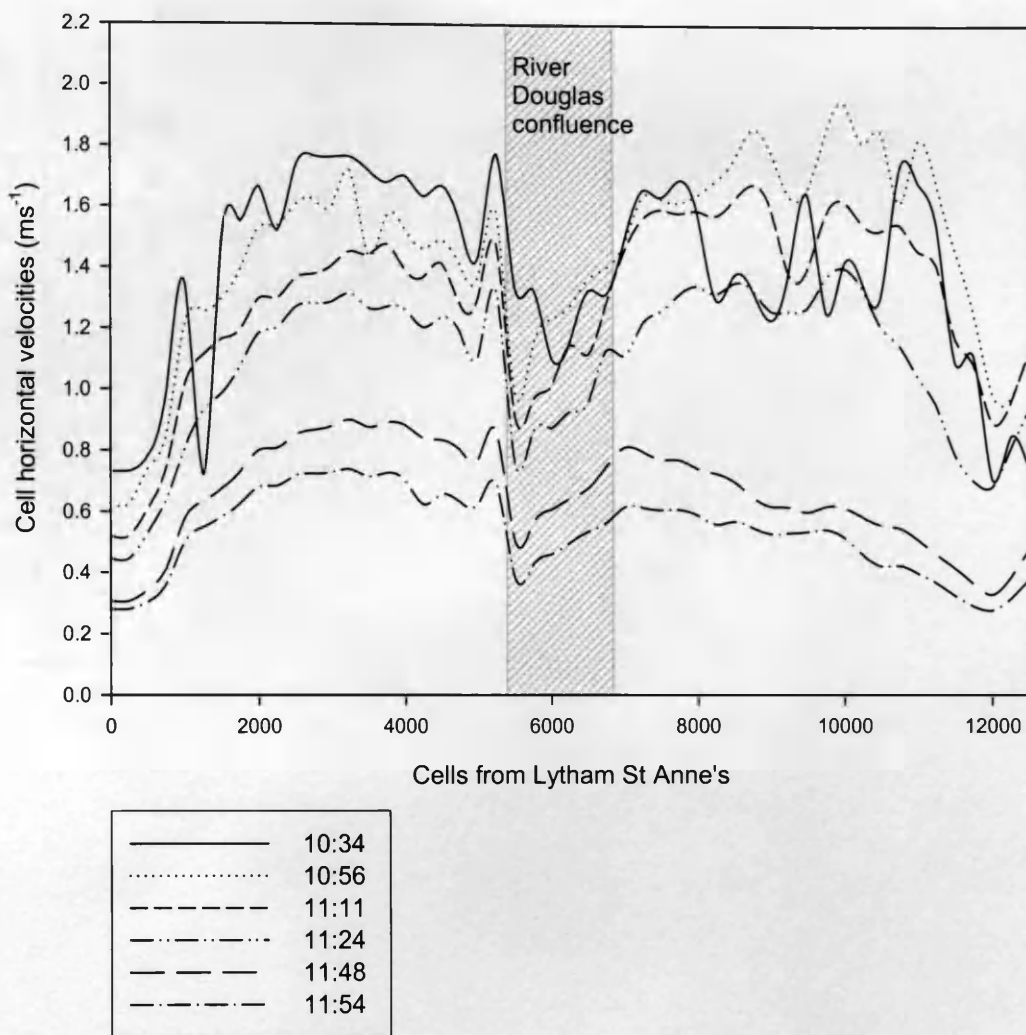


**Figure 5-6** Cell velocities from Lytham St Anne's to Preston Docks showing flow in the morning 15<sup>th</sup> July 2003.

Maximum flow appears to occur during the 10:34 and 10:56 flights on the 15<sup>th</sup> July, with the maximum flow rates occurring within the confined intertidal zones located close to Warton Bank and the upper estuarine zone above the River Douglas confluence. At the confluence, flow rates are modelled to fall by approximately half their pre-confluence velocities, gradually increasing

towards the upper estuarine zones to a maximum horizontal flow rate of  $1.95 \text{ ms}^{-1}$ .

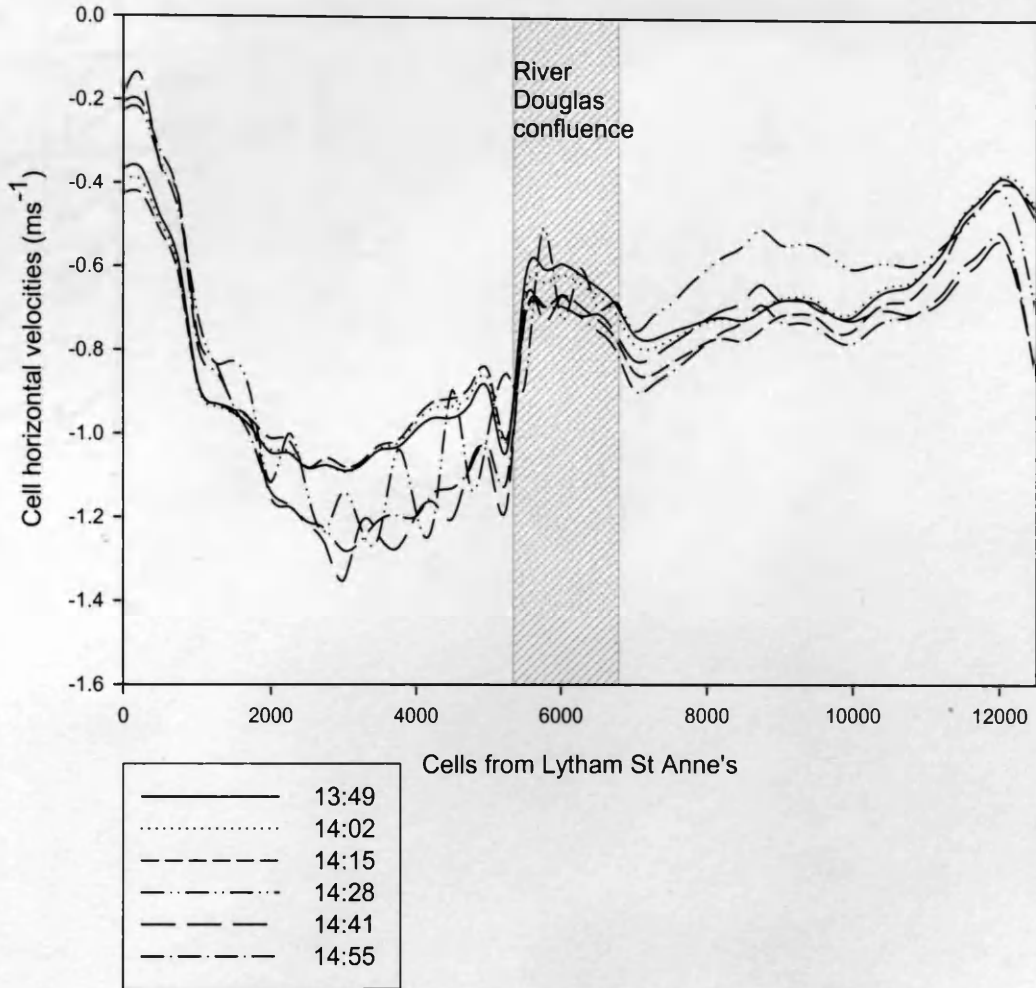


**Figure 5-7** Cell velocities from Lytham St Anne's to Preston Docks showing flow in the morning 15<sup>th</sup> July 2003.

Flow velocities for the initial April 2003 imagery demonstrate a positive flow for the lower/middle sections of the estuary, whilst the upper estuarine zone shows a negative or down estuary flow velocity direction. However, the velocity direction switches over the course of the in-coming flood tide,

reaching maximum flow velocities of  $1.95 \text{ ms}^{-1}$  just prior to the River Douglas confluence zone. During the ebb tide flow, horizontal flow velocities are modelled to be approximately half that of the main flood horizontal velocities (Figure 5.8). Again, the River Douglas confluence appears to have an effect on the flow velocities, with velocity reducing as it approaches the confluence and rapidly accelerating after the confluence zone.

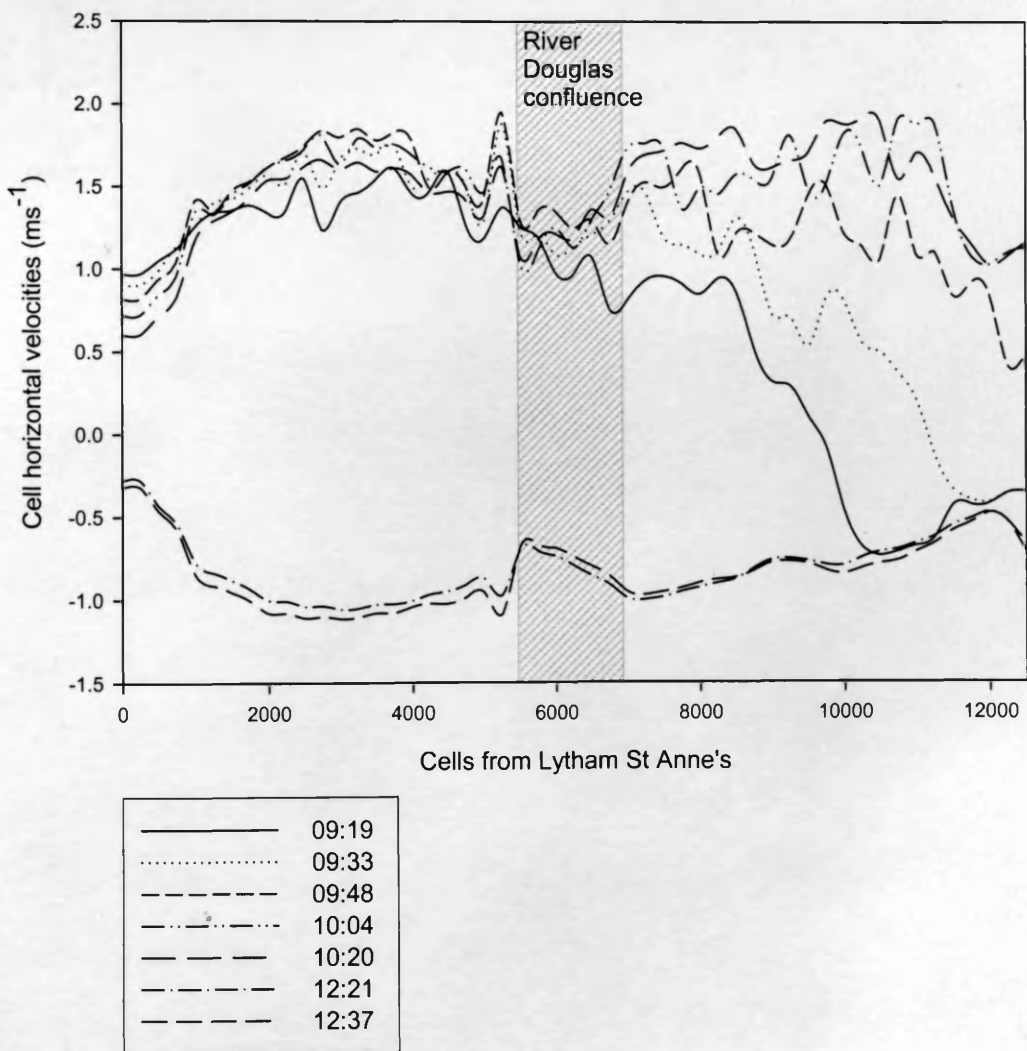


**Figure 5-8** Cell velocities from Lytham St Anne's to Preston Docks 16<sup>th</sup> April 2003.

## **5.6. Results**

### **5.6.1. Introduction**

The results are divided into two distinct sections. The first describe the point measurement data retrieved in association with the July 2003 time series imagery, providing validation and calibration data the subsequent CASI time series imagery. Following on from these important reference data are the two sets of time series imagery obtained on the 16<sup>th</sup> April and 15<sup>th</sup> July 2003.

### **5.6.2. Ground reference data**

#### **SSC**

The suspended sediment results derived during the July 2003 time series flights of the Ribble Estuary, show that there is little variation in the mean grain size (Table 5.5) across all the samples. However, there is a difference in the clay, silt and sand percentages for the concluding sample. This sample (8) shows large percentages of sand, which far exceeds any of the previous seven samples. The location of the sampling was situated above the southern intertidal surface, which with a lowering ebb tide, became much shallower and the resulting suspended sediment in the water column could have been generated from the basal layer of the water column.

Sample No.	Location (Easting)	Northing	Mean Grain size (um)	Clay %	Silt %	Sand %	SSC (mg l <sup>-1</sup> )
1	38786	26186	16.0	1.1	98.8	0.2	18.9
2	38944	26343	16.7	1.7	98.1	0.3	71.2
3	39060	26302	14.1	1.1	98.9	0.0	23.4
4	29298	26227	14.4	1.3	98.7	0.0	27.9
5	39031	26210	16.0	1.2	98.8	0.0	40.2
6	39060	26309	15.2	1.1	98.9	0.0	45.6
7	38984	26439	20.9	3.4	93.3	3.3	47.2
8	38942	26102	13.4	16.8	45.6	47.0	47.4

**Table 5-6** Sample locations and grain size distribution for concomitant ground control points for July 2003 CASI imagery. Also sampled SSC within the surface waters of the estuary

The SSC values obtained from the collected samples demonstrate that the range is from 18.9 to 71.2 mg l<sup>-1</sup>. Table 5.5 shows that there is an increase in the SSC over the course of the sediment sampling period. The initial 4 samples (except for Sample 2, which was obtained at the axial convergence front), are approximately half that of the subsequent samples which were obtained during the initial ebb tidal period. This point measurement data, when compared to the 1997 data, demonstrates that the SSC are all in the lower quartile of the data distribution. This is because sampling only took place at high water slack and over the subsequent ebb tide and not over the highly turbid initial flood period. Therefore, SSC and <sup>137</sup>Cs were relatively low in comparison to the values obtained by Atkin (2000) in 1997.

#### *Calibration of <sup>137</sup>Cs from SSC*

Because of the relatively small data set generated by the eight sample bottles, it was necessary to demonstrate that any linear relationship between SSC and <sup>137</sup>Cs activity concentrations were within previously measured parameters. Subsequently any previous identified linear relationships in SSC/<sup>137</sup>Cs activity

concentrations could then be applied to present imagery of the Ribble Estuary to generate estimates of total inventory of  $^{137}\text{Cs}$  transported over the flood and ebb tide. Atkin (2000) demonstrated that there was a linear relationship between suspended sediment concentrations and  $^{137}\text{Cs}$  and because the results were obtained during consecutive summers (1996 and 1997), a temporal seasonal stability may be interpreted from the data (Figure 5.12).

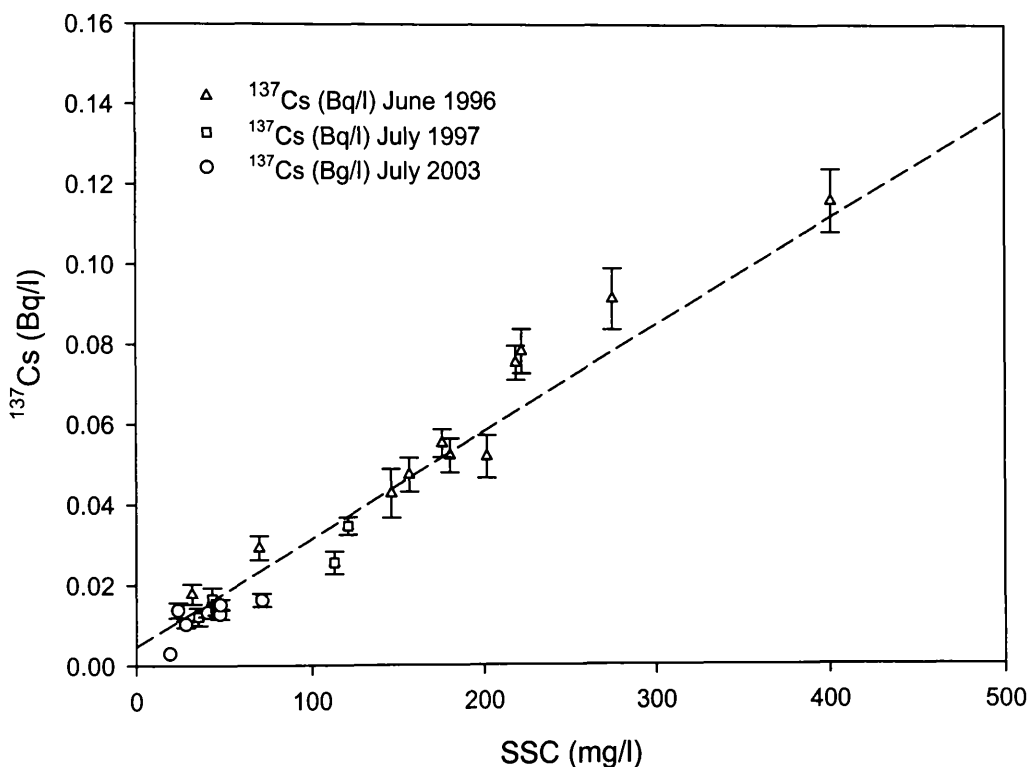


**Figure 5-9** The environmentally derived relationship between suspended sediment and the associated  $^{137}\text{Cs}$  concentration and its temporal stability (Atkin 2000), in comparison to the July 2003 sampling data.

### Depth profiling of the estuarine water column

Figure 5.10 demonstrates that the turbidity of the estuarine water column does not vary greatly with depth, except for the basal layer where the turbidity probe was probably embedded within the mobile bed sediments. The sampling periods coincided with the high tide slack water period and the initial phases of the ebb tidal period, when water stratification might be expected.

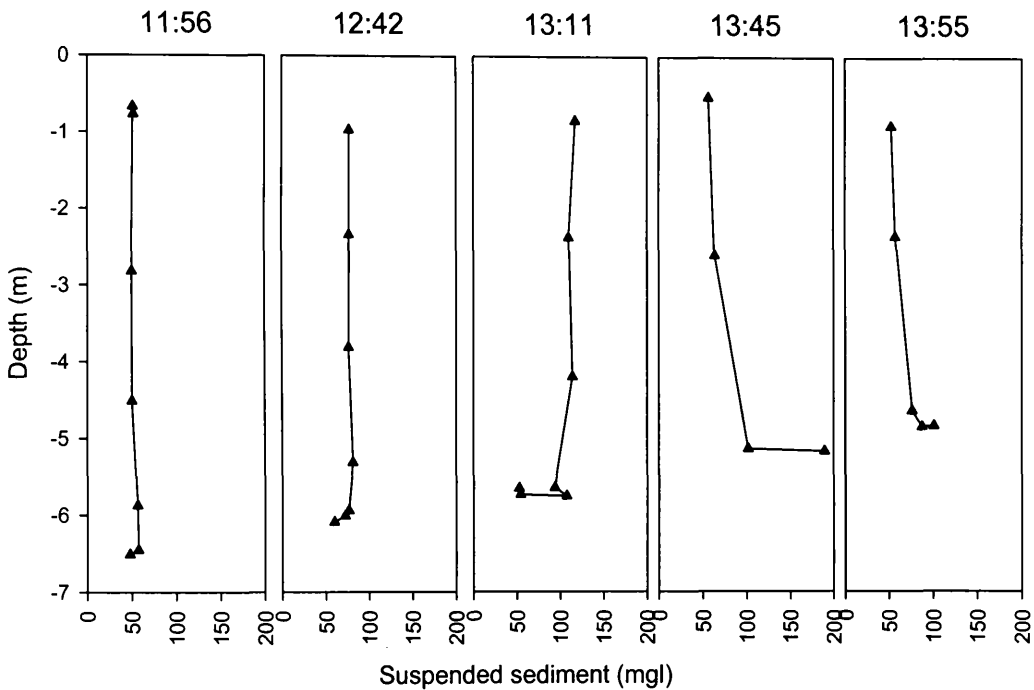


**Figure 5-10** SSC for the Ribble Estuary, obtained concurrently with the July 2003 time series CASI imagery.

### 5.6.3. Time series imagery

For the purposes of image presentation and understanding, each individual image is reproduced in full, with two subsections enlarged and highlighted to identify important sections of the estuary at the different stages of the tidal cycle. The second smaller window viewing Preston Docks is used to demonstrate how effective and the image normalisation techniques conducted

above are. This is because Preston Docks represent a fixed body of water (due to lock gates) that has no significant in-flux of water into the dock environment over the course of the flood and ebb tide event. Therefore, assuming that the water properties of the data remain relatively constant there should be little change in SSC within this water body and consequently can be used as a control zone.

#### **5.6.4. Image analysis – 15<sup>th</sup> July 2003**

##### *Data quality*

It is evident from the initial images (Figures 5.14 – 18) that there is a significant presence of sun glint at the southern edge of the imagery, which exaggerates the underlying trends in SSC. However, within Figure 5.14, upstream of the River Douglas confluence, there is a marked increase in SSC, from 60 - 100 mg l<sup>-1</sup> prior to confluence rising to 120 – 319 mg l<sup>-1</sup>. These values appear to drop rapidly after approximately 3 km from the convergence zone, falling back values typical of the eastern side of the confluence. This feature of increased SSC subsequently appears in figures 5.15 – 5.18, although it is less pronounced within some of the imagery. However, the axial convergence front is present within all the initial imagery gathered during the flood tide stage of the tide. This feature then disappears during the subsequent ebb tide images (figures 5.19 – 5.23), indicating no strong lateral circulatory currents on the ebb tide, which generate the axial convergence fronts.

It is apparent within the Preston dock subsection that the average SSC values registered during the flood tidal sequence are all confined to approximately 20 – 60  $\text{mg l}^{-1}$ , except for the cloud shadow effect in figure 5.14a. It is also evident that there is a slight gradient in SSC along the length of the docks, with higher SSC values found around the moored boats and adjacent to the dock gates.

### *Suspended sediment calibration*

Subsequent to image-to-image normalisation with the July 1997 midday image (Atkin, 2000), the linear model of estimated suspended sediment generated from comparison of ground control points collected concomitant with 1997 imagery and image radiance values from CASI band 10 (SeaWifs setting), can then be applied to the normalised imagery of the April and July 2003 data (Figure 5.11). The mean radiance values were obtained from the imagery by assessing 3x3 grids of pixels at each sampling location within the imagery and compared to the measured SSC. It is apparent from Figure 5.10 that the largest uncertainty is associated with the actual measured values of SSC and not through the radiance values and it is this linear regression model that is applied to the data to convert image data to SSC.

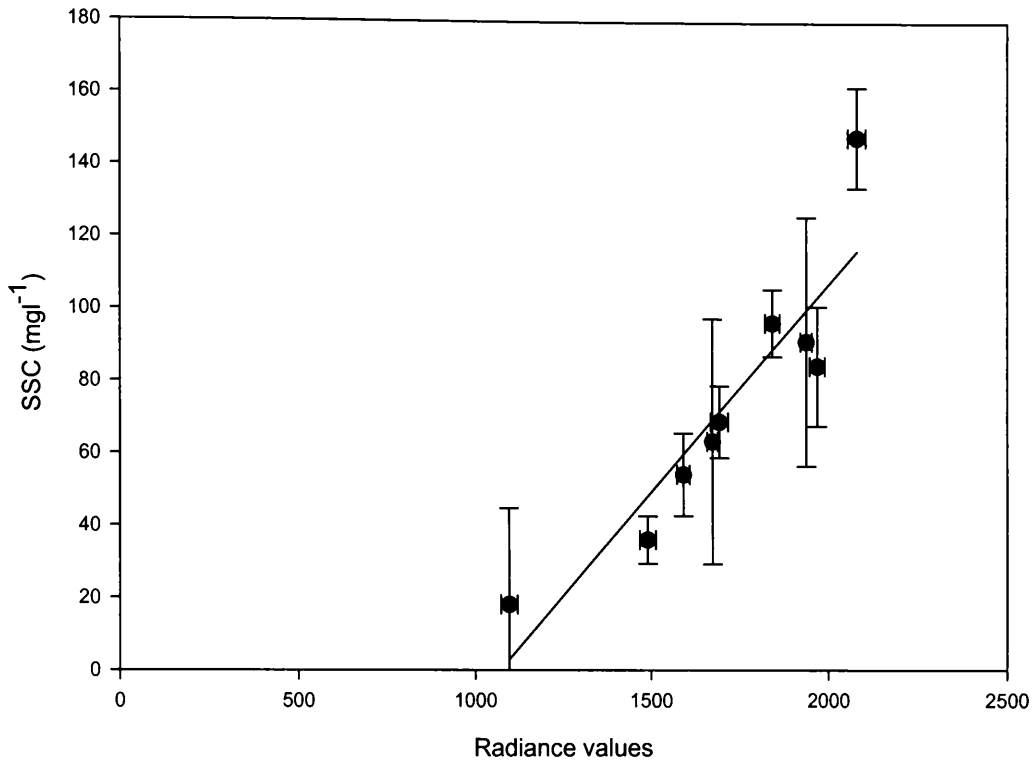


**Figure 5-11** Measured SSC values compared to image radiance values obtained from Atkins' (2000) July 1997 imagery, band 10 CASI.

$$SSC = 0.1153x - 123.49 \text{ imageradiance}$$

**Equation 5-1**

It is evident from Figure 5.11, that the measured and estimated SSC values generated by the application of the linear model (Equation 5.1) demonstrate a very good coefficient of determination ( $R^2$ ) of 0.83. It is also apparent from the Figure 5.11 that the lower and upper regions of the estimated SSC are being under estimated, which could lead to underestimation of SSC during slack water periods and also during the initial periods of the flood tide.

### Validation of SSC relationships

The effects of cloud shadow coincided with flight overpasses and reference data collection, rendering seven of the eight points inappropriate for validation purposes. From the remaining sample point, a 5x5 pixel average was obtained using the ENVI region of interest tool. Mean and standard deviation values were generated and compared to measure SSC. This produced a measured value of  $23 \text{ mg l}^{-1}$  and an estimated value of  $23.5 \text{ mg l}^{-1}$  ( $\pm 2.5 \text{ mg l}^{-1}$ ) from the ARS imagery of the area. This is a good comparison, and although limited to one point of reference, provides some confidence in the correction procedure. Therefore an un-calibrated sampling location was identified at Preston Docks to provide independent validation of the image correction procedures outlined above. Figure 5.12 demonstrates that within the Preston Dock, the mean SSC in each image demonstrates a greater homogeneity across the image data set, in comparison to the estuary channel, thus providing a non-calibrated validation point within the imagery.

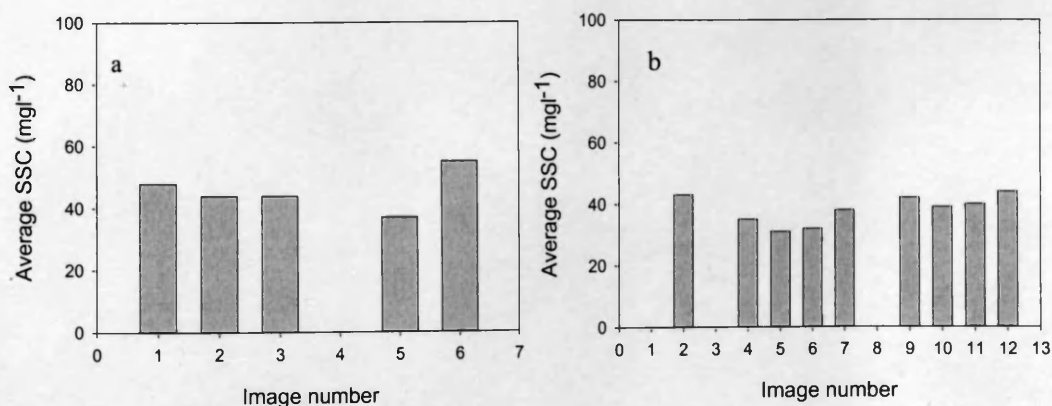


**Figure 5-12** Average SSC within Preston Docks a: April 2003 & b: July 2003. Blank spaces represent areas where data is not available due to reduced flight lines or cloud cover over dock area.

The uniformity of the SSC for Preston Docks (Figure 5-12) demonstrates that it is effectively a closed system, in terms of the tidal cycle. It could be expected that there is some input of fresh estuarine water during the high tide period, but with no evident circulation patterns in the inner dock area, it should only influence the area adjacent to the dock gates (Figures 5.17 – 5.19). This means that there is a marked difference between the relatively stable inner dock water body and the main estuary channel that demonstrates great variability, in terms of SSC, over the course of a flood and ebb tidal cycle.

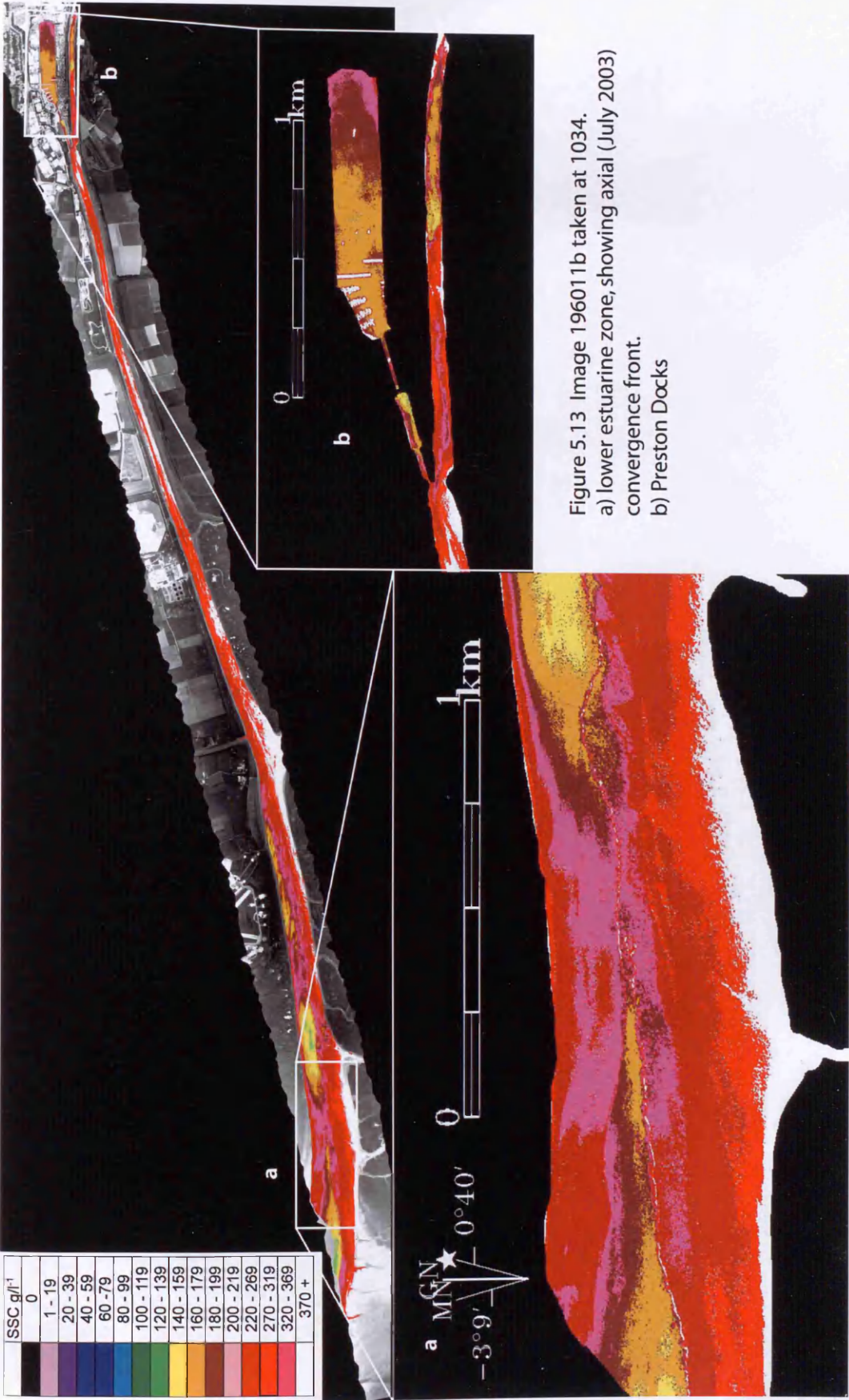


Figure 5.13 Image 196011b taken at 1034.  
 a) lower estuarine zone, showing axial convergence front.  
 b) Preston Docks

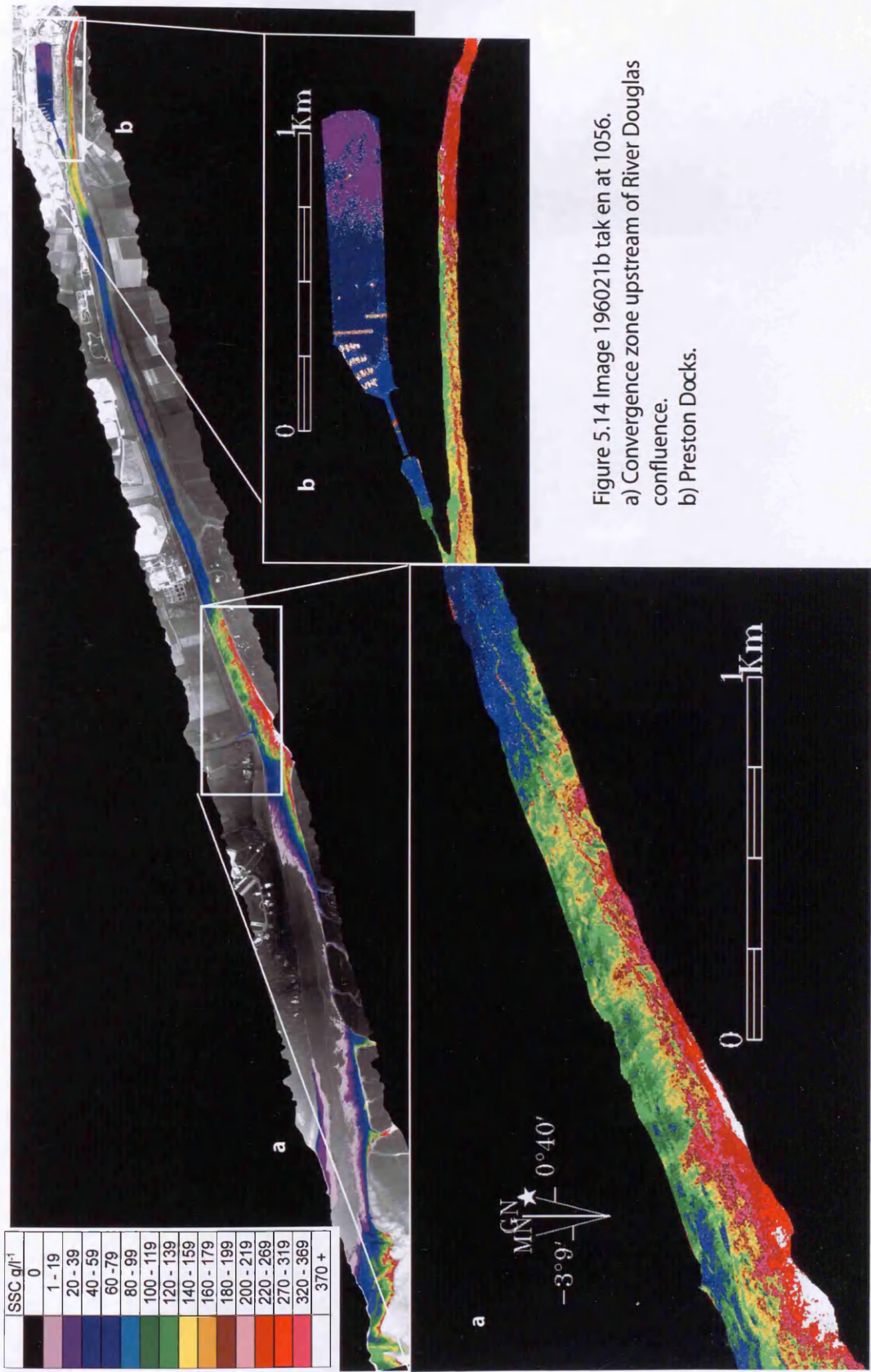


Figure 5.14 Image 196021b taken at 1056.  
 a) Convergence zone upstream of River Douglas confluence.  
 b) Preston Docks.

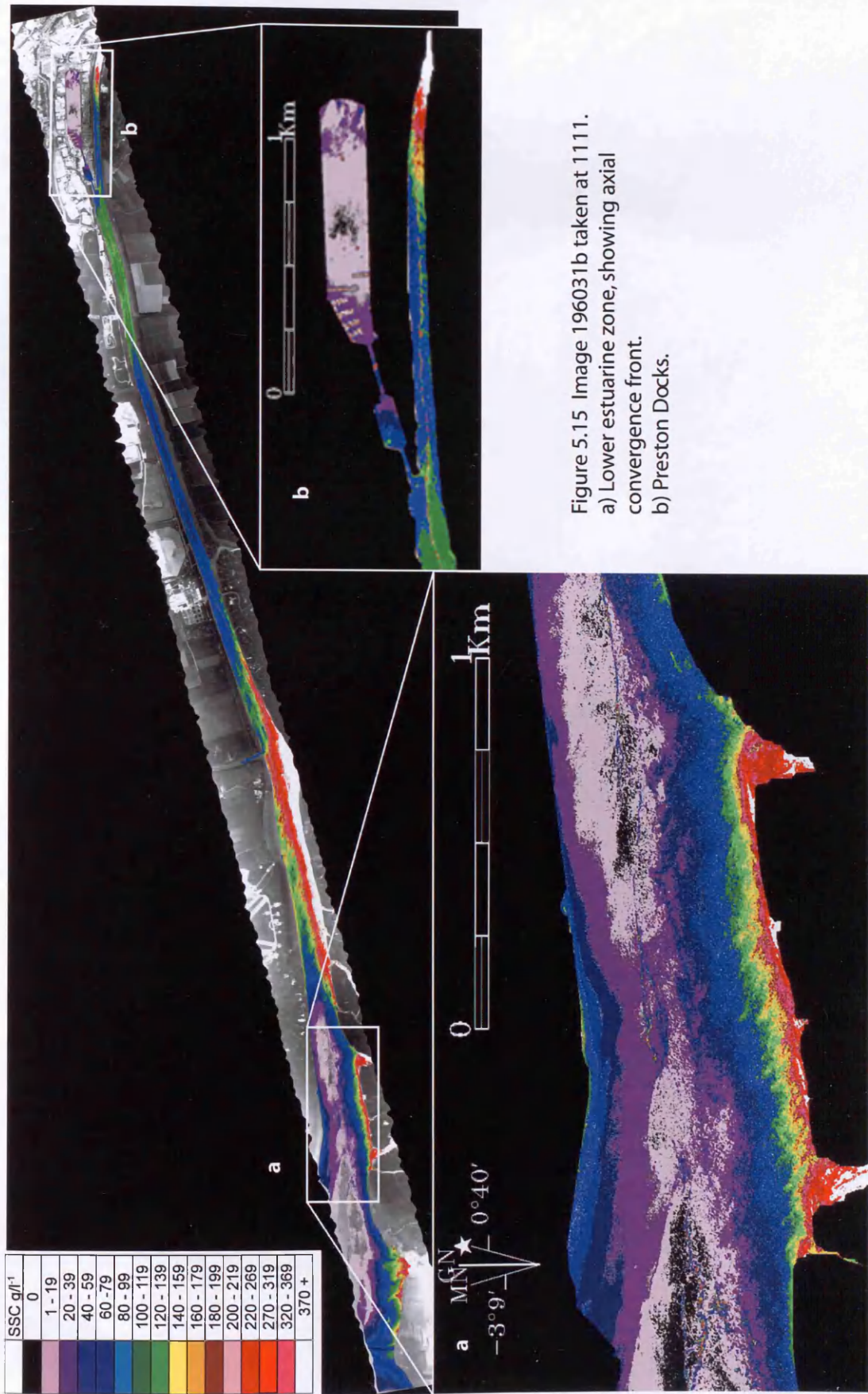


Figure 5.15 Image 196031b taken at 1111.  
 a) Lower estuarine zone, showing axial convergence front.  
 b) Preston Docks.

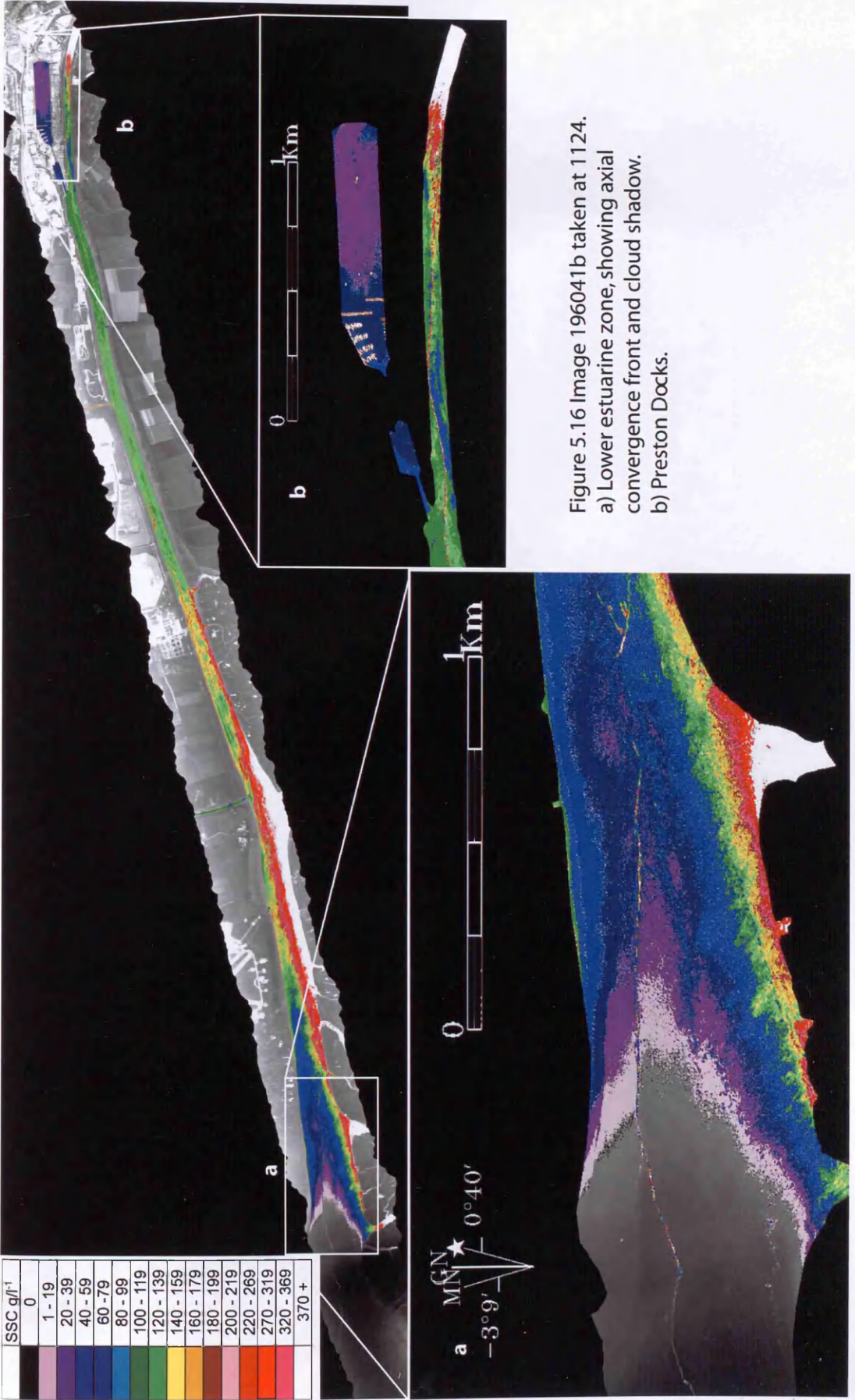


Figure 5.16 Image 196041b taken at 1124.  
 a) Lower estuarine zone, showing axial convergence front and cloud shadow.  
 b) Preston Docks.

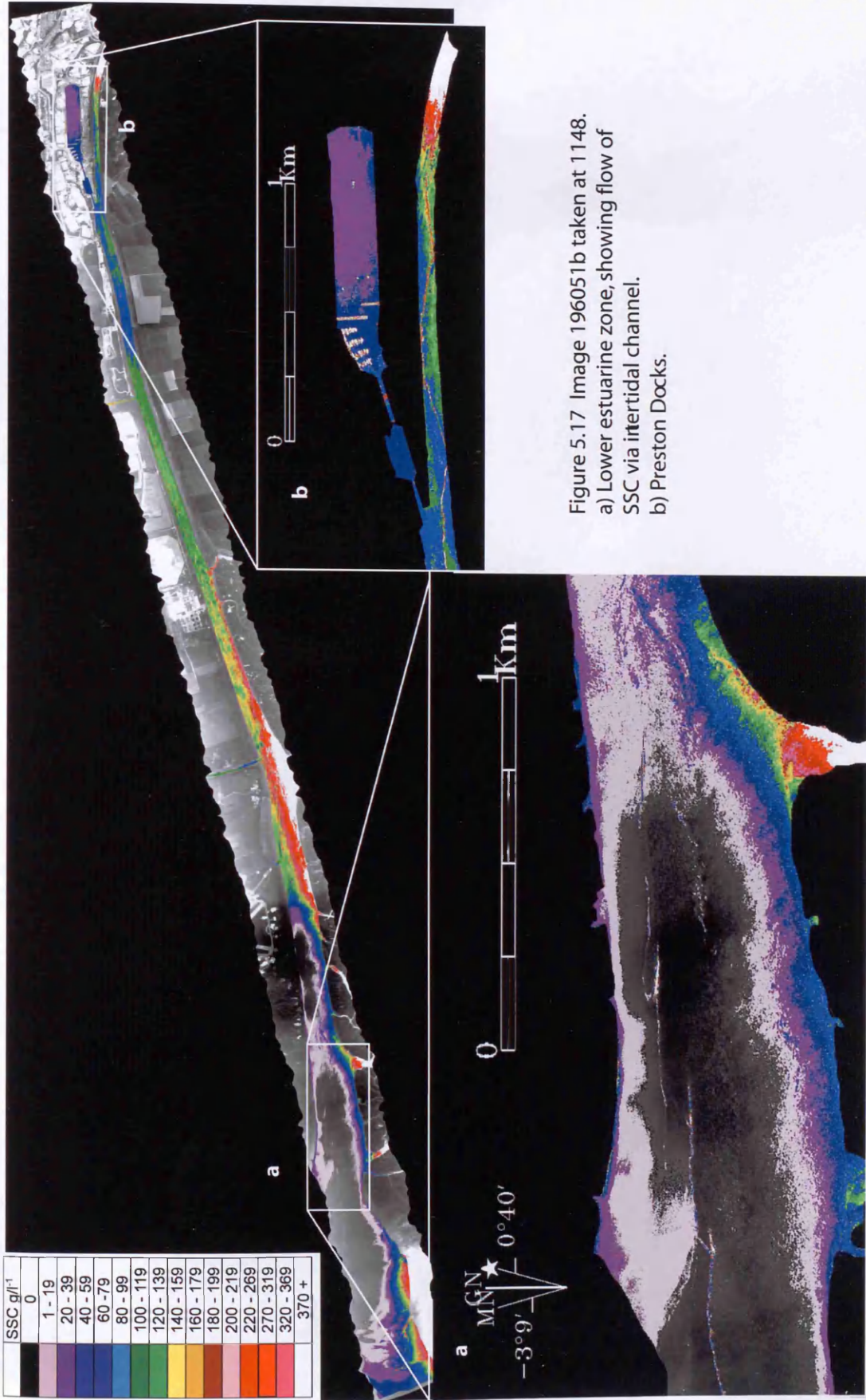


Figure 5.17 Image 196051b taken at 1148.  
 a) Lower estuarine zone, showing flow of SSC via intertidal channel.  
 b) Preston Docks.

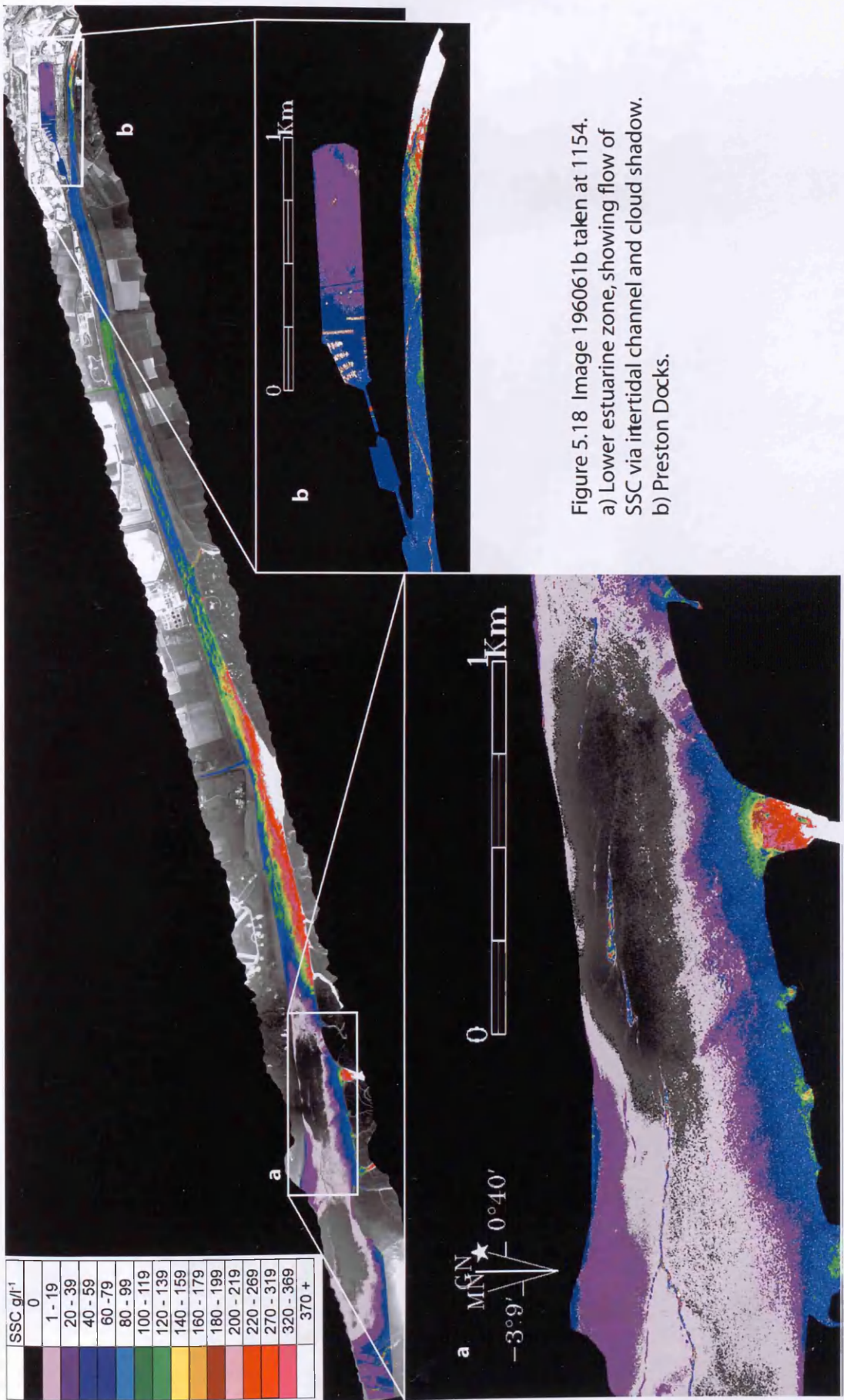


Figure 5.18 Image 196061b taken at 1154.  
 a) Lower estuarine zone, showing flow of SSC via intertidal channel and cloud shadow.  
 b) Preston Docks.

During the time series imagery data that captured the start of the ebb tide during the 17<sup>th</sup> July 2003. The SSC values estimated from the imagery (Figures 5.19 – 5.24) were lower than the values obtained for the flood tide imagery. There appears to be little or no effect from sun glint on the southern boundary of the imagery. Reassuringly, the SSC mapped within Preston Docks appears to have stayed similar throughout the morning flood tide imagery. Flow patterns can be seen in figures 5.19 & 5.20, indicating that there is an injection of suspended sediment into the main channel from the southern intertidal channels. It is also noticeable that the areas outside the main, entrained estuary channel have higher values of SSC than within and which only increase over time as the tide falls in subsequent images (seen clearly in Figure 5.23). The radiometric resolution is sensitive enough to pick out the effects the mile marker posts have on SSC in their localised area. This is demonstrated within Figure 5.24a, where in the central section of the enlarged image, there is a noticeable plume of higher suspended sediment downstream from the mile marker (Figure 5.24 a (i)).

Flow patterns are being identified within the SSC images from the July 2003 time series data set. Each image exhibits unique flow structures and patterns within the surface waters of the estuary. Within Figure 5.16, for example, the axial convergence is present throughout the estuary system, where it is clearly marked by a thin section of high SSC located within the central section of the estuary channel. Unfortunately, sun glint masks the flow patterns defined at the Douglas/Ribble interface.

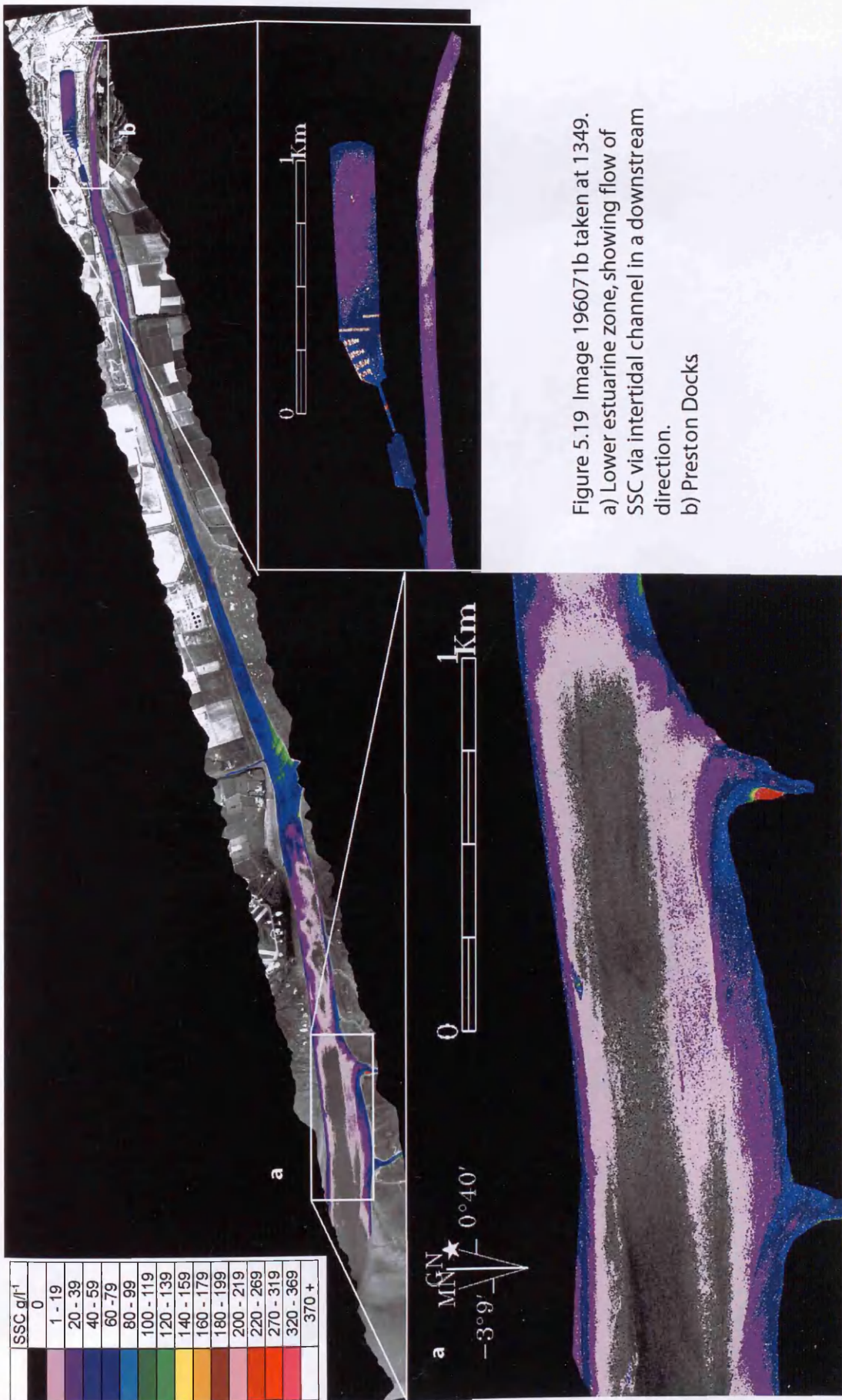


Figure 5.19 Image 196071b taken at 1349.  
 a) Lower estuarine zone, showing flow of SSC via intertidal channel in a downstream direction.  
 b) Preston Docks

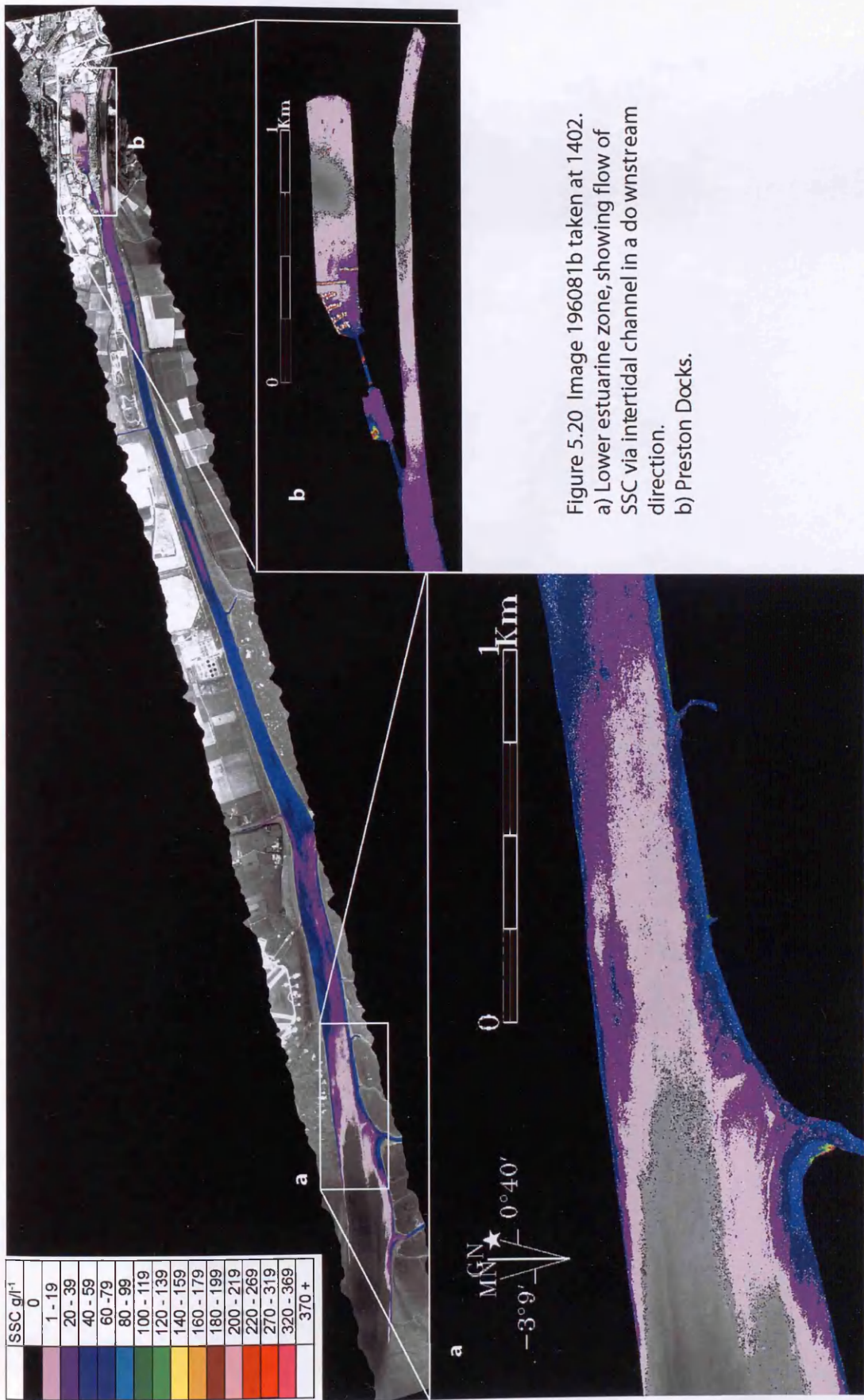


Figure 5.20 Image 196081b taken at 1402.  
 a) Lower estuarine zone, showing flow of SSC via intertidal channel in a do wnstream direction.  
 b) Preston Docks.

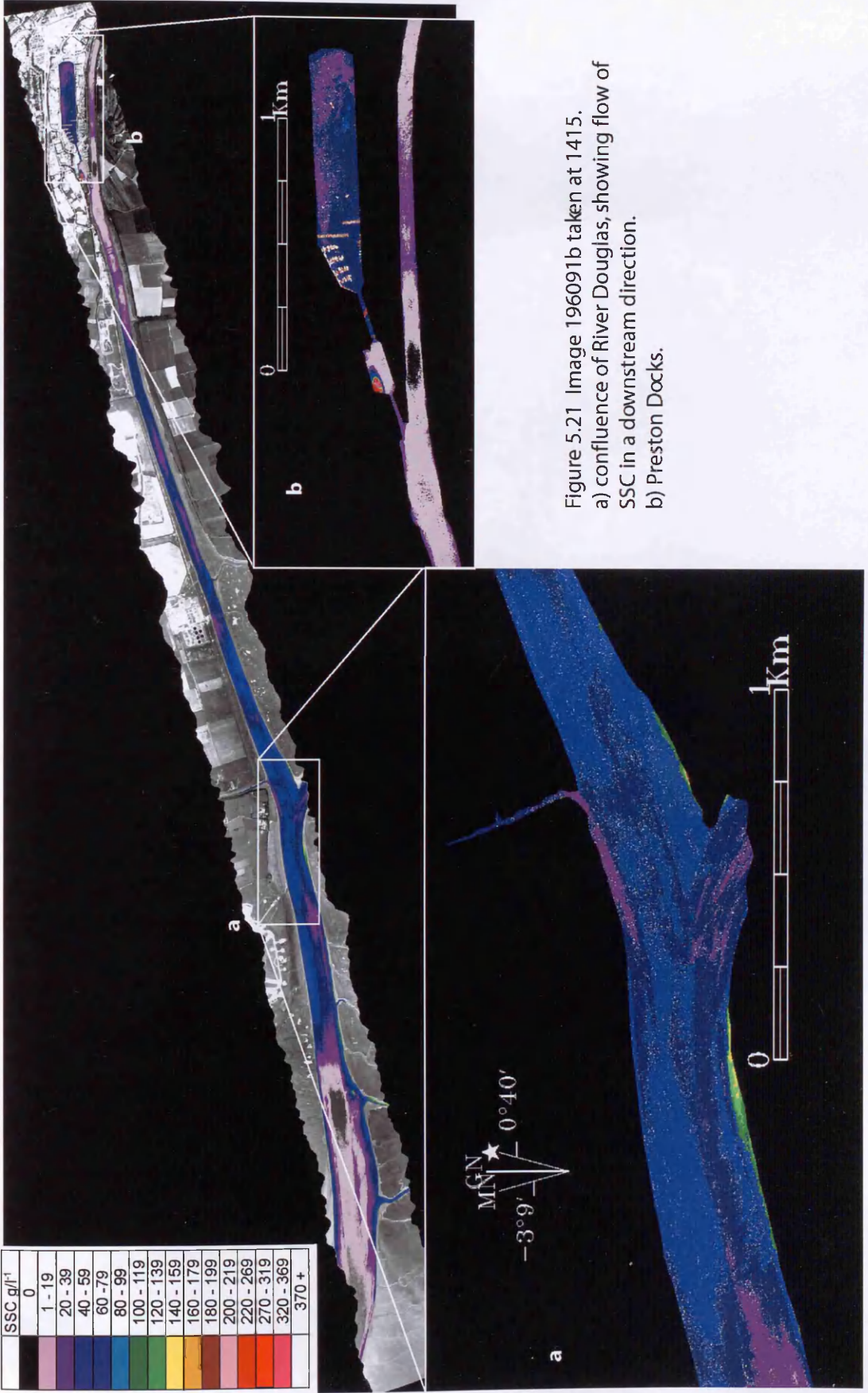


Figure 5.21 Image 196091b taken at 1415.  
 a) confluence of River Douglas, showing flow of SSC in a downstream direction.  
 b) Preston Docks.

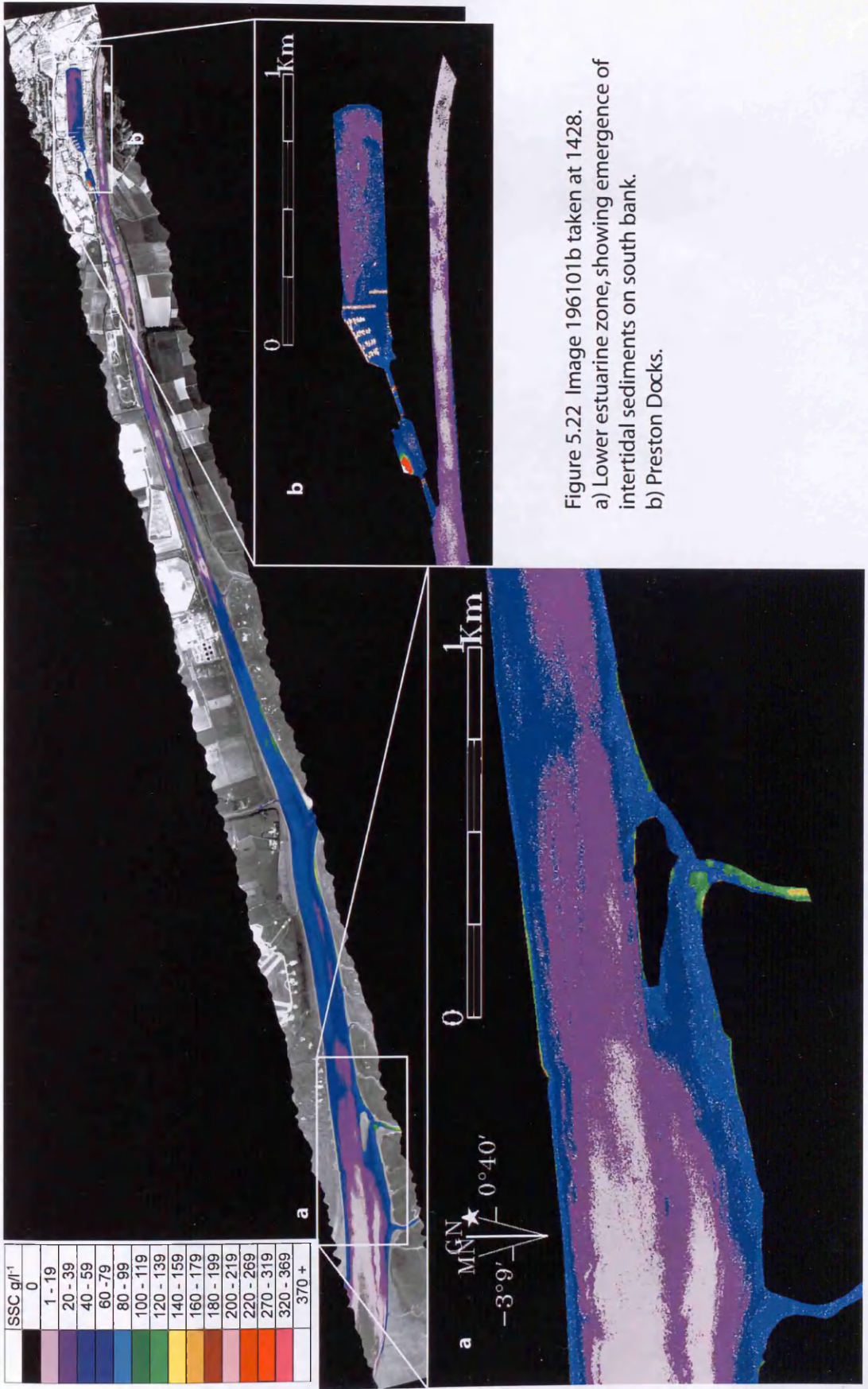


Figure 5.22 Image 196101b taken at 1428.  
 a) Lower estuarine zone, showing emergence of intertidal sediments on south bank.  
 b) Preston Docks.

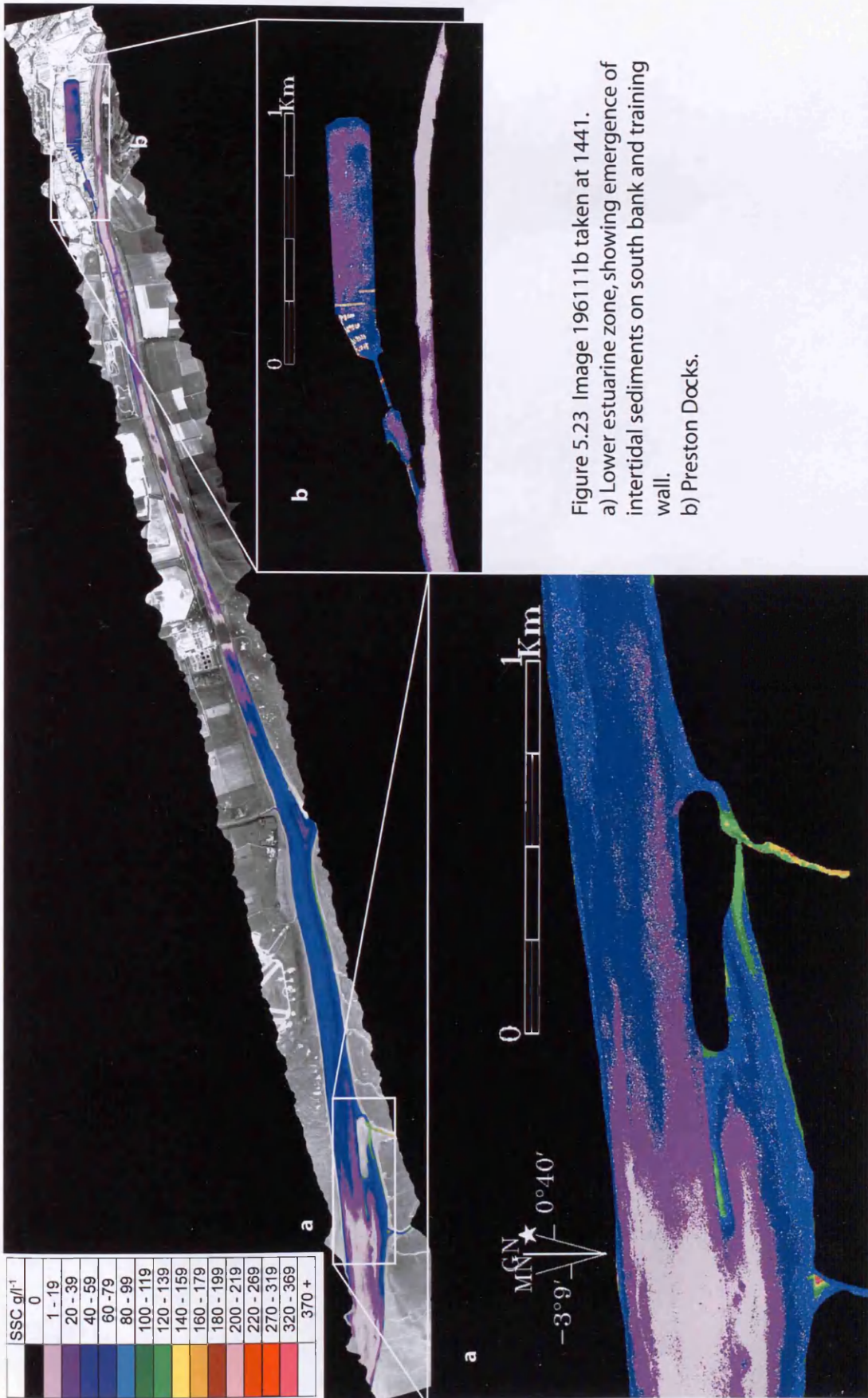


Figure 5.23 Image 196111b taken at 1441.  
 a) Lower estuarine zone, showing emergence of intertidal sediments on south bank and training wall.  
 b) Preston Docks.

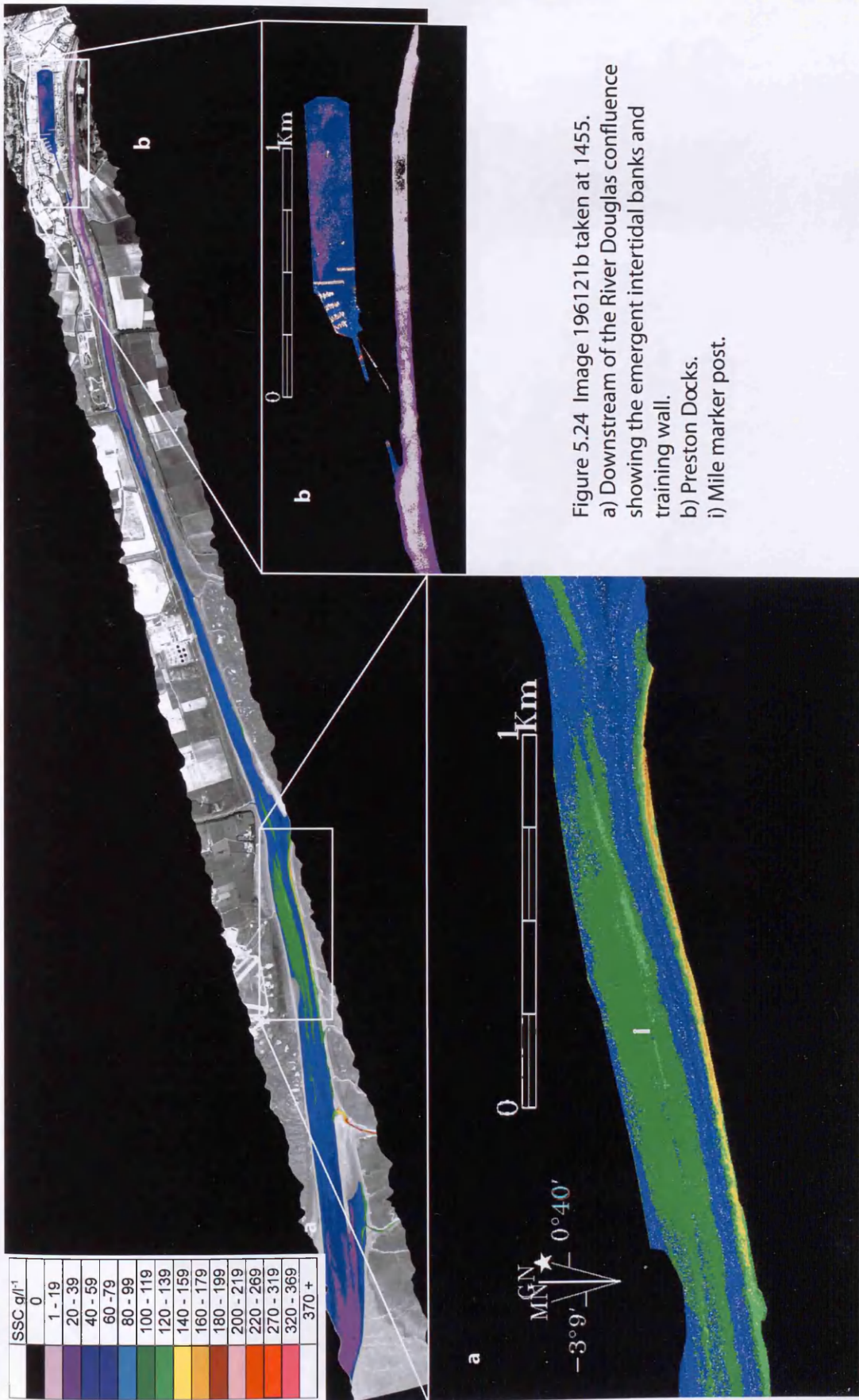


Figure 5.24 Image 196121b taken at 1455.  
 a) Downstream of the River Douglas confluence showing the emergent intertidal banks and training wall.  
 b) Preston Docks.  
 i) Mile marker post.

### **5.6.5. Image analysis – 16<sup>th</sup> April 2003**

The April 2003 data series relies on the assumption that SSC radiance calibration values will be temporally stable over the summer months and that the assumptions that are applied to the July 2003 time series data can also be applicable for the April 2003 data. Again, Preston Dock can be used to validate the image calibration process (Figure 5.12), demonstrating good inter-image comparison for the April 2003 data, as well as showing good inter-data similarity.

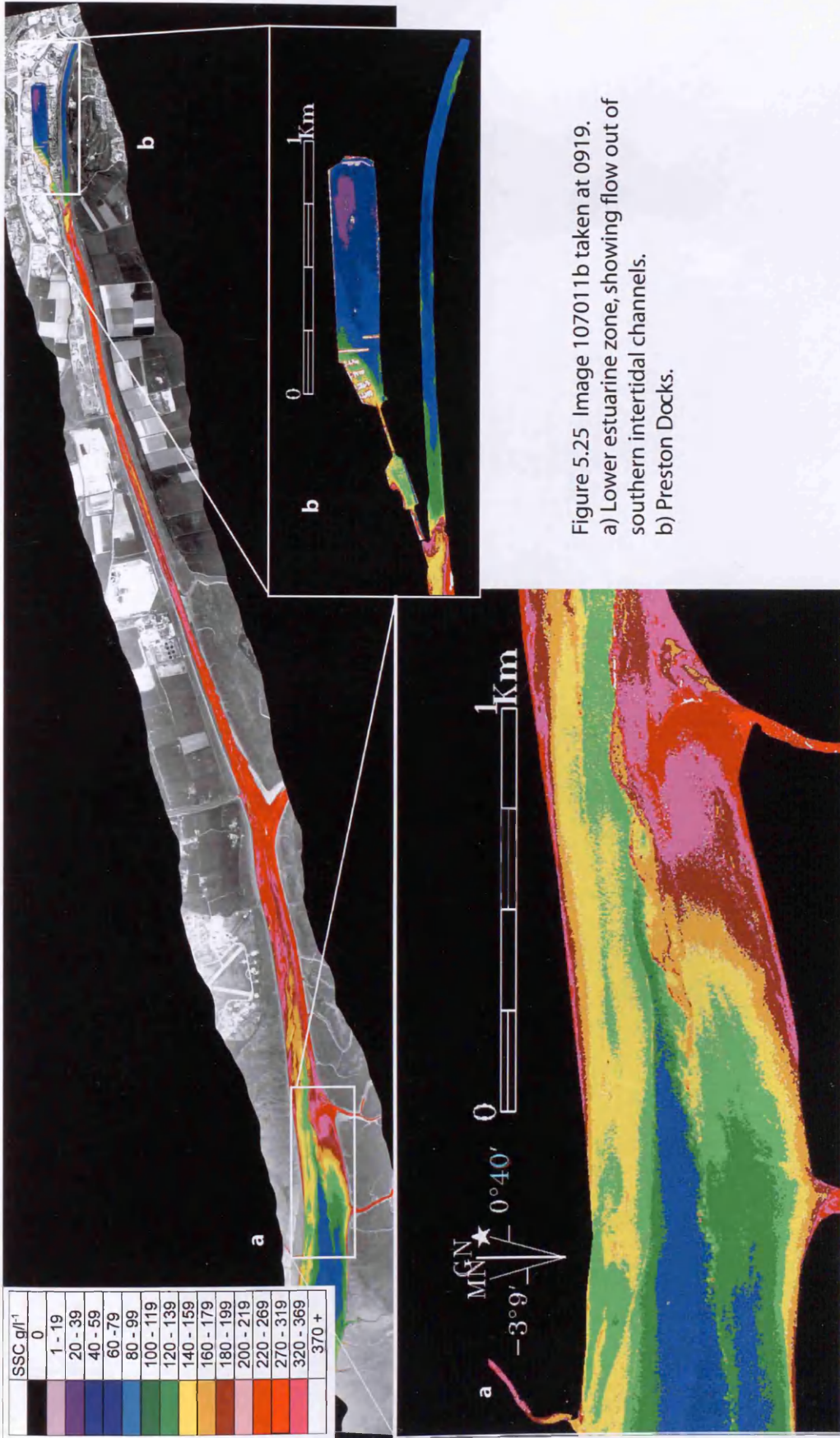


Figure 5.25 Image 107011b taken at 0919.  
 a) Lower estuarine zone, showing flow out of southern intertidal channels.  
 b) Preston Docks.

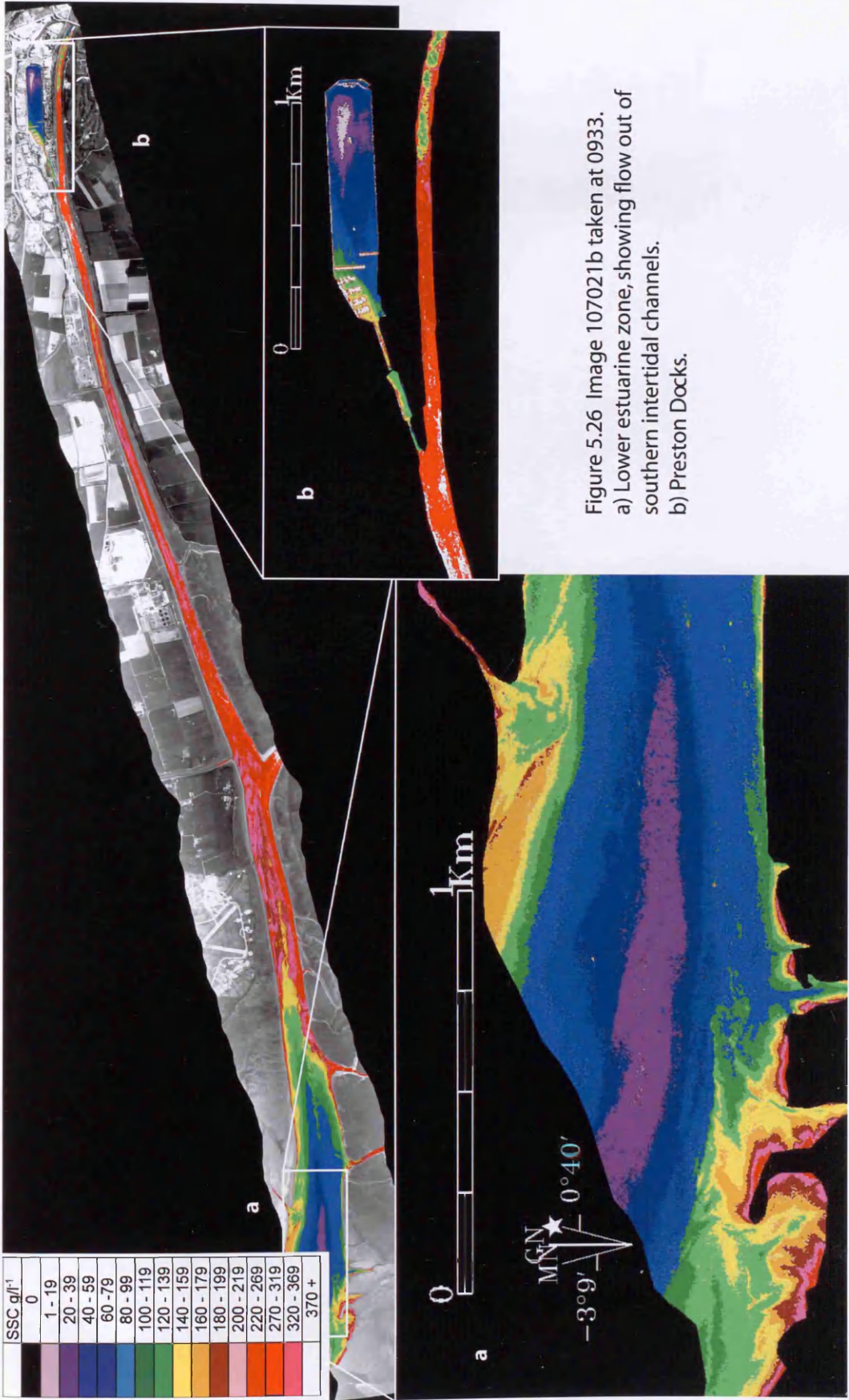


Figure 5.26 Image 107021b taken at 0933.  
 a) Lower estuarine zone, showing flow out of southern intertidal channels.  
 b) Preston Docks.

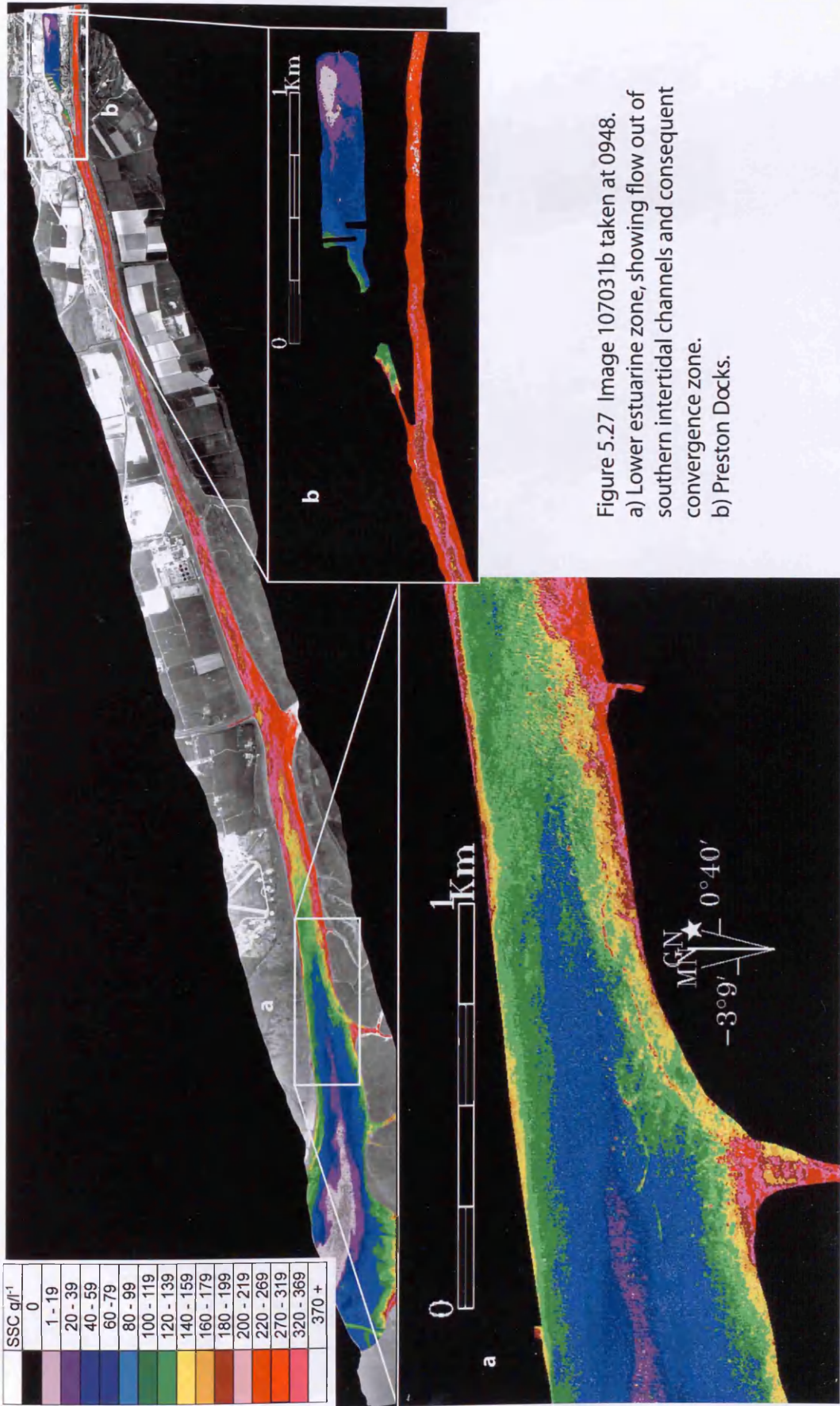


Figure 5.27 Image 107031b taken at 0948.  
 a) Lower estuarine zone, showing flow out of southern intertidal channels and consequent convergence zone.  
 b) Preston Docks.

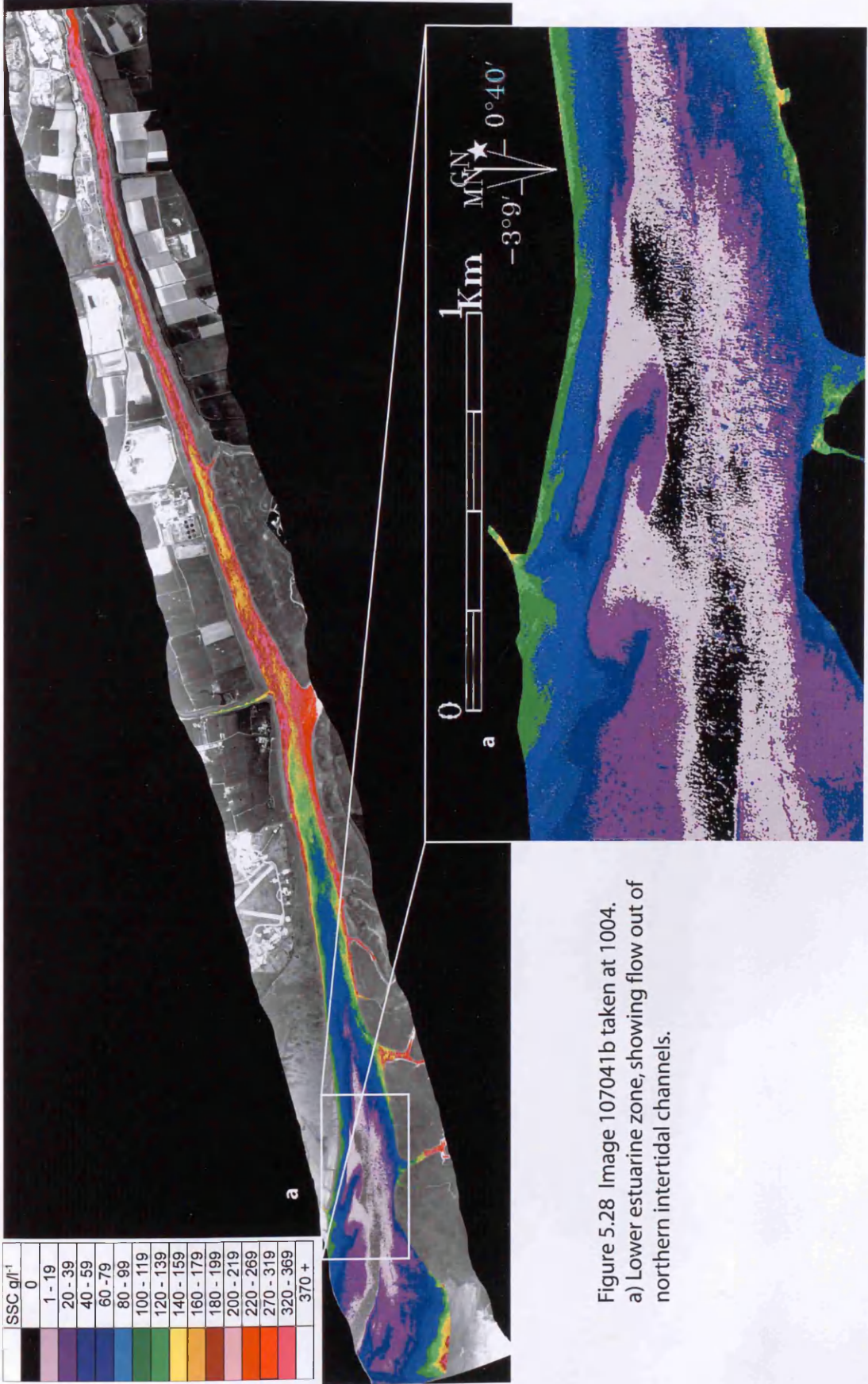


Figure 5.28 Image 107041b taken at 1004.  
 a) Lower estuarine zone, showing flow out of northern intertidal channels.

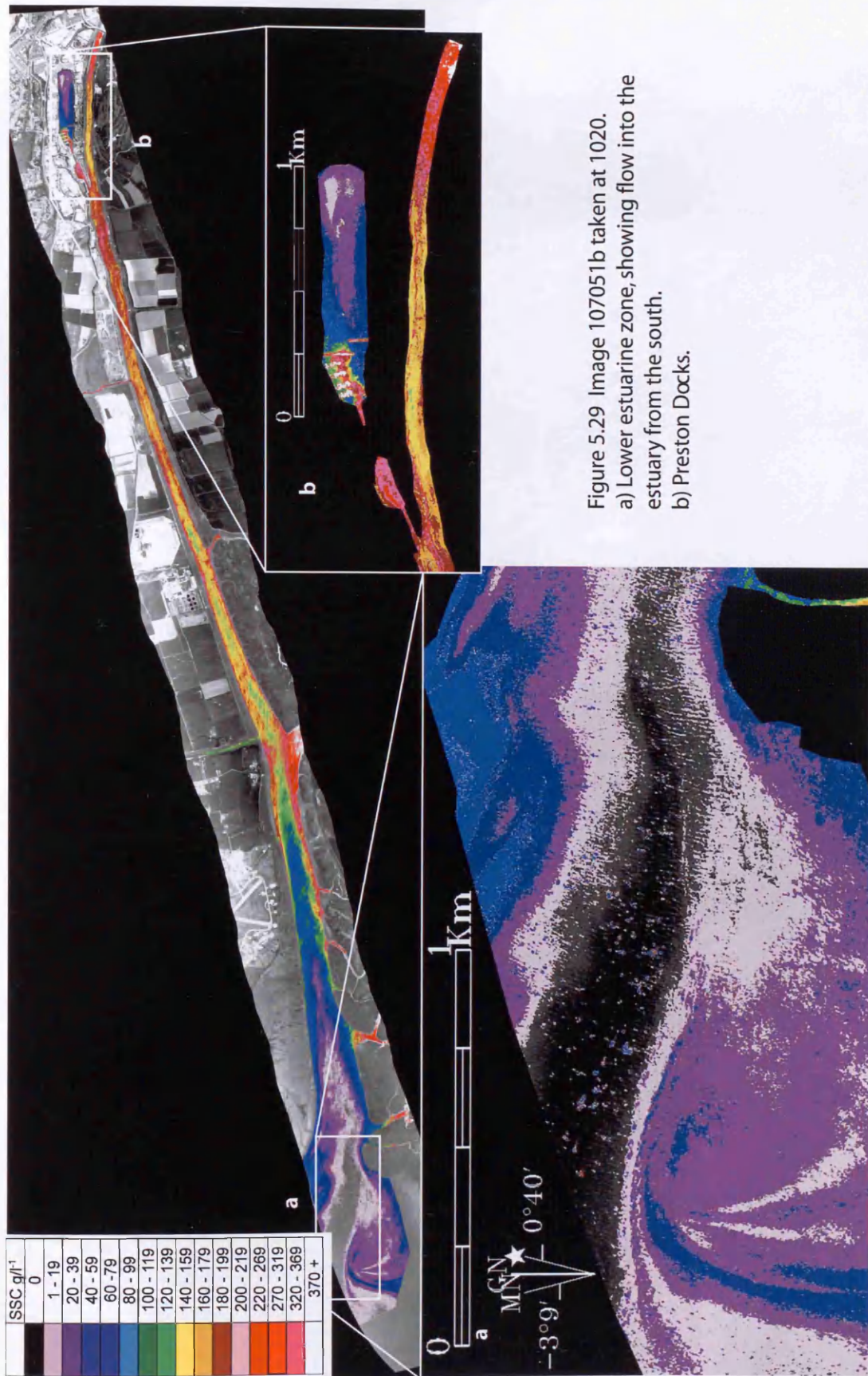


Figure 5.29 Image 107051b taken at 1020.

- a) Lower estuarine zone, showing flow into the estuary from the south.
- b) Preston Docks.

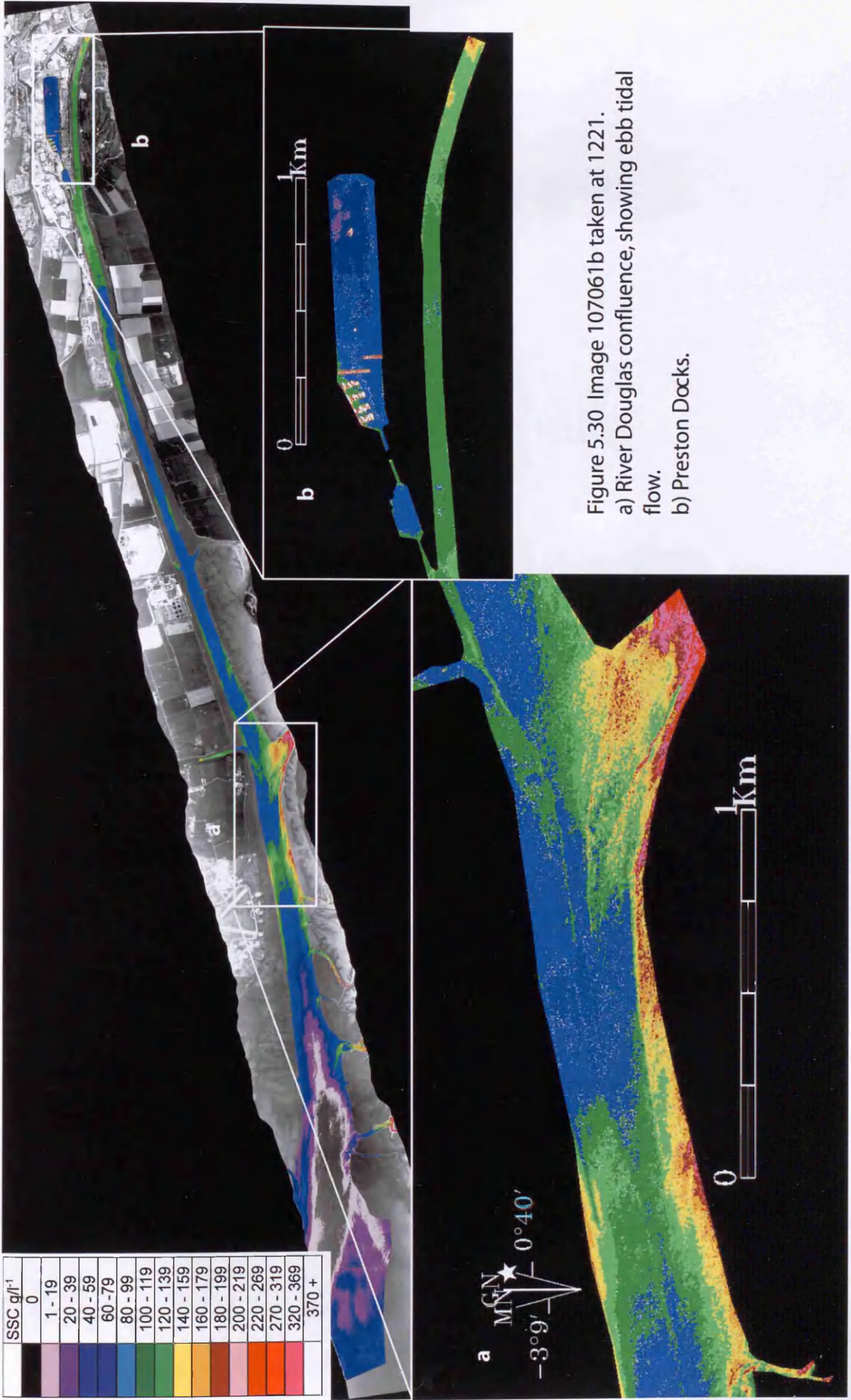


Figure 5.30 Image 107061b taken at 1221.

a) River Douglas confluence, showing ebb tidal flow.

b) Preston Docks.

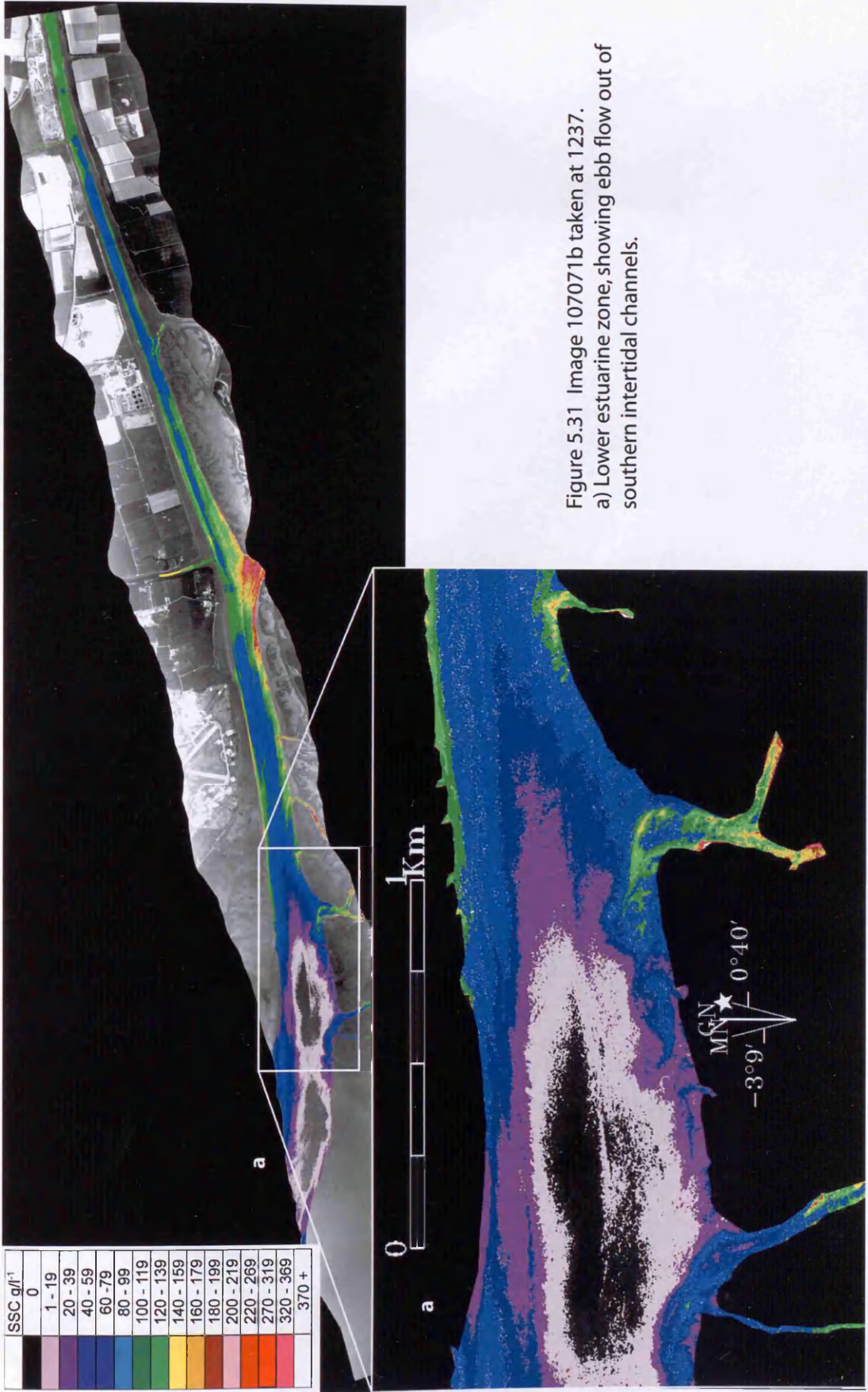


Figure 5.31 Image 107071b taken at 1237.  
 a) Lower estuarine zone, showing ebb flow out of southern intertidal channels.

It is apparent that the April 2003 data (Figures 5.25 – 5.31) are devoid of any cloud shadow and of any visible sun glint. The initial image gathered at 09:19 GMT (Figure 5.25) shows the convergence front approaching Preston Docks (Figure 5.25b), which is due to the rapid increase in the turbidity of the surface waters. Importantly, in this initial image as well as subsequent images, the SSC within Preston Docks is similar to that of the July 2003 data series. However, during the course of the image series acquisition, the lock gates were opened to allow a boat to enter the inner dock. This results in a plume of water with higher SSC ( $140 - 159 \text{ mg l}^{-1}$ ) entering into the western side of the inner dock. This plume of suspended sediment does not appear to penetrate into the central or eastern zones of the inner dock, although some overall increase in SSC is shown within Figure 5.30 (12:21 GMT).

The first two images (Figure 5.25 & 5.26) show SSC in excess of  $200 \text{ mg l}^{-1}$  in the upper estuarine environment, with no discernable increase in SSC after the River Douglas confluence. However, the images do show a plume of 'clean' water entering the estuary from the Irish Sea, with relatively low SSC ( $20 - 60 \text{ mg l}^{-1}$ ). This plume migrates in an upstream direction over the course of the flood tide, until it reaches the Douglas interface, after which trace of the plume is lost. It is also noticeable within the April 2003 flood tide images (Figures 5.25 – 5.29) that there appears to be a perceptible flow from the intertidal channels that feed into the main channel. It is also evident that sediment is being transported into the estuary from the south (Figure 5.29a) during the later middle stage of the flood tide.

In the final two images (Figures 5.30 & 5.31), the tide is beginning to ebb. The intertidal/saltmarsh channels are transporting quantities of sediment into the main channel which is then being transported in a downstream direction.

#### **5.6.6. Estimation of total sediment fluxes April 2003 and July 2003**

In the calculation of the total sediment loads transported over the course of the flood and ebb tide from ARS imagery, certain assumptions must be made. One key factor is the assumption of homogeneity of the water column, with respect to SSC. During the course of the flood tide Atkin (2000) postulated, that through turbulent mixing generated by the incoming flood tide, the water column would be relatively well mixed. Unfortunately, this is not assumed to be the case over the course of the ebb tide, where stratification is believed to take place due to lower flow speeds experienced over the ebb period (demonstrated in Section 5.4). Therefore, to accurately measure the change in SSC with depth during the ebb tide, a depth-sensitive turbidity meter was deployed to gather information on the stratification of the water column. The results from the truncated July 2003 ground truthing of the estuarine water column over slack water high tide and the following initial ebb tide, demonstrated no obvious stratification of the water column. Therefore, surface SSC are assumed to be representative of the entire water column. In conjunction with the VERSE modelled volumetric data (Section 5.4), estimates of total suspended sediment can be calculated, and hence, the total activity inventory for  $^{137}\text{Cs}$ , associated with SSC.

It is evident within the July 2003 image data set that there are zones of cloud shadow present and during estimation of total suspended sediment, these shadowed zones were discounted from the actual estimation process. However, within Figure 5.31 the effects of cloud shadow and sun glint on estimating total sediment loads are clearly demonstrated. Another potential problem with using the time series imagery is that there is a significant time gap in the middle of both the April and July 2003 data sets, which is highlighted in figures 5.32 and 5.33. This break in data acquisition will lead to uncertainties in the calculation of SSC, although the VERSE model can produce estimates of transported sediment during these periods.

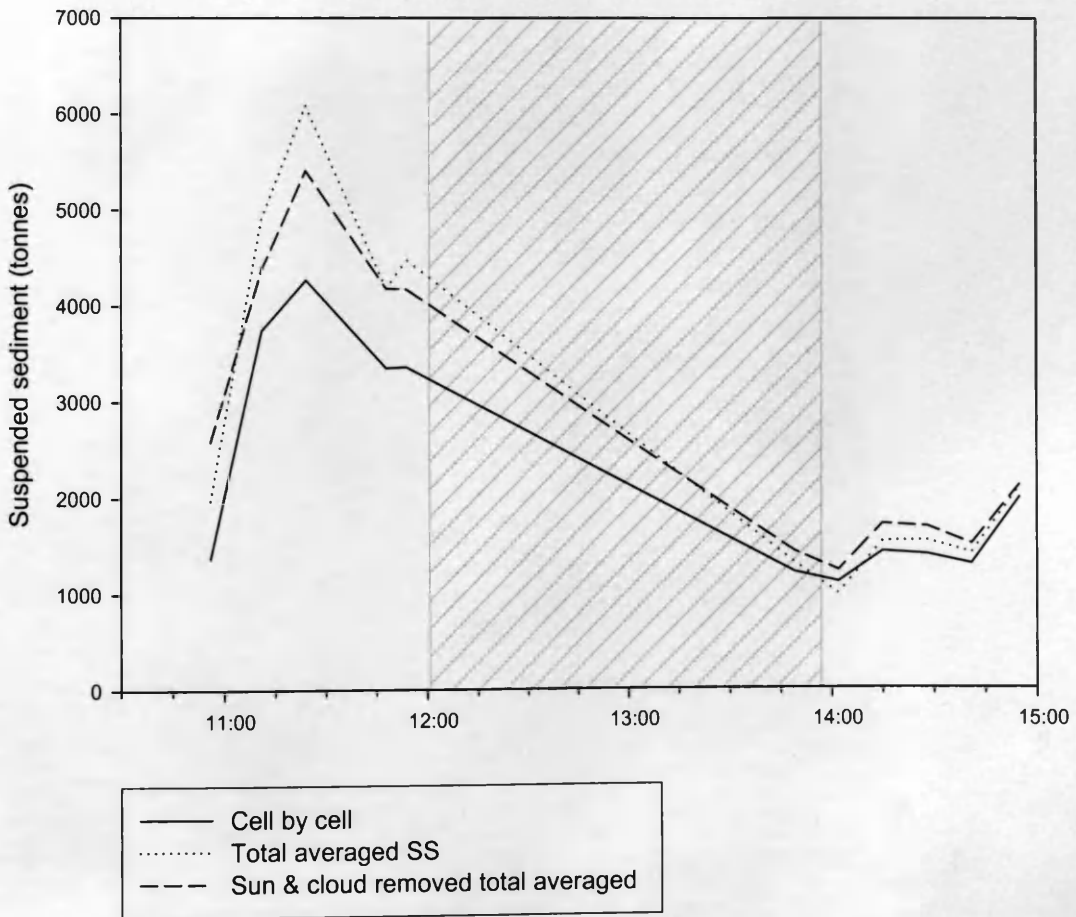


**Figure 5-32** Variation in total suspended sediment loads for the 15<sup>th</sup> July 2003

Figure 5.32 shows that the total suspended sediment loads transported by the estuary during the course of the flood and ebb tide sequence are of the magnitude of thousands of tonnes. However the methods used to obtain estimates of total suspended sediment can dramatically affect the sediment loads. Three separate approaches were used to obtain total sediment loads from the normalised and corrected imagery (Figures 5.13 – 5.31).

The most *simplistic* approach used was to create a region of interest around the entire image and obtain the mean SSC value of this area and apply it to the VERSE derived water volume for that image (dotted line Figure 5.32). This produced the highest estimate of suspended sediment over the flood tide, but lowers values for the ebb tidal flow.

The second *net simplistic* approach is to remove any zones within the imagery that were affected by either cloud shadow or sun glint (dashed line figure 5.32). This had the effect of lowering the estimated mean sediment load, in comparison to the simplistic approach, whilst estimating higher suspended load transportation over the ebb tidal period.

The final *cell-by-cell* approach adopted, required the imagery to be segmented into 250 m long cells (east-west orientation), in alignment with the cells generated by the VERSE model for estimates of water volume. Mean SSC values were obtained from the image for each individual cell, with careful avoidance of the any areas affected by cloud shadows and sun glint. These were then applied to the corresponding water volume to generate the estimate

of total suspended sediment (solid line Figure 5.32). From this technique the total loads estimated for the flood tide were reduced by approximately 2000 tonnes, in comparison to the *simplistic* approach. However, the estimates for total sediment load transportation over the ebb tide lies within the same order of magnitude of the other two estimation techniques.

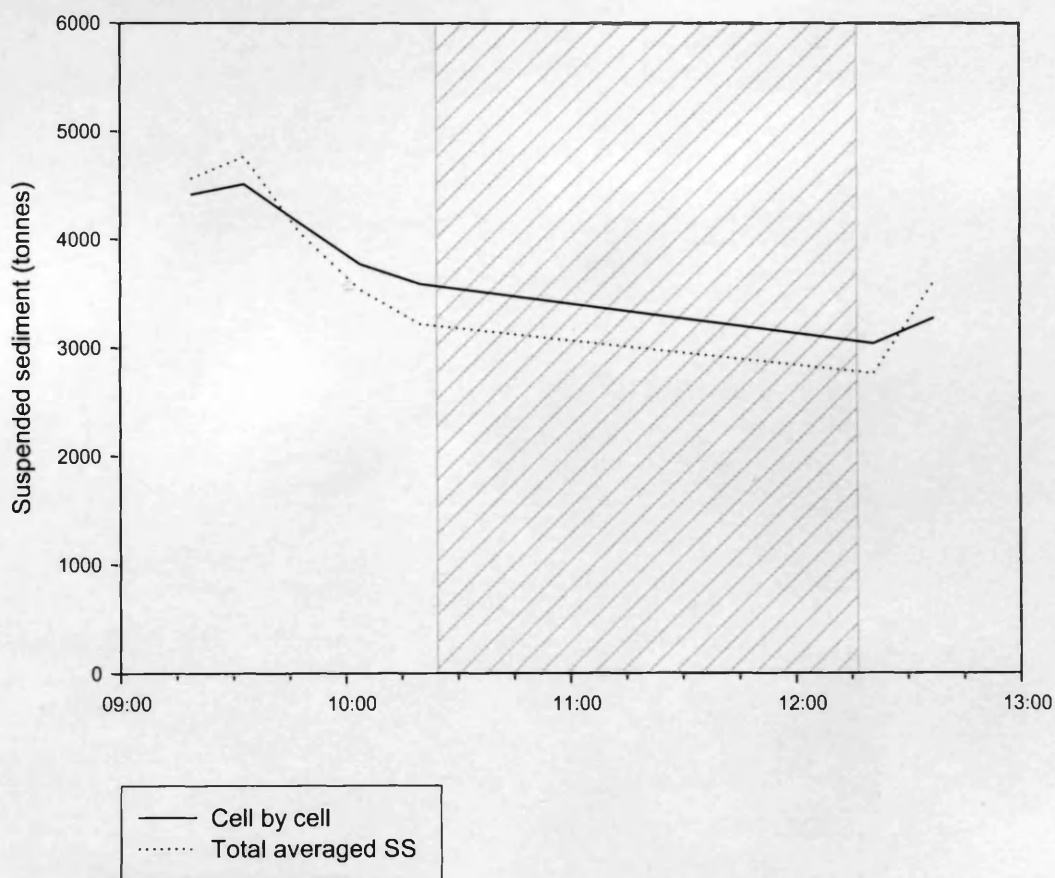


**Figure 5-33** Variation in total suspended sediment loads for the 16<sup>th</sup> April 2003

The *simplistic* and the *cell-by-cell* approach was also applied to the April 2003 imagery (Figure 5.33). The removal of shadow effect and sun glint approach was not used as these features are not apparent within the image data series. This data series captures a greater percentage of the flood tide sequence than

the July 2003 time series imagery, with high tide occurring at 11:17 GMT. Again, there is a significant time gap between the morning data series and the afternoon time series, resulting in a zone of uncertainty with regard to sediment loads. From the comparison of the total averaged suspended sediment and the cell by cell approach, it is obvious that there is little difference between the methods used to estimate the suspended sediment loads. The data obtained from the April 2003 imagery provides some confidence that the plateau, in the region of no data, may be a reasonable approximation.

#### *Estimation of suspended sediment loads*

Due to the zone of uncertainty in estimating suspended sediment loads within each time series data set, created by the NERC aircraft to land for re-fuelling, it is necessary to postulate the change in the suspended sediment loads within this zone. However, it is also necessary to calculate the pre- and post-suspended loads transported out with the time series imagery. Therefore an initial base line sediment load must be assigned to the imagery, replicating the quantity of suspended sediment being transported during the later stages of the ebb tide and the period before tidal inundation during the initial stages of the flood tide. This load should be representative of the sediment transported by the river waters, but will vary depending upon the volume of water that is being discharged on a daily basis.

It is apparent from Figure 5.32, that the zone of uncertainty generated by the break in the image acquisition in July, 2003 demonstrated that the sediment

load was beginning to drop as slack water high approached (high tide at 12:06 (GMT)). The subsequent image (Figure 5.19) produces an estimate of 1200 tonnes, which is approximately one third of the last morning image. It could be postulated that the intervening drop in suspended sediment quantities is a linear relationship. Assuming a linear drop in suspended sediment quantities within the estuary allows for a predictable drop in suspended sediment throughout this data gap, permitting an estimation of the quantities of sediment that are being transported during this period. It should also be noted that there is a similar profile between the observed suspended sediment loads for the April and July time series imagery, which could validate the April image series.

Therefore by applying estimated baseline suspended sediment quantities to the pre- and post-image and the use of a linear depreciation line to plot the potential uniform drop in suspended sediment quantities, it should be possible to obtain total estimates of net deposition over the course of the flood and ebb tidal cycle for both April and July 2003 image data series.

#### *Net sediment load transport for flood and ebb tide.*

From the estimation of the water volume and the predicted SSC within that water, a prediction of the baseline flow can be made. With the estimation of baseline suspended sediment load during this period, this quantity of sediment can be removed from the subsequent values obtained during the course of the flood and ebb tide sequence. To quantify the erosion and depositional volumes of sediment that occurs over the course of the tidal cycle, the

trapezium rule is used to calculate the sum of the trapeziums under the curve. This rule (Equation 5.2) allows for the estimation of the volumes of sediment that are eroded during the erosion phase and then what is deposited during the depositional phase.

$$y = 1/2h[(Y_0 + Y_n) + 2(Y_1 + \dots + Y_{n-1})] \quad \text{Equation 5-2}$$

Where h = gap between intervals,  $Y_0$  = starting value and  $Y_n$  = end value

This trapezium rule was applied to the July data sets, to estimate the cycle of erosion and deposition that occurs during the tidal phase. Using hypothetical values of SSC ( $20 \text{ mg l}^{-1}$  per litre) for the water column during the periods before and after the tidal period and by applying modelled volumetric estimates from VERSE, it was then possible to estimate the basal flow within the estuary generated by the low riverine flow rates at the time of the flight. This estimate (approximately 60 tonnes), was then deducted from the erosion and depositional cycles (Figure 5.34) and the resulting areas of erosion and deposition estimated.

In utilizing this trapezium rule method to estimate the sediment budget within the estuary, it was possible to break the tidal cycle into two distinct sets of erosion and deposition phases (Figure 5.34 and Table 5.7). The first phase correlates to the flood and high water slack period of the tide and the second period represents the ebb flow transporting sediment in a seaward direction. Calculating the initial period of erosion/deposition during the tidal cycle, is achieved by subtracting the quantity of sediment that is eroded during tidal

inundation from the deposited sediment during the flood period of the tide. This generates an estimated 13,125 tonnes of sediment that is deposited over the sub and intertidal surface of the estuary. This is then allayed against the amount of sediment that is eroded and deposited over the ebb tidal period of the tide, which is approximately 3,188 tonnes. Therefore, for the entire tidal cycle on the 15<sup>th</sup> July 2003 there was a net accretion of approximately 9,938 tonnes across the entire spatial extent of the estuary.

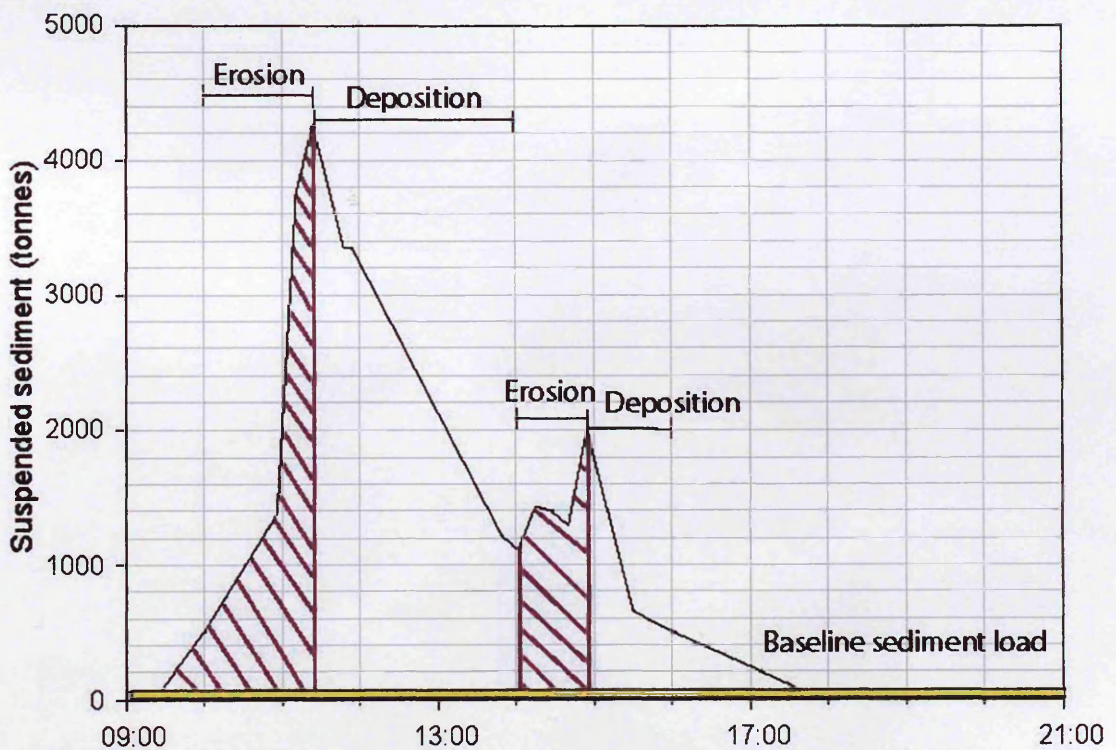


Figure 5-34 Erosion and depositional cycle of the estuary during the July 2003 overflight.

Section	Total sediment (Tonnes)	Net deposition (Tonnes)	Uncertainty ± (Tonnes)
1st Erosion phase	17938		
1st deposition phase	31063	13125	3383
2nd Erosion phase	14250		
2nd Deposition phase	11063	-3188	2135
Total deposition (tonnes)		9938	4000

**Table 5-7** Deposition and erosion of sediment over course of flood and ebb tidal cycle and the associated uncertainties with them.

However, this figure then needs to be put in context with the impact on deposition rates within the estuary. The spatial extent of the maximum flood tide image was obtained via ENVI's spatial analysis tool. The tidal waters covered a region of approximately 4.3 million m<sup>2</sup>, thus the calculated 9,938 tonnes of sediment was dispersed throughout this area. The average depth of deposition should be greatly affected by the bulk density of the sediment, which will vary depending upon the percentage mud (<63 µm) content of the suspended sediment in relation to sand content of the deposited sediment. Flemming & Delafontaine (2000) demonstrated that the wet bulk density of the sediments will be much lower when there is an increased silt content within the sediment, thus it is probable that the bulk density of the suspended sediment could be positioned towards the lower end of the wet bulk density range, due to the measured suspended sediment within the estuary demonstrating a predominantly mud composition. Deposition rates will vary from location to location over this area, but assuming a wet bulk density of between 1,250 - 1,750 kg/m<sup>3</sup> for this suspended sediment, then a net deposition of between 1.4 mm/m<sup>2</sup> (1,750 kgm<sup>-3</sup>) and 1.8 mm/m<sup>2</sup> (1,250 kgm<sup>-3</sup>) across the entire estuary would be achieved over a flood and ebb tide event.

### 5.6.7. Deposition of $^{137}\text{Cs}$ over tidal event

The quantity of suspended sediment that has been deposited over the course of this single flood and ebb tidal sequence of this study is predicted to be approximately 9,938 tonnes, which can be used to calculate  $^{137}\text{Cs}$  loading, by using the equation given by Atkin (2000) (Equation 5.3) (Figure 5.35). Table 5.8 demonstrates the total suspended sediment load and associated  $^{137}\text{Cs}$  for each time series image. Applying this same calculation to the estimated suspended sediment deposited over the course of the tidal cycle generates an estimated 2.72 GBq of  $^{137}\text{Cs}$  deposited over the spatial extent of the estuary in a single tidal event (Table 5.8).

$$^{137}\text{Cs} = 0.0003(\text{SSC})$$

Equation 5-3

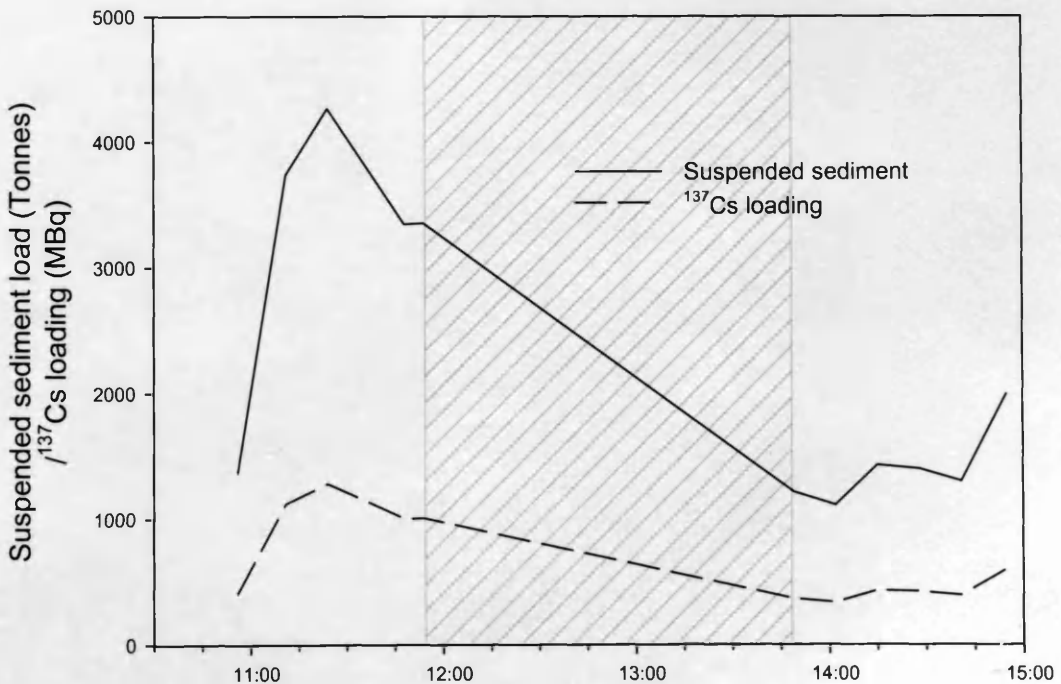


Figure 5-35 Comparison of suspended sediment load against  $^{137}\text{Cs}$  loading for each flight line.

Time	Suspended sediment (tonnes)	<sup>137</sup> Cs (GBq)
10:56	1368.5	0.41
11:11	3737.6	1.12
11:24	4265.9	1.28
11:48	3345.1	1.00
11:54	3353.4	1.01
13:49	1212.8	0.36
14:02	1108.6	0.33
14:15	1425.5	0.43
14:28	1394.6	0.42
14:41	1296.8	0.39
14:55	1986.9	0.60

**Table 5-8** The total suspended sediment and <sup>137</sup>Cs load for each time series flight line for July 2003

### 5.7. Warton Bank suspended sediment transport pattern

A more focused study was directed at the one kilometre area in proximity to Warton Bank coinciding with the point sampling site. This area starts 2,250 meters upstream from the edge of the VERSE model at Lytham and extends one thousand meters in an up-stream direction. Volumetric estimates were obtained from VERSE and SSC were gathered from the cell-by-cell breakdown of the ARS imagery.

It is highlighted in Figure 5.35 that suspended sediment loads during the April 2003 imagery are larger than those of the July 2003 imagery, which should be expected due to the higher tidal conditions during the April imagery. However, they both do appear to show the same profile in respect of sediment loads transported over the course of the tidal cycle. They both show a high initial suspended sediment load (432 and 409 tonnes respectfully), which then

rapidly drops off. Unfortunately, during the near midday imagery in July, there appears to be some effect from cloud shadow across the area masking SSC. Examination of the un-validated April imagery, suggests that the rapid reduction in suspended sediment loads during this period is real, although not as dramatic. Following the period of slack water, the amounts of suspended sediment increase with the out going tide. This increase appears to occur as the water column depth over the intertidal zones of Warton Bank decreases (approximately 1 meter deep during the 14:55 image). Unfortunately, there is no subsequent image which could show the emergence of the main extent of the intertidal zone and the confinement of the remaining estuarine waters within the main entrained channel.

Therefore, two estimated values were added to the beginning and end of both time series data sets to allow estimations of the total suspended sediment load deposited upon the intertidal surface at Warton Bank during the April and July 2003 time series imagery (Table 5.9).

	Apr-03	Jul-03
1st Erosion event (tonnes)	1238	1163
1st Depositional event (tonnes)	3350	2475
2nd Erosion event (tonnes)	2763	1213
2nd Depositional event (tonnes)	1350	1050
<b>Total deposition (tonnes)</b>	<b>700</b>	<b>1150</b>
mm per m <sup>-2</sup> (assuming bulk density of 1250 kg m <sup>-3</sup> )	1.50	2.47

**Table 5-9** Depositional estimation of Warton Bank sedimentation from the April and July 2003 time series imagery (Figure 5.35)

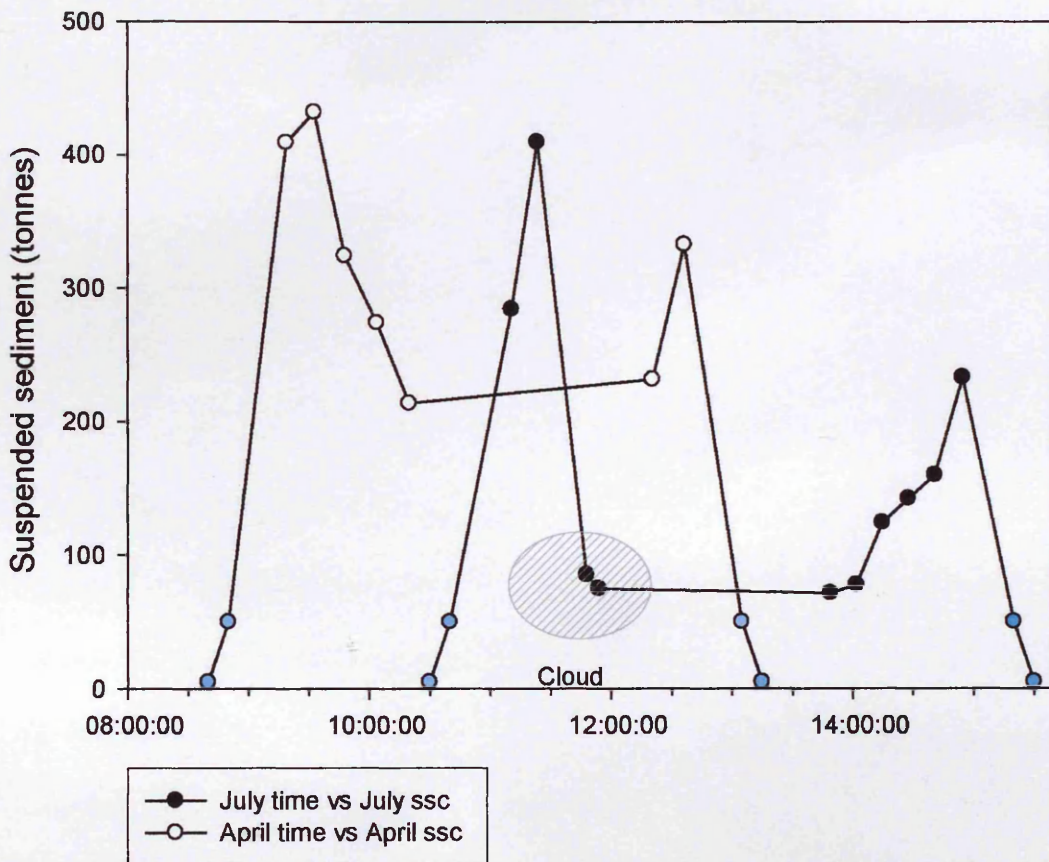


**Figure 5-36** Warton Bank – April and July 2003 suspended sediment loads during course of imagery (blue sample points are estimations of suspended sediment load prior and after time series acquisition) (April high tide at 11:17 GMT (9.79m) and July 2003 high tide at 12:06 GMT (8.69m) .

The estimates of net deposition of sediment over this one kilometre section of the estuary at Warton Bank produce an estimated 1.5 mm of sediment for the April 2003 time series and 2.47 mm for the July 2003 imagery. Both of these estimates assume a bulk sediment density of  $1250 \text{ kg/m}^3$  for the deposited sediments and compare favourably to the overall estuary net deposition for the July 2003 time series imagery.

These values compare favourably with the monthly sampling investigation carried out on either side of the time series flights. The total deposition at Lytham and the lower sites at Warton Bank all showed accretionary values comparable to the estimated values obtained through the application of the time series remote sensing.

### 5.8. Consideration of uncertainties

There are a number of possible sources of uncertainty associated with the estimation of the net sediment deposition rates over the course of the time series imagery. The possible uncertainties are tabulated within table 5.10, allowing absolute errors to be calculated for the quantification of sediment deposition over the course of a flood and ebb tide cycle.

		Values (Tonnes)	Baseline estimate (%)	Slack water assuption (%)	Volume error (%)	Vertical mixing* (%)	Total uncertainty (%)	Absolute error ± (tonnes)
Flood tide	Erosion	17938	3.34	0	7.18	2.5	8.31	1490
	Deposition	31063	1.93	6.7	6.38	2.5	9.78	3037
Ebb tide	Erosion	14250	4.21	0	7.47	5	9.93	1414
	Deposition	11063	5.42	0	8.91	10	14.45	1599

**Table 5-10** Uncertainties associated with the calculation of the net deposition of sediments during the July 2003 time series imagery (\* - estimated sources of error).

Initially, the largest potential source of uncertainty is the modelled water volumes produced by the VERSE model. One of the main sources of error within the model is the bathymetric file associated with providing the lateral extent of the model. It was found that at Warton Bank that the model's bathymetric profile, obtained by side-scan sonar in 1995, was different to the 2003 transect profile (Appendix 4). This source of error (Table 5.10) could

lead to differences of between six and nine percent for the actual volumetric estimates for the estuary, allowing an underestimation of the total sediment flux over the course of a tidal cycle.

Secondly and perhaps most ambiguous source of uncertainty within the suspended sediment calculations is the assumption of uniform suspended sediment within the water column. Within the strong flood tide period it is assumed that the water column is well mixed and that surface SSC are comparable to those at depth. However, this assumption could not be applied to the ebb tide images without conducting point sampling studies concurrent with the time series flights. Subsequent to the collection and analysis of these depth profiles at high water slack and the initial two hours of the ebb tide (Figure 5.10), it was demonstrated that the surface SSC were comparable to the SSC at depth within the water column. Therefore, the use of the mean surface SSC for each 250 m cells (for incorporation into the VERSE modelled volumetric data) was validated for producing estimates of total suspended sediment within the Ribble Estuary.

Assessing the variation in suspended loads (Figure 5.32) produces large differences in the possible quantities of suspended sediment that are actually obtained from the remote sensing imagery. It is clear that accurately calculating the suspended sediment load will impact on the possible quantities of sediment transported during the flood tide section of the tidal cycle, with reducing effects on the ebb tidal sequences. The *cell-by-cell* approach was ultimately selected to provide the best estimate of averaged cell SSC, which

was then applied to volumetric data obtained from the VERSE model. However, during the slack water period of the high tide, when no imagery was obtained, there are uncertainties as to how rapidly the SSC decrease over that period. This work assumes a linear decrease in SSC, but there may be a two stage of decrease in SSC with the coarser sediments ( $>63 \mu\text{m}$ ) dropping out of suspension more rapidly, leaving the finer-grained sediments ( $<63 \mu\text{m}$ ) to settle out at a reduced rate. The error associated with this assumption is demonstrated with Table 5.10, where it appears to have a large impact on the absolute error associated with estimating the quantity of sediments during the initial depositional phase of the tidal cycle.

The affects of the assumed baseline flow could also impact on the calculated sediment deposition, with its effects increased during the initial and later stages of the tidal cycle. Although, it appears that it makes up a small section of the possible error in quantifying the deposited sediment within the estuary.

Finally, the validation of the image to SSC values was preformed by assessing the actual concomitant ground control points to the image value points. This was achieved by obtaining a 5 by 5 pixel average of the geocorrected image pixels within the corresponding time series image and comparing it the ground control point. Unfortunately, only one ground control point was applicable for image validation purposes, due to timing of flights and cloud shadow over collection point during image acquisition. However, this single point produced a good correlation, with a measured value of  $23 \text{ mg l}^{-1}$  and an estimated value of  $23.5 \text{ mg l}^{-1}$  ( $\pm 2.5 \text{ mg l}^{-1}$ ) for the area. Also the SSC values can also be

partially validated by comparing the average SSC within the enclosed Preston Docks (Figure 5.36). It can be seen that the average SSC stay relatively consistent over the length of the time series imagery for both April and July 2003.

By calculating the absolute error for the entire time series imagery (Table 5.10), it is then possible to generate total absolute errors for the calculated sediment,  $^{137}\text{Cs}$  activity concentrations and the possible uncertainties for the bed elevation changes (Table 5.11).

Net Deposition uncertainty $\pm$ (tonnes)	4000
Uncertainty of $^{137}\text{Cs}$ $\pm$ (GBq)	1.09
Uncertainty of 1.4 mm deposition $\pm$ (mm)	0.56
Uncertainty of 1.8 mm deposition $\pm$ (mm)	0.72

**Table 5-11** Absolute errors for calculated depositional values for the July 2003 time series imagery.

## 5.9. Discussion and Conclusions

This chapter shows a number of problem areas that have required correction in order to obtain estimates of SSC and the associated estimates of  $^{137}\text{Cs}$  activity concentration within the Ribble Estuary. Some of these problems, such as cloud shadow and sun glint, cannot be corrected easily, but it is clear from Figure 5.32 that these can have large impacts on the estimation of suspended sediment within the estuary. The three different estimates of the quantities of suspended sediment generated from each time series image show a range of approximately 2000 tonnes over the maximum flood tide image. The selection of the *cell-by-cell* approach appears to be the most

appropriate method to calculate the suspended sediment quantities transported over a tidal cycle, but the implications for quantities of sediment that could be potentially transported over the course of the tidal cycle would be significant. The selection of the *cell-by-cell* approach method to generate estimates of suspended sediment loads over each image was validated by the small case study undertaken at Warton Bank (Figure 5.34), which showed that the cell-by-cell approach replicated similar suspended sediment profiles for both the April and July. The approach will probably account for some of the variability and perhaps leads to normality in the data sets.

However, the use of the sun azimuth correction and image-to-image normalisation for the 2003 data sets demonstrate a good correlation between the two image data sets, thus validating the use of such an approach. This is confirmed by the uniform values of SSC (Figure 5.12) that are obtained from the Preston Docks area from all the image data series. The application of the surface SSC values to the entire water column over both the flood and ebb tide sequence has been validated, by a turbidity probe that was lowered into the water column at regular intervals during that sampling period. With the data from this turbidity probe, it is possible to show how well mixed the underlying water column is, and thus make the assumption that throughout the entire course of the strong flood and ebb tide that the water column is relatively well mixed. A possible explanation for this relatively well mixed water column could be found by comparing the modelled water flow velocities of the flood (Figure 5.7) and ebb tide (Figure 5.8) during the course of the data acquisition. They do demonstrate that flow velocities are lower over the

course of the ebb tide than the flood, but they are still relatively high current velocities within the ebb tidal cycle, which could impede the development of a stratified water column.

### **5.9.1. Warton Bank**

Comparing the two separate suspended sediment loads that are transported over the course of the flood and ebb tide at Warton Bank (Figure 5.35), demonstrates that although the quantity of sediments that are carried by the April time series is greater than the July tidal cycle, the actual pattern of sediment transport fits a similar profile for both sets of time series images. A possible reason for increased sediment load over the April imagery is that a higher tide was present on April 2003 (9.79 m), in comparison to July 2003 (8.69 m).

### **5.9.2. Suspended sediment transportation**

The estimated net deposition of sediment within the estuary relies on a number of criteria to be considered. As mentioned above, these criteria have been identified and solutions applied to produce a calculated approximation of net sediment deposition over the entire estuary of between  $1.4 \text{ mm/m}^2$  ( $1,750 \text{ kgm}^{-3}$ ) and  $1.8 \text{ mm/m}^2$  ( $1,250 \text{ kg/m}^{-3}$ ) of fine grained sediment across the entire estuary for a single tidal cycle.

It should be noted that this tidal pumping (Chapter Three) of sediment and the resulting calculated sediment deposition does not take into any account the

effects of storm surge/wave or extreme river flow events that will have the effect of entraining more sediment and transporting it around the estuary. The increased river flow could lead to increased sediment load transportation out of the estuary on the ebb tide, thus creating net erosion of the intertidal sediments in the estuary. From this calculated net deposition of sediment, it is then possible, by using Atkin's (2000) work, to estimate the net deposition of  $^{137}\text{Cs}$  over that same period. By using this approach, it is calculated that an estimated 2.72 GBq of  $^{137}\text{Cs}$  would be deposited in association with the fine grained sediments over the sub- and intertidal zones of the Ribble Estuary during the midday, 15<sup>th</sup> July 2003 tidal cycle.

By utilizing the VERSE model to produce volumetric data for each individual time series image, identification of zones of erosion and deposition over the course of the tidal cycle is possible, allowing the recognition of the two distinct zones of sediment transport associated with the flood and ebb tide (Figure 5.33) that is evident from the suspended sediment imagery of the estuary.

However, as noted above there are uncertainties associated with quantifying net sediment deposition. It has been calculated that there is a total absolute error of 40%, this will have implications on the quantities of sediment that is deposited over the intertidal surface. This uncertainty within the data means that the calculated sediment deposition could vary by 40%, with associated impacts on the deposition of  $^{137}\text{Cs}$  and the amount of sediment deposited upon the intertidal surface.

## 5.10. Summary

The ability to provide quantitative estimates for net sediment load transportation within an estuarine system is a valuable tool in gaining a greater understanding of estuarine dynamics. Time series imagery allows the production of high resolution (2 m pixels) maps of suspended sediment load, which can be used to firstly, identify structural patterns within the water column i.e. axial front convergence, and secondly, estimates of net sediment deposition over the spatial extent of the estuary.

This chapter has demonstrated that the net sediment flux and associated radionuclide patterns within the Ribble Estuary can be quantified and thus positively confirms the final research hypothesis of this project. Then the derived remote sensing data and associated radionuclide distributions patterns could be of value to regulatory bodies, such as the Environment Agency, as such data would allow them to identify zones of rapid accumulation and erosion within the estuary and therefore improve gamma dose risk assessments to the critical groups within the Ribble Estuary and place them in a spatial context.

It may not be realistic to further increase the 250 m resolution of the volumetric cell estimates and associated mean values of those areas, although it would be perhaps advantageous to apply LiDAR data to gain a up-to-date bathymetric profile of the estuaries intertidal profile.

This work has provided a new insight into the quantitative assessment of sediment flux patterns within the Ribble Estuary. There are associated errors in the calculation of the sediment flux patterns and depositional rates during the tidal cycle, however, the deposition rates appear comparable to the measured bed elevation changes described with Chapter Three.

## 6 Discussion and Conclusions

### 6.1. Introduction

Understanding the dynamic nature of estuarine environments is important to enable the pressures on estuaries, be they natural or anthropogenic, to be evaluated. For example, sea level rise and/or increased storminess may have consequences for sediment transport. Such as perturbation could lead to the remobilization of heavy metal contaminants that are bound to fine-grain sediments in the upper intertidal and saltmarsh sediments of estuarine environments. It has been shown that heavy metals (including radionuclides) demonstrate a high affinity for fine-grained estuarine sediments (Barr *et al.*, 1990; Middleton & Grant, 1990; Croudace & Cundy, 1995). Once these heavy metals are released to the environment they may interact with the fine-grained suspended sediments, and subsequently be removed from the water column (Lee & Cundy, 2001). Similarly, the predicted rise in global sea levels, could mean that any heavy metals deposited in either the saltmarshes or upper intertidal sediments could be reworked and redistributed (Reed, 1995). This is especially important with the anthropogenic radionuclides. For example historical discharge rates from BNFL Sellafield (especially  $^{137}\text{Cs}$  &  $^{239-240}\text{Pu}$ ) were of orders of magnitude higher than the present day authorised discharge rates (RIFE 10). Consequently, fine-grained sediments of elevated activity concentrations, which are at present buried within the upper intertidal zones and saltmarshes could be remobilised. It is therefore important to understand the spatial distribution of these deposited sediments and to

identify the largest potential sources of trace metals, or other pollutants, if subject to erosion/disturbance were to occur (Lee & Cundy, 2001). The LISP-UK investigation (Littoral Investigation of Sediment Properties, a sub-section of LOIS), obtained a large number of sediment samples that were used to assess the heavy metal contamination within the lower Humber Estuary. The results indicated that there were high levels and significant correlations with fine-grained sediments and a number of heavy metal concentrations (Pb, Zn, Cu, Al, Mn and Fe) were highest in the saltmarsh and upper intertidal mudflats. This finding demonstrates that any increase in sea-level could feasibly result in the remobilisation of contaminated sediments estuarine environments.

Here we are partly concerned with the security and the potential re-release of pollutants stored within the estuarine environment. Within the Ribble Estuary, there is a historical legacy of anthropogenic radionuclides that are stored within the sub-tidal and intertidal sediments. Consequently the processes of sediment remobilisation and the subsequent sediment flux patterns due to tides, river discharge conditions and wind induced wave action, are all important factors for understanding the temporal and spatial variability in sediment distribution patterns in estuarine environments.

Traditionally the analysis of sediment dynamics and the associated estimation of sediment depositional histories of estuarine environments have been undertaken by point sampling or modelling or a combination of the two. Although providing precise data points, these point sampling approaches are

often spatially isolated within the context of the estuary and must therefore be treated with caution especially when used within estuarine model development. Such extrapolations or generalisations of point data sources often give little more than a tacit recognition to the heterogeneity of the estuarine system they represent. However, this research has shown that the integration of ARS data with point samples has enabled maps of intertidal sediment characteristics to be generated with a good level of accuracy (Clay  $r^2 = 0.828$ ). Further, a quantitative estuary wide methodology for calculating the net depositional flux of sediments within tidal cycles has been developed with a reasonable level of precision (40%).

It is both logically and economically difficult to justify full spatial coverage of monitoring through seasonal cycles. However, this research has demonstrated that by careful examination of long-term time series point sampling measurements, coupled with intertidal imagery and short term time series (flood and ebb) ARS measurements, it is possible to gain valuable quantitative information on sediment flux patterns within the estuarine environment.

The project rationale is based around four research hypotheses that have been addressed throughout this investigation;

- i) *The inter-annual deposition of marine sediments in the Ribble Estuary shows a net accretion.*

- ii) *The intra-annual variability in sediment accretion and erosion is greater than the overall net accretion.*
- iii) *The relationship between  $^{137}\text{Cs}$  and the sediment clay percentage content is temporally stable.*
- iv) *The net flux of sediment and radionuclides over a single flood and ebb tide cycle can be estimated through time series remote sensing.*

These hypotheses, which were integral to the work contained within chapters three, four and five, will now be discussed further in terms of the results and implications for ARS and ground based investigations of the stability and fluxes of sediment in the Ribble Estuary. The following sections will examine each hypothesis in turn.

## **6.2. Inter-annual variations in sediment deposition.**

The interpretations of point sample information and estimation of total intertidal sedimentation and the sources of those sediments rely on understanding the environmental drivers that are responsible for erosion, transportation and deposition of the marine, estuarine and riverine sediments. Obtaining these quantitative measurements over the large spatial area of an estuarine environment can perhaps only be realistically achieved through the use of ARS, in conjunction with field investigations. Within this investigation, chapters three and four provide valuable information to derive the inter-annual variations in sediment movement within the estuary. Moreover, the time series

imagery in chapter five can be used to demonstrate the possible influx of marine sediment into the estuary during the initial flood tide.

It is not directly possible to put high accurate and reliable estimates of total net sediment and radionuclide accretion for the whole estuary on an inter-annual time scale, due to the expansiveness of the estuary and the geographical spacing of the intertidal sampling points, but approximations may be possible. Improved accuracy could be achieved by the assessment of a series of LiDAR images of the estuary, which would have provided estimates of volumetric change for the estuary between image capture periods. Unfortunately, as this LiDAR was unavailable, although commissioned for study, answering this first hypothesis relies on the combination of spatially isolated, time series measurements coupled with the two intertidal maps produced within Chapter Four.

### **6.2.1. Intertidal sediment properties**

The two year investigation undertaken to study the temporal and spatial distribution patterns of the intertidal sediments was based around the first three hypotheses outlined above. The investigation sought to identify the main trends in sediment distribution patterns and what environmental drivers had the most impact on these. It had been found in previous investigations (Burton *et al.*, 1995) that tidal pumping was responsible for the movement of marine derived sediments into the estuary and that large river discharges caused flushing of sediment within the estuary. However, quantifying the actual impacts that these forces have on the intertidal sediments was

important to the understanding the hydrological and sedimentological dynamics of the estuary. This was shown for the first time by the completion of the two year investigation of the intertidal sediments of the estuary, directly relating to the clay sediment fraction, and the changes in the bed height elevations of the intertidal sediments.

Within the context of this work it has been shown that point sampling is an intrinsic tool in assessing the temporal variations in intertidal sediment properties and allows the environmental drivers to be assessed in terms of sediment transport. Point sampling techniques provides a low cost approach to estuarine studies, however, the incorporation of ARS techniques allows these spatially isolated point samples to be placed within a spatial context.

### **6.2.2. Spatial distribution of intertidal sediments.**

The application of the two intertidal images (1997 (Rainey, 1999) & 2003), does not allow a quantitative estimate of estuarine sedimentation, however it does allow the change in spatial distribution patterns of sediment types, especially clay and  $^{137}\text{Cs}$  to be assessed in addition to the robustness of the image analysis technique. It is clear from these distribution patterns that there is a greater expanse of clay within the 1997 image. However, as there had been a large river flow event prior to the 2003 image acquisition, it could be argued that this is the reason that there is a reduced quantity of clay on the intertidal sediments in 2003.

### **6.3. Intra-annual variations in sediment accretion and erosion**

The erosion and accretion data contained within Chapter Three allows the second hypothesis on the intra-annual variability of the intertidal sediments to be answered here. By conducting this two year study of the intertidal sediments it was possible to compare the monthly (intra-annual) against the inter-annual time scales of sediment deposition within the Ribble Estuary. The bed height elevation changes within Chapter Three increased the conceptual understanding of sediment movement patterns within the estuary system. Best sub-set regression analysis was performed on the changes in bed elevation for the three major sampling sites (Lytham, Warton Bank and Penwortham Bridge), against the main environmental drivers responsible for the spatial distribution patterns of the clay particles within the estuary. There was no direct correlation between tidal amplitude, river discharge conditions and wind direction and the changing bed elevation levels. Therefore, the changes in bed elevation at each sampling location were further studied, to gain an understanding of the movement patterns of the intertidal sediments within the Ribble Estuary.

It was possible to demonstrate that the outer estuary sites at Lytham were dominated by the inter-annual variations in sediment deposition. However, these findings were not demonstrated by the other sites at Warton Bank and Penwortham Bridge. At these sites (Figures 3.16, 3.18 & 3.22), it is clear that the intra-annual variations in bed sediment height are in excess of the average inter-annual bed elevation for the sites. Whilst the Savick Brook site could not be compared for any inter-annual changes, it could be used to illustrate the

gradual propagation of the intertidal sediments in an up-stream direction during low river discharge rates, and the subsequent rapid removal by large riverine flow events. These bed elevation height changes indicate that the outer estuary sites are more greatly affected by the cyclic patterns of tidal pumping, whilst the middle and upper estuarine zones are more likely to be affected by episodic river discharge events.

Secondly, the rates of sediment accumulation could be measured at an intra-annual time scale (monthly) and compared to the inter-annual changes in sediment budgets. However, it is evident at Penwortham Bridge (upper estuarine zone), that due to the boulder and pebble layer of this site, the bed elevation changes over the two year investigation showed no net change.

Warton Bank showed a distinct two-tier profile with the upper and lower sections of the intertidal sediments. Here, the relative location of the intertidal zone within the estuary had implications for which environmental driver had the most effect on the intertidal sediments. The upper intertidal sites are affected by a number of different environmental processes especially tidal currents, wave action, river discharge conditions and exposure to the atmosphere. The lower intertidal sediments are mostly affected by changing tidal amplitude.

It is evident from studying the bed elevation height changes in Chapter Three that the monthly changes in sediment height, especially at Warton Bank, are in excess of the annual accumulation rates. This finding provides evidence to

support the second research hypotheses, validating the assumption that the intra-annual changes in bed sediment elevations are in excess of the inter-annual bed elevation changes. Comparing the maximum monthly depositional rates for each site within the estuary, demonstrates the variance in bed elevation height changes throughout the estuary system. Table 3.6, demonstrates that maximum daily deposition rates (averaged over the number of days between the sampling periods) are up to 2.8 mm per day for Warton Banks lower estuary site. These values will represent periods when there is net deposition on the intertidal surface, and not the net erosion events.

#### **6.4. Percentage clay and $^{137}\text{Cs}$ relationships**

Remote sensing can not directly detect the presence of radionuclides within the environment, unlike airborne gamma spectrometry systems, which spatially integrate over a 150 m radius (Tyler, 1996b; Sanderson *et al.*, 2004) (section 2.4.4). However, as noted by numerous studies within the Ribble Estuary (Aston & Stanners, 1981; Assinder *et al.*, 1997; Brown, 1997; Rainey, 1999), there is a strong relationship between percentage clay and  $^{137}\text{Cs}$  within the intertidal sediments found within the estuary. The temporal stability of this relationship had therefore to be verified over the course of this study to ensure a defined, stable relationship existed for the surface intertidal sediments, allowing the production of total activity concentration maps, derived from ATM imagery, for  $^{137}\text{Cs}$ .

Assessing the temporal stability of the percentage clay/<sup>137</sup>Cs relationships is especially important not only within the context of this investigation, but also for the possible implications it has on any environmental monitoring studies undertaken by other interested regulatory bodies i.e. Environment Agency and the Scottish Environmental Protection Agency. This research hypothesis impacts on all three research chapters. Initially Chapter Three sought to identify the inter-annual and intra-annual stability of the relationship, by comparing the regression analysis of each month's relationship to that of riverine discharge conditions (Figure 3.24). It is clear that after large (>50 cumecs) flow events, the regression analysis for percentage clay and <sup>137</sup>Cs breaks down within the estuarine sediments. This finding had impacts on the subsequent ARS study (Chapter Four), as it meant that each separate flight line had to have associated field sampling to verify the existence of the relationship and the nature of the percentage clay/<sup>137</sup>Cs relationship. It can be seen within Figure 4.14 that in comparing the September 2002 and the October 2003, there are differences in the relationships for each separate year, indicating that although there is a relationship between the clay and <sup>137</sup>Cs, the actual association varies with time and space.

The finding that the relationships alter with time is important for (i) the assessment of total activity concentrations within the intertidal sediments of the estuary, (ii) sampling times and (iii) sampling locations within the estuarine environment.

In that there are significant correlations of  $^{137}\text{Cs}$  with the fine-grained clay particles for the Ribble Estuary, it is now important to assess if other estuaries experience other statistical relationships with other heavy metal contaminants. In close proximity to the Ribble Estuary, the Mersey Estuary is also a macro tidal estuary with a tidal range of 10.4m (extreme spring tide) (Harland *et al.*, 2000). Both estuaries have constrained training walls and are/were maintained by dredging (present day dredging continues in the Mersey, but stopped in Ribble in the mid-1980s). Extensive studies have been conducted by Harland *et al.* (2000), assessing the heavy metal contamination of the sub-tidal and the inter-tidal sediments within the estuary. The report demonstrated that there is a significant correlation between mercury and other heavy metals to the silt fraction within the estuary (Taylor, 1986), although, that has not been identified in other estuaries i.e. Firth of Forth (Harland *et al.*, 2000). Therefore, if any correlations exist between other heavy metal contaminations within the Ribble Estuary i.e. Mercury, Chromium, Zinc or Cobalt then it should be possible to utilize ARS to map the spatial extent of these contaminants within the Ribble Estuary intertidal sediments. Moreover, the technique developed in this thesis may be applicable to other estuaries, although not universally or generically.

#### **6.4.1. Intertidal clay mapping**

The clay abundance differences between the 1997 (Rainey *et al.*, 2000 & 2003) and the 2003 imagery showed that the actual clay percentage distribution had reduced. The reduction in the clay distribution between the two images has two possible explanations. The first is that they were

obtained at different times of the year (May 1997 and October 2003), which would have meant that the differing river discharge conditions and possible storminess patterns may be different leading to different spatial distributions. Secondly, the change is related to the varying river discharge patterns within the estuary prior to image acquisition. It can be clearly seen that within Figure 4.24, that there was a large discharge event prior to the 2003 image acquisition that would have caused a net loss of fine-grained sediment from the intertidal sediments within the estuary, and therefore reduce the clay percentages of the intertidal sediments. This would have accounted for reduced percentage clay in the middle and upper reaches of the estuary.

#### **6.4.2. Application of clay/<sup>137</sup>Cs relationships**

After identifying that the intertidal clay/<sup>137</sup>Cs were not temporally stable over an annual basis from the two-year monthly investigation of the intertidal sediments, individual ground reference data were required for each intertidal image flight, to firstly develop the image to clay relationship and subsequently the clay to <sup>137</sup>Cs relationship to produce the maps of intertidal <sup>137</sup>Cs distribution. Two separately ground truthed ATM images were acquired for the Ribble Estuary in September 2002 and October 2003. Unfortunately, due to a sensor malfunction in the September 2002 intertidal image, the image could not be used, but the data obtained from the ground control points could be utilized. However, it was decided that imagery acquired and ground truthed by Rainey (1999) in May 1997 could be used for an image-to-image comparison.

Assessment of the two images demonstrates that the activity concentrations have reduced over the six year time period. This change is demonstrated with the comparison of the 1995, 1997, 2000 and 2003 data sets with section 3.6. Table 3.6 demonstrates that the overall activity concentrations are reducing over time, with the 2002 transects indicating a 55% drop in the mid-range (5%) clay concentrations.

Some of this change can be attributed to the different river flow conditions, but some could be associated with the dilution of  $^{137}\text{Cs}$  contaminated marine sediments by uncontaminated sediment from the riverine or the historical uncontaminated estuarine sediments (demonstrated by cores obtained at Warton Bank Chapter Three). Conversely, the reduction in activity concentration could be due to the deposition and subsequent burial of the more active older marine sediments associated with the marine discharges of  $^{137}\text{Cs}$  in the late 60's and early 70's from BNFL Sellafield.

The distribution patterns of the percentage clay/ $^{137}\text{Cs}$  have been shown to be variable with time, both at the inter- and intra-annual time scales. This has important implications for any fixed term monitoring that is undertaken within the estuary. If sampling is conducted during a period of low river discharge rates and large river discharge, the effects on the spatial distribution patterns of  $^{137}\text{Cs}$  will be large and should affect any dose calculations based on them.

Subsequent analysis of the distribution of  $^{137}\text{Cs}$  shows that there is a 52% reduction in the activity concentrations of the intertidal sediments between the

1997 and 2003 data sets. Cook *et al.* (1997) showed that within the Irish Sea sediments, the redissolution process shortened the half-life period of  $^{137}\text{Cs}$  from 31 years to 23 years for the reduction in activity concentrations within the bed sediments. However, applying this reduction in the expected activity concentration half life to the time period associated here, can only account for c.16.5% reduction over the time period. This means that there is a 35.5% of extra dilution to be accounted for with the estuary system. It must therefore be a function of;

- i. Reduced activity concentrations of incoming marine derived sediments.
- ii. Distribution of marine sediments
  - a. Introduction of uncontaminated terrestrial sediments.
  - b. Re-mobilisation of uncontaminated estuarine sediments.
- iii. Increased resorption of  $^{137}\text{Cs}$  into the water column.

These possible mechanisms for the reduction in the activity concentrations of  $^{137}\text{Cs}$  within the Ribble Estuary are all plausible methods for describing this reduction. The source of  $^{137}\text{Cs}$  within the estuary originates from Irish Sea sediments, so if uncontaminated sediments are combined with these Irish Sea derived sediments then there would be a reduction in the activity concentrations. Certainly, some of this dilution could be caused by the influx of fresh uncontaminated sediment from the Ribble catchment area, however, influxes of sediments should be relatively small in comparison to the total sediment volumes contained within the estuary. The final mechanism, the

resorption of  $^{137}\text{Cs}$  back into the water column from the sediments has been shown (Cook *et al.*, 1997; MacKenzie *et al.*, 1997) to be of importance in reducing the effective activity of  $^{137}\text{Cs}$  within the Irish Sea sediments. This process is also likely to be occurring within the Ribble Estuary, gradually reducing the activity concentrations of the sediments at an increased rate.

It is likely that all three processes interlink, jointly combining to lower  $^{137}\text{Cs}$  activity concentrations of the sediment during the six years between intertidal sediment surveys.

### **6.5. Net sediment flux of suspended sediment**

The suspended sediment research was used to validate the fourth research hypothesis, thereby allowing the quantification of net sediment transportation over a flood and ebb tidal cycle.

The extraction of estimates for net sediment transport loads during the course of a single tidal event required the relatively novel approaches of using a sequence of time series ARS imagery obtained over the course of an entire tidal cycle to estimate net sediment deposition. Atkin (2000) demonstrated the ability of the CASI SeaWifs setting to map changing SSC over the course of the flood tidal sequence. Consequently, similar methodologies were used and assumptions validated to obtain estimates of total suspended sediment load transportation during an entire flood and ebb tide within the Ribble Estuary. The inclusion of a sun azimuth to the image normalisation process was an

alteration to the methodologies demonstrated by Atkin (2000). Consequently, as this step is part of the pre-processing stage of the SSC correction, the entire 1997 time series data set had to be re-calibrated using this approach, with the subsequent alteration of the SSC relationship described within chapter five. This section of work relies heavily on the modelled volumetric predictions from the VERSE model, due to the absence of LiDAR data, which was applied to each time series image to calculate the estimates of suspended sediment transportation.

#### **6.5.1. Suspended sediment load estimations**

It can be seen from Section 5.5.9 that the estimated net sediment transport of sediment over the course of the flood and ebb tide generates an estimate of 9,938 tonnes of sediment. This estimate, when put in context with the spatial extent of the entire estuary, results in the deposition over each square metre of an estimated 1.4 to 1.8 mm/m<sup>2</sup> for the entire estuarine system. If this deposition rate was to continue unabated, the estuary would experience a rapid sediment accretion. However, as demonstrated within the context of Chapter Three, the effects of storm wave activity on the outer estuary zones and the flushing effects of excessive (>50 cumecs) river flow events should lead to net erosion over the course of a tidal cycle. Comparisons to the maximum single tidal depositional rates measured within the estuary (Table 3.7) during the course of the two year field investigation indicated that the estimated 1.4 to 1.8 mm/m<sup>2</sup> of deposition over the intertidal surface is a good approximation of the actual deposition rates within the estuary. Where the

maximum single-tide depositional rates (2.8 mm) exceed the estimated net deposition rate for the estuary from the time series remote sensing imagery.

It could be assumed that the sediment deposited over the intertidal surface, would be of a fine particle size (<63  $\mu\text{m}$ ) and as demonstrated by the intertidal images within Chapter Four, the deposition of this sediment type will predominantly occupy the upper sections of the intertidal sediment. This means that the probable surface area for deposition will be dramatically reduced, effectively increasing the sediment deposition for those areas. If the fine-grained areas of the 2003 intertidal image are assessed for the surface area (c. 1.5 million  $\text{m}^2$ ) representing fine-grained sediments, it is possible to calculate bed elevation changes of between 4.1 and 5.1  $\text{mm}/\text{m}^2$ . This alternative value would only represent net deposition over the course of one tide and would not take into account any subsequent net erosion over subsequent tides. Nevertheless, the values derived from the calculated suspended sediment deposition are in relative agreement with the two year time series investigation, when possible erosion is accounted for.

Through this estimation of total sediment deposition and the systematic relationships between SSC and the use of the SSC/ $^{137}\text{Cs}$  relationship demonstrated by Atkin (2000), it is then possible to calculate the total activity concentrations of  $^{137}\text{Cs}$  that is associated with the sediments. Thus an estimated 2.72 GBq of  $^{137}\text{Cs}$  were deposited over the course of the July 2003 time series imagery. However, due to the affinity of  $^{137}\text{Cs}$  with fine-grained sediment (clay <2  $\mu\text{m}$ ) particles, the spatial distribution patterns will be not be

uniform. It can be clearly seen from the maps of intertidal clay (Figure 4.23) that depositional patterns are not uniform with time and therefore the sediment distribution pattern will not be consistent throughout the estuarine environment. The upper intertidal zones have the greater association with the finer (<63  $\mu\text{m}$ ) particles and thus higher activity concentrations, whilst the lower sandier intertidal sediment zones, having a lower affinity to radionuclides, will have lower activity concentrations. However, it has been observed that after high river flow events, the lower intertidal sites at Lytham can be covered by a layer (~5 cm) of unconsolidated mud derived from erosion of the upper estuarine sediments. Therefore, sampling strategies must take into account this spatial variation when collecting contemporaneous field samples.

Within the course of the entire study, a small sub-section of the estuary was selected to compare the estimates of sediment flux patterns of the April and July 2003 time series imagery. Consequently, a 1.5 km section of the estuary channel was identified at Warton Bank to derive inter-comparisons for the two time series data sets (Figure 5.36). It can be concluded that they have similar suspended sediment gradient profiles, with a high initial sediment load, dropping rapidly as the slack water high approaches and subsequently a smaller secondary peak in suspended sediment that is related to the ebb flow tidal flow. Figure 5.36, demonstrates that the April 2003 imagery has a higher suspended sediment load in the course of the tidal cycle, which is comparable to the larger tide that occurs during that period (9.79 m & 8.69 m).

Importantly, the two profiles demonstrate that the process of sediment suspension and deposition are similar for both periods, with the quantity of sediments changing in response to increased tidal amplitude.

The suspended sediment concentration imagery can also be used to demonstrate the movement of marine sediments into the estuary during the initial stages of the flood tide. It can be seen that during the initial phase of the flood tide (figure 5.14 & 5.25), sediments to the south-west of the main estuary channel are being transported into the estuary. However, subsequent imagery indicates that the SSC rapidly reduces during the course of tidal cycle. This influx of this sediment from the Irish Sea will also transport the associated radionuclides into the estuary. Unfortunately, it is not directly possible to assess the total quantity of sediment that is being transported into the estuary from the SSC imagery.

#### *Sources of uncertainty associated with sediment flux estimates*

As discussed within Chapter Five, there are a number of possible sources of uncertainty associated with the estimation of the net sediment deposition rates over the course of the time series imagery;

- Modelled volumetric estimates of the estuary.
- Assumption of vertical homogeneity within the water column.
- Suspended sediment concentrations during period of slack water.
- Assumptions of baseline suspended sediment at start and end of tidal cycle.

- Accuracy of calculation approach for SSC values.

An analysis of the uncertainties was discussed within Chapter 5.8, and highlighted that the largest uncertainty within the production of suspended sediment flux totals is the assumption the modelled water volume. Due to the lack of LiDAR data, it was required to use the modelled volumetric estimates obtained from the VERSE model to quantify the total sediment loads for each time series image. There are possible sources of error associated with any model outputs, with the main one being that of age of the bathymetric study of the estuary which the model uses to predict the water volume. The bathymetric data for the VERSE model was obtained in 1995 from an extensive side-scan sonar survey, which within itself has limitations within shallow estuarine environments. Therefore, during the course of the investigation an accurate EDM transect of Warton Bank was assessed against the bathymetric profile used within VERSE (Appendix 4). It shows that there was a large difference between the 1995 bathymetric data and the 2003 EDM survey. The difference between the two profiles is approximately  $243 \text{ m}^2$ , which if expanded for the one kilometre at the sub-sectioned Warton Bank site, would mean a difference of  $243,000 \text{ m}^3$ , in the two data sets. This disparity (shown with Table 5.10), shows that the uncertainties associated with the modelled water volume are less significant (6.38%) during tidal maxima, but more significant (8.91%) during the ensuing reduction in tidal height.

This is a large volumetric difference, which would mean that VERSE would under predict the water volumes within the estuary at this location. However, it

is known from field observation that the area at and around Lytham St Anne's has undergone considerable accretion within the last 10 years. This growth in this expansive area, may well counter-balance the area of erosion difference at Warton Bank area, although not on a cell-by-cell basis. It is not expected that the middle and upper estuarine zones will have experienced significant sediment accumulation, verified by the sediment core logs obtained at Warton Bank (Chapter Three). These cores indicate that uncontaminated sediment is present at the intertidal surface and therefore no substantial deposition has occurred at the time of coring. Indeed more than a metre or more of sediment is known to have been eroded from knowledge of the field site since 1995.

Quantifying the amount of sediment settling during the period of slack water had to be estimated due to the lack of available image data during this state of the tidal cycle. It could be seen from the pre- and post image estimates of suspended sediment (figures 5.31 & 5.32) that the quantities of sediment decrease within that period of time. For the purposes of this investigation, it was assumed that sediment deposition and flocculation rates were uniform with time and therefore remain relatively constant during the period of slack water.

The assumption of baseline sediment flow is based on the supposition that the water left within the estuary during the low tide period will contain a quantity of suspended sediment. It must be recognised that this baseline volume will change with varying river discharge conditions and the lunar cycle. However, the actual volume of water within the estuary and the associated suspended

sediment load are relatively insubstantial in comparison to the net flux of sediment within the flood and ebb tide period.

The suspended sediment flux estimates are based on the assumption of a homogeneous water column. This uncertainty was assessed by conducting depth profiles concurrent with image acquisition. They showed that the water column was predominantly homogeneous throughout the course of the time series imagery, although there could be some increase in SSC near the base of the water column that would generate increased uncertainties during the ebb tide period, which is demonstrated within Table 5.10.

The calibration of the SSC to the radiance values provides another source of uncertainty within the sediment flux calculations. Due to a relatively small number of point sample, obtained during the image acquisition, a past calibration (Atkin, 2000) was used to estimate SSC within the time series imagery. This required the 2003 image data to be normalised to the 1997 imagery, thereby allowing the SSC calibration to be utilized. These image-to-image normalisations relied on the assumption that the ground reference points (Warton Aerodrome taxi-ways) have stayed the same spectrally over time. The aerodrome staff confirmed that the taxi-ways had not been re-surfaced. Consequently, the 1997 image SSC calibration could be used on the 2003 time series imagery.

## 6.6. Further related work on the Ribble Estuary

The methodologies applied in monitoring the changing environmental conditions within the Ribble Estuary have been shown to produce accurate, quantitative information for major parts of the estuarine system. However, there are several logical progressive improvements to be undertaken to obtain the maximum scientific return.

1. The successful application of these methodologies to other Irish Sea estuaries would show and allow the methodologies developed for the Ribble Estuary may have a wider application and provide a greater understanding of the fate of radionuclides the Irish Sea and its estuaries.
2. To obtain same day time series intertidal imagery prior to and after inundation of the intertidal surface and the subsequent capture of time series airborne remote sensing data with either the CASI system or a more modern hyperspectral imager system. This would allow the identification of zones of fine-grained sediments on the intertidal surface, which would provide likely sources for suspended sediment. The post-intertidal image could then be used to classify the areas of the estuary that had undergone net deposition/removal of sediments.
3. Assessment of the mineralogy of the sediment particles distributed over the intertidal zones of the estuary to determine their provenance and

how they will affect the sediment deposition rates and resorption of  $^{137}\text{Cs}$ .

4. Obtaining *in-situ* erosional shear strength measurements of the intertidal sediments, in conjunction with microphytobenthos measurements, could be used to produce maps of intertidal erosion potential using the mixture modelling approach of ATM imagery.
5. Obtaining a continuous time series image data set would provide definitive answers to the gap in knowledge experienced within this project's image acquisition of the flood and ebb tidal imagery. This would validate the assumptions made within this body of work to replicate the reduction in suspended sediment load during the high water slack period within the estuary.
6. To capture a number of LiDAR images for the estuary at predetermined stages of the year to monitor how the surface elevation changes across the intertidal sediments. These could then be compared to a monthly sediment sampling study to demonstrate which types of sediment are being transported predominantly. Allowing the assessment of LiDAR precision and potentially for estimating inventory changes in radionuclides.
7. Studies on the role of microphytobenthos in releasing radionuclides from the intertidal sediments and into the water column. This could

have implications for the remobilisation of sediment-bound radionuclides back into the solution and may be an important mechanisms in explaining the observation of Cook *et al.* (1997) and MacKenzie *et al.* (1997).

8. The deployment of a wave and wind direction buoy at the outer edge of the Ribble Estuary could provide valuable parameters for any subsequent modelling of the estuary, as wind directional data from RAF Ronaldsway (Isle of Man) demonstrates a relationship to the intertidal sediments at Lytham St Anne's.
9. The acquisition of a number of ATM images of the intertidal surface during the course of a year would allow the mapping of fine-grained sediment and subsequently the identification of the major sources and sinks of other particle reactive or related pollutants, e.g. faecal coliforms and heavy metals.
10. From the data derived from the work could then be applied to a simple box model of sediment flux, which can be used to validate sediment movement according to the tide and catchment characteristics.
11. *In-situ* gamma detection of  $^{137}\text{Cs}$  on transect profiles during any future image acquisition to obtain total activity concentrations from the intertidal surface.

## 6.7. Conclusions on method developments

The use of point sampling over an inter-annual period provides increased knowledge of estuarine sediments, which can be applied to the ARS imagery. It is clear from the field sampling that ARS must include extensive ground-truthing to produce reliable maps of intertidal clay and  $^{137}\text{Cs}$  distribution patterns within the estuary. However, it is evident that in mapping sediment flux patterns, the use of point measurement are not required to provide estimates of suspended sediment deposition within the estuary, as demonstrated by the April 2003 image data set, and perhaps provides the best spatially explicit approach to providing sedimentation estimates..

Methodologies for the identification of the intertidal sediments and the associated radionuclides produced by previous research (Rainey, 1999; Rainey *et al.*, 2000 & Rainey *et al.*, 2003) demonstrate the continued applicability of the methods. The use of the mud abundance and microphytobenthos endmembers to predict the intertidal clay distribution were shown to be still valid. However, it was not possible to apply the same percentage clay/ $^{137}\text{Cs}$  relationship demonstrated by Rainey (1999), to the 2003 intertidal imagery as this relationship has been shown to be temporally unstable with time. Subsequently, it was therefore necessary to obtain concomitant ground sampling data with image calibration. Nevertheless the application of this methodology has shown that the activity concentrations of the intertidal surface sediments are decreasing since the 1995 intertidal survey (Rainey, 1999).

## 6.8. Conclusions on the fate of sediment and radionuclide dynamics in the Ribble Estuary

The sediments and associated radionuclides within the Ribble Estuary has been shown over the period of this study to be temporally and spatially variable. The quantity of the data set has enabled linkages to be identified and quantified to a range of environmental drivers (tidal cycles, wind direction and wind induced wave action and river discharge). It is also clear that the environmental drivers effects vary from location to location within the estuary.

The main use of this information is;

- To understand and quantify sediment fluxes within estuarine environments.
- To obtain rates of change in the intertidal sediment surface.
- To understand environmental drivers within the estuarine system.
- To underpin interpretation of remote sensing data i.e. sediment type.

The key findings are:

(i) The associated clay/<sup>137</sup>Cs relationships have been shown to be temporally unstable with time, although this instability appears to be confined to the higher river discharge events. The use of the percentage clay/<sup>137</sup>Cs relationship to produce maps of total activity concentrations for the estuary is a valuable in assessing the changing spatial distribution of the radionuclides and other possible heavy metal contaminants. The comparison 1997 and 2003 image data series highlights the affect of river discharge conditions on

clay and  $^{137}\text{Cs}$  distribution patterns within the estuary. This conclusion has important implications for annual dose assessment reports conducted by the Environment Agency. Consequently, if point sampling were to occur after a large river discharge event, subsequent dose assessments made on this data would under-estimate gamma-dose levels to the critical groups within the estuary and over-estimated during periods of low river discharge conditions.

(ii) The use of time series ARS as a tool for quantifying sediment flux patterns within the Ribble Estuary has been successfully demonstrated. The use of the ARS data allows for spatially isolated point samples to be placed within a geographic setting, which could not be achieved through conventional point sampling or modelling of estuarine sediment dynamics. The quantity of depositional sediment, when evenly distributed over the entire estuary resulted in an estimated  $1.4 - 1.8 \text{ mm/m}^2$  of net sedimentation over a tidal cycle. This is verified by the monthly bed elevation height changes, which demonstrates that the estimated depositional rate is comparable to the measured values. Estimating total fluxes of sediment are not only important in estimating net sedimentation rates within estuarine environments, for the associated radionuclides, but also for estuarine management strategies. However, there are a number of uncertainties associated with the quantification of the sediment flux over the course of a tidal cycle, with the total absolute error of 40%, associated with all the calculated values.

(iii) The methodologies for the quantification of the suspended sediment flux demonstrated above has provided estimates of sediment and radionuclide flux over the course of a tidal cycle for the first time within this macro tidal estuary. Understanding these processes is also important for the assessment of geomorphic evolution of different sediment domains and the short and long term fate of anthropogenic radionuclides within estuarine environments. This investigation has demonstrated the temporal flexibility of the methodology, allowing a unique spatial insight into the processes controlling sediment distribution and flux across an estuary over a range of time scales.

## **6.9. Final conclusions**

Assessing the main finding of this investigation of the estuarine sediments within the Ribble estuary, has demonstrated a number of important facts that are important in gaining an increased understanding of the sediment and the pollution pathways within the estuarine environment of the Ribble Estuary.

- Cyclic patterns of sediment transport can occur, with estuarine sediments being tidally pumped in an upstream direction, whilst intertidal sediments undergo erosion during high river flow events (>50 cumecs). Fine-grained sediments can be eroded from upper estuary and transported down-stream and deposited over the outer estuary intertidal zones.

- Intra-annual bed elevation changes can be in excess of inter-annual changes, with net accretion in the outer estuary zone and limited inter-annual changes in bed sediment height in the middle and upper estuary intertidal sediments sometimes occurring.
- Distribution patterns of intertidal clay distribution, derived from the May 1997 (Rainey, 1999) and October 2003, show considerable variation between images. This was due to high (>50 cumec) river flows prior to the 2003 image acquisition, which may have caused the erosion of the clay particles, that did not occur before the 1997 imagery. This validates the findings from Chapter Three, where it was demonstrated that river discharge seems to control fine-grain sediment distribution in estuaries.
- The temporal stability of the clay/<sup>137</sup>Cs relationship identified by Rainey (1999), were found to be unstable under large river discharge conditions, following the two year field sampling investigation (Chapter Three). Therefore, it may be necessary to carry out extensive concomitant field sampling to identify the current clay/<sup>137</sup>Cs relationship within the intertidal sediments of other estuaries or in the future of the Ribble and not rely on previously identified clay/<sup>137</sup>Cs relationships.
- Activity concentrations of the intertidal sediments have reduced substantially (c. 52 %) between the 1995 and 2003. Natural decay of the historically higher <sup>137</sup>Cs, which were discharged from BNFL

Sellafield early 70's, can only account for 16.5 % of this reduction in activity concentrations. Therefore,  $^{137}\text{Cs}$  is either being desorbed from the estuarine sediments and transported out of the estuary or older, more contaminated sediments have been buried by fresh sediments within the estuary.

- Deriving the estimates of suspended sediment for the July 2003 time series imagery provides an apparent realistic assessment of the sediment budget within the estuary. This novel methodology of providing total estimates of sediment generated within the Ribble Estuary, demonstrates a good replication of the observed depositional rates from the monthly field sampling and thus the possibility of the techniques being more universal.

This combined approach of remote sensing with time series field monitoring data has yielded quantitative information on the distribution and flux of sediments and sediment bound pollutants, in this case BNFL Sellafield derived radioactivity. ARS in particular has proven itself to be a powerful tool in deriving estuary wide estimates of sediment flux, which would be difficult to achieve through conventional point sampling methodologies. Validating these estimates of flux and sedimentation rates, suggest that they are not only reasonably precise (40%) compared to other means of deriving estimates, but that such data should also be useful in validating models of estuarine systems, as well as providing a better understanding of the dynamics of macro-tidal estuaries.

## References

- Aldridge, J.N., Kershaw, P., Brown, J., McCubbin, D., Leonard, K.S. & Young, E.F. 2003. Transport of plutonium ( $^{239,240}\text{Pu}$ ) and caesium ( $^{137}\text{Cs}$ ) in the Irish Sea: comparison between observations and the results from sediment and contaminant transport modelling. *Continental Shelf Research*. Vol. 23, pp 869 – 899.
- Anderson, F.E. 1983. The northern muddy intertidal: a seasonally changing source of suspended sediment to estuarine waters – a review. *Canadian Journal of Fisheries and Aquatic Science*. Vol. 40, pp 143 – 159.
- Allen, J.P.L. & Duffy, M.J. 1998. Medium-term sedimentation on high intertidal mudflats and salt marshes in the Severn Estuary, SW Britain: role of wind and tide. *Marine Geology*, Vol. 150, pp 1 – 27.
- Arundale, A.M.W., Darbshire, E.J., Hunt, S.J., Schmitz, K.G. & West, J.R. 1997. Turbidity maximum formation in four estuaries. In *Cohesive Sediments.*, Burt. N., Parker. R. & Watts, J. (edi.). Wallingford, Chichester: John Wiley & Sons.
- Assinder, D.J., Mudge, S.M. & Bourne, G.S. 1997. Radiological assessment of the Ribble Estuary – I. Distribution of radionuclides in surface sediments. *Journal of Environmental Radioactivity*. Vol. 36 (1), pp 1 – 19.
- Aston, S.R., Assinder, D.J. & Kelly, M. 1985. Plutonium in intertidal coastal and estuarine sediments in the northern Irish Sea. *Estuarine, Coastal and Shelf Science*. Vol. 20, pp 761 - 771.
- Atkin, P.A. 2000 Investigating radionuclide bearing suspended sediment transport mechanisms in the Ribble Estuary using airborne remote sensing. *Ph.D Thesis*. University of Stirling.
- Avery, S.V. 1996. Fate of Caesium in the Environment: Distribution Between the Abiotic and Biotic components of Aquatic and Terrestrial Ecosystems. *Journal of Environmental Radioactivity*, Vol. 30, No. 2, pp 139 – 171.
- Bale, A.J., Tocher, M.D., Weaver, R., Hudson, S.J. & Aiken, J. 1994. Laboratory measurements of spectral properties of estuarine suspended particles. *Netherlands Journal of Aquatic Ecology*, Vol. 28 (3-4), pp 237 – 244.
- Babey, S.K. & Anger, C.D. 1989. A Compact Airborne Spectrographic Imager (CASI). *Proc. IGARSS '89, 12<sup>th</sup> Canadian Symposium on Remote Sensing*. Vol. 2, pp 1028 – 1031. Vancouver, July 10 – 14<sup>th</sup>, 1989.
- Barr, R., Watson. P.G., Ashcroft. C.R., Barnett. B.E. & Hilton. C. 1990. Humber Estuary – a case study. *Hydrobiologia*, Vol. 195, pp 127 -143.
- Beresford Hartwell, P.R., Horsington, R.W., Mamas, C.J., Randle, K., Sokhi, R.S., Taylor, E.W. & West, J.R. 1995. Changes in sedimentation and pollution in the Ribble Estuary. *ECSA 20 Symposium: The Changing coastline*. Hull.
- Bell, R.G., Hume, T.M., Dolphin, T.J., Green, M.O. & Walters, R.A. 1997. Characterisation of physical environmental factors on an intertidal sandflat, Manukau harbour, New Zealand. *Journal of Experimental Marine Biology and Ecology*. Vol. 216, pp 11 – 31.
- Berk, A.L.S., Berstein & Robertson, D.C. 1989. *MODTRAN: A moderate resolution model for LOWTRAN 7*. Hanscom Air Force Base, MA: *US Airforce Geophysics Laboratory*.

- Black, K.S. 1997. Microbiological factors contributing to the erosional resistance in natural cohesive sediments. In *Cohesive Sediments*, Burt. N., Parker. R. & Watts. J. (edi). Wallingford, Chichester, John Wiley & Sons.
- Blanchard, G.F., Paterson, D.M., Stal, L., Richard, P., Galois, R., Huet. V., Kelly, J., Honeywill, C., de Brouwer, J., Dyer, K. , Christie, M.C. & Seguignes, M.2000. The effect of geomorphological structures on potential biostabilization by microphytobenthos on intertidal mudflats, *Continental Shelf Research*. Vol. 20(10-11), pp 1243-1256.
- Boardman, J.W. 1989. Inversion of imaging spectrometry data using singular value decomposition. In *Proceedings of IGARSS '89 12<sup>th</sup> Canadian Symposium on Remote Sensing*. Vol. 4, pp 2069 – 2072.
- Børretzen, P. & Salbu, B. 2002. Fixation of Cs to marine sediments estimated by a stochastic modelling approach. *Journal of Environmental Radioactivity*, Vol. 61, pp 1 – 20.
- Bradley, S.B., & Chapman, P. 1998. Contemporary flux of radionuclide contamination saltmarsh in the Esk Estuary, Cumbria. *Water, Air and Soil Pollution*. Vol. 107, pp 175 - 184
- Brenon, I. & Le Hir, P. 1998. Modelling fine sediment dynamics in the Seine Estuary: Interactions between the turbidity patterns and sediment balance. *Physics of Estuaries and Coastal Seas* (Donkers, J. & Scheffers, M.B.A.M. ed.) The Hague, Netherlands. Rotterdam: A.A. Balkema.
- Brown, J.E. 1997. The behaviour of radionuclides in the Ribble Estuary, NW England. *Ph.D. Thesis*. Postgraduate research institute for sedimentology, University of Reading.
- Brown, J.E., McDonald, P., Parker, A. & Rae, J.E. 1999. The vertical distribution of radionuclides in the Ribble Estuary saltmarsh: transport and deposition of radionuclides. *Journal of Environmental Radioactivity*. Vol. 43, pp 259 – 275.
- Bruesseler, K.O. 1991. Do upper-ocean sediment traps provide an accurate record of particle flux? *Nature*. Vol. 353, pp 420 – 423.
- Burchard, H. & Baumert, H. 1998. The formation of estuarine turbidity maxima due to density effects in the salt wedge. A hydrodynamic process study. *Journal of Physical Oceanography*. Vol. 28 (2), pp 309 -321.
- Burton, D.J., West, J.R. & Horsington, R.W. 1995. Modelling transport processes in the Ribble Estuary. *Environmental International*. Vol. 21 (2), pp 131 – 141.
- Cahoon, D.R., Reed, D.J. & Day Jr, J.R. 1995. Estimating shallow subsidence in micro-tidal salt marshes of the south-eastern United States: Kaye and Barghoorn revisited. *Marine Geology*. Vol. 128, pp 1 – 9.
- Cahoon, D.R. & Lynch, J.C. 1997. Vertical accretion and shallow subsidence in a mangrove forest of south-eastern Florida, USA. *Mangroves Salt Marshes*. Vol. 1, pp 173 – 186.
- Camenen, B. & Larson, M. 2005. A general formula for non-cohesive bed load sediment transport. *Estuarine, Coastal and Shelf Science*. Vol. 63, pp 249 – 260.
- Cameron, F.A. & Pritchard, D.W. 1963, in *The Sea*, Hill. M.N. (edi.), John Wiley and Sons, New York.
- Chaplesworth, M.E., Service, M. & Gibson, C.E. *In press*. The distribution and transport of Sellafield derived <sup>137</sup>Cs and <sup>241</sup>Am to western Irish Sea sediments. *The Science of the Total Environment*. Vol..

- Chavez, P.S. 1975. An improved dark-object subtraction technique for atmospheric scattering correction of multispectral data. *Remote Sensing of Environment*. Vol. 24, pp 459 – 479.
- Chen, H. & Dyke, P.P.G. 1998. Multivariate time-series model for suspended sediment concentration. *Continental Shelf Research*. Vol. 18, pp 123 – 150.
- Chen, Z., Hanson, J.D. & Curran, P.-J. 1991. The form of the relationship between suspended sediment concentration and spectral reflectance: Its implications for the use of Daedalus 1268 data. *International Journal of Remote Sensing*. Vol. 12 (1), pp 215 – 222.
- Chen, Z., Kostaschuk, R. & Yang, M. 2001. Heavy metals on tidal flats in the Yangtze Estuary, China. *Environmental Geology*. Vol. 40, pp 742 – 749.
- Christie, M.C., Dyer, K.R. & Turner, P. 1999. Sediment flux and bed level measurements from a macro tidal mudflat. *Estuarine, Coastal and Shelf Science*. Vol. 49, pp 667 – 688.
- Clifton, J., McDonald, P., Plater, A. & Oldfield, F. 1997. Relationship between radionuclide content and textural properties in Irish Sea Intertidal sediments. *Water, Air and Soil Pollution*. Vol. 99 (1-4), pp 209 – 216.
- Cook, G.T., MacKenzie, A.B., McDonald, P. & Jones, S.R. 1997. Remobilization of Sellafield-derived radionuclides and transport from the north-east Irish coast. *Journal of Environmental Radioactivity*. Vol. 35 (3), pp 227 – 241.
- Couperthwaite, J.S., Mitchell, S.B., West, J.R. & Lawler, D.M. 1998. Cohesive sediment dynamics on an intertidal bank of the tidal Trent. *Marine Pollution Bulletin*. Vol. 37 (3 – 7), pp 144 – 154.
- Croudance, I.W. & Cundy, A.B. 1995. Heavy metal and hydro-carbon pollution in recent sediments from Southampton Water, Southern England: a geochemical and isotopic study. *Environmental Science and Technology*, Vol. 29, pp 1288 – 1296.
- Cundy, A.B. & Croudance, I.W. 1996. Sediment accretion and recent sea-level rise in the Solent, southern England: Inferences from radiometric and geometrical studies. *Estuarine, Coastal and Shelf Science*. Vol. 43, pp 449 – 467.
- Davies, K.S. & Shaw, G. 1993. Fixation of <sup>137</sup>Cs by soils and sediments in the Esk Estuary, Cumbria, UK. *Science of the Total Environment*. Vol. 132, pp 71 – 92.
- Donoghue, D.N.M. & Shennan, L. 1987. A preliminary assessment of Landsat TM imager for mapping vegetation and sediment distribution in the Wash Estuary. *International Journal of Remote Sensing*. Vol. 8 (7), pp 1101 – 1108.
- Donoghue, D.N.M. & Mironnet, N. 2002. Development of an integrated geographical information system prototype for coastal habitat monitoring. *Computers & Geosciences*. Vol. 28, pp 129 – 141.
- Doxaran, D., Froidefond, J.-M., Lavender, S. & Castaing, P. 2002. Spectral signature of highly turbid waters. Application with SPOT data to quantify suspended matter concentrations. *Remote Sensing of Environment*. Vol. 81, pp 149 – 161.
- Doxaran, D., Cherukuru, R.C.N. & Lavender, S.J. 2005. Use of reflectance band ratios to estimate suspended and dissolved matter concentrations in estuarine waters. *International Journal of Remote Sensing*. Vol. 26 (8), pp 1763 – 1769.
- Dyer, K.R.. 1986. Coastal and Estuarine Dynamics. Chichester, *John Wiley and Sons*
- Dyer, K.R.. 1995. Sediment transport processes in estuaries. In *Geomorphology and sedimentology of estuaries*. Perillo, G.M.E. (edi.). Elsevier Science, pp 423 – 449.

- Dyer, K.R. 1997. *Estuaries : a physical introduction*. (2<sup>nd</sup> ed.). Chichester, *John Wiley*.
- Dyer, K.R., Christie, M.C. & Wright, E.W. 2000. The classification of intertidal mudflats. *Continental Shelf Research*. Vol. 20 (10-11), pp 1039 – 1060.
- Dyer, K.R., Christie, M.C. & Manning, A.J. 2004. The effects of suspended sediment on turbulence within an estuarine turbidity maximum. *Estuarine, Coastal and Shelf Science*. Vol. 59, pp 237 – 248.
- Eisenbud, M. & Gesell, T. 1997. *Environmental radioactivity: from nature, industrial and military sources*, 4<sup>th</sup> ed. San Diego, Academic press.
- Estes, J.A., Hajic, E.J. & Tinney, L.R. 1983. Fundamentals of image analysis: analysis of visible and thermal infrared data. *Manual of Remote Sensing* (Colwell, R.N. ed.). American Society Photogram, Falls Church, Virginia, USA.
- Eyre, P. 2002. BNFL Westinghouse UK fuel Business REPPiR report of assessment.
- Facchinelli, A., Gallini, L., Barberis, E., Magnoni, M. & Hursthouse, A.S. 2001. The influence of clay mineralogy on the mobility of radiocaesium in upland soils in NW Italy. *Journal of Environmental Radioactivity*, Vol. 56, pp 299 – 307.
- Friedrichs, C.T., Armbrust, B.D. & de Swart, H.E. 1998. Hydrodynamics and equilibrium sediment dynamics of shallow, funnel-shaped tidal estuaries. In *Physics of Estuaries and Coastal Seas* (Dronkers, J. & Scheffers, M.B.A.M.), Balkema, Rotterdam, pp 315 -327.
- Frignani, M., Sorgente, D., Langone, L., Albertazzi, S. & Ravaioli, M. 2004. Behaviour of Chernobyl radiocaesium in sediments of the Adriatic Sea off the Po River delta and the Emilia-Romagna coast. *Journal of Environmental Radioactivity*. Vol. 71, pp 299 – 312.
- Galois, R., Blanchard, G., Seguignes, M., Huet, V. & Joassard, L. 2000. Spatial distribution of sediment particulate organic matter on two estuarine intertidal mudflats: a comparison between Marennes-Oleron Bay (France) and the Humber Estuary (UK). *Continental Shelf Research*. Vol. 20, pp 1199 – 1217.
- Ganju, N.K., Schoellhamer, D.H., Warner, J.C., Barad, M.F. & Schladow, S.G. 2004. Tidal oscillation of sediment between a river and a bay: conceptual model. *Estuarine, Coastal and Shelf Science*. Vol. 60, pp 81 – 90.
- Gilvear, D., Tyler, A.T. & Davids, C. 2004. Detection of estuarine and tidal river hydromorphology using hyper-spectral and LiDAR data: Forth Estuary, Scotland. *Estuarine, Coastal and Shelf Science*. Vol. 61, pp 379 – 392.
- Gleizon, P. 1999. A vertically resolving model of sediment and radionuclide transport for the Ribble Estuary. *Proceedings of 6<sup>th</sup> SRP International Symposium*, pp 291 – 294.
- Gleizon, P., Punt, A.G. & Lyons, M.G. 2002. A computer model of sediment dynamics and radionuclide dispersion in a macrotidal estuary. *Proceedings of the Radiological – Ecotoxicology of Continental and Estuarine Environments*, ECORAD 2001. Vol. 37 (C1), pp 737 – 742.
- Gleizon, P., Punt, A.G. & Lyons, M.G. 2003. Modelling hydrodynamics and sediment fluxes within a macrotidal estuary; problems and solutions. *The Science of the Total Environment*. Vol. 314-316, pp 589 – 597.
- Grabemann, I. & Krause, G. 1998. Response of turbidity maximum in the Weser Estuary to Pulses in freshwater runoff and to storms. In *Physics of Estuarine and Coastal Seas* (Dronkers, J. & Scheffers, M.B.A.M. eds.), The Hague, Netherlands, Rotterdam: A.A. Balkema.

- Green, A.A., Berman, M., Switzer, P. & Craig, M.D. 1988. A transformation for ordering multispectral data in terms of image quality and implications for noise removal. *Transactions on Geoscience and Remote Sensing*. Vol. 26 (1), pp 65 -74.
- Guezennec, L., Lafite, R., Dupont, J-P., Meyer, R. & Boust, D. 1999. Hydrodynamics of suspended particulate matter in the tidal freshwater zone of a macrotidal estuary (the Seine Estuary, France). *Estuaries*. Vol. 22, pp 717 – 727.
- Hakvoort, J.H.M., Heineke, M., Heymann, K., Kuhl, H., Riethmuller, R. & Witte, G. 1998. A basis for mapping the erodibility of tidal flats by optical remote sensing. *Marine Fresh Water Research*. Vol. 49, pp 867 – 873.
- Harland, B.J., Taylor, D. & Wither, A. 2000. The distribution of mercury and other trace metals in the sediments of the Mersey Estuary over 25 years 1974 – 1998. *The Science of the Total Environment*, Vol. 253, pp 45 – 62.
- Han, L. 1997. Spectral reflectance with varying suspended sediment concentrations I clear and algal waters. *Photogrammetric Engineering and Remote Sensing*. Vol. 63 (6), pp 701 – 705.
- Hardisty, J. & Rouse, H.L. 1996. The Humber Observatory: Monitoring, modelling and management for the regional environment. *Environmental International*. Vol. 21 (2), pp 143 – 149.
- Hird, A.B. & Rimmer, D.J. 1995. Total caesium-fixing potentials of acid organic soils. *Journal of Environmental Radioactivity*. Vol. 26 (2), pp 103 – 118.
- Honeywell, C., Paterson, D.M. & Hagerthey, S.E 2002. Determination of microphytobenthic biomass using pulse-amplified modulated minimum fluorescence. *European Journal of Phycol*. Vol. 37, pp 485 – 492.
- Hudson, S.J., Moore, G.F., Bale, A.J., Dyer, K.R. & Aiken, J. 1994. An operational approach to determining suspended sediment distribution in the Humber Estuary by airborne multi-spectral imagery. *Proceedings of the first Airborne Remote Sensing Conference and Exhibition*, Strasbourg, France. 11 – 15<sup>th</sup> September, 1994.
- International Atomic Energy Agency. 2003. International Atomic Energy Agency guidelines for radioelement mapping using gamma ray spectrometry, Austria, IAEA.
- Jay, D.A., Geyer, W.R., Uncles, R.J., Vallino, J., Largier, J. & Boynton, W.R. 1997. A review of recent developments in estuarine scalar flux estimates. *Estuaries*. Vol. 20, pp 262 – 280.
- Jorgensen, P.V. & Edelvang, K. 2000. CASI data utilisation for mapping suspended matter concentrations in sediment plumes and verification of 2D hydrodynamic modelling. *International Journal of Remote Sensing*. Vol. 21 (11), pp 2247 – 2258.
- Kashefipour, S.M., Lin, B., Harris, E. & Falconer, R.A. 2002. Hydro-environmental modelling for bathing water compliance of an estuarine basin. *Water Research*. Vol. 36, pp 1854 – 1868.
- Kelly, M.R. & Emptage, M.R. 1992. Distribution of radioactivity in the Esk Estuary and its relationship to sedimentary processes. Department of Environment Report 1992. pp 124.
- Kemeny, J. 2005. Time-dependent drift degradation due to the progressive failure of rock bridges along discontinuities. *International Journal of Rock Mechanics and Mining Sciences*. Vol. 42, pp 35 -46.
- Kershaw, P.J., Woodhead, D.S., Malcolm, S.J., Allington, D.J. & Lovett, M.B. 1990. A sediment history of Sellafield discharges. *Journal of Environmental Radioactivity*. Vol. 12, pp 201 – 241.

- Kershaw, P.J., Dennon, D.C. & Woodhead, D.S. 1999. Observations on the redistribution of plutonium and americium in the Irish Sea sediments, 1978 to 1996: concentrations and inventories. *Journal of Environmental Radioactivity*. Vol. 44, pp 191 – 221.
- Kircher, G. & Ehlers, H. Sediment geochronology in changing coastal environments: Potentials and limitations of the  $^{137}\text{Cs}$  and  $^{210}\text{Pb}$  methods. *Journal of Coastal Research*. Vol. 14 (2), pp 483 – 492.
- Kluson, J. 2001. Environmental monitoring and *in situ* gamma spectrometry. *Radiation Physics and Chemistry*. Vol. 61, pp 209 – 216.
- Kneizys, F.X.E.P., Settle, L.W., Abreu, J.H., Chetwynd, G.P., Anderson, W.O., Gallery, J.E.A, Selby, & Clough, S.A. 1988. User guide to LOWTRAN 7. Hanson Air Force Base: *US air force geophysics laboratory*; 1988137.
- Knoll, G.F. 1989. *Radiation detection and measurement*, 2<sup>nd</sup> ed. Singapore, John Wiley and Sons, Inc.
- Lawler, D.M., West, J.R., Couperthwaite, J.S & Michell, S.B. 2001. Application of a novel automatic erosion and deposition monitoring system at a channel bank site on the tidal rive Trent, UK. *Estuarine, Coastal and Shelf Science*. Vol. 53, pp 237 – 247.
- Lawler, D.M. 2005. The importance of high-resolution monitoring in erosion and deposition dynamics studies: examples from estuarine and fluvial systems. *Geomorphology*. Vol. 64, pp 1 – 23.
- Lee, S.V. & Cundy, A.B. 2001. Heavy metal contamination and mixing processes in sediments from the Humber Estuary, Eastern England. *Estuarine, Coastal and Shelf Science*. Vol. 53, pp 619 – 636.
- Le Normant, C., Peltier, E. & Teisson, C. 1998. Three dimensional modelling of cohesive sediment transport in estuaries. *Physics of Estuaries and Coastal Seas* (Donkers, J. & Scheffers, M.B.A.M. eds.) The Hague, Netherlands. Rotterdam: A.A. Balkema.
- Le Hir, P., Roberts, W., Cazaillet, O., Christie, M., Bassoullet, P. & Bacher, C. 2000. Characterization of intertidal flat hydrodynamics. *Continental Shelf Research*. Vol. 20, pp 1433 – 1459.
- Le Hir, P., Ficht, A., Jacinto, R.S., Lesueur, P., Dupont, J.P., Lafite, R., Brenon, I. Thouvenin, B. & Cugier, P. 2001. Fine sediment transport and accumulation at the mouth of the Seine Estuary (France). *Estuaries*. Vol. 24, pp 950 – 963.
- Li, C. 2002. Axial convergence fronts in a barotropic tidal inlet-sand shoal inlet, VA. *Continental Shelf Research*. Vol. 22, pp 2633 – 2653.
- Lillesand, T. & Kiefer, R. 2000. *Remote Sensing and Image Interpretation*, forth edition. New York, John Wiley and Sons, Inc.
- Liu, H.H., Salve, R., Wang, J.S., Bodvarsson, G.S. & Hudson, D. 2004. Field investigation into unsaturated flow and transport in a fault: model analysis. *Journal of Contaminant Hydrology*. Vol. 74, pp 39 – 59.
- Livens, F.R., Horrill, A.D. & Singleton, D.L. 1994. Plutonium in estuarine sediments and the associated interstitial waters. *Estuarine, Coastal and Shelf Science*. Vol. 38, pp 479 – 489.
- Lumberg, U. & Windlin, A. 2003. Hydrography and cohesive sediment modelling: application to the Rome Dyb tidal area. *Journal of Marine Systems*. Vol. 38, pp 287 – 303.
- Lyons, M.G. 1997. The dynamics of suspended sediment transport in the Ribble Estuary. *Water, Air and Soil*, Vol. 99, pp 144 – 148.

- MacKenzie, A.B., Scott, R.D., Allan, R.L., Ben Shaban, Y.A., Cook, G.T. & Pulford, I.D. 1994. Sediment radionuclide profiles: implications for mechanisms of Sellafield waste dispersal in the Irish Sea. *Journal of Environmental Radioactivity*. Vol.23, 39 – 69.
- MacKenzie, A.B., Cook, G.T., McDonald, P. & Jones, S.R. 1997. The influence of mixing timescales and re-dissolution processes on the distribution of radionuclides in north east Irish Sea sediments. *Journal of Environmental Radioactivity*. Vol. 39, pp 35 – 53.
- MacKenzie, A.B., Cook, G.T. & McDonald, P. 1999. Radionuclide distribution and particle size associations in Irish Sea surface sediments: implications for actinide dispersion. *Journal of Environmental Radioactivity*. Vol. 44, pp 275 – 296.
- Mamas, C.J.V., Earwaker, L.G. & Sokhi, R.S. 1995. An estimation of sedimentation rates along the Ribble Estuary, Lancashire, UK, based on radiocaesium profiles preserved in intertidal sediments. *Environmental Radioactivity*. Vol. 21 (2), pp 151 – 165.
- McCartney, M., Kershaw, P.J., Woodhead, D.S. & Denoon, D.C. 1994. Artificial radionuclides in the surface sediments of the Irish Sea, 1968 -1988. *The Science of the Total Environment*. Vol. 141, pp 103 – 138.
- McDonald, P., Vives-Battle, J., Bousher, A. & Chambers, N. 2001. The availability of plutonium and americium in Irish Sea sediments for re-mobilisation. *The Science of the Total Environment*. Vol. 267, pp 109 – 123.
- Middleton, R. & Grant, A. 1990. Heavy metals in the Humber Estuary: *Scrobicularia* clay as a pre-industrial datum. *Proceedings of the Yorkshire Geological*, Vol. 48, pp 75 – 80.
- Mikkelsen, O.A.. 2002. Variation in the projected surface area of suspended particles: Implications for remote sensing assessment of TSM. *Remote Sensing of Environment*. Vol. 79, pp 23 – 29.
- Milovich, J.A., Frulla, L.A. & Gagliardini, D.A. 1995. Environment contribution to the atmospheric correction for Landsat-MSS images. *International Journal of Remote Sensing*. Vol. 16 (14), pp 2515 – 2537.
- Mitchells S.B., Lawler, D.M., West, J.R. & Couperthwaite, J.S. 2003. Use of continuous turbidity in the prediction of fine sediment transport in the turbidity maximum of the Trent Estuary, UK. *Estuarine, Coastal and Shelf Science*. Vol. 58, pp 645 – 652.
- Mudge, S.M., Bourne, G.S. & Assinder, D.J. 1997. Radiological assessment of the Ribble Estuary – II. Beta and Gamma dose rates and dose to critical groups. *Journal of Environmental Radioactivity*. Vol. 36 (1), pp 21 – 41.
- Nimmo Smith, W.A.M. & Thorpe, S.A. 1999. Dispersion of buoyant material by langmuir circulation and tidal currents. *Marine Pollution Bulletin*. Vol. 38 (9), pp 824 – 829.
- Norris, J. 2004. Investigating the factors controlling intertidal sediment erosivity *Unpublished BSc. Dissertation*, University of Stirling.
- Novo, E.M.M., Steffen, C.A. & Braga, C.Z.F. 1991. Results of a laboratory experiment relating spectral reflectance to total suspended solids. *Remote Sensing of the Environment*. Vol. 36 (1), pp 67 – 72.
- Nybakken, J.W. 2001. Marine Biology, 5<sup>th</sup> edition. *Library of congress cataloguing-in-publication data*.
- Parker, A. & McCann, C. 1988. Percussion corer and extrusion device for unconsolidated sediments. *Journal of Sedimentary Petrology*. Vol. 58, pp 752 – 753.
- O'Brien, D.J., Whitehouse, R.J.S. & Cramp, A. 2000. The cyclic development of a macrotidal mudflat on varying timescales. *Continental Shelf Research*. Vol. 20, pp 1593 – 1619.

O'Neill, A.J., Galloway, T.S., Brown, M.A., Dissanayake, A. & Depledge, M.H. 2004. Evaluation of toxicity in Tributaries of the Mersey Estuary using the isopod *Asellus aquaticus*(L.). *Marine Environmental Research*, Vol. 58 (2-5), pp 327 – 331.

OSPAR, 1998. SINTRA Statement. *Summary record OSPAR 98/14/1*, Annex 45. OSPAR, London.

Oughton, D.H., Børretzen, P., Salbu, B. & Tronstad, E. 1997. Mobilisation of <sup>137</sup>Cs and <sup>90</sup>Sr from sediments: potential sources to arctic waters. *The Science of the Total Environment*, Vol. 202, pp 155 – 165.

Paterson, D.M. 1997. Biological mediation of sediment erodibility: ecology and physical dynamics. *Biological mediation of sediment erodibility: ecology and physical dynamics*. (Eds.) Burt, N., Parker, R. & Watts, J., Cohesive Sediments, Wiley & Sons, pp. 215-229.

Paterson, D.M. & Black, K.S. 1999. Water flow, sediment dynamics and benthic biology. In *Advances in ecological research*, Raffaelli, D. & Nedwell, D. (eds). London, Academic Press.

Paterson, D.M. & Black, K.S. 2000. Temporal variability in the critical erosion threshold of salt marsh and upper intertidal sediments. In *British Salt Marshes*, (Sherwood, B.R., Gardiner, B.G., & Harris, T. eds.) J. Linnaean Soc London.

Paterson, D.M. & Hagerthey, S.E. 2001. Microphytobenthos in contrasting coastal ecosystems: biology and dynamics. In *Ecological comparisons of sedimentary shores*, Reise, K. (edi). Germany, Springer-Verlag.

Perkins, R.G., Paterson, D.M., Sun, H., Watson, J. & Player, M.A. 2004. Extracellular polymeric substances: quantification and use in erosion experiments. *Continental Shelf Research*. Vol. 24 (15), pp 1623 – 1635.

Perry, E.M., Warner, T. & Foote, P. 2000. Comparison of atmospheric modelling versus empirical line fitting for mosaicing HYDICE imagery. *International Journal of Remote Sensing*. Vol. 21 (4), pp 799 -803.

Peters, H & Bokhorst, R. 2001. Microstructure observations of turbulent mixing in a partially mixed estuary, Part II: salt flux and stress. *Journal of Physical Oceanography*. Vol. 31, pp 1105 – 1119.

Pinckney, J., Papa, R. & Zingmark, R. 1994. Comparison of high-performance liquid chromatographic, spectrophotometric and fluorometric methods determining chlorophyll a concentrations in estuarine sediments. *Journal of Microbiological Methods*. Vol. 19 (1), pp 59 - 66

Postma, H. 1967. Sediment transport and sedimentation in the estuarine environment. *American Association of Advance Science*. Vol. 83, pp 158 – 179.

Rainey, M.P. 1999. Airborne remote sensing of estuarine intertidal radionuclides concentrations. *PhD Thesis*. University of Stirling.

Rainey, M.P., Tyler, A.N., Bryant, R.G., Gilvear, D.J. & McDonald, P. 2000. The influence of surface and interstitial moisture on the spectral characteristics of intertidal sediments: implications for airborne image acquisition and processing. *International Journal of Remote Sensing*. Vol. 21 (16), pp 3025 – 3038.

Rainey, M.P., Tyler, A.N., Bryant, R.G., Gilvear, D.J. & McDonald, P. 2003. Mapping intertidal estuarine sediment grain size distributions through airborne remote sensing. *Remote Sensing of Environment*. Vol. 86, pp 480 – 490.

Reed, D.J. 1995. The response of coastal marshes to sea-level rise; survival or submergence? *Earth Surface Processes and Landforms*, Vol. 20, pp 39 – 48.

- Ridgeway, J. & Shimmiel, G. 2002. Estuaries as repositories of historical contaminants and their impact on shelf seas. *Estuarine, Coastal and Shelf Science*. Vol. 55, pp 903 – 928.
- RIFE -7. 2002. Environment Agency and Food Standards Agency.
- RIFE -9. 2003 Environment Agency and Food Standards Agency.
- RIFE -10. 2004. Environment Agency and Food Standards Agency.
- Ritcher, R., Muller, A. & Heiden, U. 2002. Aspects of operational atmospheric correction of hyperspectral imagery. *International Journal of Remote Sensing*. Vol. 23 (1), pp 145 – 157.
- Robinson, M-C., Morris, K.P. & Dyer, K.R. 1998. Deriving fluxes of suspended particulate matter in the Humber Estuary, UK. Using airborne remote sensing. *Marine Pollution Bulletin*. Vol. 37 (3-7), pp 155 – 163.
- Robinson Swift, M., Fredriksson, D.W. & Barbaros Celikkol. 1996. Structure of an axial convergence zone from acoustic Doppler current profiler measurements. *Estuarine, Coastal and Shelf Science*. Vol. 43, pp 109 – 122.
- Rosales-Hoz, L., Cundy, A.B. & Bahena-Manjarrez, J.L. 2003. Heavy metals in sediment cores from a tropical estuary affected by anthropogenic discharges: Coatzacoalcos Estuary, Mexico. *Estuarine, Coastal and Shelf Science*. Vol. 58, pp 117 – 126.
- Ruiz, F. 2001. Trace metals in estuarine sediments from the south-western Spanish coast. *Marine Pollution Bulletin*. Vol. 42 (6), pp 482 – 490.
- Sanford, T.B., Suttles, S.E. & Halka, J.P. 2001. Reconsidering the physics of the Chesapeake Bay estuarine turbidity maximum. *Estuaries*. Vol. 24, pp 655 – 669.
- Sanderson, D.C.W., Cresswell, A.J., Hardeman, F. & Debauche, A. 2004. An airborne gamma-ray spectrometry survey of nuclear sites in Belgium. *Journal of Environmental Radioactivity*. Vol. 72, pp 213 – 224.
- Sawnhey, B.L. 1966. Kinetics of caesium sorption by clay minerals. *Soil Science Society of America Proceedings*. Vol. 30, pp 565 – 569.
- Settle, J.J. & Drake, N.A. 1993. Linear mixing and the estimation of ground cover proportions. *International Journal of Remote Sensing*. Vol. 14 (6), pp 1159 – 1177.
- Shainburg, J. & Kemper, W.D. 1967. Ion exchange equilibria in montmorillonite. *Soil Science*. Vol. 103, pp 4 – 9.
- Sharples, J., Simpson, J.H. & Brubaker, J.M. 1994. Observations and modelling of periodic stratification in the upper York River Estuary, Virginia. *Estuarine, Coastal and Shelf Science*. Vol. 38, pp 301 – 312.
- Siegel, H., Gerth, M. & Mutzka, A. 1999. Dynamics of the Ode River plume in the southern Baltic Sea: Satellite data and numerical modelling. *Continental Shelf Research*. Vol. 19, pp 1143 – 1159.
- Smith, C.N., Goshawk, J.A., Charles, K., McDonald, P., Leonard, K.S. & McCubbin, D. 2003. MEAD (part II) – predictions of radioactivity concentrations in the Irish Sea. *Journal of Environmental Radioactivity*. Vol. 68, pp 193 – 214.
- Stanners, D.A. & Aston, S.R. 1981. Factors controlling the interactions of <sup>137</sup>Cs with suspended and deposited in estuarine and coastal environments. *Impacts of radionuclide release into the marine environment*; Vienna. IAEA

Stanners, D.A. & Aston, S.R. 1982. Desorption of  $^{106}\text{Ru}$ ,  $^{134}\text{Cs}$ ,  $^{137}\text{Cs}$ ,  $^{144}\text{Ce}$  and  $^{241}\text{Am}$  from intertidal sediment contamination by nuclear fuel reprocessing effluents. *Estuarine, Coastal and Shelf Science*. Vol. 14, pp 687 – 691.

Stuckless, J.S. & Dudley, W.W. 2002. The geohydrologic setting of Yucca Mountain, Nevada. *Applied Geochemistry*. Vol. 17, pp 659 – 682.

Tattersall, G.R., Elliot, A.J. & Lynn, N.M. 2003. Suspended sediment concentrations in the Tamar Estuary. *Estuarine, Coastal and Shelf Science*. Vol. 57, pp 679 – 688.

Taylor, D. 1986. Changes in the distribution patterns of trace metals in sediments of the Mersey Estuary in the last decade. *The Science of the Total Environment*, Vol. 49, pp 257 – 295.

Thomas, S. & Ridd, P.V. 2004. Review of methods to measure short time scale sediment accumulation. *Marine Geology*. Vol. 207, pp 95 -114.

Thomson, A.G., Eastwood, J.A., Yates, M.G., Fuller, R.M., Wadsworth, R.A. & Cox, R. 1998a. Airborne remote sensing of intertidal biotopes. *Marine Pollution Bulletin*. Vol. 37, pp 164 – 172.

Thomson, A.G., Fuller, R.M. & Eastwood, J.A. 1998b. Supervised versus unsupervised methods for classification of coast and river corridors from airborne remote sensing. *International Journal of Remote Sensing*. Vol. 19 (17), pp 3423 – 3431.

Tolhurst, T.J., Black, K.S., Shayler, S.A., Mather, S., Black, I., Baker, K. & Paterson, D.M. 1999. Measuring the *in-situ* erosion shear stress of intertidal sediments with the cohesive strength meter (CSM). *Estuarine, Coastal and Shelf Science*. Vol. 49, pp 281 – 294.

Tolhurst, T.J., Black, K.S., Paterson, D.M., Mitchener, H.J. Termaat, G.R. & Shayler, S.A. 2000. A comparison and measurement standardisation of four *in-situ* devices for determining the erosion shear stress of intertidal sediments. *Continental Shelf Research*. Vol. 20, pp 1397 – 1418.

Trowbridge, J.H., Geyer, W.R., Bowen, M.M. & Williams, A.J. 1999. Near-bottom turbulence measurements in a partially mixed estuary: turbulent energy balance, velocity structure, and along-channel momentum balance. *Journal of Physical Oceanography*. Vol. 29, pp 3056 – 3072.

Tyler, A.N., Bryant, R., Gilvear, D., McDonald, P., Teasdale, I., Brown, J. & Ferrier, G. 1995. The spectral characterisation of radionuclide bearing sediments in the Ribble Estuary. In *Proceedings of the 21<sup>st</sup> Annual Conference of the Remote Sensing Society*, pp 433 – 440.

Tyler, A.N., Sanderson, D.C.A. & Scott, E.M. 1996. Estimating and accounting for  $^{137}\text{Cs}$  source burial through *in-situ* gamma spectrometry in salt marsh environments. *Journal of Environmental Radioactivity*. Vol. 33 (3), pp 195 – 212.

Tyler, A.N. 1999. Monitoring anthropogenic radioactivity in salt marsh environments through *in situ* gamma-ray spectrometry. *Journal of Environmental Radioactivity*. Vol. 45, pp 235 – 252

Tyler, A.N. 2004. High accuracy of radiometric mapping. *Journal of Environmental Radioactivity*. Vol. 72, pp 195 – 202.

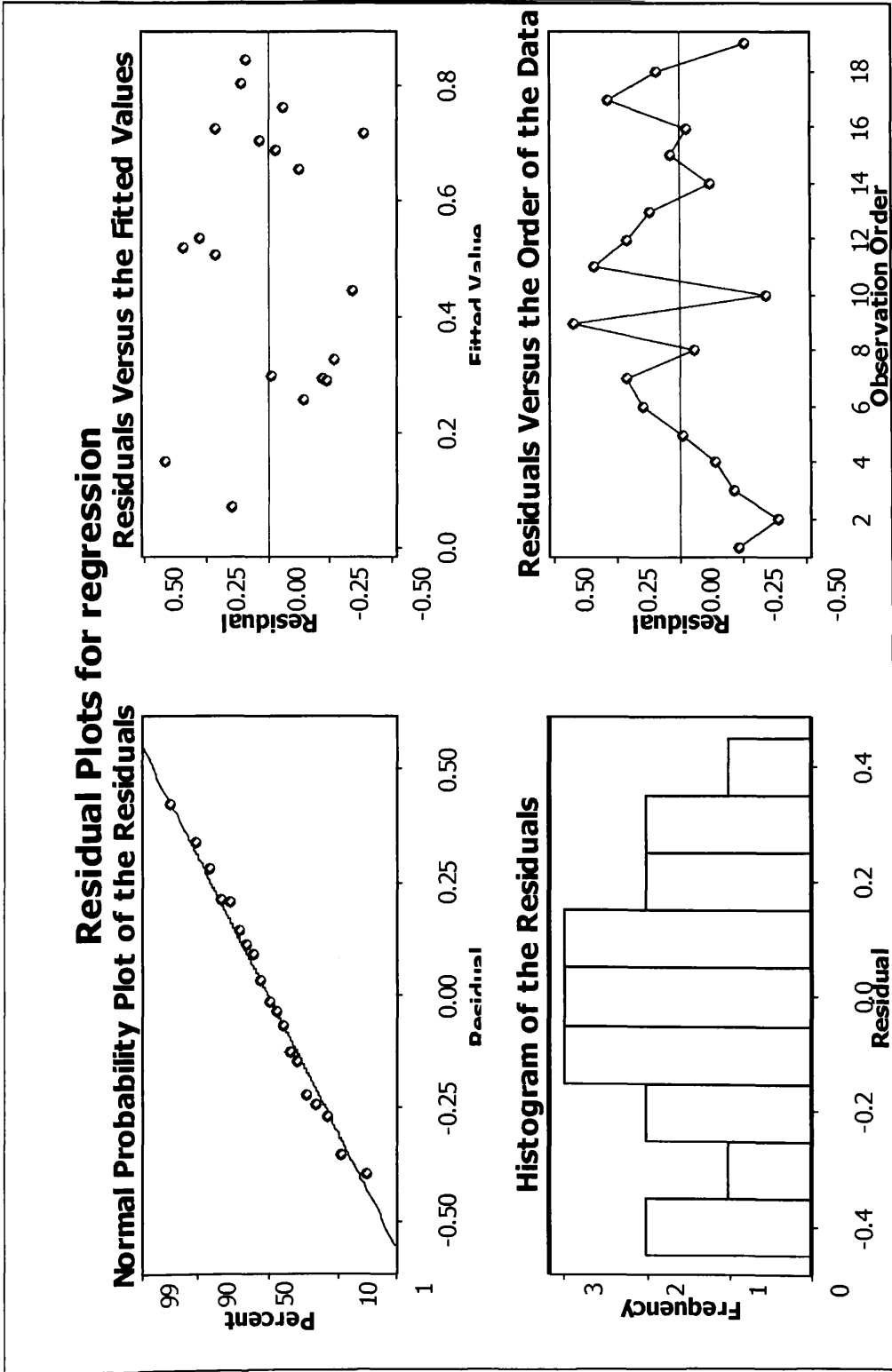
Tyler, A.N., Wakefield, R.J.; Rainey, M.P., McDonald, P. & Gilvear, D.G. (in prep). Deriving accurate intertidal radionuclide concentrations at high spatial resolution through airborne remote sensing. *Environmental Science and Technology*.

- Tyler, A.N., Atkin, P., Wakefield, R., Gilvear, D.J. & McDonald, P. (In prep)(b). Estimate Sediment and radionuclide deposition over a flood tide sequence through airborne remote sensing. *Estuarine and Coastal Shelf Science*.
- Ueda, S., Ohtsuka, Y. & Kondo, K. 2004. Inventories of  $^{239+240}\text{Pu}$ ,  $^{137}\text{Cs}$  and excess  $^{210}\text{Pb}$  in sediment cores from brackish Lake Obuchi, Rokkasho Village, Japan. *Journal of Radioanalytical and Nuclear Chemistry*. Vol.261 (2), pp 277 – 282.
- Uncles, R.J. & Stephens, J.A. 2000. Observations of currents, salinity, turbidity and intertidal mudflat characteristics and properties in the Tay Estuary. *Continental Shelf Research*. Vol. 20, pp 1531 – 1549.
- Uncles, R.J. 2002. Estuarine physical processes research: Some recent studies and progress. *Estuarine, Coastal and Shelf Science*. Vol. 55, pp 829 – 856.
- Underwood, G.J.C. & Paterson, D.M. 2003. The importance of extracellular carbohydrate production by marine epipellic diatoms. *Advances in Botanical Research*. Vol. 40, pp 184 - 240
- Van der Ham, R. & Winterwerp, J.C. 2001. Turbulent exchange of fine sediments in a tidal channel in the Ems/Dollard estuary. Part II. Analysis with a 1DV numerical model. *Continental Shelf Research*. Vol. 21 (15), pp 1629 – 1647.
- Van der Wal, D., Pye, K. & Neal, A. 2002. A long term morphological change in the Ribble Estuary, northwest England. *Marine Geology*. Vol. 189 (3-4), pp 249 – 266.
- Van der Wal, D. & Pye, K. 2003. The use of historical bathymetric charts in a GIS to assess morphological changes in estuaries. *The Geological Journal*, Vol. 169, No. 1, pp 21 – 31.
- Weaver, P. P. & Schulthies, P.J. 1990. Current methods for obtaining, logging and splitting marine sediment cores. *Marine Geophysical Researches*. Vol. 12, pp 85 – 100.
- Widdows, J. & Brinsley, M. 2002. Impacts of biotic and abiotic processes on sediment dynamics and the consequences to the structure and functioning of the intertidal zone. *Journal of Sea Research*. Vol. 48, pp 143 – 156.
- Williams, K..H., Thorne, M.C., Thopson, J.G. & Paulley, A. 2002. Development of a solution method for the differential equations in the biosphere module of the BNFL's suite of codes MONDRAIN. *Annals of NUCLEAR ENERGY*. Vol. 29, pp 1019 – 1039.
- Wiltsire, K.H. & Schroeder, F. 1994. Pigment patterns in suspended matter from the Elbe Estuary, Northern Germany. *Netherlands Journal of Aquatic Ecology*. Vol. 28 pp 255 – 265.
- Wolanski, E. & Spagnol, S. 2003. Dynamics of the turbidity maximum in King Sound, tropical Western Australia. *Estuarine, Coastal and Shelf Science*. Vol. 56, pp 877 – 890.
- Wu, Y., Falconer, R.A. & Uncles, R.J. 1998. Modelling of water flows and cohesive sediment fluxes in the Humber Estuary. *Marine Pollution Bulletin*. Vol. 37, pp 182 – 189.
- Yates. M.G., Jones, A.R., McGrorty, S. & Goss-Custard, J.D. 1993. The use of satellite imagery to determine the distribution of intertidal surface sediments of the Wash, England. *Estuarine, Coastal and Shelf Science*. Vol. 36, pp 333 – 344.
- Zagolski, F. & Gastellu-Etchegorry, J.P. 1995. Atmospheric corrections of AVIRIS images with a procedure based on the inversion of the 5S model. *International Journal of Remote Sensing*. Vol. 16 (16), pp 3115 – 3146.

Appendix 1 – Example of meteorological data for RAF Ronaldsway, Isle of Man. (April, 2003)

RONALDSWAY		LATITUDE 54_5N		LONGITUDE 4_38W		ALTITUDE		16m	
MONTH	APR	YEAR		2003					
DAY	MAXTEMP (Deg C)	MINTEMP (Deg C)	RAIN (mm)	SUN (hours)	GRASS MIN (Deg C)	WIND SPEED (knots)	WIND DIRECTION (degrees)	GUST (knots)	WEATHER (see key)
1	11.1	8.2	2.5	5.0	6.6	22	270	50	h
2	10.5	2.9	1.3	5.7	1.7	15	310	37	
3	13.1	6.7	0.0	9.7	0.4	11	340	37	
4	12.9	8.5	0.0	5.0	6.4	12	280	29	
5	14.5	4.6	0.0	6.0	0.7	5	70	11	f
6	10.9	3.5	0.0	4.2	-1.0	9	80	23	
7	7.8	5.9	0.0	0.0	4.5	10	100	21	
8	9.4	3.3	0.0	10.2	-0.2	9	90	16	
9	9.4	2.0	0.0	7.1	-2.0	7	100	23	
10	8.4	2.2	0.0	11.8	-2.6	8	90	19	
11	10.5	2.0	0.0	7.3	-2.1	8	250	18	
12	11.0	5.3	0.0	3.6	1.2	6	90	16	
13	12.4	6.1	2.7	0.4	2.2	15	110	26	
14	15.7	8.5	0.0	1.3	7.7	15	70	25	
15	15.9	9.7	0.0	8.8	7.2	8	70	22	
16	20.1	9.2	0.0	11.4	6.2	8	70	21	
17	19.5	11.1	0.0	12.6	6.6	15	70	27	
18	18.7	10.2	0.0	11.0	7.1	13	70	26	
19	12.5	7.6	0.0	12.6	2.8	13	60	26	
20	14.3	6.2	0.9	4.3	3.5	16	50	31	
21	10.4	6.6	1.2	0.0	5.2	11	50	28	
22	11.6	6.3	0.0	8.3	2.4	8	230	18	
23	14.6	3.1	0.0	11.8	0.4	9	80	19	
24	11.6	7.6	3.5	4.2	4.6	14	90	27	
26	11.3	8.0	5.6	1.8	6.3	16	120	29	
26	12.7	8.8	0.3	4.9	6.5	16	170	29	
27	13.1	8.8	14.2	7.2	7.1	17	230	29	
28	11.6	8.1	1.2	0.0	8.8	14	100	29	
29	13.2	8.6	12.0	9.0	7.1	11	240	26	
30	13.0	8.4	6.8	10.8	7.6	12	200	23	
<b>Monthly Sum/Average</b>	12.7	6.6	52.2	196.0	3.8	12	--	Max 50	
<b>1971-2000 Average</b>	10.8	4.9	53.4	169.2	2.7	11.7	--	--	--

Appendix 2 – Residual plots for regression of percentage clay versus  $^{137}\text{Cs}$  relationships.



**Appendix 3** Best subset regression of the image unmixed image values of mudabundance and microphytobenthos abundance from the September 2003 imagery.

**Best Subsets Regression: real nl versus unmix all, unmix micro**

Response is real nl

43 cases used, 2 cases contain missing values

Vars	R-Sq	R-Sq(adj)	Mallows C-p	S	l r
1	83.6	83.2	1.0	0.39830	X
1	5.4	3.1	191.5	0.95615	X
2	83.6	82.8	3.0	0.40323	X X

**Appendix 4.** Comparison of the EDM survey at Warton Bank and the bathymetric profile obtained from within the VERSE model.

